COPPE
Instituto Alberto Luiz Coimbra de Pós-Graduação e Pesquisa de Engenharia
UFRJ

HYPERSALINE BRINES TREATMENT USING OSMOSIS-BASED PROCESSES: FUNDAMENTALS AND FEASIBILITY

Sara Regina Osipi

Tese de Doutorado apresentada ao Programa de Pós-graduação em Engenharia Química, COPPE, da Universidade Federal do Rio de Janeiro, como parte dos requisitos necessários à obtenção do título de Doutor em Engenharia Química.

Orientadores: Cristiano Piacsek Borges
Argimiro Resende Secchi
Meagan Stumpe Mauter

Rio de Janeiro
Dezembro de 2019

HYPERSALINE BRINES TREATMENT USING OSMOSIS-BASED PROCESSES: FUNDAMENTALS AND FEASIBILITY

Sara Regina Osipi

TESE SUBMETIDA AO CORPO DOCENTE DO INSTITUTO ALBERTO LUIZ COIMBRA DE PÓS-GRADUAÇÃO E PESQUISA DE ENGENHARIA (COPPE) DA UNIVERSIDADE FEDERAL DO RIO DE JANEIRO COMO PARTE DOS REQUISITOS NECESSÁRIOS PARA A OBTENÇÃO DO GRAU DE DOUTOR EM CIÊNCIAS EM ENGENHARIA QUÍMICA.

Orientadores: Cristiano Piacsek Borges
Argimiro Resende Secchi
Meagan Stumpe Mauter

Aprovada por: Prof. Cristiano Piacsek Borges
Prof. Argimiro Resende Secchi
Prof. Frederico de Araújo Kronemberger
Prof. André Luiz Hemerly Costa
Prof. Luiz Antonio Pessan

RIO DE JANEIRO, RJ - BRASIL
DEZEMBRO DE 2019

Osipi, Sara Regina

Hypersaline brines treatment using osmosis-based processes: Fundamentals and feasibility/Sara Regina Osipi. – Rio de Janeiro: UFRJ/COPPE, 2019.

XXVIII, 180 p.: il.; 29, 7cm.

Orientadores: Cristiano Piacsek Borges
Argimiro Resende Secchi
Meagan Stumpe Mauter

Tese (doutorado) – UFRJ/COPPE/Programa de Engenharia Química, 2019.

Referências Bibliográficas: p. 90 – 113.

1. Dessalinização. 2. Avaliação de custos. 3. Permeabilidade hidráulica. 4. Permeabilidade a sal. 5. Correntes salinas. I. Borges, Cristiano Piacsek *et al.* II. Universidade Federal do Rio de Janeiro, COPPE, Programa de Engenharia Química. III. Título.

If I have seen further, it is by standing upon the shoulders of giants.
Isaac Newton

Agradecimentos

Gostaria de agradecer a Deus, minha família e amigos por me manterem motivada. Em especial, quero agradecer meu marido Kadu pela paciência, carinho e apoio incondicional em todos os momentos do doutorado.

Sou muito grata aos meus orientadores e quase "pais", Argimiro e Cristiano! Desde o início do doutorado e em váááários momentos de desespero, o Cristiano teve ideias num primeiro momento, malucas, e que depois se mostraram excelentes. O Argimiro, sempre muito presente, dava aquele empurrãozinho quando era necessário e sempre se prontificou a ajudar nas inúmeras intempéries da interpretação dos dados experimentais e simulados! Junto a outros excelentes pesquisadores da área de dessalinização, estatística e simulação, o Cristiano e o Argimiro são os gigantes que me permitiram ver mais longe. Muito obrigada!!

I am extremely grateful to Dr. Meagan Mauter, who made my vision of a PhD broader, motivating my research to focus on fundamental science and kindly gave me an opportunity of internship in her laboratory. Thank you so much!!

À Vera Cruz e à Luciana Santos, pessoas maravilhosas que salvaram a minha vida em diversos momentos ao longo dessa tese, muito obrigada!!

Gostaria também de agradecer aos membros da banca, Profs. Fred Kronemberger, André Hemerly e Luiz Pessan, que aceitaram o convite para avaliação desta tese. Em especial, um muito obrigada ao Prof. Fred, que fez parte da banca de acompanhamento de tese, contribuindo com a análise crítica do trabalho.

Aos meus amigos do PAM. Marcos, companheiro de RU e de debate crítico de resultados, muito obrigada! Agradeço também a Cátia, que sempre me apoiou e que melhorava a ambiência da sala 22! Obrigada também à Omayra, à Karla e ao Bruno, pelos desabafos e discussões técnicas enriquecedoras! Também gostaria de agradecer à sala 26 pela ajuda constante: Aline, Amanda, Gisele e Bruno Alves, muito obrigada!! Sou imensamente grata ao Bob e a Beth, que compartilharam sua experiência experimental e de vida em incontáveis ocasiões!

A big thanks also goes to WE^3 Lab for their excellent suggestions, friendship and help: Thanks Tim, Sneha, Xitong, Alex, Quay and Daniel! Besides, I'd like to thank Jake and Nick from NETL/DOE for their constant help and suggestions in this work!

Sou grata a meus amigos da Petrobras, Rodrigo, Mariana, Ana Levy, Scofa, Bignetti, Raquel, Sílvia e Solange! Desde a concepção da ideia de tese, sempre me apoiaram e compartilharam sua experiência comigo. Obrigada!

Por fim, gostaria de agradecer à CAPES/PDSE (88881.186982/2018-01) e à FAPERJ pelo apoio financeiro.

Resumo da Tese apresentada à COPPE/UFRJ como parte dos requisitos necessários para a obtenção do grau de Doutor em Ciências (D.Sc.)

TRATAMENTO DE EFLUENTES HIPERSALINOS USANDO PROCESSOS BASEADOS EM OSMOSE: FUNDAMENTOS E VIABILIDADE

Sara Regina Osipi

Dezembro/2019

Orientadores: Cristiano Piacsek Borges
Argimiro Resende Secchi
Meagan Stumpe Mauter

Programa: Engenharia Química

Efluentes salinos vêm sendo estudados como fontes hídricas em função da escassez de água doce e da elevada disponibilidade dessas correntes na extração de óleo e gás e captura de CO_2. No entanto, há incertezas a respeito da relação custo-benefício dos tratamentos aplicáveis. Novos processos baseados na osmose inversa estão sendo desenvolvidos com promissoras vantagens energéticas e econômicas. O objetivo geral deste trabalho é investigar os efeitos da alta salinidade em processos derivados da osmose inversa, assim como avaliar a aplicabilidade dos mesmos. A otimização dos custos de rotas de tratamento mostrou que o processo de osmose inversa assistida tem o menor custo, mesmo quando comparado com processos convencionais. Os parâmetros de transporte da membrana, como permeabilidades e parâmetro estrutural, são importantes para a viabilidade econômica desse processo. Objetivando investigar se esses parâmetros permaneceriam constantes em alta concentração de sal, membranas de triacetato de celulose foram testadas em salinidade e pressão variáveis. As permeabilidades hídrica e à sal diminuíram com o aumento da salinidade, enquanto o parâmetro estrutural aumentou com a elevação da pressão. Testes de pervaporação confirmaram que a permeabilidade hidráulica diminui até atingir um platô em salinidades acima de 50 g/L. Uma provável explicação para esse fenômeno é o desinchamento da membrana, já reportado para outros materiais. Estudos subsequentes são necessários para entender o transporte em alta salinidade e estabelecer diretrizes para o desenvolvimento de membranas e processos em condições extremas.

Abstract of Thesis presented to COPPE/UFRJ as a partial fulfillment of the requirements for the degree of Doctor of Science (D.Sc.)

HYPERSALINE BRINES TREATMENT USING OSMOSIS-BASED PROCESSES: FUNDAMENTALS AND FEASIBILITY

Sara Regina Osipi

December/2019

Advisors: Cristiano Piacsek Borges
Argimiro Resende Secchi
Meagan Stumpe Mauter

Department: Chemical Engineering

High salinity brines have been studied as potential fresh water sources due to the scarcity of other supplies and elevated saline effluent generation in activities such as oil and gas extraction and CO_2 capture. Although their availability is remarkably abundant in some regions, there are concerns regarding its cost-effective treatment. Novel reverse osmosis (RO) based process are being developed with promising energy consumption and cost advantages. The main objective of this work is to investigate the effects of high salinity on RO-based processes, as well as in the process treatment feasibility. Cost optimization showed the osmotically assisted reverse osmosis process have the lowest cost when compared to conventional processes, such as mechanical vapor compression. Membrane transport properties as permeabilities and structural parameter are important to the cost technology feasibility. Aiming to investigate whether the membrane transport properties would remain constant in higher salt concentration, cellulose triacetate membranes were tested under variable pressure and salinity. Water and salt permeability were found to decrease with increasing average salinity while the structural parameter increased with increasing pressure. Pervaporation tests supported the hypothesis of variable membrane performance, reaching a plateau for average salinities higher than 50 g/L. A possible explanation is membrane deswelling, previously reported for different materials. Further studies are needed to understand the transport under high salinity and to stablish directions for membrane tailoring and applications under extreme environments.

Contents

List of Figures

List of Tables

List of Symbols

A	Water permeability (L/(h×m^2×bar)), p. 21
A_{hx}	Heat exchangers area (m^2), p. 117
B	Salt permeability (L/(h×m^2), p. 21
BPE_b	Brine boiling point elevation (K), p. 117
BPE_f	Feed boiling point elevation (K), p. 117
C_{comp}	MVC compressor cost (US$), p. 117
C_{evap}	MVC evaporator cost (US$), p. 117
C_{hx}	Heat exchangers cost (US$), p. 117
C_{pump}	Pump and PX cost (US$), p. 37
DF	Degrees of freedom, p. 66
D_f	Salt diffusivity (m^2/s), p. 38
FF_{max},FF_{min}	F-Fisher maximum and minimum critical values, p. 122
F_i	Volumetric flowrate (m^3/h), p. 37
G	Membrane permeability coefficient (kg/(bar m^{2}h)), p. 118
H_s	Superheated vapor mass enthalpy ((kJ/kg)), p. 116
H_v	Saturated vapor mass enthalpy (kJ/kg), p. 116
$H_{v,f,m}$	Vapor mass enthalpy at feed membrane interface temperature (kJ/kg), p. 118
$H_{v,p,m}$	Vapor mass enthalpy at permeate membrane interface temperature (kJ/kg), p. 118
J_W	Volumetric water flux (L/(h×m^2), p. 36

K_m	Membrane thermal conductivity (kW/(m K)), p. 119
K_p	Permeate thermal conductivity (kW/(m K)), p. 119
K_v	Vapor thermal conductivity (kW/(m K)), p. 119
$LMTD$	Log mean temperature difference (K), p. 121
LS	Least square error, p. 122
MM	Molar mass (mol/L), p. 36
N_{exp}	Number of experimental conditions, p. 66
N_{par}	Number of fitted parameters, p. 66
N_{var}	Number of measured variables, p. 66
Nu	Nusselt number, p. 120
P_d	Condenser pressure (bar), p. 117
P_f	Feed pressure (bar), p. 65
P_s	Sweep pressure (bar), p. 65
P_v	Evaporator pressure (bar), p. 117
$P_{in,c}$	PX inlet concentrate pressure (bar), p. 36
$P_{in,f}$	PX inlet feed pressure (bar), p. 36
$P_{out,c}$	PX outlet concentrate pressure (bar), p. 36
$P_{out,f}$	PX outlet feed pressure (bar), p. 36
$P_{out,i}$	Equipment discharge pressure (bar), p. 37
$P^w_{sat,l}$	Water vapor pressure at liquid temperature, p. 68
$P^w_{sat,v}$	Water vapor pressure at vacuum side (bar), p. 68
$P_{vap,f}$	Feed vapor pressure at the membrane interface (bar), p. 118
$P_{vap,p}$	Permeate vapor pressure at the membrane interface (bar), p. 118
Pot	Pump power (kW), p. 119
Pr	Prandtl number, p. 120

R	Universal gas constant (J/(mol K), p. 121
R^2	Coefficient of determination, p. 67
Re	Reynolds number, p. 66
S	Support structural parameter (μm), p. 21
Sc	Schmidt number, p. 66
T	Temperature (K), p. 121
TFC	Thin film composite, p. 23
T_b	Brine temperature (K), p. 116
T_d	Condensing temperature (K), p. 116
T_f	Feed temperature (K), p. 116
T_s	Superheated vapor temperature (K), p. 116
T_v	Saturated vapor temperature (K), p. 116
T_w	Wall temperature (K), p. 119
$T_{f,m}$	Feed membrane temperature (K), p. 118
$T_{f,m}$	Permeate membrane temperature (K), p. 118
$T_{in,c}$	Inlet cool stream temperature (K), p. 121
$T_{in,h}$	Intlet hot stream temperature (K), p. 121
$T_{out,c}$	Outlet cool stream temperature (K), p. 121
$T_{out,h}$	Outlet hot stream temperature (K), p. 121
$T_{out,p}$	Permeate outlet temperature (K), p. 119
U	Global heat transfer coefficient (kW/(K m^2)), p. 117
VR	Volumetric ratio, p. 115
V_{water}	Annual recovered water volume (m^3/y), p. 34
W	Flow channel width (m), p. 120
ΔP	Hydraulic pressure difference (bar), p. 36

ΔP_{drop}	Head loss (bar), p. 121
ΔP_{sh}	Shell head loss (kPa), p. 117
ΔP_t	Tubes head loss (kPa), p. 117
$\Delta \dot{m}_f$	Feed mass flowrate variation (kg/h), p. 36
$\Delta \dot{m}_p$	Permeate mass flowrate variation (kg/h), p. 36
Δh_{vap}	Latent heat of vaporization (kJ/kg), p. 121
$\Delta \dot{m}_f$	Feed mass flowrate variation (kg/h), p. 38
$\Delta \dot{m}_s$	Sweep flowrate variation (kg/h), p. 38
$\Delta \pi_m$	Osmotic pressure difference at the membrane (bar), p. 36
δ	Membrane support thickness , p. 72
$\dot{F}_{pw}$	Pure water volumetric flowrate (m^3/h), p. 116
$\dot{F}_{ds}$)	Feed volumetric flowrate (m^3/h), p. 38
$\dot{F}_f$	Feed volumetric flowrate (m^3/h), p. 36
$\dot{F}_{in,c}$	Inlet coolant volumetric flowrate (m^3/h), p. 118
$\dot{F}_{in,f}$	Inlet feed volumetric flowrate (m^3/h), p. 114
$\dot{F}_{out,c}$	Outlet coolant volumetric flowrate (m^3/h), p. 118
$\dot{F}_{out,f}$	Outlet feed volumetric flowrate (m^3/h), p. 114
$\dot{F}_p$	Permeate volumetric flowrate (m^3/h), p. 36
$\dot{F}_s$	Sweep solution volumetric flowrate (m^3/h), p. 38
$\dot{m}_c$	Cool stream mass flowrate (kg/h), p. 121
$\dot{m}_h$	Hot stream mass flowrate (kg/h), p. 121
$\dot{m}_{in,f}$	Inlet feed mass flowrate, p. 114
$\dot{m}_{out,f}$	Outlet feed mass flowrate (kg/h), p. 114
$\dot{m}_{out,p}$	Outlet permeate mass flowrate (kg/h), p. 114
η_p	Pump efficiency, p. 119

η_{PX} Pressure exchanger efficiency factor, p. 36

γ Heat capacity ratio, p. 117

λ Head loss coefficient, p. 121

μ Viscosity (Pa.s), p. 83

ν_y Variance of variable y, p. 122

ϕ Osmotic coefficient, p. 121

π Osmotic pressure (bar), p. 20

π_f Feed osmotic pressure (bar), p. 115

$\pi_{m,f}$ Osmotic pressure at membrane feed interface (bar), p. 65

$\pi_{m,s}$ Osmotic pressure at membrane sweep interface (bar), p. 65

ρ Stream density (kg/m^3), p. 36

τ Membrane support tortuosity , p. 72

ε Membrane support porosity, p. 72

a Amortization factor, p. 34

a_n Element membrane area (m^2), p. 36

a_w Water activity, p. 68

a_e Evaporator area (m^2), p. 117

b_i Ionic species molality (mol/kg), p. 121

c_f Feed molar salt concentration (mol/L), p. 36

c_m Feed membrane molar salt concentration, p. 36

c_p Permeate molar salt concentration (mol/L), p. 36

c_{in} Inlet salt concentration (mol/L), p. 116

$c_{m,f}$ Feed salt concentration at the membrane interface (mol/L), p. 65

$c_{m,s}$ Sweep salt concentration at the membrane interface (mol/L), p. 65

$c_{oil,in,f}$ Inlet feed oil concentration (g/L), p. 114

$c_{oil,out,f}$ Outlet feed oil concentration (g/L), p. 114

c_{out} Outlet salt concentration (mol/L), p. 116

c_s Sweep bulk concentration (mol/L), p. 38

cp_c Cool stream specific heat capacity (J/(kg K), p. 121

cp_h Hot stream specific heat capacity (J/(kg K), p. 121

d_h Hydraulic diameter (m), p. 66

f Plant utilization factor, p. 34

h_b Brine mass enthalpy (kJ/kg), p. 116

h_f Feed mass enthalpy (kJ/kg), p. 116

$h_{conv,c}$ Coolant convective heat transfer coefficient (kW/(m^{2}K), p. 119

$h_{conv,f}$ Feed convective heat transfer coefficient (kW/(m^{2}K) , p. 119

$h_{f,b}$ Bulk feed mass enthalpy (kJ/kg), p. 119

$h_{in,c}$ Feed inlet mass enthalpy (kJ/kg), p. 118

$h_{in,f}$ Feed inlet mass enthalpy (kJ/kg), p. 118

$h_{out,c}$ Feed inlet mass enthalpy (kJ/kg), p. 118

$h_{out,f}$ Feed outlet mass enthalpy (kJ/kg), p. 118

$h_{out,f}$ Permeate outlet mass enthalpy (kJ/kg), p. 118

$h_{p,w}$ Permeate mass enthalpy at wall temperature (kJ/kg), p. 119

i Interest rate, p. 34

j_W Massic water flux (kg/(m^{2}h)), p. 118

j_s Mass salt flux (g/(h×m^2), p. 36

k_f Feed mass transfer coefficient (m/s), p. 36

k_{ds} Draw solution mass transfer coefficient (m^2/s), p. 115

n Investment period (y), p. 34

q	Heat (kW), p. 116
q_c	Heat transferred at the cooling wall (kW/(m^2), p. 118
q_m	Heat transferred through the membrane (kW/(m^2), p. 118
spc	Specific water cost (US$/m^3), p. 34
v_v	Specific volume (m^3/kg), p. 117
y	Calculated variable, p. 122
y^{exp}	Experimental variable, p. 122
z	Flow channel depth (m), p. 120

List of Abbreviations

AFM	Atomic force microscopy, p. 79
AGMD	Air gap membrane distillation, p. 17
BPE	Boiling point elevation, p. 48
BTEX	Benzene, Toluene, Ethyl-benzene and Xylenes, p. 8
CAPEX	Capital expenditures, p. 34
CA	Cellulose acetate, p. 25
CCRO	Closed circuit reverse osmosis, p. 23
CEPCI	Chemical Engineering Plant Cost Index, p. 34
CFRO	Counterflow Reverse Osmosis, p. 2
CGS	Carbon geological storage, p. 8
COMRO	Cascading osmotically mediated reverse osmosis, p. 24
CP	Concentration polarization, p. 39
CTA	Cellulose triacetate, p. 25
DI	Deionized water, p. 62
DSARO	Draw solution assisted reverse osmosis, p. 24
FO	Forward osmosis, p. 18
FTIR	Fourier transform infrared spectroscopy, p. 79
HDH	Humidification-dehumidification, p. 18
HPRO	High-Pressure Reverse Osmosis, p. 2
MD	Membrane distillation, p. 17

MED	Multieffect distillation, p. 13
MED	Multieffect evaporation, p. 13
MF	Microfiltration, p. 34
MSF	Multistage flash, p. 13
ND	Non detectable, p. 6
NORM	Naturally Occurring Radioactive Materials, p. 7
NR	Not reported, p. 6
OARO	Osmotically Assisted Reverse Osmosis, p. 2
OPEX	Operational expenditures, p. 34
O&G	Oil and gas, p. 6
PAH	Polycyclic Aromatic Hydrocarbons, p. 8
PALS	Positron annihilation lifetime spectroscopy, p. 79
PAO	Pressure assisted osmosis, p. 61
PA	Polyamide, p. 25
PRO	Pressure retarded osmosis, p. 21
PW	Produced Water, p. 5
PX	Pressure exchanger, p. 22
QCM-d	Quartz Crystal Microbalance with dissipation, p. 79
RO	Reverse osmosis, p. viii
RTEA	Retro-techno-economic analysis, p. 29
SAGD	Steam assisted gravity drainage, p. 16
SANS	Small angle neutron scattering, p. 79
SAR	Sodium absorption ratio, p. 12
SDG	Sustainable Development Goal, p. 1
SWRO	Seawater reverse osmosis, p. 34

TDS	Total dissolved solids, p. 9
TGA	Thermogravimetric analysis, p. 79
TOC	Total organic carbon, p. 6
TOG	Total oil and grease, p. 6
TTD	Terminal temperature difference, p. 41
TVC	Thermal vapor compression, p. 13
VC	Vapor compression, p. 13
XRD	X-ray diffraction, p. 87
ZLD	Zero liquid discharge, p. 10

Chapter 1

Introduction

1.1 Background and Relevance

Recently, it has been shown that only the usage of conventional water sources (rivers, lakes, wells and snow melting) is insufficient to meet current water demand [21]. Thus, the utilization of unconventional supplies, such as saline streams, is mandatory to meet the availability of clean water, described in the Sustainable Development Goal (SDG) 6 [21]. Water scarcity is an growing concern for world's agriculture, industry and population. It is estimated that almost half of world's population already experiences lack of water at least one month a year [22]. Water crises were also identified as one of the top 10 global risks both in impact and likelihood at the World Economic Forum [23].

Although Brazil accounts for almost 20% of the world's freshwater [24], 1 out of 6 municipalities has a risk related to water scarcity [25]. In this country, nearly 72% of the water is consumed in crop irrigation [24]. In places where severe drougths are common, as the Northeast region, deplection of agricultural and industrial activity can happen due to lack of water supplies [26] and priorization of water for domestic use.

With shortage of fresh water, the demand for higher recovery treatment processes and usage of saline streams and effluents is increasing. Activities such as oil and gas extraction [27, 28] and CO_2 geological storage [29, 30] generate impressive quantities of brines, specially onshore. The availability, allied to the cost and envinromental concerns associated with inland saline effluents disposal [21, 31, 32] settle the hypersaline streams as actual water supplies.

Despite the considerable volumes, the raw quality of hypersaline brines is usually not adequate to most usages in agriculture or industry because of the saline content [31, 33]. Hypersaline brines are defined as streams with salinity higher than 70 g/L and may contain expressive concentrations of scaling salts [34]. In order to meet

the required quality for reuse, in which salinity normally ranges from 0.1 mg/L to 5 g/L, a desalination step is often necessary.

Although there are conventional technologies that do desalinate brines, such as thermal processes, those are energy-intensive operations [3, 4, 35]. On the other hand, the current benchmark for salinities up to seawater level is reverse osmosis, a mature and low-energy technique, but not feasible for higher salinity due to pressure and recovery constraints. RO is inspiring novel membranes processes, such as counterflow reverse osmosis (CFRO), osmotically assisted reverse osmosis (OARO) and high-pressure reverse osmosis (HPRO) [1–4, 36]. These processes claim to expand the RO conventional limits on recovery and on feed salinity by using a sweep/draw solution (CFRO and OARO) or even higher pressures (HPRO).

Whereas RO-based technologies are theoretically promising, it is necessary to understand how these novel systems would perform at harsher conditions of pressure and mostly, salinity. There is some evidence in literature that membrane morphological properties do change in high salinity [12, 37], but it is still not completely understood if and how these modifications would be converted in performance changes. Besides, the existence of concentration polarization in osmotic processes makes the proper quantification of the changes in these properties more challenging. Because of these uncertainties, current methodologies used for evaluating membrane properties in mature membrane processes might not be representative of the new applications.

Additionally to the understanding of the effects involved in process performance, it is also important to address their impact on energy and cost for brine treatment. In particular, cost comparison is important to show the differences not only in terms of energy but also to prospect the key variables and parameters to increase process feasibility and guide future research.

Questions about the membrane behavior under high salinity and cost-effective RO-based processes are extremely relevant since they are aiming to substitute conventional desalination process and decrease treatment cost and energy consumption. The feasibility of these routes, as well as their common assumptions should be addressed in order to better support the decisions on desalination technologies.

1.2 Objectives

The main purpose of this work is to evaluate the feasibility of osmotically assisted processes in desalination of hypersaline brines. The specific objectives to be discussed in the next chapters are:

- Study and optimization of main variables of osmotic and osmotically assisted processes.

- Analysis of the most promising cost-benefit routes in desalination of higly saline streams.
- Investigation on the effect of high salinity in membrane properties.

1.3 Defending propositions

The defending propositions and contributions of this thesis are:

- The investigation and cost comparison of several desalination technologies for brines, showing OARO has promising cost and energetic consumption.
- A novel application of retro-techno-economic analysis for desalination by RO-based processes, showing that parameters as water permeability and structural parameter may determine the cost feasibility.
- Water and salt permeabilities were detected to decrease with salinity for a commercial CTA membrane, using different sorption-diffusion processes.
- CTA deswelling was evidenced in preliminary tests in quartz crystal microbalance and may be associated with the decrease of permeabilities.

1.4 Thesis structure

Additionally to the present chapter, this document is structured in four other chapters, as described below:

Chapter 1: Introduction, which contains the motivation and relevance of the work, as well as the objectives.

Chapter 2: Literature Review, which presents theoretical background of hypersaline brines and effluents characteristics, the desalination processes applied for treating them, focusing on osmotic processes and their state-of-art. Regarding the aforementioned processes, membrane properties and cost are also discussed.

Chapter 3: Cost assessment of osmotic processes, where desalination technologies (consolidated and novel processes) costs are mapped under the common assumptions on literature in a technical-economic study.

Chapter 4: Effect of salinity on osmosis membrane properties, in which the hypothesis of constant membrane parameters is tested experimentally over a range of salinity and pressure. Besides, analytical techniques to support the hypothesis are discussed and tested.

Chapter 5: Conclusions and future work, which summarizes the main points of previous chapters and suggests future studies.

In this document, the common measurement units for membrane science are used, such as (L/(h m^2)) or mmHg for vacuum pressures, despite the International System of Units.

1.5 Publications of the research

The research described in this document was published in Desalination and submited to Journal of Membrance Science, which are detailed in the next chapters. Partial results of this work were presented in poster format at the AIChE Annual Meeting, Pittsburgh/PA (2018), North American Membrane Society NAMS 28th Annual Meeting (2019), Pittsburgh/PA and I Brazilian Congress on Process Systems Engineering 2019, Rio de Janeiro/RJ. The cost analyses presented in this work generated a book chapter in *Current Trends and Future Developments on (Bio-) Membranes - Reverse and Forward Osmosis: Principles, Applications, Advances*, Elsevier (2020).

Chapter 2

Literature review

This chapter addresses the main definitions and concerns regarding hypersaline brines, their production and characteristics, as well as potential users of desalted water and the desalination processes to obtain the required quality. It focus on theory not covered by the other chapters.

2.1 Hypersaline brines: main sources and characteristics

2.1.1 Oil and gas produced water

Despite the expanding participation of renewable energy resources [23], fossil fuels consumption, oil and natural gas in particular, are still the largest portion of world's energy supply. As reported by British Petroleum [38], 2018 oil worldwide production reached 94 billion of barrels per day, in average, representing an annual increase of 2.4%. Although relatively abundant and cheap energy sources, oil and gas exploration rises environmental concerns. One of the main effluents, produced water (PW), is the combination of the saline water naturally present in oil fields, known as formation water, and the water injected to keep the reservoir pressurized, injection water [39]. In natural gas conventional fields, produced water emerges as a mixture of water condensed from natural gas and formation water [40], representing less expressive volumes than oil fields.

The top conventional oil producing countries explore oil mainly from onshore fields, such as Saudi Arabia and Iran, or with equal parts of each sort of exploration (onshore and offshore), such as USA and Russia [38]. Furthermore, onshore produced water generation contributes to nearly two thirds of overall effluents from oilfields [41]. It is expected that produced water generation to reach 500 million barrels worldwide per day in 2020 [28]. In Brazil, the majority of the produced water comes

from offshore fields, being disposed after free oil removal [42]. However, oil onshore fields in Brazil's Northeast region produce large quantities of PW, with water as more than 90% of the well outlet.

Besides the growing amount of PW associated with the increasing oil and gas (O&G) production, other factors might also affect produced water quantity, as oil well drilling and completion method, water injection as secondary recovery, reservoir characteristics, water/oil separation technology in surface and oil well age [28, 40, 43]. In particular, the more mature an oilfield is, the more water it produces. Another aggravating point is the increasing share of unconventional oil and gas, especially those which use hydraulic fracking. These exploration methods can produce large amounts of produced water and consume expressive quantities of freshwater, mainly in the early drilling stages [28]. Around 3800 m^3 of water per well can be consumed just in shale gas drilling stage [27] and up to 15000 m^3/well can be used in fracking. Due to the low life of shale wells and effluent variability, modular treatment, such as membrane-based, is preferred.

Conventional and unconventional onshore fields are generally under higher disposal restrictions and water supply limitations than offshore ones [42, 44, 45]. Besides, in some countries, as OSPAR signatories and Canada, environment concerns are supporting several recommendations of lower or even zero effluent discharge for new offshore oil facilities [45]. The scenarios of water-stress zones and effluent disposal resctrictions point out to water reuse as an attractive, and sometimes mandatory, solution [41]. Another reason that supports reuse and desalination is a higher oil recovery when injection water has low salinity (< 1.5 mg/L) [46, 47].

Additionally, oil depots also handles saline effluent and are under onshore regulations for treatment and disposal [44, 48, 49]. São Paulo state, where are located four refineries and oil depots, was extremely impacted with a water shortage that led environmental and regulatory committees to reevaluate water grant to local industries [50].

Produced water, after leaving well or through addition of injection water, can receive chemical products to assist water/oil separation or to control corrosion, foam, fouling, bacterial growth and H_2S release. Drilling fluids can be part of produced water among formation water and injection water, in the early stages of well production [27]. Chemical additives used in oil and gas drilling or exploitation can be a downside in produced water treatability, in case of conventional process [27, 51].

Concerning to salinity, one of the main specific characteristics of produced water is the usually high ionic concentration, when compared to seawater, with total dissolved solids ranging from 3 mg/L to more than 300 g/L. Salt distribution and other main characteristics are presented on Table 2.1.

Despite of being usually more saline, these streams have individual ion concen-

Table 2.1: Physicochemical parameters for produced water and seawater [16–18].

Parameter	Produced water	Seawater (average)
Sodium (g/L)	0.132 - 97	11.2
Chloride (g/L)	0.08 – 200	20.6
Magnesium (mg/L)	8 - 6000	1300
Calcium (mg/L)	13 - 25800	314
Barium (mg/L)	1.3 - 650	NR[a]
Strontium (mg/L)	0.02 - 1000	10
Sulfate (mg/L)	<2 - 1650	2300
Bicarbonate (mg/L)	77 - 3990	83
pH	4.3 - 10.0	8.1
Total oil and grease (TOG) (g/L)	2-565	NR[a]
Total organic carbon (TOC) (g/L)	ND[b]- 1500	NR[a]
Suspended solids (g/L)	1.2 - 1000	NR[a]

[a] Not reported
[b] Non detectable

trations that also differ from seawater, with possible presence of barium, cadmium, chromium, copper, iron, lead, nickel and zinc in larger proportions. Generally, just some of these metals are present in produced water [40, 52]. This ionic distribution, mainly of minor constituents, is dependent on formation reservoir geology [52, 53], with constant predominance of sodium and chloride ions, as shown in Table 2.1.

In brine treatment and handling, there are concerns regarding scaling, as some salts concentrations as calcium carbonate and barium and strontium sulfates may be above saturation limit. Salt precipitation lowers heat exchange in thermal processes and decrease water flux in dense membrane applications [30]. Another complication relies on different salts behavior with temperature, which may change during exctracting and processing. For example, calcium carbonate tends to become more insoluble with temperature increase whereas silica solubility is elevated in high temperatures [52].

Aside from conventional salts, geothermal fluids, like PW, can contain Naturally Occurring Radioactive Materials (NORM), mainly radium isotopes [39, 52]. These contaminants can concentrate in alkaline earth precipitates, like barium sulfate, or biofilm deposits [52].

Substances such as benzene, toluene, ethyl-benzene and xylenes (BTEX), polycyclic aromatic hydrocarbons (PAH) and organic acids are the most abundant dissolved organic compounds in produced water [39, 54] and may need specific removal in restricter reuse cases. Hydrocarbons can be present in minor quantities, as their solubility is lower with salinity increase [55, 56]. Generally, produced water contain less diversity of organic compounds than refinery wastewater, since there are several processes like cracking and coking in oil refining that contribute to organic variety

[57].

Depending on well characteristics, H_2S, ammonia and volatile organic compounds can be also present [40] and leak during processing, since produced water temperature may range from 50 to 90 °C [51, 58]. Besides potential corrosion in copper alloys, ammonia levels were found toxic to some algae species by Andrade [59].

Although produced water pH is variable, it tends to acid range [39, 60]. Depending on the field, H_2S and CO_2 can be present due to bacterial activity [39] and can contribute to the acid pH. According to Doran *et al.* [61], calcium and magnesium scaling are lower at acid pH and from this point of view, it is interesting to correct pH when it is alkali. Additionally, oily organic fouling tends to be more intense in lower pHs [62], although higher pHs usually enhance silica rejection in pressure-driven membrane processes. Therefore, optimum operation pH depends on feed water characteristics and treatment particularities.

Sulfate reducing, anaerobic and gram-positive aerobic bacteria may be present in suspended solids on produced water [56]. Sand, silt and other formation minerals are also expected to be present [40]. As these solids can foul membranes and deposit on equipment and piping, their removal is important.

Another emerging hypersaline stream is the one produced in carbon dioxide storage and is addressed in the next section.

2.1.2 Formation water from CO_2 storage

Following the aforementioned usage of fossil fuels, the emission of greenhouse gases is also a subject of concern. A widespreading alternative to mitigate the effects of carbon dioxide in the atmosphere is by capturing and injecting it in a geological CO_2 storage (CGS) [63, 64]. This option may take place in different reservoirs, such as deplected oil and gas wells and saline formations [63, 64]. While the former generally have known geology and traps avoiding leakage [65], the latter possess the greatest capacity of depth storage [64], allowing the disposal of the equivalent CO_2 of decades. Potential geological reservoirs for carbon dioxide have been identified around the world [63, 64], including in Brazil [66, 67]. As the gas is injected in the supercritical phase, the reservoirs must be at least 800m deep to keep carbon dioxide in this state [64, 67]. A schematics of CGS is presented in Figure 2.1.

In CGS, there can be a pressure build up when carbon dioxide is injected in subsurface reservoirs, which need to be monitored and controlled, in order to avoid seismic activity and CO_2 leakage [29, 68]. One method to control the reservoir pressure is by extracting the formation water naturally present in the subsurface porous formations [68]. The rate of extraction depends on the characteristics of rock formation: the more porous it is, the easier is to equalize internal pressure and

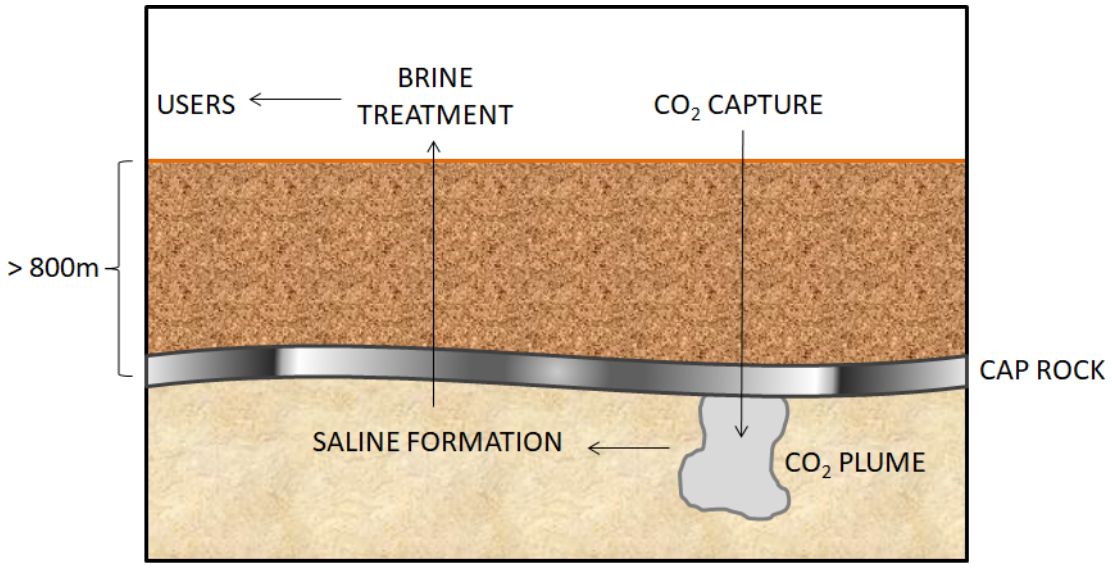

Figure 2.1: Carbon dioxide capture schematics. CO_2 in supercrytical stage is injected in a reservoir with a cap rock. To allow more carbon dioxide injection, the pressure is reliefed by extracting saline water from the reservoir.

the lower the volume of extracted formation water. In a case of low permeability rock, a 5Mt CO_2/yr storage unit was estimated to extract up to 540 m^3/h of brine [29].

While the lower salinity limit for formation water is usually considered to be 10 g/L [67], it can reach up to 200 g/L [69]. A few potential CGS formation water characteristics are presented in Table 2.2. Even though the three formation waters have similar sodium concentrations, their total dissolved solids (TDS) and concentrations of other ions, specially divalents ones, have high variability.

Table 2.2: Potential CGS formation waters.

Parameter	Oriskany [69]	Frio [70] [a]	Lower Tuscaloosa [71, 72]
Sodium (g/L)	48.7	43.6	43.7
Chloride (g/L)	122.9	73.4	92.2
Magnesium (mg/L)	1540	490	1035
Calcium (g/L)	25.1	2.4	11.8
Barium (mg/L)	847	62.9	9.55
Strontium (mg/L)	11800	116.7	696
Sulfate (mg/L)	-	44	238
Potassium (mg/L)	2720	109	412
pH	2.2	6.9	5.4
TDS (g/L)	221	109	149

[a] Concentrations calculated by given molalities assuming a solution at 25°C

Besides these naturally-occuring saline streams, saline industrial effluents such as landfill leachate [73, 74], coal-to-chemical wastewater [75] and textile effluents [76] could also be treated and reused, specially in regions where new plants are being demanded to have zero liquid discharge (ZLD) processes or very low saline content [34, 74–77]. Concerns regarding cost and environmental restrictions of reverse osmosis brine disposal [21, 31] also point to the increasing total water recovery.

2.1.3 Possible uses for saline water

The available uses, treatments and disposals for saline waters depend highly on site-specific characteristics, such as their raw quality, proximity to potential users and costs associated [52, 78]. Among the common possibilities, the main destinations to saline effluents are generally injection in oilfields, discharge (in deep wells or aquifers) or reuse [52, 78].

The first possibility generally evaluated is the reinjection in oil reservoirs to keep them pressurized, saving fresh water transport costs. However, this alternative is not always possible, as in gas fields. Besides, it usually demands hardness removal, oil removal and compatibility analysis between injection water and reservoir [78, 79]. Shell Company was reported to reinject more than a half of produced water of its fields [32].

Other disposal options are the discharge into the sea (for offshore facilities) or into deep wells, according to local regulations [27, 32, 42]. The majority of drilling fluids from onshore non-conventional fields in US is disposed in a special type of injection wells [80]. Though, the development of new facilities for saline effluents disposal can be challenging, due to high costs, time and ambient restrictions, besides potential geological obstacles [79] and eventual salinity limitations of injection water. It is important to highlight that salt contamination in shallow aquifers and long term well behavior are questions not solved yet, although this method is said as most economical choice for onshore brine disposal [31]. Brines contamined with specific compounds, such as NORMs, are being injected into deep wells in United States [31].

Site-specific uses, such as industrial reuse, irrigation, usage as livestock supply and even as potable water can be suitable options [52, 61]. Some of these possibilities, as well as their quality recommendations, are summarized in Table 2.3.

In irrigation case, besides the quality recommendations cited in Table 2.3, there can be particular ionic constraints [31], which may be crop-dependent. For example, chloride limits in plants root zone range from 350 to 2800 mg/L [33]. Additionally, to reach irrigation conditions, every substance toxic to plants and consumers shall be also removed from the saline stream.

Table 2.3: Recommended water compositions for various applications. The dash symbol (-) represents limits or recommendations not reported.

Parameter	Potable water	Irrigation [a]	Livestock	Surface discharge [b]	Cooling water make up [c]	Steam generation
TDS (mg/L)	1000	2000	5000	-	200	-[d]
Sodium (mg/L)	200	[e]	2000	-	-	0.01
Chloride (mg/L)	250	100-700	1500	-	60	-
Hardness (mg/L $CaCO_3$)	500	[e]	-	-	80	ND [f]
Ammonia (mg/L N)	1.5	-	-	<20	-	-
Sulfate (mg/L)	250	-	1000	-	60	-
TOG (mg/L)	-	-	-	<20	-	<0.2
References	[84]	[48, 85, 86]	[48, 85]	[44, 49]	Typical Petrobras limits	[87]

[a] There can be limits in roots zone [33].
[b] According to Brazilian law, discharge can not change the water body quality after mixture zone [44, 49].
[c] Considering 5 concentration cycles.
[d] Typical demineralized water conductivity: < 0.2 μS/cm.
[e] Limited through SAR (Sodium Absorption Ratio).
[f] ND: Non detectable.

An additional option is the industrial usage, which generally requires desalination steps in order to reach the required quality for cooling water reposition, steam generation or specific process application. In the Brazilian case, industrial and irrigational use are promising alternatives for reusing O&G produced water [81, 82]. There are also efforts to reuse produced water as drilling fluid in shale gas facilities [27, 83], combining the availability of PW with the expensive cost of fresh water transportation and short well life. Reuse of water as drilling fluid implies the stream not to have fouling salts or any substance harmful to the reservoir, pipes or equipments. Therefore, in most shale gas cases, for being short in duration, produced water is reused to drill next well (as hydraulic fracking).

Another potential use for saline streams is potable water, specially in water scarce areas [61]. In this case, several restrictions in treated water must be followed, as salinity, toxicity and aromatic compounds content [61, 84]. Generally, this solution has been investigated in locations with clear regulations for potable water generated via reuse, which is not the Brazilian case yet.

Hypersaline brines can also be used as feedstock in mineral production [52, 88] and often require desalination steps to concentrate the target compound before further purification. However, very few of the projects related to mineral recovery proved to be economically feasible [52].

The typical treatment and discharge unit cost for produced water can vary from 0.15 to 15 US$/m^3, depending on the oilfield and the water destination [32]. Although final water quality has a major influence in cost treatment [47], specific disposal costs can generate scenarios in which reusing is a cheaper approach.

In order to reach the target composition for reuse or discharge, desalination is normally a required step for reusing saline water, since the most users require a minimum of 5 g/L on total dissolved solids. The available technologies to desalinate brines are generally divided by their driving force: thermal technologies use heat to evaporate water while osmotic processes use hydraulic pressure to overcome the osmotic pressure. Both groups and their applications are discussed in the next section.

2.2 High salinity treatment technologies

2.2.1 Thermal processes

Thermal desalination processes are based on distillation principle: energy is given to the feed, evaporating part of the water. Due to robustness, high quality treated water and applicability to highly saline feeds, thermal technologies have been proposed and applied in O&G industry for produced water treatment [39, 89] and used widely in

the Middle East [31, 39], representing around 31% of world desalination capacity [52].

As these technologies use the phase change from liquid to vapor and the latent heat of condensation for water is high, they usually consume an expressive amount of energy. Recent designs make use of energy recycling by preheating feed with latent heat of condensation for vapor stream [90]. Still, to reach an energy efficiency similar to reverse osmosis in seawater desalination, they would have to apply a maximum terminal temperature difference of only 1°C [35]. However, to avoid excessive heat exchange area and cost, they work at lower efficiencies.

The main technologies in thermal desalination are multistage flash (MSF), multieffect distillation (MED) or evaporation (MEE) and vapor compression (VC) in seawater desalination [91] and also used for produced water treatment [39, 89]. They differ basically due to heat exchange method and particularities in equipment design [92]. These processes can also be combined, as MED-TVC, which is a hybrid of MED and thermal vapor compression (TVC) [91].

MSF and MED use several stages or effects in series to enhance recovery and reduce energy consumption [35]. In MSF, sequential vessels operate in different pressure levels, allowing flash to occur. Generally, there is no heat source in each stage, unless the first one, as can be seen in Figure 2.2 [89, 92]. Erosion and corrosion can occur in MSF equipment [39], mainly in flash chamber due to turbulence [90] and due to elevated temperatures, in the range of 90 – 110°C [91].

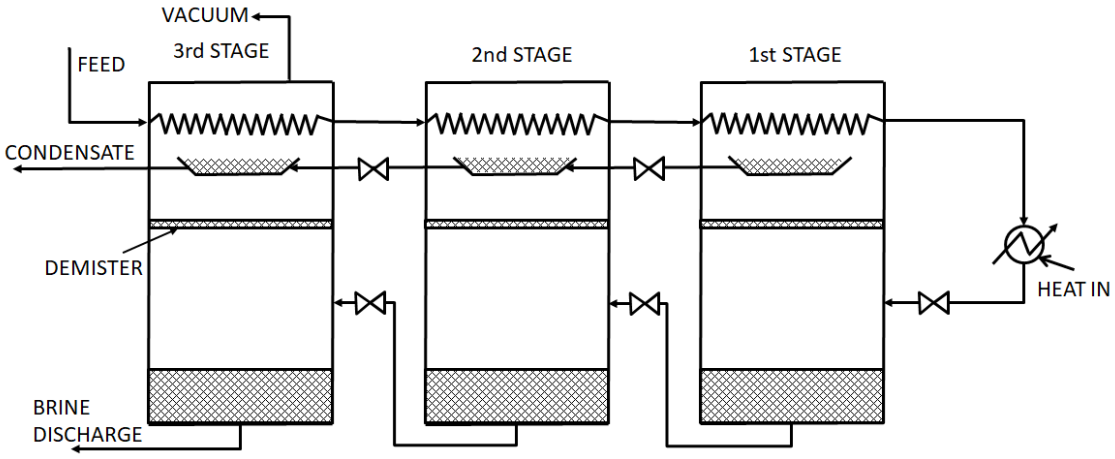

Figure 2.2: Multistage flash typical configuration with 3 stages. The feed is preheated with the vapor generated, which condenses and flows to a collector. There is a demister in each vessel to avoid brine drag to condensate and valves to promote the different flash pressures. The external heat source gives heat to the first stage.

Multistage flash technology typically recovers from 10 – 20 % water and has an energy consumption of 55-66 kWh/m^3 [91], considering seawater as feed. This technology is widely used in Middle East for seawater desalination [31], even with

membrane desalination advent. The main reasons for MSF being more popular than RO are based on water particularities (very high saline content) and thermal availability, since there are many cogeneration plants coupled to desalination units [31, 39].

In general, MED uses steam generated in a earlier stage as heat source for the next one. Additionally, mainly old MED designs spray the feedwater onto heat exchanger tubes [89, 92]. This option usually may reduce heat exchange due to scaling and deposits on tubes external surface. An example of configuration is shown in Figure 2.3.

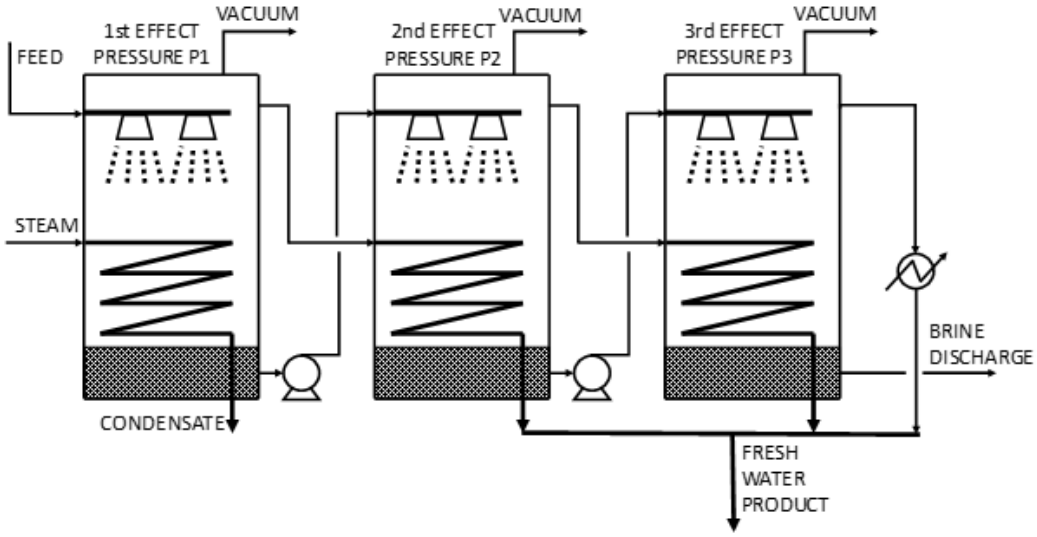

Figure 2.3: Multieffect distillation configuration with three stages. The feed of each vessel is sprayed over the tubes in which steam is condensing. The brine from a earlier stage is feeded to the next one, at a lower pressure level, while the vapor from the earlier stage condenses in the next one, providing heat to evaporate more water. The external heat source is steam, at the first stage, and heat is removed at the last stage to condensate the last vapor stream.

Typical thermal energetic demand for MED systems varies between 54 and 80 kWh/m^3 [90] while their water recovery ranges from 20 to 35%. Additionally, typical MED operating temperatures vary from 64 to 70°C [91].

Some data reported for desalination technologies include electrical equivalent energy consumption or specific mechanical work. This quantity is defined as the electrical amount which would be produced if the thermal energy was used by a turbine generator [93]. In case of many desalination plants combined with cogeneration, it makes sense to use this parameter, but depending on the steam source (turbine exit or "throttled" from boiler) and pressure, it can lead to distinct electrical equivalent consumptions.

As oilfield and CGS sites may not have steam turbines for power generation and sometimes neither steam, for better comparison purposes, data showed at this

document will focus on thermal energy itself. However, it is important to highlight that energy requirement values in electrical equivalent can be much lower than original thermal energy consumption. For example, for a MSF case [94], the electrical equivalent ranges from 4 to 25 kWheq/m^3, while the thermal energy requirement can be two times higher.

Conventional thermal processes usually are less pretreatment demanding (particularly oil and solid removal), in comparison with processes with membranes that have hydraulic pressure as a driving force. Besides, they have less influence caused by changes in feed salinity [27]. However, volatile compounds such as NH_3 and H_2S may impair distillate quality in thermal processes and energy consumption can reach 95% of its operational costs [27, 40], specially if there is no available heat source.

Among the thermal desalination technologies, mechanical vapor compression is particularly interesting due to the lower energy consumption when compared to MSF or MED. VC may be applied using two possible drivers: mechanical or thermal, originating the terms MVC and TVC [90]. These two systems differ from actuator mode: MVC uses a mechanical compressor while TVC often uses a steam jet [90, 91]. As MVC does not require any steam and has low energy consumption, it would be used in comparisons to membrane processes.

MVC is a thermal desalination process that uses the temperature increase of water vapor caused by compression, as well as its latent heat, as main heat source. This technology handles many internal heat exchangers to maximize energy recovery, as shown at Figure 2.4. The feed enters in a preheating step, and after this, the saline solution at the evaporator is cirulated over tubes, in which superheated vapor flows. Part of the water is vaporized and feeds the compressor, which overheats the generated vapor, providing energy to vaporize more water. Water condenses at tubes outlet and still pre-heats part of the feed. The concentrated saline solution is drained from main heat exchanger and also supplies energy to part of the feed in another exchanger.

MVC technologies are usually of falling film type, with vertical or horizontal tubes. This process consist of a film around tubes to enhance evaporation and reduce scaling, since the liquid film constantly generates movement and deplete depositions [91].

The main advantages of MVC are its modularization, operational simplicity and low energy input. The latter occurs mainly due to internal energy integration and temperature steadiness during heat exchange (latent heat) [91]. The major energy consumption in MVC is the compressor, that often requires high voltage electrical network [95]. Combined with the pumping eletrical requirement, the specific energy consumption reaches 11 kWh/m^3 for 40% of water recovery in seawater desalination [95]. Its operating temperature is generally around 60°C [96].

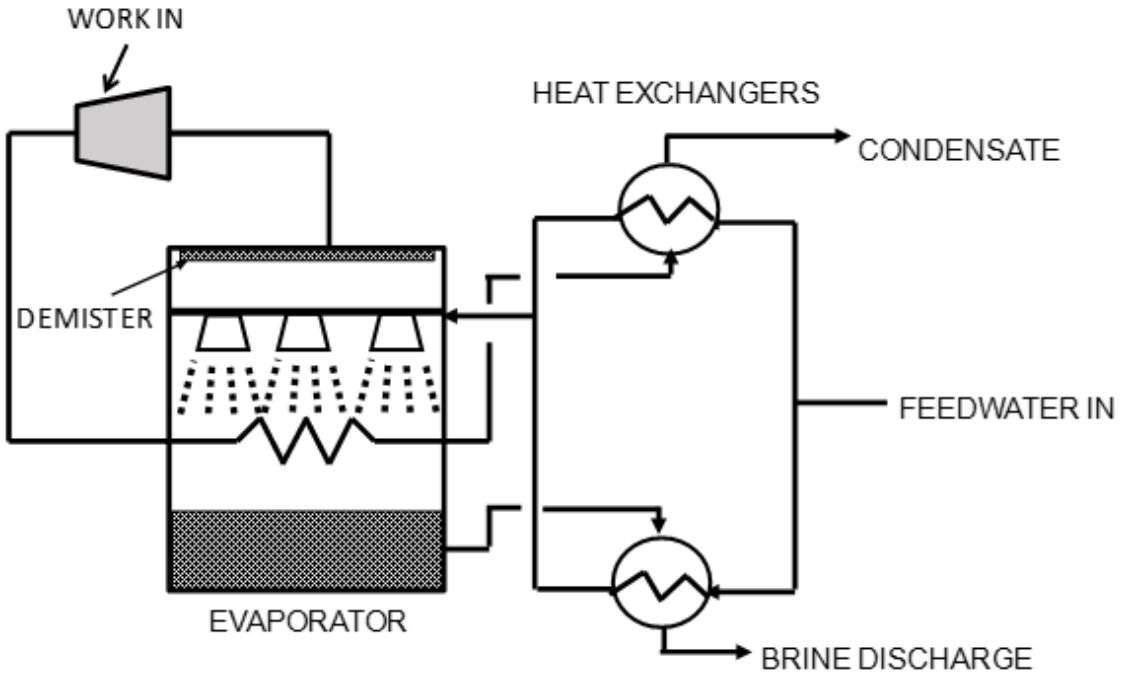

Figure 2.4: Mechanical vapor compression operation. The feed is preheated in condensate and brine heat exchangers and is sprayed over tubes, in which superheated steam flows. The vapor generated in the vessel is compressed, heating the feed and generating the condensate.

The downsides for MVC, as well as for other thermal processes, rely on the necessity of a postreatment when volatile compounds are present on feed and the relative high energy consumption when compared to RO in seawater desalination [31]. In one produced water reuse case for irrigation, the treated stream was found to be still toxic to algae *P. subcapitata*, although no acute toxicity occurred in others organisms tested (lettuce, worms and fish species) [82]. In this case, toxicity was attributed to ammoniacal nitrogen present even after MVC treatment. Besides ammonia, in some tests, treated effluent also contained benzene and toluene in concentrations above Brazilian limits [44, 48]. There was also identified a salting out effect of volatile organic matter for the studied produced water, at a total dissolved solids of 30 g/L [82], supported by other studies using sodium chloride [97, 98]. As NaCl correspond to the major salt concentration in hypersaline streams, the contamination with volatile organics can happen in using produced water as a feed, demanding posterior treatment.

As a mature technology, MVC is broadly employed in seawater desalination [61] and also to treat produced water in heavy oil fields in Germany, Netherlands [96] and Canada [99]. The Canadian case aims to generate steam for steam assisted gravity drainage (SAGD) activities from produced water, making thermal process specially interesting due to the high purity of the treated water.

The typical pretreatment for saline feeds in MVC processes employs suspended

solids removal, pH adjustment, antiscalant dosing and oil removal when applicable [61, 99]. Additionally, chemicals can be dosed in order to avoid precipitation on exchanger tubes [91, 96]. A particular MVC cathegory called seeded MVC claims to need less pretreatment, but specific seed minerals are needed in order to perform the system correctly.

The membrane distillation (MD) process contains both thermal driving force and a porous hydrophobic membrane to allow transport in the vapor phase [100]. As it involves phase change, this process tends to use more energy than conventional membrane processes like RO. Commercial membranes applicable to MD are made of polypropylene, polytetrafluorethene and polyvinylidene fluoride [101].

MD processes can be classificated depending on module permeate side [102], as presented in Figure 2.5. When the cold fluid gets in contact to membrane, it is classified as direct contact membrane distillation. On the other hand, when there is an air gap between membrane and cold plate surface, the process is defined as air gap membrane distillation (AGMD). Finally, when the low vapor pressure is generated by a vacuum pump, it is defined as vacuum membrane distillation.

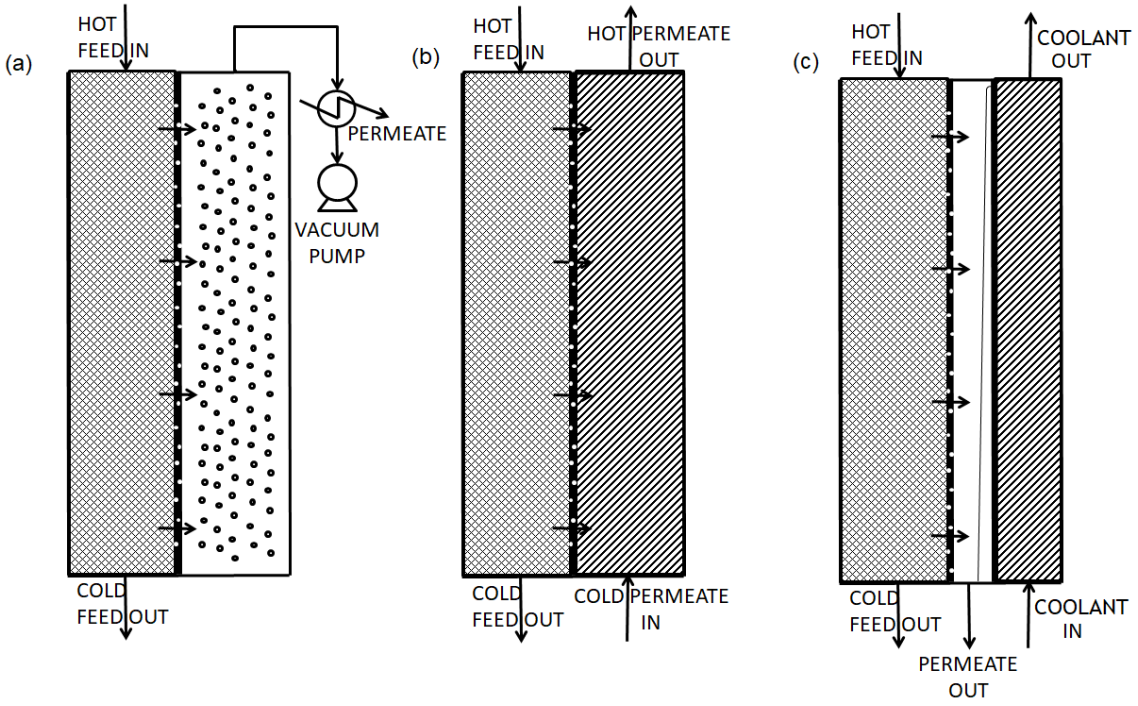

Figure 2.5: Common membrane distillation types. The feed is heated, causing only vapor to flow accross a hydrophobic membrane. The vapor can be either be cooled in vacuum mode (a), directly condensed in a cooler solutions in direct contact mode (b), onto a cool surface in air gap (c).

AGMD has advantages over other MD variations, mainly due lower heat loss since the air gap is an insulating layer [102]. Thus, the heat utilization for evaporating is improved. When compared to conventional thermal technologies (MSF and MED),

MD outperforms due to its lower operating temperatures and footprint [35, 102].

One promising advantage of MD, as a thermal desalination technology is the tendency of low flux variation due to the increase of salinity [101]. For instance, when the feedwater NaCl concentration was increased from 35 g/L to 75 g/L, the water flux only decreased 5%. However, when the concentration reached 350 g/L, the flux decay was almost 50%, likely because of the steep decrease of water activity [101].

A summary of studies using MD in produced and formation water desalination is presented in Table 2.4. The use of pretreatment is important when dealing with contamined streams, as produced water. While a study of a pre-treated produced water of 248 g/L TDS shown the water flux was constant over time and sodium chloride rejection was higher than 99% [103], a low salinity (15.7 g/L TDS) produced water without pretreatment caused water flux decline, pore wetting and rejection loss [104]. In this case, cleaning cycles were needed and oil traces were found in the permeate water, reinforcing the need of pretreatment when using a membrane.

As other thermal processes, MD is susceptible to contamination by volatile organics [103, 105], specially in elevated temperatures for produced water. Another concern when treating effluents that may contains organics is the pore wetting [104, 106], which leads the rejection to decrease. It happens due to poor pressure control and/or presence of surfactants in the feedwater [104]. Moreover, when oil and grease are present in the stream, the liquid entry pressure was found to severely reduce probably due to coating of oil internally to the pores [106]. Besides oil and grease, polyvalent ions as barium and calcium also contribute to wetting [106].

Recently, MD is being studied in combination to other processes, as forward osmosis (FO) [107]. Another possibility is the integration of MD as a complimentary step for MVC, substituting the brine heat exchanger by membrane distillation module [108]. This solution increases the total recovery and decreases cost, even comparing MD to the brine heat exchanger. However, it is advantageous for salinities near seawater, with lower gains with increasing salinity.

There are also other thermal processes, as humidification-dehumidification (HDH) [3, 35]. This process allows water to evaporate from a feed source to an air stream, which is cooled below dew point and water condenses. Besides the high energetic demand [3], expected heat transfer area is high, since air has a lower heat transfer capacity than steam, used in MED or MVC. Additionally, any air impurities can contaminate the treated water stream [35].

Additionally to performance characteristics, such as water flux and temperature levels, it is interesting to compare alternatives in terms of cost and energy consumption. A summary of thermal desalination technologies applied to hypersaline streams is presented in Table 2.5.

Table 2.4: Summary of MD processes applied to produced water treatment.

Salinity (g/L)	Feed Temperature (°C)	Coolant temperature (°C)	Flux (kg/m^{2}s)	Pretreatment	Reference
3	95 - 125	30	70 - 180	(synthetic PW)	[105]
187	40 - 80	5 - 25	3.6 - 12.0	Microfiltration	[102]
248	50 - 70	25	0.2 - 14	Microfiltration and activated carbon	[103]
15.7	64 - 84	-	10 - 50	None	[104]
150	60	20	5 - 33	None	[106]
92 - 308	< 100	30	10 - 39	None	[111]

Table 2.5: Reported applications of thermal processes in saline streams treatment.

Technology	Salinity (g/L)	Recovery (%)	Energy consumption (kWh/m^3)	Cost (US$/m^3)	Reference
MED-MVC	70	76.7	29	6.80	[112]
MVC	170	42.3	19	-	[3]
HDH	170	42.3	370	-	[3]
MD	170	42.3	510	-	[3]
MD[1]	40	80.0	-	0.59	[109]
MD	40	80.0	-	4.47	[109]
MD1	100	66.6	591	1.11 [2]	[110]
MD	100	66.6	591	8.55 [3]	[110]

[1]Membrane distillation without external thermal energy input.
[2]Converted from 0.74 US$/m$^3_{feed}$ [110]
[3]Converted from 5.70 US$/m$^3_{feed}$ [110]

While thermal process may benefit from formation and produced water high temperatures [52], they still need an expressive energy input to promote the separation. In this aspect, cost drastically rises in membrane distillation applications when there is no available heat source in the analysis [109, 110]. Despite having internal heat recovery design, the cost of MD treated water is an order of magnitude greater than the other reported thermal processes.

Though conventionally less used in high salinity applications due to the pressure limit [113], reverse osmosis based process are developing to expand salinity limits while maintaing the RO advantages as low energy consumption. These process are presented in the sext section.

2.2.2 Osmotic processes

An important category of treatment technologies for hypersaline brines is based on the osmotic process. It can be defined as the flux of water from a small ionic strength solution to a more concentrated stream when they are separated by a semipermeable membrane [100]. The pressure exerted on the hypertonic solution to cease flux is denominated osmotic pressure π. In order to obtain a purified stream, it is possible to apply an hydraulic pressure higher than the osmotic pressure, reversing flux direction. This process is defined as reverse osmosis (RO). These concepts are represented in Figure 2.6.

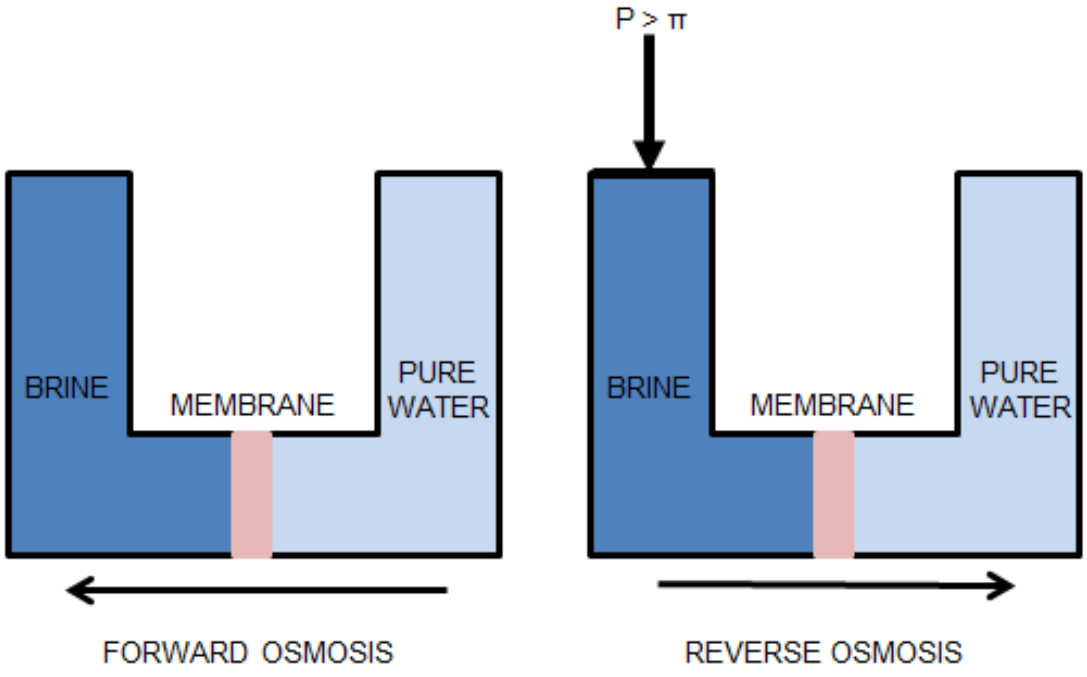

Figure 2.6: Forward and reverse osmosis operation principle.

Forward osmosis

The water flux in forward osmosis happens due to use of a more concentrated stream, designated draw solution or osmotic agent, and has two exit streams: a concentrated feed and the diluted, but still highly saline, draw solution. Although the standalone forward osmosis process does not desalinate, but generates a permeate dilute solution, it has been employed in osmotic dilution for shale gas produced water treatment [27]. In this situation, as the treated water is used in new drillings, only scaling agents (mostly divalent ions) are required to be removed.

If a lower salinity is required by the final user, the diluted draw solution can be desalinated in further processes, such as MD [60, 95, 107, 114, 115], MVC [116] or even RO [3, 117, 118] in combined processes. FO acts as advanced pretreatment for the conventional desalination processes, since it prevents potential fouling (organics, solids, oils, insoluble salts) to the following processes [27, 107]. Additionally, as forward osmosis does not apply hydraulic pressure, it has less irreversible fouling tendency and may have easier or even absent pretreatment before it [80, 117]. Although extensively applied FO to oily effluents as produced water [27, 119, 120], oil and organic matter presence has found to be harmful to the membrane and reduce water flux [80, 120–123].

The main properties of osmotic membranes that define their performance are the water (A) and salt (B) permeabilities and the support structural parameter S [124]. While the first two properties are related to the selective layer of assymetric membranes, the structural parameter is a measurement of the mass transport resistance of the structural support, lumping important characteristics such as thickness, tortuosity or porosity [124]. When high, S deplects the osmotic pressure difference, which is the driving force for FO, and makes the process lose efficiency [124].

Different configurations can be used in forward osmosis equipment: when the draw solution faces the membrane selective layer, the configuration is called pressure-retarded osmosis (PRO) mode. However, when the feed faces the selective layer, the process is defined as FO itself. The former configuration typically leads to higher fluxes when only salt content is considered [124]. When treating streams with high TDS or organic matter concentration, FO mode is preferred, since fouling is minimized as solids or oil do not contact to porous support [123].

When the draw solution is applied and recovered by a desalination step, there are concerns regarding salt reposition and contaminants accumulation in this stream [83]. Besides, any processes in which FO draw solution is effectively recovered consume more energy than a standalone feedwater desalination, due to the higher ionic content [3, 35].

Although the main process variables and research interest are related to the

draw solution characteristics [125–129], flowrate, module design and temperature have also been investigated to increase water flux [80, 117]. Polymeric membrane materials are generally sensitive to temperature and its increase tends to rise osmotic pressure, mass transfer coefficient and both water and salt permeabilities [117, 124].

Current state-of-art research in FO focus in development of easily recovery draw solutions as magnetic nanoparticles, thermoresponsive polymers and polyelectrolytes [129, 130]. Another fundamental branch is the study and development of membranes with lower structural parameter S and good fouling resistance [123, 124, 131, 132].

In the aspect of decreasing S, it is possible to enhance the hydrophilicity by treating the support [131], incorporing nanoparticles in the membrane [132] or other adding hydrophilic materials to the support fabrication, as polyacrylic acid [133]. The later alternative was found to decrease four times the structural parameter from a polysulfone-based support. Additionally to hydrophilicity increase, electrospun PVA nanofibers were reported to also increase support porosity and decrease tortuosity [134].

Reverse osmosis

Reverse osmosis is a process in which water flows through a semipermeable membrane due an applied hydraulic pressure greater than the osmotic pressure [100], as presented in Figure 2.6. It is widely used due to its low energy consumption, specially in seawater desalination [3, 31, 35, 52, 100, 113].

The factors that minimized the energy requirements in the last years of research include development of high efficiency energy recovery methods, as pressure exchanger (PX) [31, 91]. In this device, presented in Figure 2.7, the power is directly transferred to part of the RO feed, without converting it to mechanical energy [31]. The low pressure stream is pressurized inside the rotor due to direct contact with the high pressure concentrate, similarly to a piston pump. As the energy recovery is very high, the feed stream only pass by a booster pump before entering the RO module. However, the contact between streams usually results in a small mixing [31].

Whereas thermal process are generally employed for concentrating solutions up to 250 g/L in ZLD processes, the salinity for the concentrated stream in conventional RO lies at maximum 80 g/L, due to the hydraulic pressure contraints [34, 77].

Although RO has been applied for produced water treatment [40, 81, 86], the maximum salinities are still low when compared to hypersaline brines described earlier. While the maximum commercial hydraulic pressure for RO is set up to 80 bar [113], there are reports on specific applications up to 200 bar and feed salinities of 80 g/L [73, 135, 136]. Besides the use of spiral wound membranes in RO and some HPRO early applications [31, 113, 135], a plate and frame configuration for

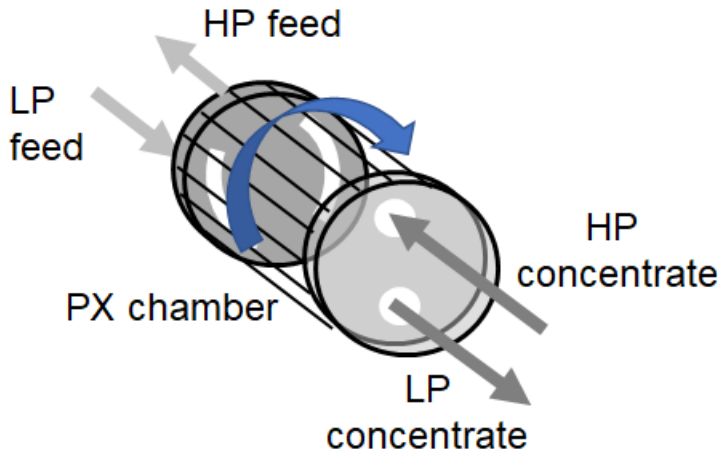

Figure 2.7: Working principle of pressure exchanger. The low-pressure (LP) feed enter a piston chamber, in which the high-pressure (HP) concentrate transfer hydraulic energy to it.

HPRO was reported by Gunther (1996) [136].

Recently, membrane manufacturers reported to have design spiral wound modules to support up to 120 bar [137]. As HPRO is theoretically able to reach very low energy consumption when treating hypersaline streams [3, 34], it has been object of study specially for membranes and modules mechanically resistent and also in the fundamental membrane transport under high pressure and salinity [34, 138]. McGovern *et al.* [138] verified the water permeability decreased more than 50% while the rejection was constant at more than 99 % for a conventional thin film composite (TFC) RO membrane up to 172 bar.

Due to extremely high pressure and saline content, one concern when using HPRO is the need of an efficient pretreatment. For instance, in a leachate treatment, a nanofiltration step is applied to the concentrated stream before entering HPRO module [73]. Additionally, the reported feed velocity in this module is about 1.5 m/s, ten times higher than the conventional RO feed velocity [73], to increase mass transfer and avoid scaling.

Recent researches in RO have been focusing in different configurations, such as batch-mode or closed-circuit (CCRO) [139, 140]. In batch mode, the feed enters in the system only at the beginning and the concentrated stream is recirculated over time. At the end, the brine leaves the system [140]. In CCRO, or semi-batch mode, the RO concentrate is totally recirculated and mixed with the continuous feed, while pressure gradually increases, until the target recovery is reached. There is no brine discharge during the cycle. Batch and CCRO is reported to increase conventional RO recovery and decrease energy consumption [140].

Another RO variation is osmotically assisted reverse osmosis, also known as coun-

terflow reverse osmosis [1], osmotically enhanced dewatering (OED) [141] or draw solution assisted reverse osmosis (DSARO)[36]. In this process, a saline stream defined as draw or sweep solution is applied to decrease the osmotic pressure difference accross the membrane [4, 36]. Differently from FO, the sweep solution has lower concentration than the feed. The diluted sweep stream can be fed to a RO process or another OARO stage, in order to meet the pressure and salinity before a final reverse osmosis [4, 142]. This process is very promising, since it can expand the feed salinity and water recovery limits for conventional RO while keeping favorable energy consumption [4, 36, 141, 142].

While the first designs of OARO employed the sweep solution in closed loops [4, 36], new approaches as split-feed CFRO/OARO and cascading osmotically mediated RO (COMRO) [2] eliminated this need by using part of the feed or concentrate as sweep solution. Examples of these configurations are presented in Figures 2.8 and 2.9. The optimal concentration of each stage, as well as the number of stages and the split of the feeds (to use them as sweep solution) are process variables that would influence the energy consumption and operating pressure.

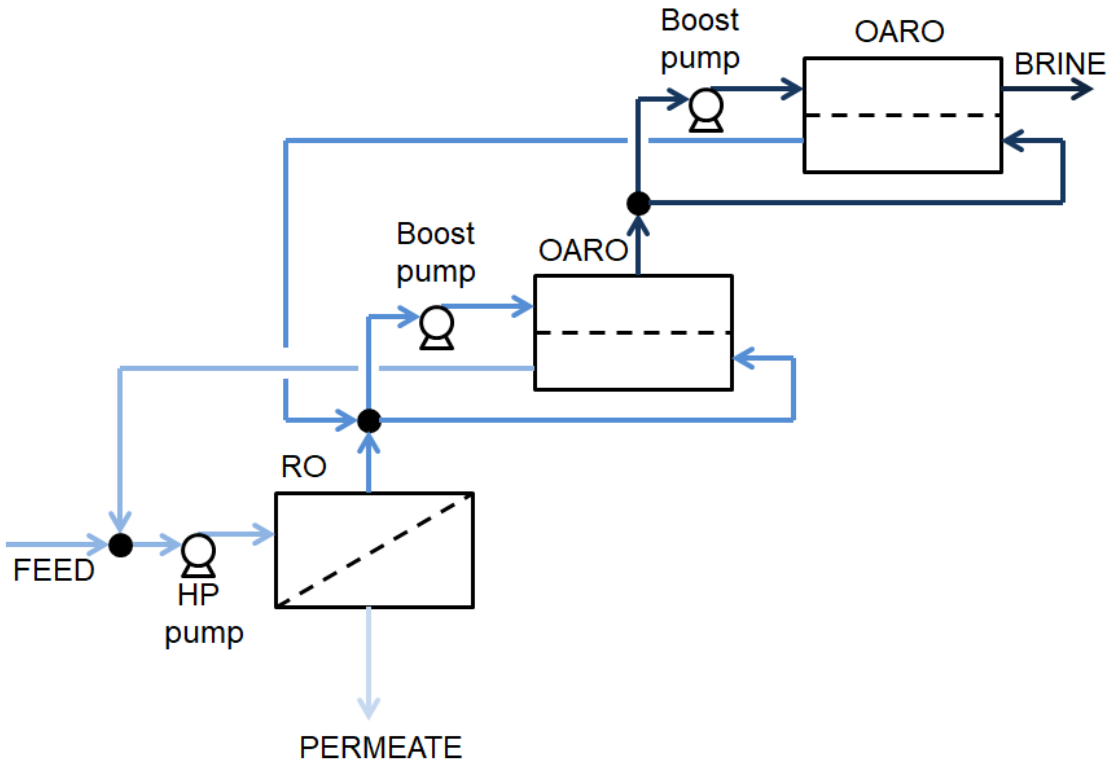

Figure 2.8: Example of split feed OARO configuration based on [1]. The color intensity corresponds to higher salt concentrations. The highest salinity stage uses part of its own feed stream as sweep solution, which is diluted along the other stages. The final stage is a conventional RO module.

The main advantages of not using loop streams consist on avoiding contaminants

accumulation and even on benefiting from a low-rejection membrane [1]. These technologies also claim to need lower operating pressure by using feed stream as sweep. COMRO is said to decrease the operating pressure not only for brine desalination but also for seawater applications [2]. As high pressure may decrease water permeability by membrane compaction [138] and might require special module designs, it may be more cost-effective to search for combined RO-based processes at lower pressure levels.

The optimal concentration of each stage, as well as the number of stages and the split of the feeds (to use them as sweep solution) are process variables that would influence the energy consumption and operating pressure.

The use of sweep solutions and counterflow modules give a wider range of application for RO, promising low energy consumption when compared to thermal technologies. A comparison among these processes is presented in Table 2.6.

Although promising, these technologies may demand special design due to high pressure and/or counterflow module and might not be as economically interesting as expected. Thus, it is important to estimate their cost, even if in a preliminary basis, to understand if and where they can be improved, and what are the major cost components. Secondly, it is important to test the processes experimentally to check if the membranes would behave as expected, since their performance is still highly dependent on the membrane properties, such as water permeability, salt permeability and structural parameter. In high salinity application, by treating more concentrated brines or by increasing recovery from seawater desalination, it even more important to verify experimentally if the membrane would perform as expected.

Membranes characteristics

The commercial membranes for FO and RO are basically from two categories: TFC, with polyamide selective layer (PA), and CA/CTA (cellulose acetate and/or cellulose triacetate) [143], although their exact composition is generally not reported by manufacturers.

The first type of membrane is made of an aromatic and/or semi-aromatic polyamide by interfacial polymerization and possess a high degree of crosslinking [12, 15]. These membranes have a porous support, generally made of polysulfone, in which the polyamide selective layer is held. TFC membranes normally have a non-woven fabric for RO applications [15]. Due to the low thickness (100 nm [144]), these membranes have high water permeability [15]. Their salt rejection is very high, which consolidated their usage for commercial seawater applications [31]. The crosslinking feature is what gives the membrane the robustness and strength not to burst in high pressure operation [15].

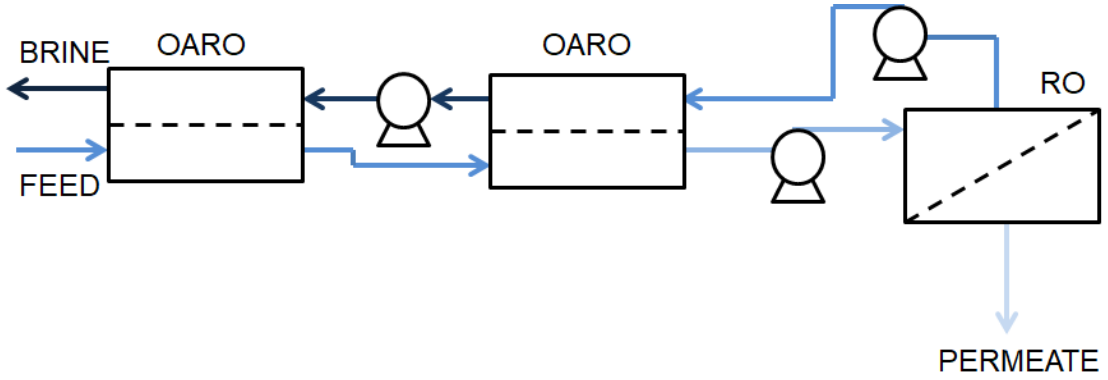

Figure 2.9: Example of cascading osmotically mediated reverse osmosis configuration based on [2]. The color intensity corresponds to higher salt concentrations. The feed streams enters as a sweep solution for the first stage, being diluted until conventional RO desalination at the last stage. The concentrate stream returns to the earlier stages as feed.

Table 2.6: Comparison among RO-based processes applications.

Technology	Salinity (g/L)	Recovery (%)	Energy consumption (kWh/m^3)	Maximum pressure (bar)	Reference
DSARO	35	40	1.7 - 2.5	36 - 52	[36, 148]
OARO	100 - 140	35 - 50	6 - 19	65	[4]
COMRO	70	50	3.2 - 3.8	68.3	[2]
CFRO	35	81	3.9	68	[1]
HPRO	70	50	7.5	150	[34]
HPRO	70	72	13	300	[34]

The polyamide used in RO possess inherent ionizable groups (carboxyl and amino groups) [145] due to incomplete polymerization [146]. The membranes tend to have slightly negative zeta potential in the common pH range [31, 147]. The PA polar groups enhance rejection because of local dipole formation [31]. However, PA membranes are generally more prone to fouling, what was associated to its elevated roughness and hydrogen bonding with foulants [119, 121]. Besides, PA has more carboxyl groups, which have stronger adhesion forces than hydroxyl groups from CA/CTA membranes [119, 121].

The second category includes single or combination of cellulose-esters. The membranes are generally assymetric and made by phase-inversion [143, 149]. Some of the membranes may have an internal woven support to give mechanical strength to the membrane [124]. They are usually thicker than PA. These materials were the first to be used in reverse osmosis [150], but were surpassed by PA in RO due to its higher water permeability. However, with the application of forward osmosis to streams with high salinity and/or organic matter and the need to combine antifouling properties to low structural parameter, this material have gained attention lately [145].

For the application in high salinity, there are evidences the membranes may change transport and morphological characteristics [12, 37, 149, 151–154]. In case of transport properties, it is not well known if the changes are happening in the membrane or due to concentration polarization or both, since the determination of these parameters can be quite complex using saline streams. There are reports that associate the decrease of performance only with concentration polarization (CP) [126, 155], while others postulate the membrane can be dehydrating/deswelling [145, 152, 153] and even an increase of water permeability at higher salinity was reported [156].

Specifically in the case of deswelling, it is worth to mention this effect was detected for nanofiltration PA (lower degree of crosslinking) and associated with the flux decrease [12, 15]. Additionally, an interesting analysis performed by Drazevic *et al.* [15] gathered data on RO membranes volumetric water content and water and salt permeability. They obtained an empirical correlation in which higher water volumetric fraction corresponds to higher permeabilities.

Another important field of study is the standardization of membrane transport characteristics measurements, which may be affected by the employed driving force and testing conditions [157, 158]. Although FO is proposed for high salinity applications [27, 116], the majority of the membrane and draw solution performance testing uses deionized water or seawater as feed [125–129]. A major difficulty in this investigation is the complex mass transport involved, since there is salt polarization on both sides of the membrane, what makes the correct quantification of permeabilities

more challenging [124, 158].

Although not commercially available yet, novel materials are being studied to enhance membrane properties, such as zeolites, nanomaterials and graphene [143, 144, 159–162]. Besides, hollow-fiber membranes are being applied for FO and assisted processes [8, 10, 123, 155] and may be promising options, since these typically do not need external support such asin spiral wound or in plate and frame and have expressive packing density [100]. [checar uma das referencias]

In high salinity applications, the current research also focus on developing mechanically resistent membranes and the fundamental transport phenomena under high pressure and salinity [34, 138].

Process cost

Cost is a major issue in desalination, particularly because the separation for salt and water is much more energy-intensive than conventional tapwater treatments. Therefore, energy is a major component for operational cost of thermal and membrane desalination technologies, representing more than 30% of treated water cost [35, 118]. Additionally, equipment also account for a considerable share of RO fixed costs, as reverse osmosis systems need high pressure vessels, pumps and piping [163]. Pretreatment and membrane reposition expenses may also be significative depending on the feed water quality [31].

Although there can be site-specific peculiarities, earlier studies for seawater RO have shown there is a cost minimum for a water recovery around 50%, which equilibrates the increasing costs of the membrane treatment caused by the increasing concentrate salinity and lower flux to the decreasing expenses of side operations, as pumping and pretreatment[35]. Knowing major components of cost also subsidizes research and development of more efficient equipment, as pressure exchanger and higher permeability membranes [31, 35].

For emerging technologies, it is even more important to understand the key cost drivers and their relation to process variables and parameters. One of the greatest influences and determinant on forward osmosis economic feasibility, for example, is membrane cost [118, 164]. On the other hand, MD cost is completely influenced by energy expenses: it may reach an 8-fold increase when there is no available low-grade energy [109, 110].

Sensitivity analysis is also helpful to analyze the extent and the cost response to process parameters. Linares *et al.* [118] reported that FO water fluxes lower than 10 L/m^2h determined the module cost as the biggest expenses share, while its influence decrease for higher fluxes. Tavakkoli *et al.* [110] determined for a MD study case that the influence of feed salinity on final water cost was small. In case of RO-based processes, there are very few studies reporting cost and sensitivity analysis [36, 142].

A novel tool to investigate cost feasibility regions for technologies is retro-techno-economic analysis (RTEA), which was reported for biorefineries [165]. It consists on determining isoeconomic regions formed by combination of process parameters (such as conversion, selectivity or selling price) to study its feasibility ranges and thresholds [165]. While RTEA was reported for a process in which the economic metric is the null present value, it is reasonable for desalination processes to use this methodology using the specific treated water cost. Instead of analyzing profit, it is possible to compare the cost to the conventional technologies and evaluate the range of applicability or improvement the new RO-based technologies have. A techno-economic assessment will be described in the next chapter.

Chapter 3

Cost assessment of osmotic processes

This chapter is focused in fulfilling the objectives of the study and optimization of osmotic and osmotically assisted processes and the analysis of the most cost-effective desalination routes for brine treatment.

Even with environmental and regulations issues, water reuse has to be based on a cost analysis considering the available technologies, plant information, utilities data, among other inputs. This is the main reason which encouraged a preliminary case study to analyze a high salinity desalination. As a tool for analysis and orientation for next steps, some technologies were simulated with cost comparison. Conventional and novel technologies were investigated through optimization focusing in process variables and membrane characteristics. In spite of some approaches that tried to compare technologies for desalination of produced water, most of them compared isolated costs or characteristics. Thiel *et al.* [3] simulated different technologies for energy consumption comparison in produced water desalination. However, some particular design issues, as low-grade heat availability, or high operation pressure, can lead to different judgment and choice. Herein, the chosen variable which will contain the design information and the impact of other variables is the specific cost, which can be defined as cost per cubic meter of recovered water.

At this moment, detailed treated water quality was not addressed, since it depends on the water further usage. Nevertheless, a simplified comparison was carried out based on literature data and simulation and optimization techniques.

The following study was published in *Desalination* journal, v. 430, pp. 107-119 in 2018 [166].

3.1 Introduction

Great amounts of produced water are generated in O&G exploration, handling and processing. These quantities can be more expressive than oil production itself, mainly in mature fields, reaching values higher than 90% of the outlet stream [81]. Generally, water can also be required the most in the later years of an oilfield, mainly for secondary and tertiary recoveries. An aggravating circumstance for water management in O&G facilities is the development of unconventional sources (as shale gas and oil and tarsands), which can be even more water-intense than conventional ones, not just during the production but mainly during drilling and fracking [27].

As effluent discharge or water intake constraints can limit industrial capacity of O&G operations in water-stressed zones or under stricter environmental regulations, produced water reuse by desalination may be an economic option. Brazillian Northeast semi-arid region, where there is most of onshore oil production in the country, have been experiencing extreme droughts over the past years [26]. This condition led to water restriction to cities, crops, energy generation and industrial activity [26]. At the same time, onshore oil exploration in this region is both a water consumer and an expressive effluent generator, since the oilfields are predominantly mature.

Produced water, as the main effluent of oil exploration, is a water source which can be valuable for oil production as well as local uses. Treatment and discharge unit cost for produced water can vary from 0.15 US$/m^3 to 15 US$/m^3 [32], depending on the oilfield and water destination. Although final water quality has an influence in treatment cost, specific disposal costs can describe a scenario in which reusing is a cheaper approach. On the other hand, stricter disposal restrictions and water supply limitations can also restate produced water reuse as an attractive, or even mandatory scenario [167].

Several papers have been addressing produced water reuse for potable [61], irrigational [59] and fracking purposes [27]. Treatment often includes oil and organics removal, and sometimes, desalination [40, 61, 81]. For the latter step, recent approaches have been focusing on forward osmosis, that can be coupled with thermal recovery [27, 80, 116, 117], and membrane distillation [102, 103, 109, 110], mainly when there is low-grade heat available.

At the same time, new technologies modifications for seawater and saline effluents are being investigated. Membrane distillation to enhance recovery in mechanical vapor compression was proposed for seawater desalination [108] and could lead to savings also in produced water treatment. Another promising modification is the use of RO assisted with sweep solution. It was proposed as an alternative to minimize vessels working pressure for seawater [36] and minimizing energy consumption

compared to thermal processes [4, 30].

Regarding to energy consumption, which is a major concern in high salinity applications, Thiel *et al.* [3] evaluated electrical and thermal energy inputs for several technologies, showing significant comparison results. The needed theoretical energy for RO is much lower than other thermal and membrane processes, from conventional to new ones, even for high salt content. As these processes vary in material and design, it is mandatory to compare them not just in energy terms, but also in economic assessments. Although energy consumption [3, 116] and sparse desalination cost [32, 109, 110] have been discussed for produced water, there is a lack of cost comparative analysis for produced water routes. This is a mandatory issue, since pressure ratings or the absence of available heat, for example, can culminate in prohibitive costs.

Thus, the main objective of this chapter is to address an analysis on process variables and costs for desalination processes applicable to a specific case study of a Brazilian produced water, aiming to choose most suitable routes and to investigate new technologies limitations by a retro-techno-economic-analysis [165].

The available technologies for desalination are discussed, as well as Brazilian produced water characteristcs and its most suitable reuse options, which can affect process design choice. In the next topic, proposed desalination routes and its main variables are presented and justified. Further information on modeling of each step can be found in Appendix A. After introducing the optimization strategy and the concept of retro-techno-economic-analysis, the results on cost and energy are examined and guidelines are discussed.

3.2 Modelling Framework

In produced water treatment, many technologies have been proposed for removal of oil and grease [40, 168, 169]. In case of desalination processes, suitable technologies are similar to those applied to seawater treatment, as multistage flash, multieffect distillation or evaporation, mechanical vapor compression, reverse osmosis and recently, membrane distillation [39, 59, 102].

As stated by Ettouney *et al.* [91], MSF and MED generally have high capital cost. Additionally, they are potentially more expensive in terms of energy cost than RO and MVC and are usually coupled with cogeneration plants [39, 170], that is not commonly the case of produced fluids treatment. It is worth to highlight that thermal or hybrid technologies are usually more suitable when there is a heat source availability and could be good options for specific cases, as membrane distillation for oilfields which use SAGD [109]. However, as the present case study does not have available low-grade energy, only MVC and RO were chosen to represent conventional

technologies in this study, since both processes need an electrical energy source only. Another point of interest was to analyze whether RO would still be the cheapest option even with a maximum pressure constraint, in accordance with Thiel *et al.* [3].

For route design, this study considered an onshore produced water with salinity of 90 g/L and oil and grease of 100 ppm [169]. Even though this effluent was assumed to be a sodium chloride solution, it is important to stress that there can be also organic matter and scaling salts in produced water, as shown in Table 3.1. As the main objective is to evaluate differences in routes cost caused mainly by colligative properties and separation principles (as hydraulic pressure or temperature), other contaminants/parameters were not modeled. However, in real operation, these contaminants may negatively affect system performance or even require specific treatment [3, 59, 91, 96].

Table 3.1: Physical and chemical parameters for Brazilian produced waters.

Parameter	Value	Reference
Sodium (g/L)	18.9 - 36.8	[88, 171, 172]
Chloride (g/L)	22.5 - 58.9	[88, 171–173]
Calcium (mg/L)	769 - 2500	[88, 173]
Magnesium (mg/L)	678 - 730	[88, 171]
pH	6.3 - 7.3	[88, 173]
TOC (mg C/L)	113 - 386	[172, 173]
TDS (g/L)	77.8 - 98.8	[172, 173]

Not only feed water quality, but also product water quality can influence suitability on certain desalination routes. Aiming to investigate the more common destinations in an onshore oilfield, this study considered three main options of reuse: irrigation, livestock and industrial water. Despite the fact that each one has several constraints, as toxicity, scaling potential and others, this work only considered total dissolved solids, assumed to be equal to salinity, and total oil and grease limits.

For the three studied reuse options, oil and grease concentration should be zero. Water for irrigation and livestock were limited at 2000 mg/L and 5000 mg/L of TDS, respectively [48, 85, 86]. Industrial water was assumed to have TDS of 200 mg/L, according to oil companies corporate data on main water users.

3.2.1 Proposed Technologies and Economic Assessment

To achieve the desirable compositions, combinations of technologies were analyzed. In some alternatives, microfiltration (MF) was applied as pretreatment for oil removal, and in others, forward osmosis was employed, since it has been proposed to

this specific purpose [27, 119, 120].

Another important consideration is the absence of progressive fouling, due to difficult quantification, which causes lack of performance in membranes or heat exchange equipment. Besides, as there can be solute loss or gain in assisted processes, proposed routes were considered to be in steady-state operation by adding a makeup stream or purge, also considered in operational costs.

For costs analysis, all equipment expenses were considered at year 2016 and the equipment cost equations were corrected using Chemical Engineering Plant Cost Index (CEPCI) [174]. Additionally, membrane modules (FO, RO and OARO) were simulated using finite volumes for better detailing. Combinations of processes were simulated in EMSO (Environment for Modeling, Simulation and Optimization), which is an equation-oriented process simulator [175], using relative and absolute accuracies of 10^{-3} and 10^{-6} in algebraic equations system solving, and 10^{-6}, for both accuracies, for optimization variables and constraints violation. EMSO data on thermodynamic properties were also used.

For specific treated water cost (spc) calculation, Eq. 3.1 and Eq. 3.2 were used.

$$spc = \frac{a\,CAPEX/f + OPEX}{V_{water}} \tag{3.1}$$

$$a = \frac{i(1+i)^n}{(1+i)^n - 1} \tag{3.2}$$

In these equations, V_{water} is the annual recovered water volume, f is the plant utilization factor, i is the interest rate, n is investment period, $OPEX$ are the operational expenditures, $CAPEX$ are the capital expenditures and a is the amortization factor. Contingency, freight, insurance and other minor contributors were not considered explicitly due to their low relevance in the overall cost and similarity for all proposed routes.

In order to analyze several possible desalination routes, conventional and new technologies were combined involving FO, RO, OARO, MF, MVC and MD. A detailed modelling for RO and OARO are presented in the next sections. For the sake of compactness, other technologies are briefly discussed here. Further information on these processes modelling is discussed in Appendix A.

The main hypotheses considered are:

- Membrane properties are constant and independent on pressure and salinity. Particularly, the values for the structural parameter were based in FO and PRO membranes;
- The maximum operational pressure is 120 bar [176] and the cost equations for seawater reverse osmosis (SWRO) were assumed to be valid;

- Produced water behaves as a sodium chloride solution;
- The treated water quality is suitable for irrigation, livestock or industrial use. To allow a fair comparison, when a process reached a lower salinity than needed, microfiltrated produced water was blended to standardize the exact composition for all routes, characterizing a bypass of the desalination stage;
- The pressure drop for membrane processes follow reported behaviors [177].

The specific optimization variables are discussed in each description for the following sections.

Microfiltration and Reverse Osmosis (MF-RO)

This route uses microfiltration, which was assumed to remove completely oil and grease [169], as pretreatment step for posterior reverse osmosis recovery. There is also a pressure exchanger in this configuration in order to integrate energy from a high-pressure source (RO concentrate) to a low-pressure stream (RO feed). Reverse osmosis process uses hydraulic pressure to overcome osmotic pressure, allowing water to flow from a hypertonic to a hypotonic solution. After desalination, RO permeate can be mixed to MF permeate, to achieve a predetermined quality, or follow to a RO second pass to remove more dissolved solids, if necessary. Depending on the second pass operating pressure, there can also be a second PX.

Membranes used in industrial RO processes are generally made of polyamide and the process is commonly employed for seawater desalination and effluent treatment [31, 40]. Proposed process for produced water desalination is presented in Figure 3.1.

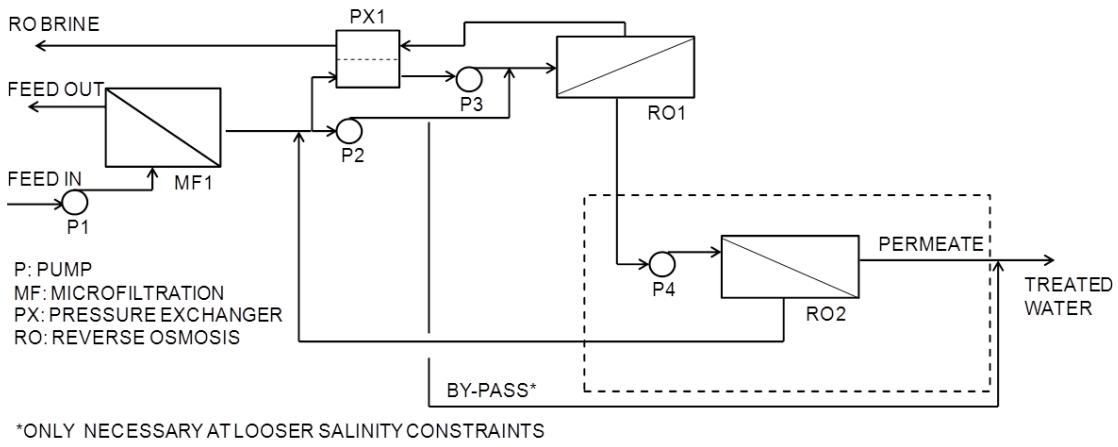

Figure 3.1: Schematic representation of MF-RO route. The dashed region represents a second RO pass which may be necessary to meet the required quality.

Simplifying produced water as a described earlier, volumetric water flux, J_W, and massic salt flux, j_S, can be described according to Eq. 3.3 and Eq. 3.4, respectively [178, 179].

$$J_W = A(\Delta P - \Delta\pi_m) \tag{3.3}$$

$$j_S = B(\Delta c_m) \tag{3.4}$$

Where $\Delta\pi_m$ is the osmotic pressure, Δc_m is the salt concentration and ΔP is hydraulic pressure differences across the membrane. A and B are water and salt membrane permeabilities, respectively.

Permeate salt molar concentration c_p is a function of water and salt fluxes, as well as salt molar mass (MM), according to Eq. 3.5.

$$c_p = j_S/(MMJ_W) \tag{3.5}$$

Salt concentration at the membrane feed side surface, c_m, is a function of water flux, feed concentration c_f and mass transfer coefficient k, according to Eq. 3.6. It was considered no polarization effect at the permeate side.

$$(c_m - c_p)/(c_f - c_p) = exp(J_W/k_f) \tag{3.6}$$

Mass balance in each membrane element of volume includes the variations of feed and permeate mass flowrates ($\Delta\dot{m}_f$ and $\Delta\dot{m}_p$, respectively), as well as water flux (J_W), stream density (ρ) and element membrane area (a_n), according to Eq. 3.7.

$$\Delta\dot{m}_f = -J_W a_n \rho = -\Delta\dot{m}_p \tag{3.7}$$

Similarly, salt molar balance relates feed and permeate salt molar variations $\Delta(c_f\dot{F}_f)$ and $\Delta(c_p\dot{F}_p)$, respectively, and salt flux, according to Eq. 3.8. $\dot{F}_f$ and $\dot{F}_p$ are the feed and permeate volumetric flowrates, respectively.

$$MM\Delta(c_f\dot{F}_f) = -j_S a_n = -MM\Delta(c_p\dot{F}_p) \tag{3.8}$$

The pressure exchanger energy balance is represented by Eq. 3.9, assuming volumetric flowrates are equal. Entrance energy in the PX is the stream pressure multiplied by its volumetric flowrate and an efficiency factor, η_{PX}. The calculation expression involves feed pressures in, $P_{in,f}$, and out, $P_{out,f}$, besides concentrate pressures in, $P_{in,c}$, and out, $P_{out,c}$.

$$P_{out,f} - \eta_{PX} P_{in,f} = \eta_{PX} P_{in,c} - P_{out,c} \tag{3.9}$$

RO cost calculations were based on Choi *et al.* [180] and Malek *et al.* [178]. Although the equations were designed for seawater desalination, it was considered they are a good estimation for produced water below 120 bar. It is important to remind that real capital cost can be higher due to material specification changes (due to higher chloride content). RO equipment cost calculation considered basically membranes and pumping equipment. Eq. 3.10 was used for pumps and PX cost calculation, C_{pump}, in US dollars, and corrected with CEPCI [174].

$$C_{pump} = 52 \sum_{i=1}^{n} P_{out,i} F_i \tag{3.10}$$

In this equation, $P_{out,i}$ is equipment discharge pressure (in atm) and F_i, respective volumetric flowrates (in m^3/h). In PX case, the higher pressure was considered as P_{out}.

On the other hand, OPEX estimation considered annual energy consumption, draw solution reposition, in cases which FO was applied together with RO or MVC, and membrane reposition (33%/year), assumed to be higher than the usual of 20%/year [91]. It is worth to highlight that produced water can affect membrane replacement, especially standalone RO, due to constant cleaning caused by organic matter attachment [86].

Due to system simplicity, the only chosen optimization variable was recovery ratio at RO. Although seawater optimal recovery ranges from 40 to 55% [31], it was considered in the present study a range from 10 to 50%. This range was also applied in other routes in which RO recovery was employed as a optimization variable. Pressure at RO inlet was defined as a constraint for systems involving reverse osmosis. Commercial limits for seawater desalination or even special applications usually range from 70 to 120 bar [4, 113, 176]. It is important to emphasize that although the recovery ratio could vary in a broad range, for RO processes optimized here, the maximum recovery will be limited by the pressure constraint of 120 bar. Thus, the effective recovery ratio range may be lower than presented.

Microfiltration, Osmotically Assisted Reverse Osmosis and Reverse Osmosis (MF-OARO-RO)

Osmotically assisted reverse osmosis uses a sweep solution to minimize hydraulic pressure requirement through the membrane. In Park *et al.* work [36], it was considered that membrane characteristics for this process would be similar comparing to conventional RO. OARO was claimed to consume less energy and to be cheaper than

conventional RO [36]. A recent study by Bartholomew *et al.* [4] has found interesting results about energy consumption, which was lower than MVC requirements and potentially would have lower cost.

In the proposed configuration, diluted sweep solute, which is OARO permeate exit stream, needs to be treated by a conventional RO to allow low salinity water production. RO concentrated stream (sweep), assumed to be a sodium chloride solution, returns to the OARO module, after having its salt composition set by a drain/make up, as presented in Figure 3.2. This route also includes PX and high pressure pumps, following the information from the previous section.

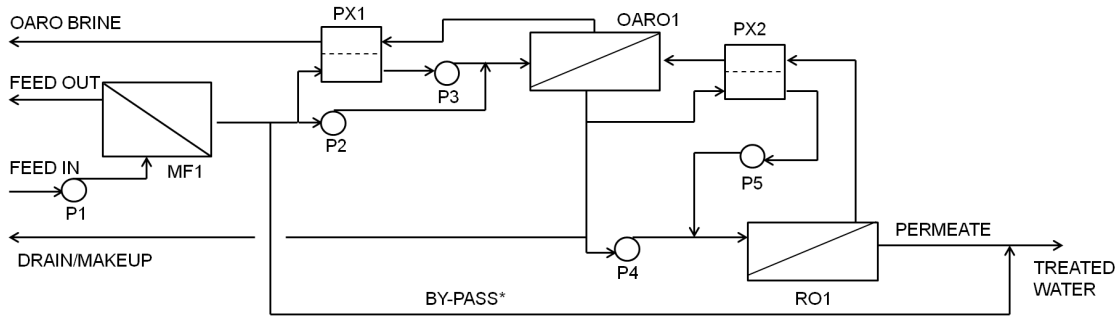

OARO: OSMOTICALLY ASSISTED REVERSE OSMOSIS
P: PUMP
MF: MICROFILTRATION
PX: PRESSURE EXCHANGER
RO: REVERSE OSMOSIS
*ONLY NECESSARY AT LOOSER SALINITY CONSTRAINTS

Figure 3.2: Schematic representation of MF-OARO-RO route.

For OARO modelling, Park *et al.* [36] assumptions for feed facing the active layer were used, after including an internal CP term, similarly to forward osmosis. Concentration difference across the membrane (Δc_m) can be calculated by Eq. 3.11 [4, 36]. In this equation, c_f and c_s are the feed and sweep solution bulk concentrations, respectively, S is the membrane structural parameter and D_f is salt diffusivity. The other variables and parameters were defined previously.

$$\Delta c_m = \frac{c_f \exp(\frac{J_W}{k^f}) - c_s \exp(-\frac{J_W S}{D^f})}{1 + \frac{B}{J_W}\left[\exp(\frac{J_W}{k^f}) - \exp(-\frac{J_W S}{D_f})\right]} \tag{3.11}$$

Similarly to other membrane processes modelled in this study, balance equation includes mass flowrate variation of feed, $\Delta \dot{m}_f$, and sweep solution, $\Delta \dot{m}_s$ for a membrane element of volume, as given by Eq. 3.12.

$$\Delta \dot{m}_f = -J_W a_n \rho = -\Delta \dot{m}_{ds} \tag{3.12}$$

Sodium chloride mass balance is described according to Eq. 3.13, including molar variations in sweep solution $\Delta(c_{ds}\dot{F}_{ds})$ and in the feed stream $\Delta(c_f \dot{F}_f)$.

$$- MM\Delta(c_f \dot{F}_f) = j_S a_n = MM\Delta(c_{ds} \dot{F}_{ds}) \tag{3.13}$$

Water and salt fluxes are calculated in a similar way to conventional reverse osmosis (Eq. 3.3 and Eq. 3.4), but the osmotic pressure gradient is lower than in RO, minimizing the needed inlet pressure.

In produced water treatment, since it is likely to overcome RO commercial pressure limits due to high osmotic pressure of feed stream, assisted reverse osmosis could be an interesting option. However, much effort is still necessary to properly design OARO module and operation.

The chosen optimization variables for MF-OARO-RO processes were OARO recovery, sweep solution concentration and volumetric ratio, which is the ratio between sweep solution and feed volumetric flowrates. In this case, recovery ratio was varied from 10 to 50 %, the sweep solution concentration from 30 g/L to 110 g/L and volumetric ratio from 0.3 to 1.5. The pressure limit of 120 bar was also applied to OARO.

Forward Osmosis with Reverse Osmosis (FO-RO)

Forward osmosis uses osmotic pressure difference as a driving force for water flux. Because of sorption-diffusion membrane mechanism, similar to reverse osmosis, rejections of salt and organics are high [27, 119, 120]. Aside from this, FO is claimed to be a low-fouling process, since the cake layer is looser than in RO [80, 123]. Because of these features, this process is recommended as a pretreatment for streams with high scaling and fouling propensity.

In spite of similarities with RO, FO flux is highly impacted due to concentration polarization (CP), internal (in the porous support) and external (on membrane surfaces)[124], tending to have low water fluxes. As Thiel *et al.* [3] elected FO-RO as a good process in terms of energy usage, this configuration was addressed in this study.

The route proposed is presented on Figure 3.3. In this configuration, NaCl was used as osmotic agent.

Similarly to MF-RO, a pressure exchanger is used to enhance energy recovery and to minimize cost. Feed is pretreated in forward osmosis (FO1) and recovered water permeates to the draw solution stream, which goes to a recovery step composed by one or two RO passes, depending on the required quality. In this case, if necessary, there can be also a second PX to recover energy. Also, drain/makeup line regulates salt concentration in draw solution, which was taken into account for cost calculation. For the same salinity comparison in the product, there can be a desalination bypass. It is important to notice that, in routes in which this mixture

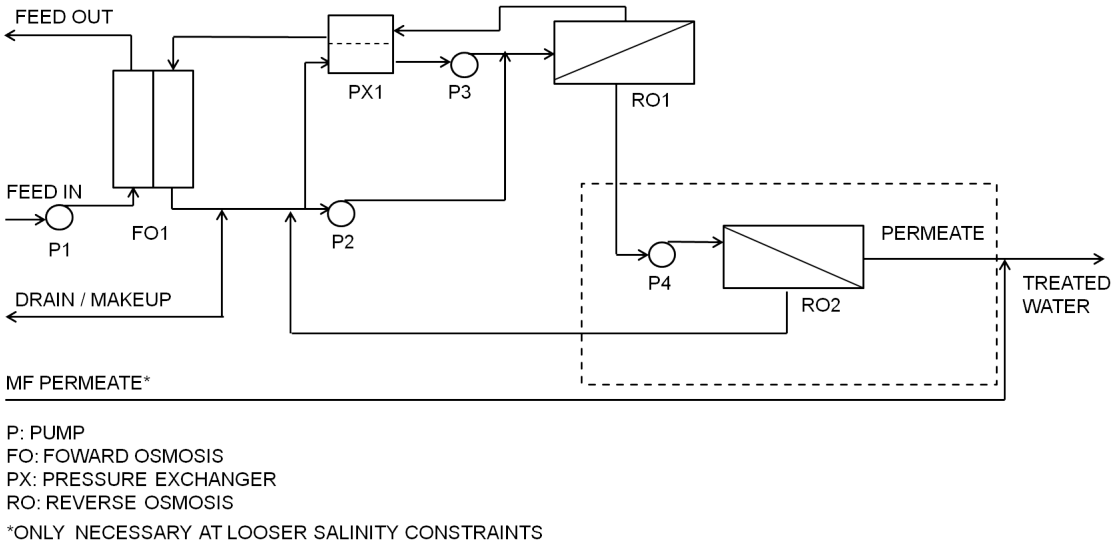

Figure 3.3: Schematic representation of FO-RO route. The dashed area includes a second RO pass, which can be necessary depending on the required water quality.

of microfiltrated produced water and permeate occurred, MF stream (TDS of 90 g/L) was substantially small (less than 2% of final stream), since one stream has nearly zero salt content and the goal concentration is closer to zero. Therefore, costs relative to MF were not considered.

For this process, optimization variables were volumetric ratio, draw solution concentration and FO recovery. The first variable was based on Tow *et al.* [181], who found the optimal condition to be 0.8, varying due recovery strategy and feed water. The volumetric ratio balances flow effects on membrane, modifying flux, area, and pumping costs. Variation range was set from 0.3 to 1.5.

Draw solution concentration is responsible for the driving force in FO and can affects directly RO recovery step. Draw solution concentration lower limit is final feed salinity plus a terminal concentration difference, since the module is counter-current. Upper boundary is defined by NaCl solubility limit (about 360 g/L). Draw solution concentration, when higher, increase pumping and make up costs, while membrane area is decreased.

FO recovery was varied from 10 to 50%, as already mentioned. On the other hand, RO recovery was not specified because two optimization variables related to it, FO recovery and volumetric ratio, are already defined. In this route, there was also a pressure limit for RO at 120 bar, which constrained not just the effective RO recovery range, but mainly the draw solution effective concentration range in the optimization routine.

Microfiltration and Mechanical Vapor Compression (MF-MVC)

Although MVC is a thermal process, it can use only electrical energy power in separation. This energy drives a compressor, responsible for pressurizing steam formed from brine evaporation. With total condensation, the steam heats the brine, allowing more water to evaporate. Additionally, two heat exchangers recover heat to enhance global system performance. A simplified diagram for this route is presented in Figure 3.4.

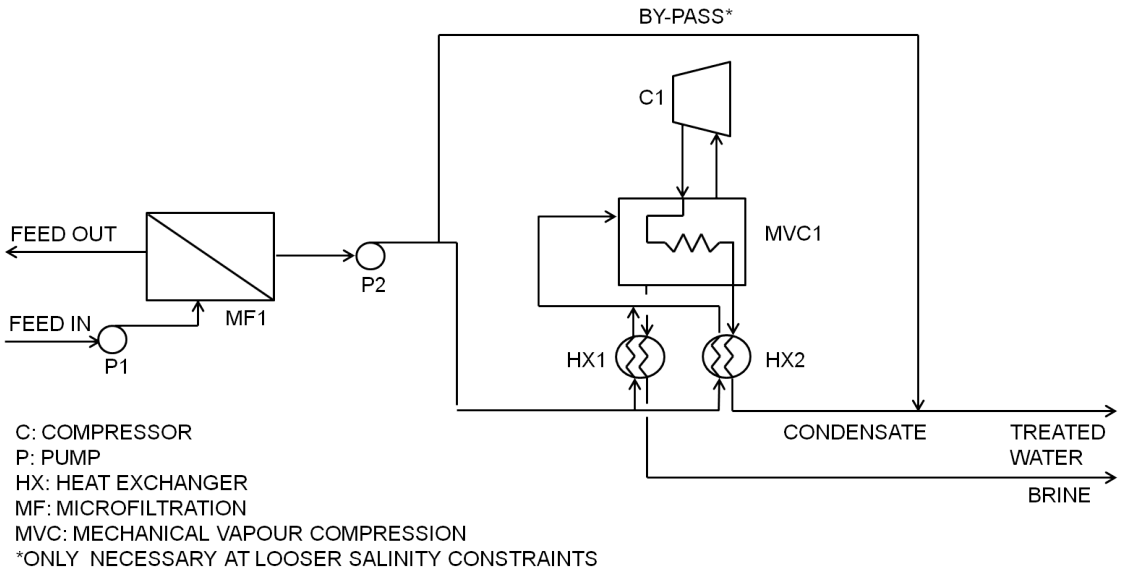

Figure 3.4: Schematic representation of MF-MVC route.

Chosen optimization variables for this system were MVC recovery, evaporator temperature, terminal temperature difference (TTD), which is the difference between the temperatures inside the evaporator and condenser. Evaporator temperature was studied from 333K to 353K, which are typical practiced temperatures, and TTD from 1K to 10K [182].

A variation of this process was proposed by Swaminathan *et al.* [108] and also addressed in the present study. These authors suggested a membrane distillation module instead of brine heat exchanger for seawater desalination, as represented in Figure 3.5. MD module improves recovery with the residual evaporator heat, although it has a larger area than a conventional heat exchanger [108]. It is important to mention that this MD module does not need external thermal energy source, since it uses the residual energy from the main evaporator. Thus, the focus in electrical-driven desalination processes is maintained.

Forward Osmosis with Mechanical Vapor Compression (FO-MVC)

A particular configuration using MVC with forward osmosis pretreatment was also evaluated via simulation and optimization, as presented in Figure 3.6.

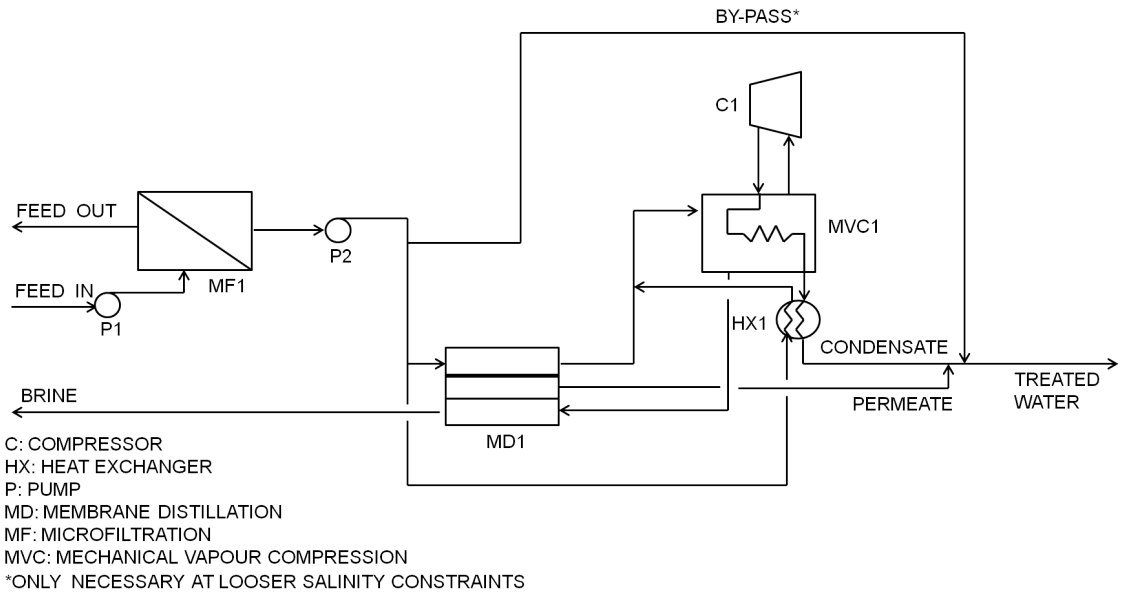

Figure 3.5: Schematic representation of MF-MVC-MD route.

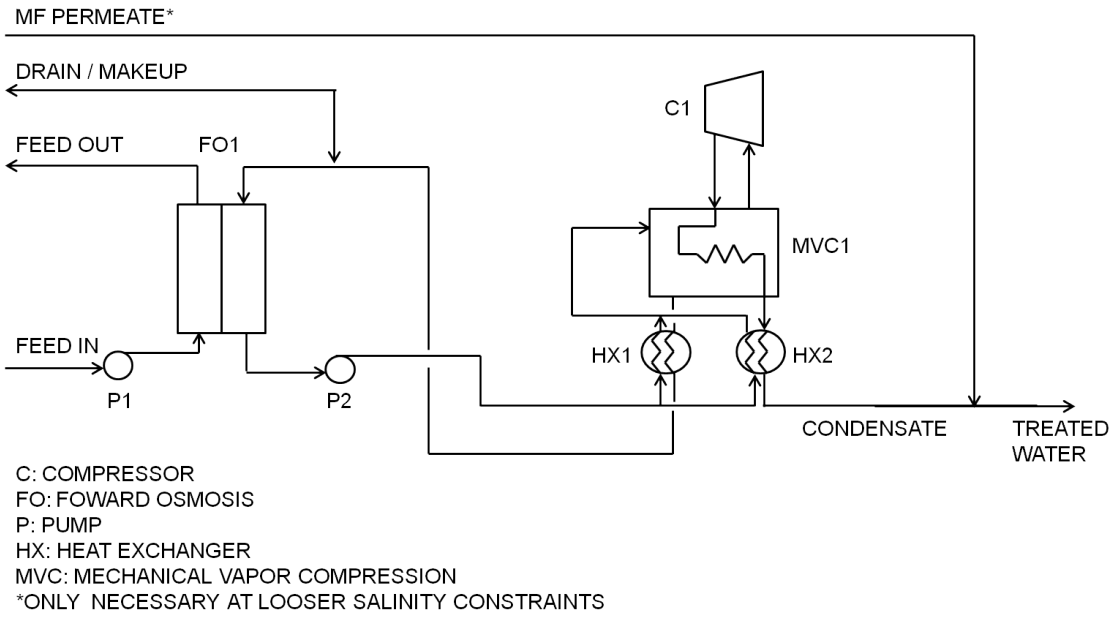

Figure 3.6: Schematic representation of FO-MVC route.

As MVC could not achieve some volatile matter restrictions [59], FO pretreatment was proposed to handle these contaminants and also remove foulants and harmful dissolved compounds which could impair MVC performance [116]. Because of this pretreatment and, consequently, scaling salts removal, it was thought that MVC could intensify recovery and operation temperature. There would be benefits for FO due to removal of compounds such as benzene, toluene and ammonia, besides any scalants that could harm thermal equipment. Sodium chloride was also used in draw solution, in consonance with previous routes.

In the optimization procedure, draw solution concentration, volumetric ratio

(similarly to MF-OARO-RO and FO-RO), FO recovery, evaporator temperature and TTD were defined as key variables, with the same ranges proposed in previous sections, unless for evaporator temperature, which was allowed to vary until 367K due to increase pretreatment quality, explained above.

3.2.2 Initial Data and Parameters

The main parameters and considerations for simulation are presented in Table 3.2. The proposed configurations were investigated for cost optimization and energy consumption for salinities from 50 to 150 g/L. The flowrate of 50 m^3/d was set to represent a small produced water facility, while the feed temperature was assumed to be 293 K.

In order to analyze differences caused by other aspects, as energy usage, equipment cost or operational expenses, plant utilization factor value was the same for all technology combinations. The economic parameters were based on Brazilian industries overview for the year of 2016, while the energy cost is equivalent to hydroelectrical power generation [187]. Regarding the processes, RO water flux, number of membrane leaves, MVC pump discharge pressure and pre-heaters heat transfer coefficient were set to typical or estimated design values, as well as MD channel depth and recirculation ratio. Additionally, pump efficiency for small RO tend to be lower due to hydraulic losses, therefore the energy consumption was penalized [35].

Regarding to membranes cost for MD, an average value of 90 US$/$m^2$ was used [101, 110], although MD tends to have a small influence in total MF-MVC-MD cost. For RO membranes, a cost of 40 US$/$m^2$ [184] was used. It was assumed that FO would have the same membrane cost for RO, since the technology is at a high rate of development. On the other hand, as OARO is a new technology, it was assumed that membrane cost would be twice the RO membrane cost. This cost variation was studied in RTEA.

Details on cost equations are presented in Appendix A, while the EMSO models are described in Appendix G. For CAPEX estimation based on these equations and on membrane costs, references listed in Table 3.3 were used. Percentages presented in this table are referred to total CAPEX.

It is important to remind that cost estimation by main equipment can differ due to site particularities (e.g. civil works, necessity to treat final brine, interest taxes, etc.) and influence the analysis depending on which place it is taken.

3.2.3 Retro-Techno-Economic Analysis

In order to prospect developments in membranes, a RTEA was performed. The analysis consists of choosing the most important variables (or parameters) of the

Table 3.2: Summary of parameters and initial data for routes simulation.

Parameter	Value	Reference
General data		
Treated water flowrate	50 m^3/d	–
Treated water quality (Irrigation) – Base case	2 g/L	[86]
Salt feed concentration	90 g/L	[169]
Pump efficiency	50 %	[35]
Compressor efficiency	60 %	[182]
Pressure exchanger efficiency	98 %	[183]
NaCl diffusivity[a]	$1.33x10^{-9}m^2/s$	[124]
Feed temperature	293 K	–
Energy cost	0.05 US$/kWh	–
Investiment duration	20 years	–
Interest rate	10 %	–
Plant utilization factor	0.90	[110]
FO/RO/OARO		
RO/OARO average water flux	15 $L/(m^2h)$	–
Hydraulic FO membrane permeability[b]	4.301 $L/(m^2h\ bar)$	[124]
Hydraulic RO membrane permeability	0.997 $L/(m^2h\ bar)$	[179]
NaCl permeability in FO[b]	1.939 $L/(m^2h)$	[124]
NaCl permeability in RO/OARO[c]	0.108 $L/(m^2h)$	[179]
FO/RO/OARO channel width	1.27 m	[179]
FO/RO/OARO channel thickness	$7.11x10^{-4}m$	[179]
Structural parameter (FO/OARO)[b]	$1x10^{-4}m$	[124]
Number of membrane leaves[d]	16	–
Membrane cost (FO/RO)	40 US$/$m^2$	[184]
Membrane cost (OARO)	80 US$/$m^2$	–
MF		
Recovery ratio	90 %	[169]
Average oil concentration	100 mg/L	[169]
Membrane cost (with housings)	720 US$/$m^2$	[169]
MVC		
Pre-heaters heat transfer coefficient	3 kW/m^2K	–
Feed pump discharge pressure	2 bar	–
MD		
Membrane permeability	$22x10^{-7}kg/(m^2sPa)$	[185]
Membrane width	1 m	[185]
Channel depth	1 mm	–
Vapor conductivity	0.0188 W/(mK)	[185]
Membrane conductivity	1.2 W/(mK)	[185]
Membrane thickness	200 μm	[185]
Recirculation ratio	12.5	–
Membrane cost	90 US$/$m^2$	[101]

[a] Sodium chloride diffusivity may range from 1.2 to 1.6 $\times 10^{-9}m^2/s$ depending on the measurement technique [186]

[b] Parameters for OASYS TFC interpolated for 293K [124].

[c] Estimated using a rejection of 99.73%.

[d] Used to adjust Reynolds number for region of interest for spiral wound modules.

Table 3.3: Cost references for CAPEX estimation.

Technology	Cost element	Cost range	Adopted value	References
RO/OARO[a]	Equipment [b]	38.1[c]- 55.8% [d]	45.0%	[36, 118, 178]
FO	Membrane	29.4 %	29.4 %	[118]
MD	Membrane	50.0 %	50.0 %	[101]
MVC	Equipment	20.0 - 40.0 %	27.0% [e]	[188, 189]
MF	Membrane & housing	30.0%	30.0%	[169]

[a] Park *et al.*[36] considered the same cost for both seawater RO and OARO. For this study, it was considered the same equations and rations, but a different cost for membrane.

[b] Including membranes, pumps, pressure recovery devices, etc.

[c] Linares *et al.*[118] considered 30.5% as equipment cost in total CAPEX, but included in others 46% pre-treatment and intake cost. Pre-treatment is taken into account separately in the present work and intake is not considered. Intake and pre-treatment would be around 20% of total CAPEX [163]. So, in this analysis, equipment cost would be 38.1% (30.5% of 80%).

[d] Malek *et al.* [178] developed cost modeling for SWRO considering a Lang Factor of 1.411, equivalent to 70.8% of CAPEX related to equipment, including intake and pre-treatment At the time of this publication, there was no data on pre-treatment by MF/UF. So, it was considered that together to intake costs, they would represent 15% of the total, remaining 55.8% as RO equipment of the total.

[e] Equivalent to a Lang factor of 3.68 [188]

process and calculating their threshold values for an economic metric[165]. Even though the approach was based on Furlan *et al.* [165], it did not consider the NPV itself, but the treated water specific cost. Another difference is the use of optimized points for the obtained values, rather than changes in simulation. Comparisons baselines were conventional technologies lowest cost, as MF-MVC, when applicable.

As the systems had their main variables optimized at this point, external parameters related to process design were selected for the analyses. For MF-OARO-RO system, membrane properties as structural membrane parameter, water permeability and salt permeability were studied, as well as membrane cost, energy cost, interest rate and pump efficiency.

3.3 Results and Discussion

In this section, optimized systems are addressed for possible reuses, focusing on irrigation (final streams standardized with 2 g/L sodium chloride and zero concentration of oil and grease). Afterwards, membrane parameters (physical or economical) impact is discussed, with focus on process feasibility. This scope intends to guide future study on desalination routes for produced water.

3.3.1 Optimal points and salinity variation

An important variable is feed salinity, which could represent route ability to handle different sources of produced water or variation of specific produced water within time, as consequence of field stratification. Desalination processes for produced water treatment should be versatile to handle this inherent salinity variation [27]. Results obtained for a salinity range from 50 to 120 g/L are summarized in Figure 3.7.

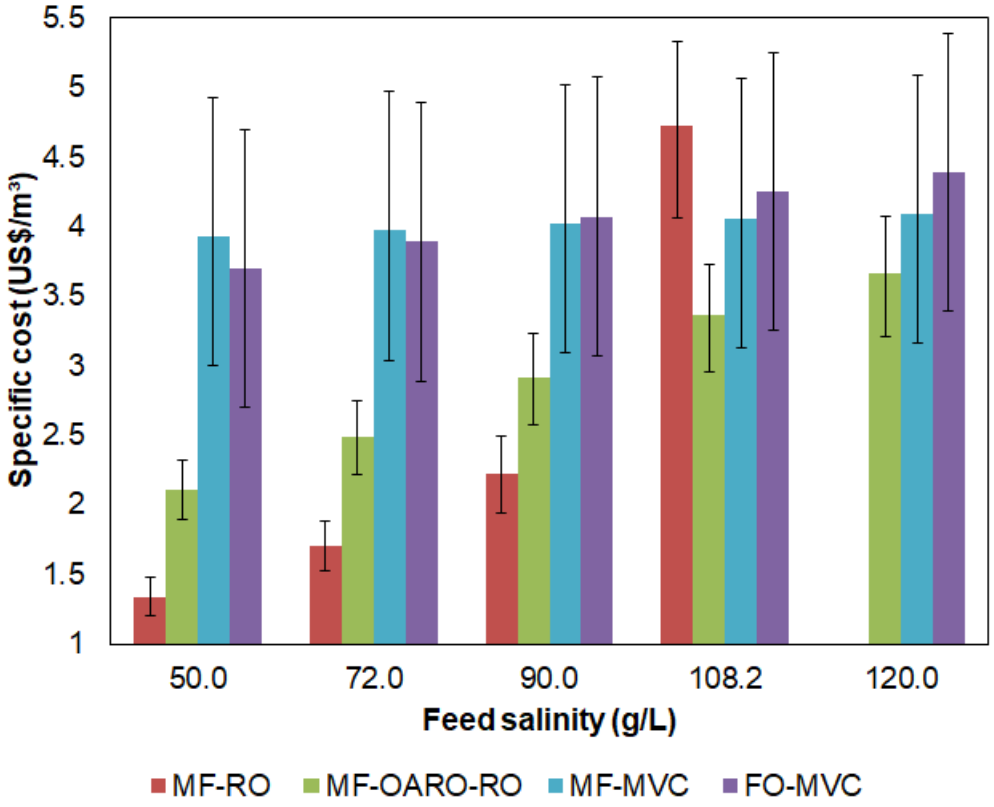

Figure 3.7: Specific cost behavior as function of feed concentration aiming to reuse water for irrigation.

Error bars presented in Figure 3.7 are the result of CAPEX variation according to ranges presented in Table 3.3 for RO/OARO and MVC. Routes MF-RO and MF-OARO-RO have similar behavior because the analysis relies on admitting equal cost function (equipment cost variation range) for both. Lang factor, which can be related to percentages referent to equipment cost, tends to be smaller in compact units [188], which is commonly the case of membrane technologies. MVC-based technologies become more competitive to others under higher salinities or tighter treated water quality.

MF-RO is the cheapest of all routes optimized for salinities up to 90 g/L. For higher salt concentrations, the mandatory pressure limit of 120 bar was activated, thus, no feasible point was found for the average flux of 15 LMH, since concentration

polarization was too intense. The higher the feed salt concentration, the steeper the flux decay along the module is: fluxes at the end of the module reached values near zero, while fluxes at module entrance were too high. The discrepancy between those fluxes led the routine not to find a solution that would satisfy all the equations and constraints for the highest salinity tested. For 108.2 g/L, a feasible point was found for flux of 14 LMH, although recovery ratio was very low (16%), bringing specific costs to high values. At this point, OARO would be more interesting.

For MF-OARO-RO, optimal point at 90 g/L had an overall cost of 2.92 US$/m^3. Although the total recovery was higher (46%) than MF-RO, inlet pressure for OARO was lower due to the effect of the sweep solution (59.3 g/L). While the pressure inlet was 119 bar for MF-RO, MF-OARO-RO had 70 bar in the first step (OARO) and 49.5 bar in conventional step (RO) for base case. In spite of having a prominent effect on total cost, increase of salinity did not lead OARO to overcome 120 bar. Therefore, for the highest tested salinity, specific cost for this route was the lowest. This could be an interesting design to handle high salinities that standalone RO is out of range. MF-OARO-RO presented more ability to handle different salinity scenarios because it has three optimization variables, which could compensate salinity effects, as they are the main cost drivers. Because of this, it could be suitable for small salinity variations due to its flexibility using draw solution.

For FO-RO, at the optimal point without pressure constraint, RO feed pressure would be 165 bar, with a recovery of 46% at this step. However, for the ranges tested with pressure constraint, the optimal point would be at 10% FO recovery and a staggering cost of 5.45 US$/m^3 for base case. Although Minier-Matar *et al.* [117] have proposed FO-RO as a potential lower capital and operating cost, preliminary results showed this route as the most expensive of all tested. Low driving force in FO, in order to reach 120 bar or less, makes costs increase quickly and does not allow high water recovery. Because of the great difference between this route and others, this configuration had no further study for the present work.

MF-MVC system had an optimal cost of 4.02 US$/m^3 at maximum recovery, evaporator temperature at 333K and TTD of 3.4K. Higher operating temperatures are preferred due to higher vapor pressures and better overall heat transfer coefficients at the evaporator. However, as exit temperature at heat exchangers is defined as well as cold fluid stream, heat exchange area is increased, and this effect was predominant. Additionally, produced water is a potential scaling stream and more aggressive than seawater. Lower evaporator temperatures are more suitable for salt scaling control, mainly because of sulfates solubility limits [190].

Of all routes tested, MF-MVC had the smallest effect of salinity on the specific cost. When salt content increases, and consequently BPE (Boiling Point Elevation) increases, the minimization routine tends to keep evaporator temperature constant

by slightly decreasing TTD. A similar effect was found for FO-MVC, which is a little more expensive than the MF-MVC route for salt concentrations higher than 80 g/L, despite the fact of allowing higher temperatures and recoveries in MVC equipment. When compared to MF-MVC, MF-MVC-MD did not reach a detectable increase in recovery due to high salinity of MVC brine. Swaminathan *et al.* [108] achieved savings up to 8%, but for seawater MVC at 40% recovery. For higher recoveries (80%), savings were reduced to less than 1%, which would be approximately the salinity range of the present MVC concentrate. MF-MVC-MD can be an interesting route to intermediate salinities, since for maximum salinity tested or higher recoveries, the effects of adding a MD step are too small.

For FO-MVC at 90 g/L, the volumetric ratio achieved the lower limit of 0.3 at the optimal point, with a cost of 4.07 US$/m^3 at base case. With volumetric ratio increase, flux at FO tends to be maximized, but it is compensated with a rise in MVC equipment cost. As flux can be maximized with draw solution concentration, volumetric ratio was reduced to the lower limit to minimize capital cost, even below MF-MVC standalone CAPEX. Because of this predominant effect, FO-MVC cost was slight lower than MF-MVC cost for salinities of 50 g/L and 72 g/L. Another influence factor is the high ceramic membrane cost, even though MF flux is at least ten times higher than FO flux.

Because of MVC relative independency of salinity, draw solution concentration at FO-MVC has reached 270 g/L, even though salinity increase drives to higher salt leakage at FO. The impact on FO area surpassed the salt loss at this point. Salts generating higher osmotic pressure, like potassium pyrophosphate [191, 192], would be good candidates for this route, since the draw solute loss is minimized.

Another point of discussion is the feasibility of reaching high fluxes with produced water having no pretreatment step prior to FO. Several authors have pointed FO as a step for oil removal, although this contaminant can decrease flux [27, 119, 120]. This effect could lower water flux and increase costs. On the other hand, if a MF pretreatment is added, cost can increase about 0.30 US$/m^3.

Optimization of FO-MVC route indicates that feed salinity has a more significant change on cost than MF-MVC alternative. For high salinities, an increase in draw solution concentration to keep the permeate flux has a small effect on cost when compared to a decrease in recovery. Moreover, even optimizing salt permeability and concentration in draw solution, specific costs are significantly higher than MF-OARO-RO cost.

Aiming to address different water users, a comparison was performed for the main processes discussed here at base case point (90 g/L). For irrigation (2 g/L) and livestock (5 g/L) reuse purposes, the achieved costs remained approximately the same (Figure 3.7). However, to achieve industrial water quality (200 mg/L),

MF-RO process cost is increased to 2.80 US$/m^3, while MF-OARO-RO reached 3.24 US$/m^3. For MF-MVC and FO-MVC, costs practically remain constant. This is an indicative that increasing salinity and/or stricter constraints bring membrane and thermal processes costs closer. At low and moderate feed salinities (near 90 g/L), even though pressure constraint limits maximum recovery, MF-RO would still be the cheapest process for all users studied here.

However, in qualitative comparison, it is likely for thermal processes to allow ammonia or volatile content to pass and to contaminate treated water. Because of this, further post-treatment as stripping or chlorination could be necessary and could add an extra expense to achieve desirable water quality.

In terms of quality, OARO routes are particularly interesting because they could deal with various contaminants in produced water with a double RO pass and could remove volatile content for more demanding water users.

3.3.2 Energy consumption

In order to compare with the literature and discuss some specific benefits of each route, the impact of tested routes on the energy consumption under salinity variation was studied. Results are presented on Figure 3.8.

It is interesting to note that energy consumption is consequence of optimization and not the optimization objective itself. For example, in routes involving MVC, higher TTD implies in greater energy consumption (compressor pressure ratio increases with an elevation of condenser temperature, calculated by TTD). However, the higher the terminal temperature difference, the lower the evaporator area.

There also may be a slightly energy consumption disparity for MVC to previous reports [3] due to different considerations, as compressor efficiency [182]. Despite the fact of energy consumptions are not represented for the same exact recovery and fluxes, range of data obtained have equal magnitude order of similar routes [3, 4], since the optimization searches the lowest cost together to other key variables. Besides, energy consumption of the present work accounts for all pumping requirements (including pretreatment steps listed in previous sections).

For MF-RO and MF-OARO-RO simulated routes, because of considerable difference in optimal recoveries, energy consumptions have different behaviors and values. MF-RO has little variation until 100 g/L and energy consumption is smaller than MF-OARO-RO in this range. However, as the pressure constraint becomes active at 90 g/L optimization, recovery ratio is lowered to meet the constraint for higher salinities. Pumping requirements become higher for smaller quantities of treated water [3], so energy consumption leads MF-RO cost to overcome MF-OARO-RO cost for 108.2 g/L feed salinity. Pressure constraint is not active for the latter route, so the

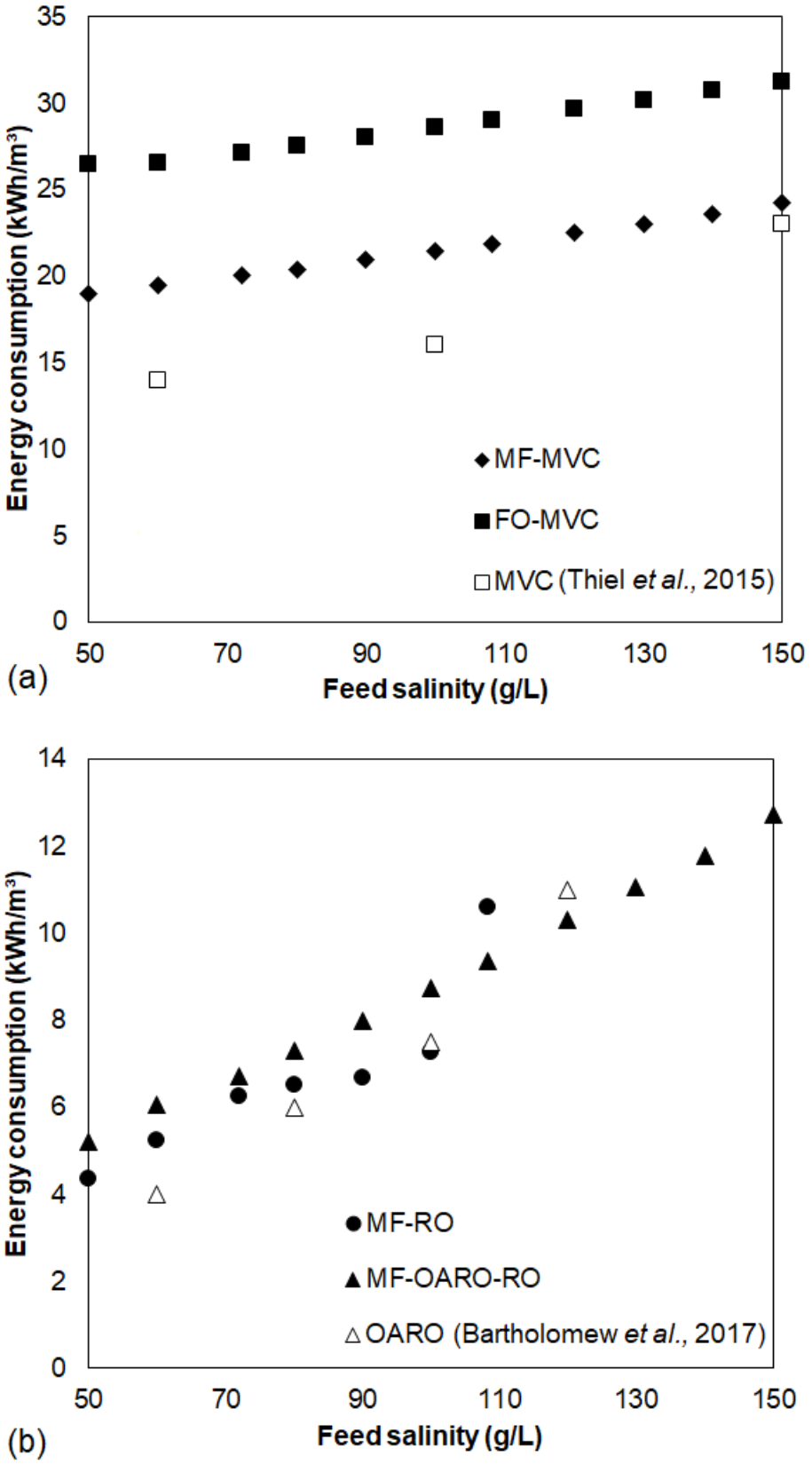

Figure 3.8: Energy consumption with feed salinity for irrigation reuse purposes. A) MVC-based processes. B) RO-based processes. MVC data based on ref. [3] and OARO based on ref. [4].

behavior is practically linear in studied range. To better understanding, feasibility region is more detailed in Figure 3.9.

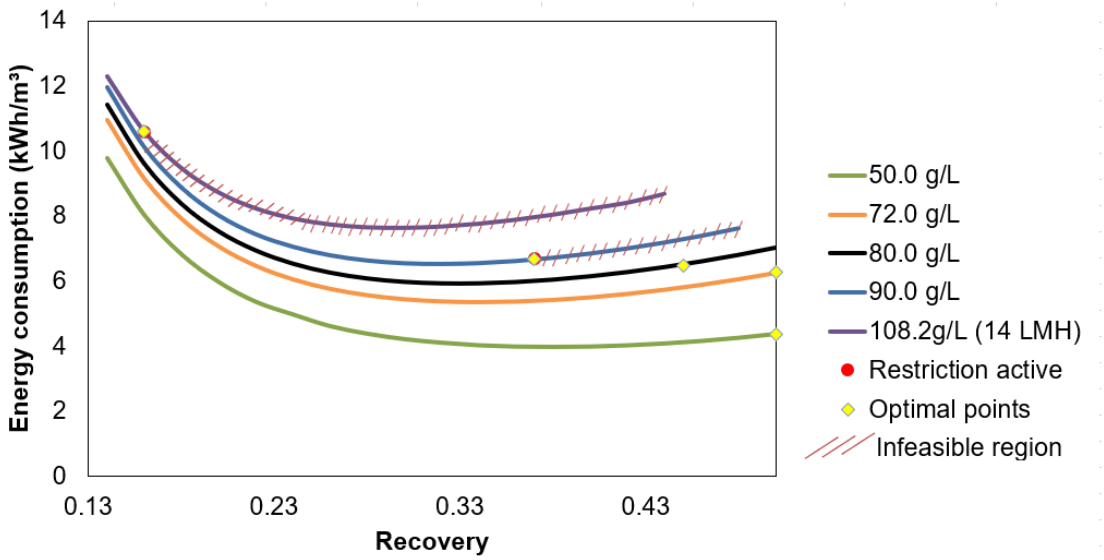

Figure 3.9: Energy consumption as function of recovery and salinity for MF-RO. Optimal points are obtained by cost optimization. The infeasible region represents the points that violate pressure constraint of 120 bar.

According to Figure 3.9, it is possible to note the cost optimization path for MF-RO. As the optimization objective is to minimize cost, the optimal point is not coincident to minimal energy consumption, since the cost function has also influence of capital expenditure costs. It is clear that for salinities greater than 90 g/L, the feasible region is too constrained for MF-RO, leading to high costs and high energy consumption, as presented in Figure 3.7 and Figure 3.8, respectively.

Values obtained for MF-OARO-RO in Figure 3.8 are slightly different from literature [4], probably because in the present study it was used a smaller value for pump efficiency, even though the process cost was optimized. Another important point to emphasize are the different fluxes, pressure and structural parameter [4], which also influence energy consumption calculation. Particularly, the structural parameter from [4] is more conservative when compared to those obtained for FO/PRO membranes [124], that based some considerations for this paper. A conclusion is the need of membranes that can combine some reverse osmosis characteristics (as high water permeability and low salt permeability) to forward osmosis membranes with low structural parameter [4].

When a structural parameter of 1000μm is used [4], at a constant membrane cost for 108.2 g/L salinity, there is a cost increase of only 10% higher for the present work, although higher values have been found to strongly change energy consumption and cost [142, 148].

Even though there is no clear correlation between higher membrane burst pres-

sures and structural parameters, as presented in Figure 3.10, tests for the same membrane type have shown increasing pressure tends to increase the structural parameter, specially for opener support spacers [193]. This type of spacers also tends to increase pressure loss in the channel when the membrane is compacted, as well as deforming the membrane, as described in Appendix E.

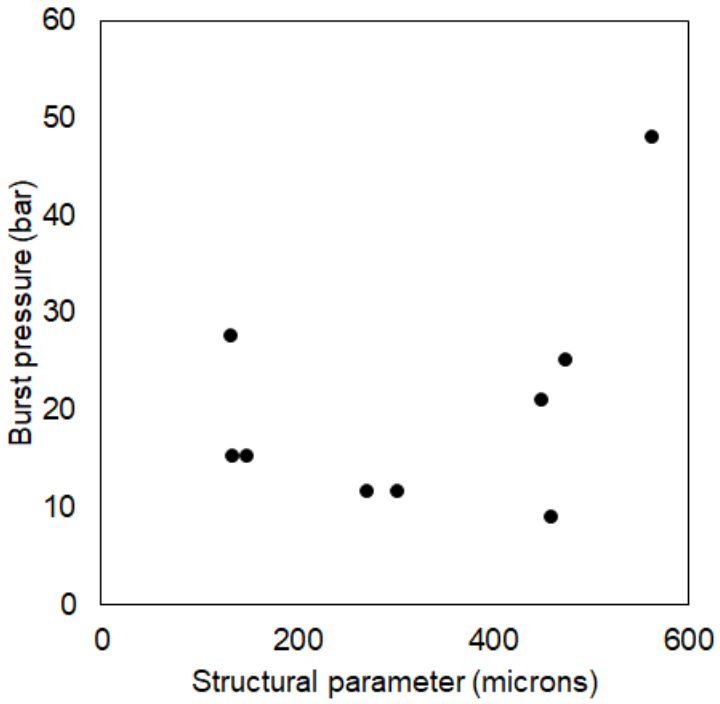

Figure 3.10: Burst pressure and structural parameter for PRO membranes [5–11].

Another concern that should be addressed is the process ability to reach fluxes as high as 15 L/(m^2.h), compatible to RO fluxes. In case they are too constrained, OARO economic feasibility may be limited. Therefore, satisfactory fluxes should be pursued by membrane and module design. An important work on assisted reverse osmosis [142] employed multiple stages instead of operating at higher pressures. This choice makes better use of energy and provides lower energy consumption [139]. Differently from the results of this study, this optimization routine used a fixed feed pressure, limited in 65 - 80 bar and variable water flux, mostly around 1 - 5 LMH. This water flux is mostly limited by the conservative higher structural parameter used in this analysis.

It is interesting to note that processes in which MVC is included are less sensible to salinity variations in terms of cost and energy requirements (Figure 3.7 and Figure 3.8). Additionally, OARO configurations are close following MF-RO trends in energy consumption for salinities up to 70 g/L, despite having higher specific cost due to higher membrane expenses (80 US$/$m^2$ for OARO and 40 US$/$m^2$ of conventional RO) and more pieces of equipment.

For MF-OARO-RO route, CAPEX and OPEX breakdown are presented in Figure 3.11. According to this figure, pumps and pressure exchangers represent the second most representative part of CAPEX, after "Others", in which are included site development, indirect capital costs and utility works, for example (Table 3.3). This proportion occurs probably because of the higher equipment demand, which is more elevated for MF-OARO-RO than for MF-RO. Interestingly, membrane reposition plays an important role for OPEX, since it was considered that membrane reposition would occur in 3 years. An aspect to be better investigated is the possibility to enhance membrane life for such application, so OPEX breakdown could change behavior and decrease total cost, changing also the optimal point.

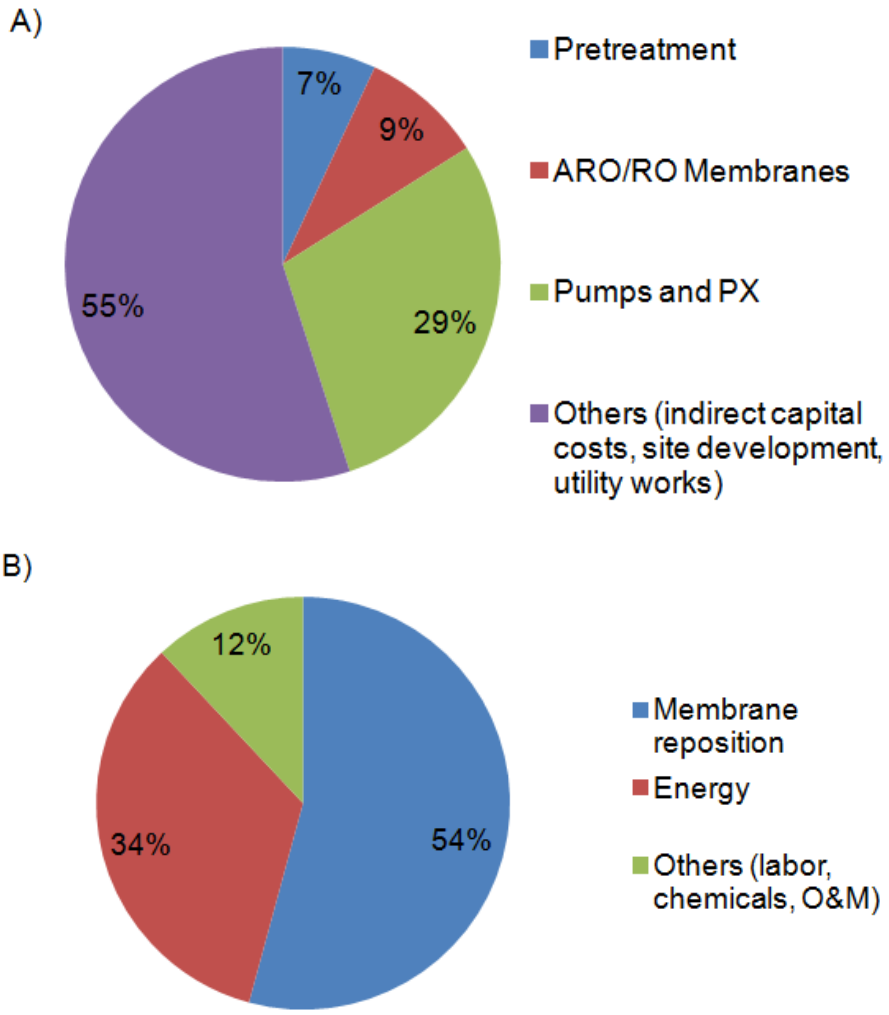

Figure 3.11: CAPEX (A) and OPEX (B) composition for MF-OARO-RO at base case.

3.3.3 RTEA

In order to investigate MF-OARO-RO economic feasibility, a retro-techno-economic analysis was performed with six parameters: membrane characteristics (A, B and S), membrane cost, energy cost, pump efficiency and interest rate for optimal points. Results for feed salinity of 90 g/L are presented in Figure 3.12.

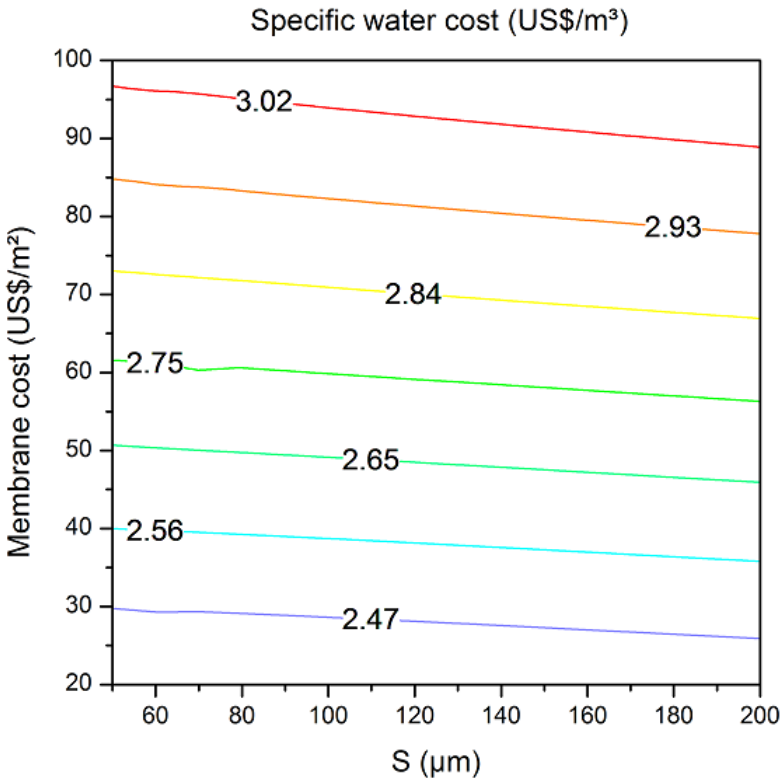

Figure 3.12: Specific cost optimal points (US$/m^3) for MF-OARO-RO (feed salinity of 90.0 g/L) as a function of membrane cost and structural parameter.

According to Figure 3.12, membrane cost has the major influence on specific cost. However, even with same membrane cost for OARO and RO (40 US$/m^2), which is unlikely, specific cost for MF-RO is lower (2.20 US$/m^3). In this analysis, there is no feasible point for MF-OARO-RO to overcome MF-RO at the studied range. Another point of interest is the structural parameter influence that could be responsible for a more effective use of driving force. Even with a decrease from 200 μm to 50μm, for a fixed membrane cost of 40 US$/m^2, the impact on specific cost would be less than 0.10 US$/m^3. Therefore, although this range was based on FO/PRO reported values [124], S may be different, specially at higher operating pressures.

When comparing higher salinities, MF-OARO-RO is competitive to conventional MF-MVC, as presented in Figure 3.13. It is worth to highlight that all points in

this RTEA are optimal points. Therefore, the parameter influence can be damped by optimization variables change (recovery ratio, sweep solution concentration and volumetric ratio).

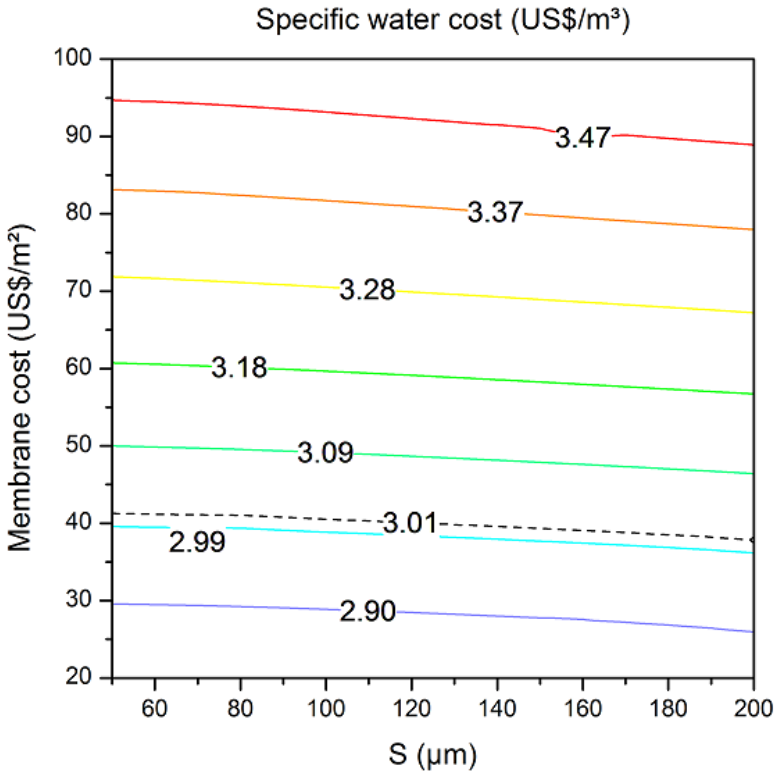

Figure 3.13: Specific cost optimal points (US$/m^3) for MF-OARO-RO (feed salinity of 108.2 g/L) as a function of membrane cost and structural parameter. The dashed line represents the lowest cost for MF-MVC.

In this case, the feasible region contains values of cost is less than 3.01 US$/m^3, which is the lowest possible cost for MF-MVC, (lower error bar in Figure 3.7). In other words, the process would be cheaper than MF-MVC in conditions where the membrane cost should be near RO cost and with structural parameter below 120 μm or even a broader range for the average, and not minimum, MF-MVC cost. In cases in which the complete treatment is weighted, MF-OARO-RO could clearly outstand where ammonia and other volatiles removal is necessary. Besides, specific site particularities, like energy cost, could modify the shape and region of the curves.

When a broader range in investigated for A and S, it is possible to note a combination effect, according to Figure 3.14. Higher structural parameter effect on cost is potentialized by low water permeabilities, since two mass transport resistances (membrane active layer and porous support) increase at the same time, directly affecting water flux, membrane area and cost. This synergic effect corroborates the need for lowering the resistances and specially, support structural parameter, which

has the strongest effect in this range.

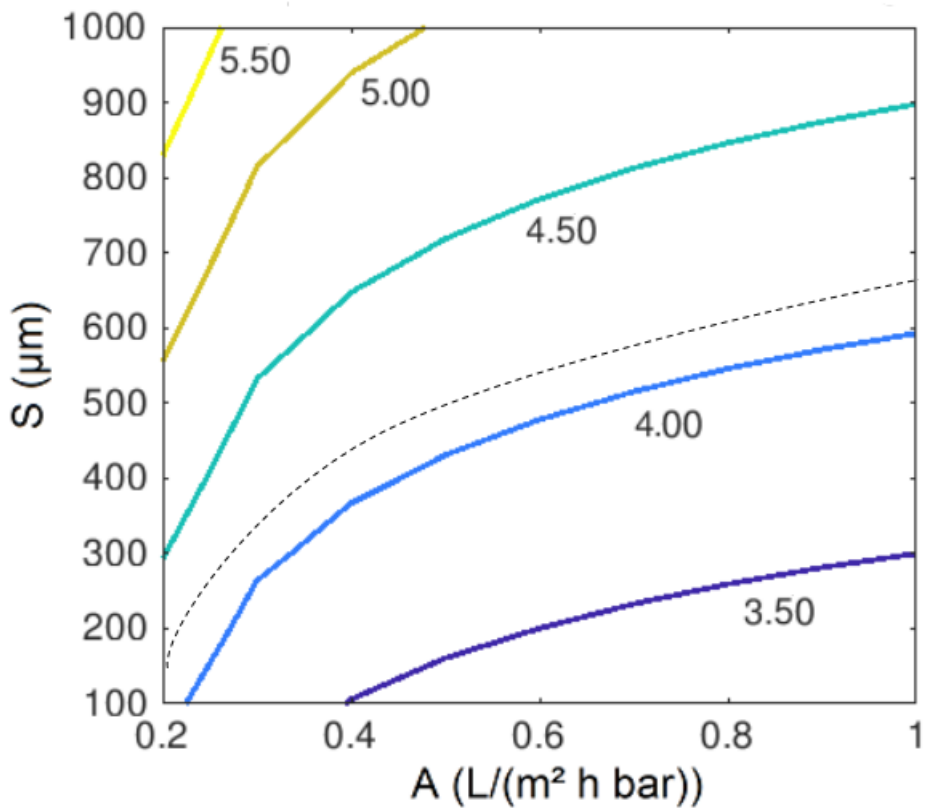

Figure 3.14: Specific cost optimal points (US$/m^3) for MF-OARO-RO (feed salinity of 108.2 g/L) as a function of water permeability and structural parameter. The dashed line is the average MF-MVC cost.

Regarding to membrane permeabilities (A and B), specific cost behavior is shown in Figure 3.15. In spite of having small influences on process cost, values shown in Figure 3.15 resulted in large variation for optimization variables to accommodate the changes. Recovery ratio varied from 38.7% to 41.9%, while sweep solution concentration changed from 73.0 to 110.0 g/L. Volumetric ratio between entrance sweep solution and feed flowrates ranged from 0.55 to 0.67. It is interesting to note that sweep solution concentration is the main cost driver for this process, and although it had the broadest variation range, specific cost varied less than 5 %. Combining conclusions on structural parameter, MF-OARO-RO cost seems to be relatively stable for expressive changes in membrane properties.

Even with optimization, energy cost and interest rate affected significantly specific cost, as shown in Figure 3.16. The impact was specially high for interest rate, since it affects CAPEX and OPEX relative weight on total cost. Combining effects of these site-dependent parameters can result in almost 35% variation in process cost, the highest range observed in this study.

Pump efficiency and energy cost impacts, presented in Figure 3.17, were also

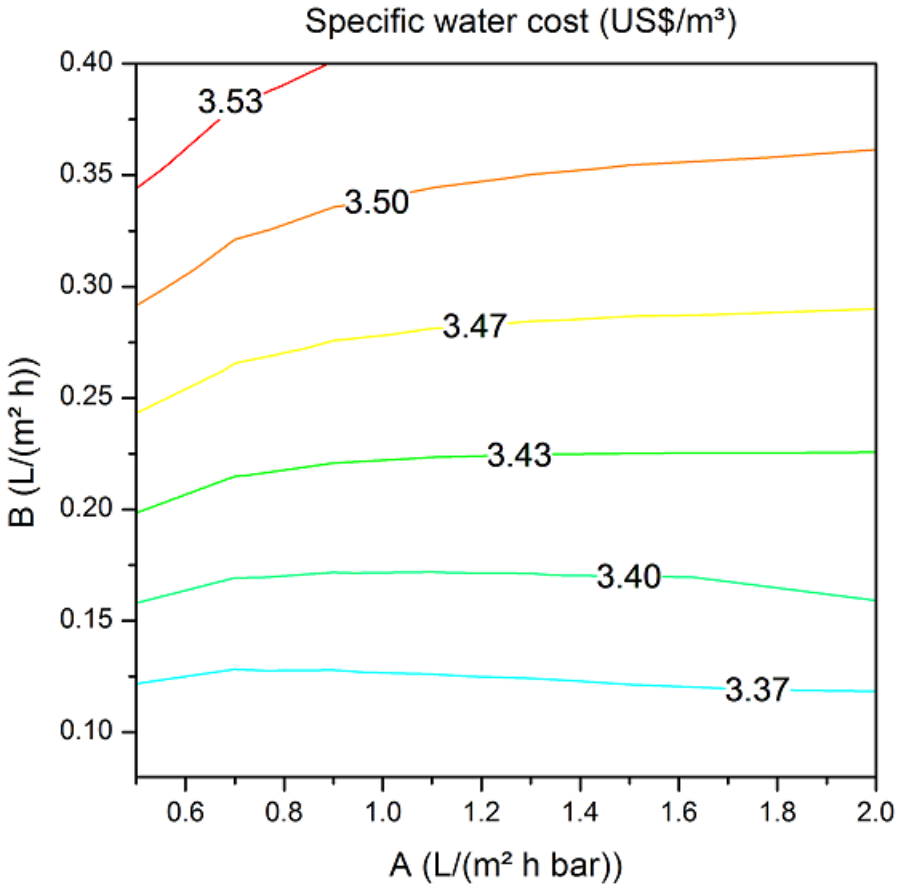

Figure 3.15: Specific cost optimal points (US$/m^3) for MF-OARO-RO (feed salinity of 108.2 g/L) as a function of membrane water permeability (A) and salt permeability (B).

studied. For this specific case, probably due to higher CAPEX proportion caused by the interest rate of 10 % and small plant size, pump efficiency did not play an important role and had little influence on specific cost. On the other hand, energy cost had impact on cost, as expected for desalination technologies [3].

In conclusion, MF-OARO-RO is definitely a process that should be object of further study and improvement, because it has potential to compete and overcome conventional technologies performance for high salinity effluents.

3.4 Final Remarks

According to modeling and route optimization, it was verified that:

- MF-RO still represents the cheapest and lowest energy consumption configuration in desalination for salinities below 90 g/L and final water quality of

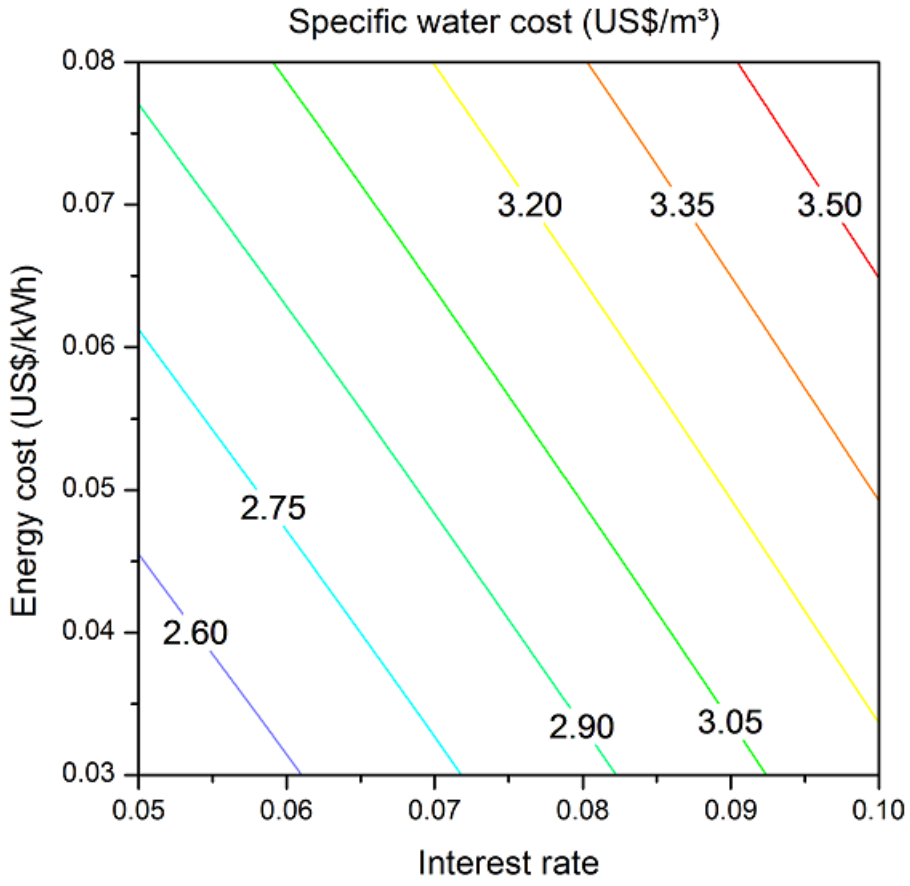

Figure 3.16: Specific cost optimal points (US$/m^3) for MF-OARO-RO (feed salinity of 108.2 g/L) as a function of energy cost and interest rate.

irrigation, livestocks or industrial water. Above this salinity level, with a pressure constraint of 120 bar, recovery is penalized and cost is increased;

- MF-OARO-RO is an interesting route when MF-RO recovery is too low, since sweep solution make suitability broader even when OARO membrane cost is twice RO membrane cost;

- FO-RO is a very expensive process at the studied salinity range, mainly due to RO pressure constraint. However, when a double membrane pass is desirable and for lower salinities, it could be a suitable process;

- The structural parameter in 50-200 μm range and at high water permeabilities did not have an expressive influence for specific cost. However, in the range of low permeability and high structural parameter (up to 1000 μm), both have a strong influence in cost.

- OARO membrane permeabilities changes can be damped by optimization vari-

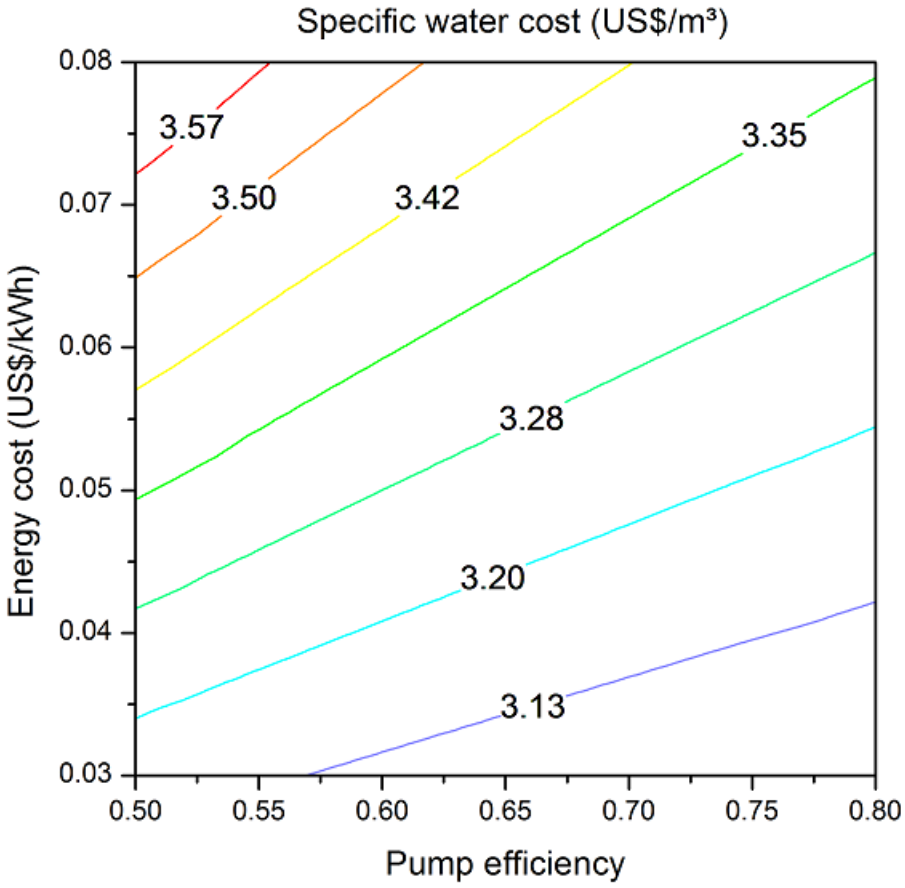

Figure 3.17: Specific cost optimal points (US$/m^3) for MF-OARO-RO (feed salinity of 108.2 g/L) as a function of energy cost and pump efficiency.

ables, having negligible final impact on cost.

- Site-dependent parameters, as energy cost and interest rate, play important roles in cost, even with process optimization. Pump efficiency has a small influence for this case study.
- The rate of cost increase with feed salinity is less expressive for thermal processes containing MVC, even though they have prominent energy consumption.
- FO-MVC is an expensive route, but it can be considered when a very strict quality level is pursued at final users. However, it should also be considered an eventual pretreatment prior to FO depending on feed characteristics.

Chapter 4

Effect of salinity on osmosis membranes properties

This chapter describes a study on the effect of high salinity in membrane materials commonly used in osmotic processes, in order to verify the common assumption of constant permeability coefficients (Section 4.1) and possible changes in morphological properties (Section 4.2). The first part was submitted as a paper to *Journal of Membrane Science*, while the second contains preliminary results on analytical techniques for CTA. This material was chosen to be studied due to its availability as an FO membrane and ease to generate thin films for the properties investigation (Section 4.2), specially when compared to polyamide.

4.1 Membrane transport properties

High salinity streams are generated during many energy-related activities, such as oil and gas extraction [95, 194, 195], CO_2 storage [30, 196, 197], and RO concentrate. These high salinity brines raise both environmental and economic concerns, as their disposal and treatment are typically difficult and costly [113, 195, 198–202]. The high treatment cost occurs mostly due to the use of conventional energy-intensive thermal processes to desalinate the brines and produce low salinity distillate.

As the cost benchmark for seawater desalination [31, 113, 194, 203], RO is being constantly studied and modified to reach high feed salinities at minimum expense and energy consumption. For example, HPRO aims to operate at pressures higher than 100 bar [34], while the conventional maximum pressure ranges from 65 - 80 bar [113]. Another development is the addition of a sweep or draw solution to assist the conventional RO in the permeate stream and lower the osmotic pressure difference across the membrane, such as OARO [4, 142] osmotically-enhanced dewatering RO (OED-RO) [141], DSARO [36], and COMRO [2]. Although the assisted processes

may require an extra RO step, their estimated cost could be competitive with current conventional processes [142, 166], as well as significantly lowering their energy consumption.

These previously reported cost estimations rely on the membrane properties: water permeability, solute permeability, and structural parameter, which can be determined through FO and/or RO experiments [124, 157, 158, 204]. However, the testing conditions (35 – 58.5 g/L) are generally very distant from the expected operational conditions of salinity (up to 200 g/L) and pressure.

For this reason, more appropriate operating conditions of salinity and pressure should be used to characterize membranes using RO-based experiments, as was performed for other nanofiltration and FO membranes [158, 205]. Previous energy/cost analyses have assumed that the transport parameters are constant values, though membrane properties may be affected by the environment, especially salinity [12, 37, 149, 151–154]. The water and salt permeability coefficients for commercial membranes were correlated to the membranes volumetric water content [15], which could be affected by the operating conditions. For example, Freger (2004) [12] verified that nanofiltration polyamide membranes were susceptible to deswelling in a high salinity environment. These changes leave questions regarding the membrane behavior and the transport fundamental mechanisms in high salinity environments. It is critical to accurately determine the transport parameters of membranes to be used in RO-based processes at their appropriate operating conditions in order to predict more effectively the performance of these technologies [34, 199] and to separate the effects of CP and membrane structural changes.

In this study, flat-sheet CTA membranes were tested in a lab-scale experimental setup for osmotic processes. Tests were operated over a range of conditions between 0-200 g/L sodium chloride and in various operation modes and pressures, including RO, FO, OARO and pressure-assisted osmosis (PAO). Transport measurements from experiments were used to determine the best fit A, B, and S parameters for the CTA membrane with confidence analysis to determine the uncertainties of the estimates. Additionally, pervaporation using the CTA membrane was also performed to estimate the parameter A in another sorption-diffusion process with less external resistances. Finally, the impact of these parameters on the technoeconomic feasibility of osmotically driven processes for high salinity brine treatment and how the design of membranes for RO-based applications can be improved are discussed.

4.1.1 Materials and Methods

Membrane and materials

The membranes used in the experiments were made of cellulose triacetate (1121821 - FTSH2O Flat Sheet Membrane, CTA, FO, CF04) and supplied by Fluid Technology Solutions (FTS, Albany, OR). The samples were stored in sodium bisulfate solutions at 4°C. The solutions used as feed, sweep and draw were made daily using deionized (DI) water and sodium chloride (Fisher Scientific CAS 7647-14-5). Although the solutions were not buffered, their pH were nearly constant at the value of 6.

Osmotic processes

In order to simultaneously fit the main parameters related to transport [158], experiments of reverse osmosis, pressure-assisted osmosis, forward osmosis and osmotically assisted reverse osmosis were performed using the setup presented in Figure 4.1.

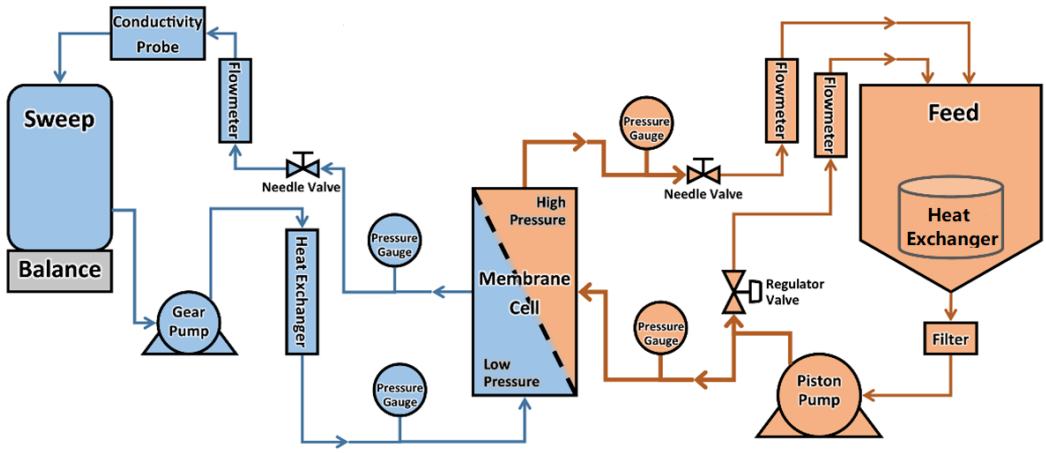

Figure 4.1: Diagram of an OARO experiment set-up. A high salinity feed solution is cycled through a pump and series of instruments and flows across a membrane, allowing water and salt to transverse the membrane. The sweep/draw side circulates a lower salinity solution along through similar instruments to measure changes in salt concentration and weight of the sweep/draw side solution.

The membrane cell has an active area of 42 cm^2 (Sterlitech, Kent, WA) and all the experiments were made with the active layer facing the high-pressure side. Stainless steel wire cloths (McMaster-Carr, Elmhurst, IL) of different mesh grades were used to support the membrane inside the cell.

A preliminary testing set was made to minimize head loss in the draw/sweep solution side. Different combinations of wire cloths were used while permeability and rejection were monitored together with the pressure loss, in order to check for possible deforming. Commercial RO feed diamond spacers were found to deform the membrane, as described in Appendix E. The best configuration, used in subsequent

experiments, used a stack of five different cloths as demonstrated in Figure 4.2, with the finer one facing the membrane porous support and reaching less than 0.2 bar of head loss. Although compatible to lab purposes, this value must be decreased for industrial applications.

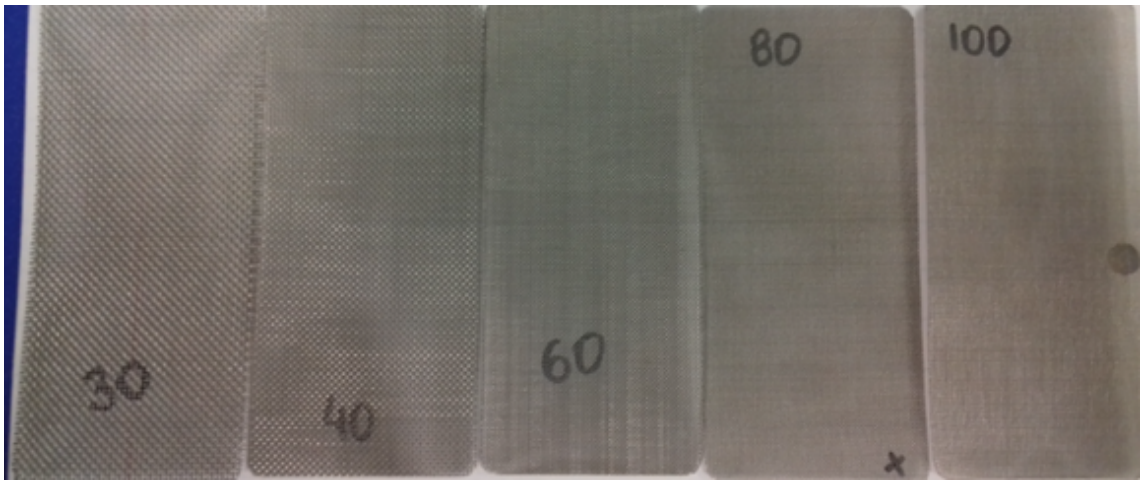

Figure 4.2: Optimal combination of wire cloths for supporting the membrane. The numbers depicted in each cloth represent their mesh grade.

In the sweep/draw solution cycle, there is a gear pump (Hydra-cell, Warner Engineering, Minneapolis, MN), pressure gauges to monitor the pressure drop in the membrane cell, a conductivity probe (Hanna Instruments, Woonsocket, Rhode Island) and a flowmeter. The tank in this circuit was used to calculate the water flux, using a balance (Ohaus, Parsippany, NJ).

Similarly, the feed cycle contains a reservoir, pressure gauges, flowmeters, valves to adjust pressure and flowrate and a high-pressure piston pump (Danfoss, Nordborg, Denmark). A shell and tube heat exchanger in the sweep cycle and a submerged heat exchanger in the feed tank were used to maintain the streams at 20°C.

In RO operation, the system described earlier was modified: one of the exits of membrane cell was capped and the reservoir with balance was used directly to collect the permeate. A laboratory conductivity meter was used to monitor the conductivity inside the tank.

In all experiments, the online instruments such as balances and line conductivity meters were monitored using a routine in LabVIEW. The data acquisition was set to 60 seconds.

The tests were performed in three different labs using slightly different pumps, reservoirs and conductivity meters: WE^3 Lab, Carnegie Mellon University; National Energy Technology Laboratory-DOE NETL; and PAM, at Universidade Federal do Rio de Janeiro. Despite this, every effort was made to ensure reproducibility, as the employment of similar piping path and validation of baselines to ensure no

leaking. For identical experimental conditions, the difference in collected parameters in different labs was lower than 15%.

The experiments were carried out under different sets of conditions: feed salinity, draw/sweep salinity or pressure were varied to get different operating conditions. Each set used a new piece of membrane. An example of these sets is presented in Figure 4.3. In high pressure experiments, the membrane was pre-compacted until the water flux was stabilized (lasting at most 3 hours). In FO, there was no significant effect in the estimated parameters due to pre-compaction prior to testing.

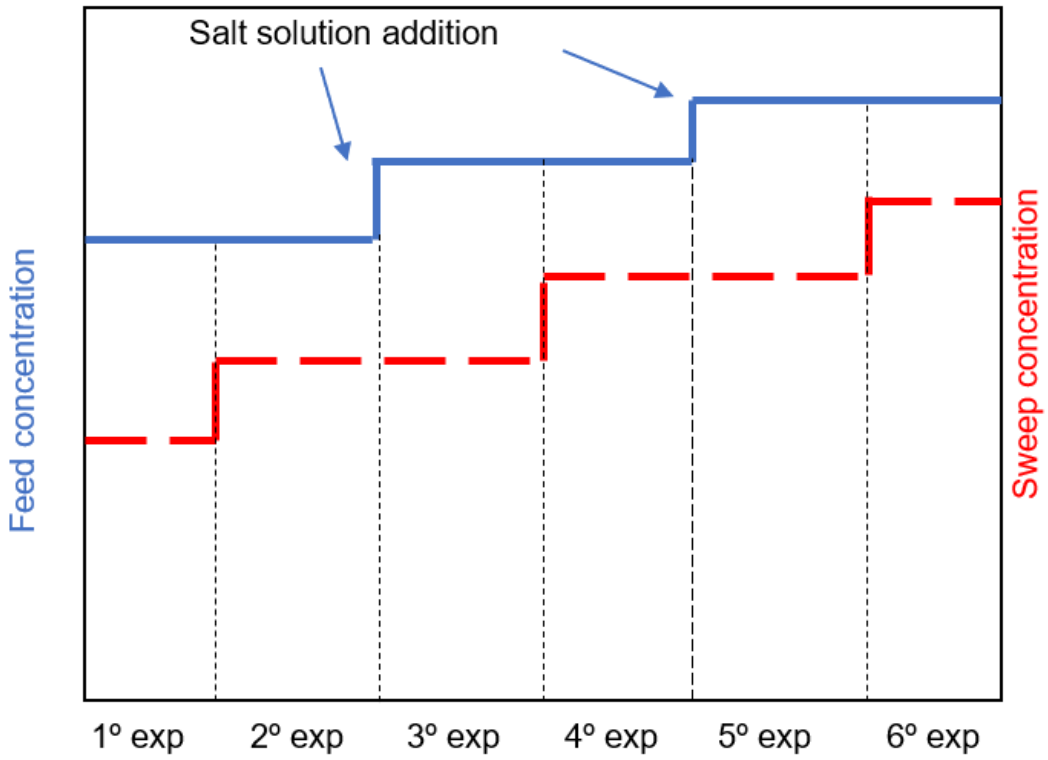

Figure 4.3: Representation of operating conditions inside a set of experiments. In this example, feed and sweep concentrations were varied by adding concentrated salt solution to modify the concentrations. Each pair of feed and sweep concentrations were a new experiment. In some cases, pressure was also varied to obtain new conditions.

Each different condition was monitored during for at least an hour, enough to reach stable values. The measured variables were water and salt flux: the first was calculated using the sweep/draw mass variation in each minute, while salt fluxes were calculated using sodium chloride mass balance, based on the conductivity measurements. The fluxes used in the parameter fitting correspond to the last 30 minutes of each condition.

Additional information on flowrates, pressures and ranges applied in the experiments are summarized in Table 4.1.

Table 4.1: Osmotic processes experimental conditions.

Feed flowrate	75.7 L/h (20 gph)
Feed pressure	0 – 60 bar
Permeate/sweep/draw solution flowrate	37.8 L/h (10 gph)
Permeate/sweep/draw solution pressure	< 0.2 bar
Temperature	20°C
Data acquisition time	1 minute
Condition duration time	1 hour (minimal)

The present work was based on a methodology previously developed to simultaneously fit the parameters A, B and S for FO [158], avoiding possible interference of different driving forces and/or membrane compaction effects. This method uses measured water and salt fluxes, as well as concentrations, pressures and temperatures to estimate the parameters using the least squares method. A routine in EMSO software (Environment for Modelling, Simulation and Optimization) [175] was used to fit these values using the optimization solver "COMPLEX", based on the flexible polyhedron method [206]. The accepted absolute and relative errors in the routine were 1×10^{-10}.

For the osmotic processes, the water flux J_W was calculated using the water permeability coefficient A and the hydraulic and osmotic pressure differences (ΔP and $\Delta\pi$) at the membrane interface, according to Eq. 4.1. Likewise, the salt flux j_S uses the solute permeability coefficient B and the sodium chloride concentrations at the same interface, as described by Eq. 4.2. The osmotic pressures are calculated using Pitzer expressions [207]. In Eq. 4.1, P_f and P_s are the hydraulic pressure at feed and sweep/draw solutions sides and $\pi_{m,f}$ and $\pi_{m,s}$ are the osmotic pressures at the membrane feed and sweep/draw solution interface, respectively.

$$J_W = A(\Delta P - \Delta\pi) = A[(P_f - P_s) - (\pi_{m,f} - \pi_{m,s})] \tag{4.1}$$

$$j_S = B\Delta c = B(c_{m,f} - c_{m,s}) \tag{4.2}$$

The feed and sweep/draw solution concentrations at the membrane interface, $c_{m,f}$ and $c_{m,s}$, are calculated using Eqs. 4.3 – 4.4 and bulk feed and sweep concentrations $c_{b,f}$ and $c_{b,s}$, respectively. The equations account for the concentration polarization on feed surface using the mass transfer coefficient k_f and in the membrane porous support using the structural parameter S. The sodium chloride diffusivity D_f was fixed as $1.5 \times 10^{-9} m/s^2$ [186].

$$c_{m,f} = c_{b,f} exp\left(\frac{J_W}{k_f}\right) - \frac{j_S}{J_W}\left[exp\left(\frac{J_W}{k_f}\right) - 1\right] \tag{4.3}$$

$$c_{m,s} = c_{b,s} exp\left(\frac{J_W S}{D}\right) + \frac{j_S}{J_W}\left[1 - exp\left(\frac{-J_W S}{D_f}\right)\right] \tag{4.4}$$

It should be noted that the structural parameter S described in Eq. 4.4 accounts for all mass transfer resistances in the sweep/draw solution side, including eventual external concentration polarization. The detailed modelling has been previously described in literature [142].

The feed mass transfer coefficient k_f was estimated theoretically using the laminar flow expression below, Eq. 4.5 [208]. It was estimated to be 2×10^{-5} m/s and varies by less than 10% between low and high salinity conditions, at the same flowrates, and was kept constant, which is subject of further discussion.

$$\frac{k_f d_h}{D_f} = 1.85\left(Re\, Sc\, \frac{d_h}{L}\right)^{0.33} \tag{4.5}$$

This expression uses the hydraulic diameter d_h, the salt diffusivity D_f, as well as Reynolds (Re) and Schimdt (Sc) dimensionless numbers and the channel length L.

A summary of the tested membrane processes, their measured variables and the fitted parameters are presented in Table 4.2. The low magnitude of salt flux and the limited precision of conductivity monitoring used to estimate bulk salinities prevented the calculation of B for all sets of experiments. Instead, for experiments in which it was not possible to calculate B, this value was kept constant at the average value measured in RO for pressurized systems fitting and the FO average for high salinity FO. The validity of this assumption is discussed further in this analysis.

Table 4.2: Processes and fitted parameters.

Process	Measured variables	Fitted parameters	Constant parameters
RO	J_W, j_S	A and B	k_f
PAO	J_W	A and S	k_f and B
OARO	J_W	A and S	k_f and B
FO	J_W, j_S	A, B and S	k_f

The number of different conditions on sets varied, but a minimum degree of freedom (DF) of 2 was maintained in order to get a good estimation. The calculation of DF is presented in Eq. 4.6 and uses the number of different conditions, N_{exp}, number of measured variables, N_{var}, (water and salt fluxes, where applicable) and number of fitted parameters N_{par} [209]. When it was not possible to get the salt fluxes, B was not estimated, but kept constant as mentioned earlier.

$$DF = N_{exp} N_{var} - N_{par} \tag{4.6}$$

The parameter fitting considered a minimum R^2 of 0.90 for both water and salt fluxes and a minimum parameter significance of 80%, calculated in EMSO using t-Student test.

Pervaporation experiments

In order to exclude the mass transfer resistance from the flux measurements and water permeability coefficient calculation, pervaporation tests were performed with the same membrane used in osmotic processes. The most accepted theory for pervaporation is also sorption-diffusion [100], so it should be susceptible to the same hypothetical effects observed in osmotic processes. Additionally, pervaporation allows measurements at both very low hydraulic pressure difference /compaction and low salinity, which is not possible in FO. Another feature is the magnitude of the water fluxes, near 1 $L/(h \times m^2)$ (LMH), which makes the overall contribution of resistance from S insignificant, which will be discussed in the next section. The system used in pervaporation data acquisition is presented in Figure 4.4. The vacuum pressure applied was 2 mmHg and the feed temperature, 21°C. The feed solution was recirculated at a flowrate of 75 L/h.

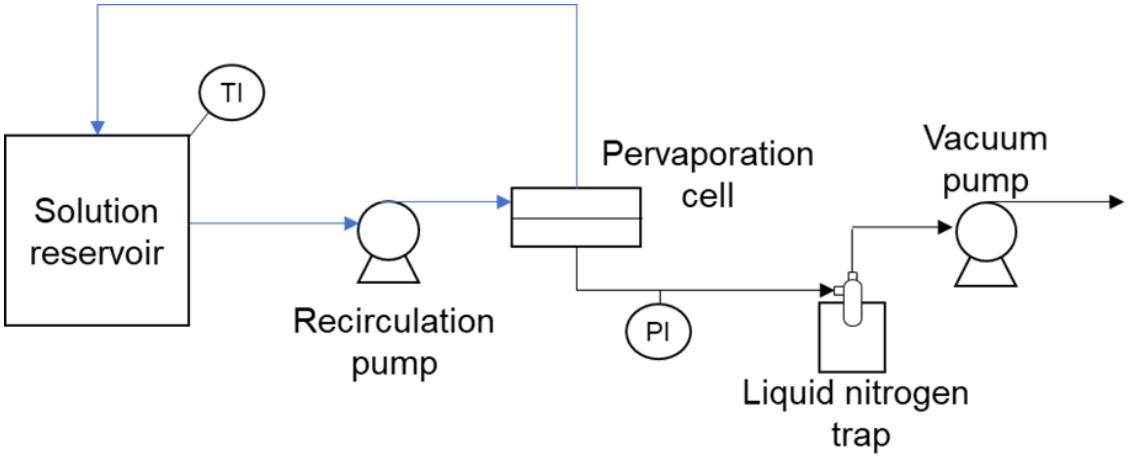

Figure 4.4: Schematic of pervaporation setup. The feed solution is circulated without detectable hydraulic pressure through a pervaporation cell. In the permeate side, water vapor flows and it is collected in a liquid nitrogen trap.

In this setup, there was a stainless-steel custom-made cell with an active area of 5.7 cm^2. The membrane was supported with porous stainless steel. In this loop, there was also a reservoir and a recirculation pump (Flojet – Xylem, Rye Brook, NY). In the vacuum side, there was a pressure gauge (Fieldpiece Instruments, Orange, CA) and a vacuum pump (Edwards, Burgess Hill, England). The pervaporation setup used an analytical balance (Shimadzu, Kyoto, Japan) to weight the permeate collected in the liquid nitrogen trap. Temperature and absolute pressure were monitored in the solution reservoir and in the vacuum line, respectively. The duration

of each experiment was 2.5h: the first 0.5h was used to stabilize the system, and a trap was collected and weighted each subsequent hour to calculate water flux. To avoid membrane dehydration due to lack of solution in the porous side [208], the experiments were run with the active layer facing the vacuum side.

The system was controlled for membrane dehydration and scaling effects on CTA membrane by monitoring membrane opacity and performing experiments on both increasingly and decreasingly saline conditions. No visual changes were observed in the CTA membrane, such as opacity, that would indicate membrane dehydration. Additionally, there was no significant change in water flux due to increasing or decreasing salinity feed for a single membrane, suggesting there was no sodium chloride precipication and active area blockage.

The water permeability coefficient (A) was calculated using water flux J_W, water activity at the solution salt concentration a_w, the vapor pressure at the liquid temperature $P^w_{sat,l}$ and the pressure in the vapor line, $P^w_{sat,v}$, according to Eq. 4.7. Note that this pressure is equal to the water vapor pressure, since the system does not contain any other vapor, gas and sodium chloride is not volatile. A Pitzer correlation was used to calculated water activity [210, 211].

$$J_W = A(a_w P^w_{sat,f} - P^w_{sat,v}) \tag{4.7}$$

In this case, salt flux has no impact on water permeability since pervaporation is a vapor pressure driven process.

In contrast to the osmotic processes estimation, this fitting was performed with only one flux at a given concentration, but the experiments were performed at least in duplicates.

4.1.2 Results and Discussion

Osmotic processes estimation

In Figure 4.5, the estimated water permeability coefficient (A) for each set of experiments is presented as function of the average membrane concentration between the calculated feed ($c_{m,f}$) and sweep/draw ($c_{m,s}$) concentrations facing the membrane. These values were calculated using the bulk concentrations, mass transfer coefficient and structural parameter, according to Eq. 4.3 and Eq. 4.4, respectively. The procedure to calculate the standard deviation for the non-linear parameter estimation is described in Appendix B.

At very high salinities, the instrument sensitivity was inadequate for calculating FO parameters. This happened because this precision was dependent on the differences in water and salt fluxes for different salinities. But at high concentrations,

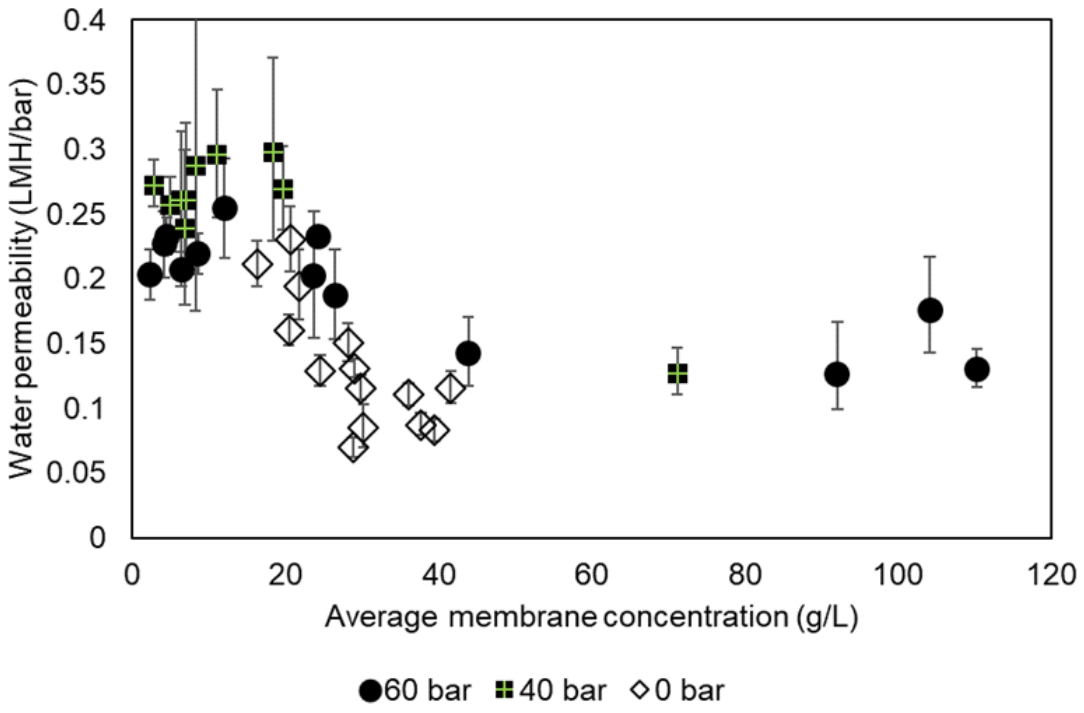

Figure 4.5: CTA Water permeability as a function of the average membrane concentration. The error bars are the 95% trust region limits keeping other parameters at their optimal value (Appendix B). Sets of experiments run at more than one pressure are plotted at the highest value.

even a difference of 20 g/L in draw solution would give a very small increase in FO water flux. As this increase was comparable or lower than the experimental error (around 0.15 LMH) and the magnitude of the water permeability was low, it was not possible to have enough parameter accuracy. This difficulty was also present in assisted processes parameter estimation, though to a lesser degre. This is the main reason why their error bars are substantial. Besides, another source of errors is the small cell active area.

Despite these errors, it is possible to note a decreasing trend in the water permeability with respect to an increase in the average concentration for all pressures tested. Non-pressurized experiments (FO) have even lower water permeability coefficients, although some of them are not statistically different from the pressurized systems. This effect might occur because higher pressures would favor the membrane compaction, and it could be less prone to deswelling. This decreasing permeability with increasing pressure was reported using polyamide membranes [138].

Regarding the uncertainties related to a possible underestimation on the mass transfer coefficient, it is worth mentioning that despite the laminar flow, there are turbulence entrance effects in the experimental module that would enhance the mass transfer when compared to theoretical values. Therefore, it is more likely for the mass transfer coefficient to be underestimated than overestimated. Also, as

the measured water fluxes are not high (mostly < 10 LMH), the influence of mass transfer in the exponential term is dampened, as described in Eq. 4.3. Thus, for very high salinities, the mass transfer coefficient would have to be severely underestimated if the water permeability coefficient was constant.

Although the salt fluxes were very low and difficult to measure, the B-values measured for RO processes and FO processes seem to follow a decreasing trend, but with a more drastic relative change than the water permeability coefficients. The described behavior is observed in Figure 4.6. The coefficient B was not calculated for all experiments due to very low salt fluxes and the lack of precision in conductivity measurements to detect changes during the experiments.

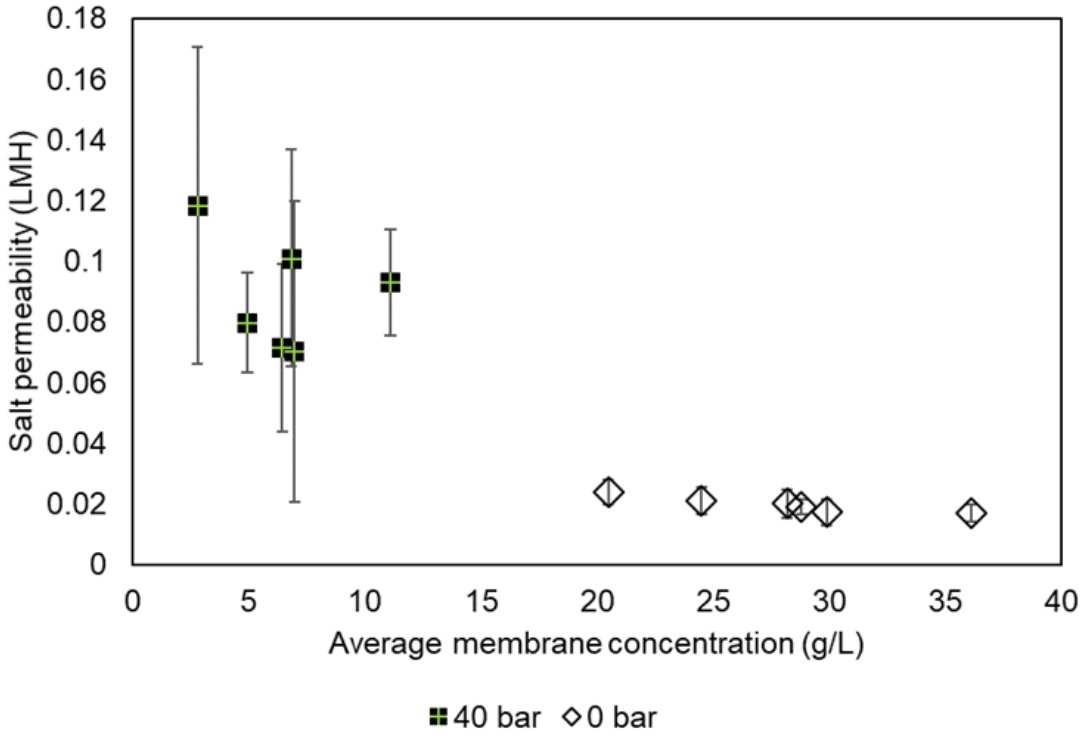

Figure 4.6: CTA Salt permeability coefficient as a function of average membrane concentration. The error bars are the 95% trust region limits keeping other parameters at their optimal value (Appendix B). Sets of experiments run at more than one pressure are plotted at the highest value.

To ensure the membranes were not deforming in high pressure, which would be a possible explanation for the trend observed in Figure 4.6, FO tests were performed with a few of the membrane samples tested at 40 bar. The salt fluxes for the compacted membrane were very similar to the ones obtained in experiments without previous pressurization, at similar salinity. However, due to the low number of points and $R^2 = 0.87$ for two of the FO points, the interpretation about salt permeability trend of decrease is suggested, but not stated.

It is sensible that the salt permeability coefficient has a sharper decrease because

sodium chloride has lower affinity with cellulose triacetate, as its transport resistance is higher than that of water. For an uncharged hydrogel, a decrease of 16% on salt permeability was reported when the feed salinity was increased from 0.01M to 1M [212]. The authors associated this effect to a reduction in the polymer water uptake, which is strongly related to both water and salt permeability for osmosis membranes [15]. In spite of that, Londsdale et al. [213] detected no changes in experimental salt sorption and diffusion coefficients for cellulose acetate in increasing salinity.

It is notable the A and B results trend seems to be exponential, as reported for salt permeability fit for an uncharged polymer [212]. A logarithmic behavior with salinity was assumed to explain flux decline as a concentration polarization effect only [126], but the observed decrease could be a combined effect of both CP and osmotic deswelling, since both appear to have logarithm/exponential behaviors [153].

An important point of interest to better understand the effects involved is the selectivity A/B. The selectivity tends to vary since A and B decay with salinity at different rates. However, at high salinities, A/B converges to a constant value, in this case, 4 bar^{-1}.

The reduction in both permeabilities suggests that the membrane could be facing an osmotic deswelling due to a high salinity environment. The feed and draw/sweep conditions could be reversibly dehydrating the membrane, and the water permeability would decrease due to a reduction in water content. The transport properties have been strongly associated with water uptake in commercial reverse osmosis membranes [12, 15].

Regarding its structure, cellulose triacetate membranes are generally made by phase inversion, with a dense skin and a porous support. In this case, it may be possible that the dense skin, or even an intermediate layer more susceptible to deswelling due to lower rigidity [12], is increasing its resistance and contributing to the overall permeability decrease. This is object of future work.

Although some RO membranes were found to not be susceptible to volumetric changes when exposed to saline water in comparison to DI-wet state, probably due to the high degree of crosslink [12], this does not necessarily mean that the water uptake is not changing, since solvent uptake has been reported as a faster process than volumetric swelling [214, 215].

Additionally, the structural parameter S, related to the porous support and mass transfer effects on sweep side, was also estimated using the experimental data and is presented in Figure 4.7.

Even though the estimated S values for a similar FTS CTA membrane in FO mode were low [216], there was an increase when the system was pressurized. It is likely that this occurred due to the compaction of the porous support in pressurized

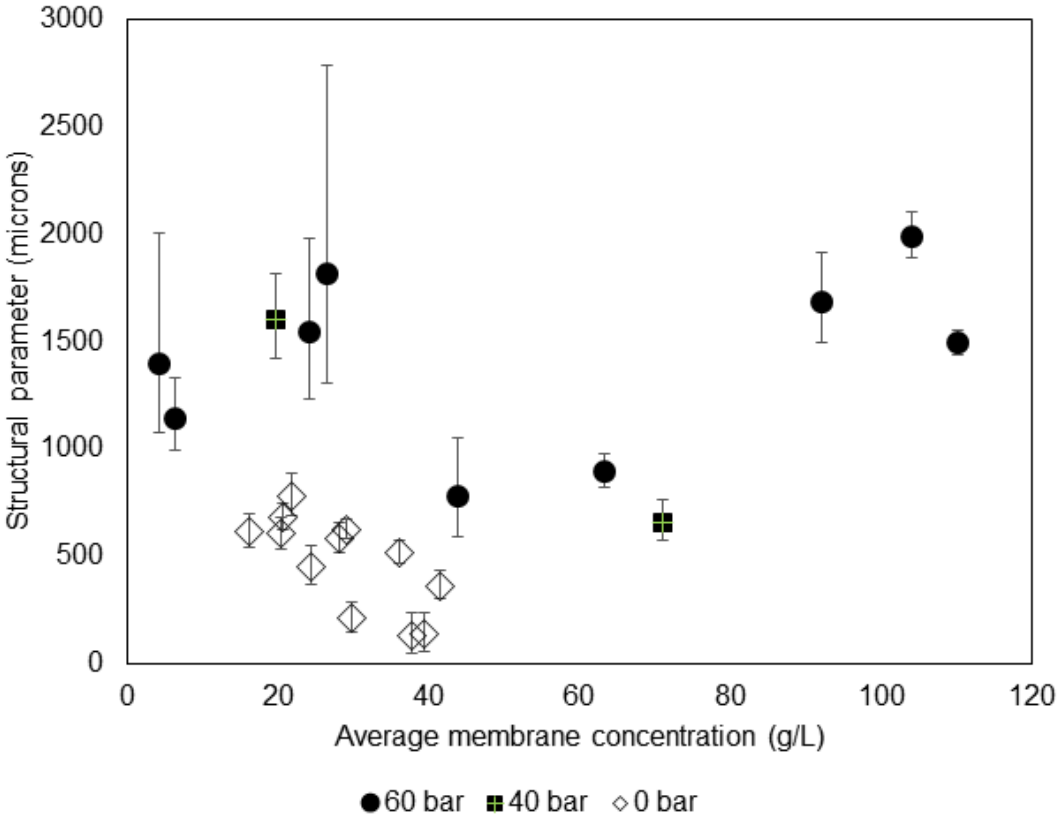

Figure 4.7: Calculated structural parameter for different sets of experiments. The error bars are the 95% trust region limits keeping other parameters at their optimal value (Appendix B). Sets of experiments run at more than one pressure are plotted at the highest value.

processes as PAO and OARO. Even though the thickness (δ) decrease would also decrease the structural parameter according to Eq. 4.8, the effects on porosity (ε) decrease and tortuosity (τ) increase are probably predominant. As this layer is usually in ultrafiltration porosity range, it would be also more prone to deformation caused by pressure.

Differently from [193], there was no clear tendency for the increase in S due to increasing pressure. A hypothesis to explain this behavior is the use of very finer spacers facing the porous support instead of coarser ones, since the use of finer spacers can change the pressure dependency [193].

$$S = \frac{\delta\tau}{\epsilon} \tag{4.8}$$

In the present case, S account not only for the membrane structural support, but also for external CP in the sweep/draw solution side. However, as the flowrate is fixed and the external supports did not deform substantially, it is not expected that the mass transfer resistance in this side varies.

It is important to note that the structural parameter was dependent on the

applied pressure. Therefore, although FO processes are generally the benchmark for the structural parameter in assisted processes such as OARO [141], they might not represent it accurately.

As the estimation for A and S was performed mostly from the same variable, the water flux, there is a strong correlation between these two parameters, presented in Figure 4.9. The calculated confidence regions show the non-linear behavior of the system in the studied range and the optimum point (least squares) for these parameters.

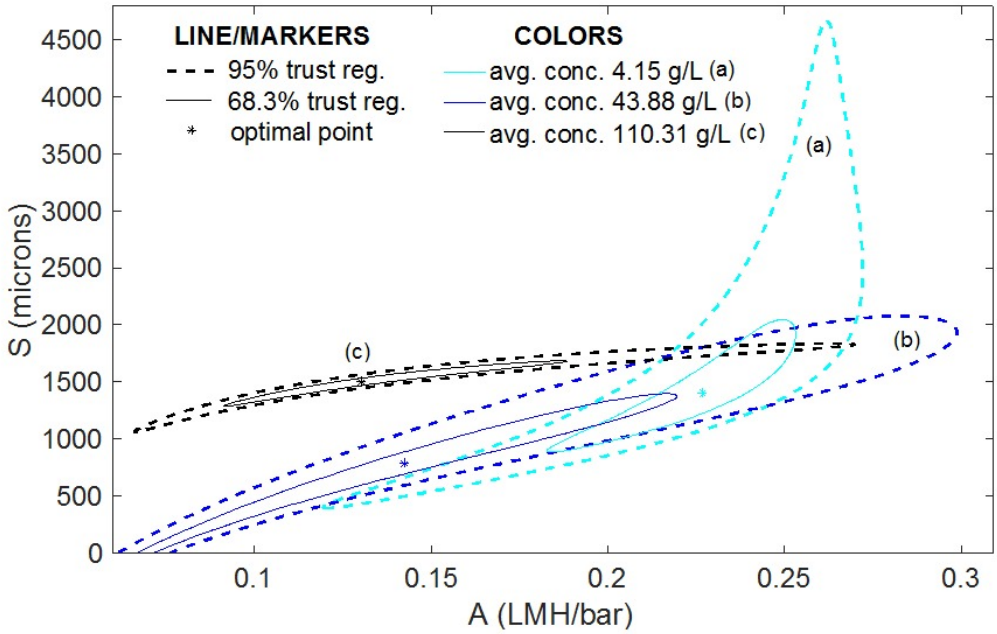

Figure 4.8: Water permeability and structural parameter trust region at 68.3% and 95% for PAO experiments. The asterisk represents the optimal solution for each set.

The trust regions intersections tend to be small at 68.3% (1 standard deviation), but significant at 95% (2 standard deviations). The higher the salinity difference between conditions, the further the trust regions are. As presented in Figure 4.7, for experiments at 60 bar, the S values were calculated to be in the same range. From the process point of view, it would make sense to have constant S values, since the pressure and flowrate are the same (mass transfer coefficient in the porous side would be similar). Thus, if we analyze the regions in Figure 4.8 at constant structural parameters, the water permeability would be significantly different at different concentrations, specially between the low salinity experiment and the medium /high salinity conditions. It makes sense for the medium and high salinity have a broader intersection, since the water permeability decreases at a lower rate with salt concentration, according to Figure 4.5.

In order to capture other possible explanations for the loss of performance in high salinity processes, as underestimations, a sensitivity analysis was performed for a PAO process. As B was maintained constant at RO-measured values, this parameter was varied to investigate if its value would change drastically A and S results. The values obtained are presented in Figure 4.9.

According to this figure, if B was significantly higher than the base case (a possible defect or bursting, for example), the water permeability would increase slightly, but not sufficiently to be compared to pure water values. Thus, an operational problem would not be enough to justify the decreasing trend at high salinities. A small increase also occurs for the structural parameter S. This behavior reinforces that S in pressurized systems is not equivalent to the value measured in low pressures, as in FO processes. Additionally, the feed mass transfer coefficient, set as a constant value in the previous calculations, was varied over a wider range to assess its impact on the same set of experiments studied in Figure 4.9 (b). In this case, k_f would have a weaker influence on the calculated A, but a stronger influence on calculated S. However, neither an underestimation nor an overestimation for the mass transfer coefficient would explain such behaviors and distinct parameters in low and high salinity experiments.

Pervaporation

In order to corroborate the previous results in a process with the same transport model, at virtually no pressure and lower interference from mass transfer resistances, pervaporation was used to calculate the water permeability coefficient.

The calculated water permeability also decreased with increasing salinity, as presented in Figure 4.10, even accounting for the water activity effect on the water vapor pressure in the liquid side (Eq. 4.7). It is also worth to mention that the hypothesis of negligible mass transfer in low fluxes was reasonable: In one example, when using exponential corrections similar to Eqs. 4.3 and 4.4, the feed concentration at the membrane is effectively the same as the bulk solution: 154 g/L instead of 150 g/L assuming $S = 400$ microns. Under these conditions, the water activity is virtually the same for both concentrations.

The values in the x-axis in Figure 4.10 are the average of the feed and permeate (assumed to be zero) bulk concentrations. A similar decreasing trend was also observed in pervaporation, supporting the results from the previous section in a process with a similar transport model.

To investigate the reversibility of water permeability decrease, a single of membrane was tested in high salinity after testing in DI water, and vice-versa. Experiments at similar salinities had similar fluxes independent on the order they were run, suggesting the effects are reversible.

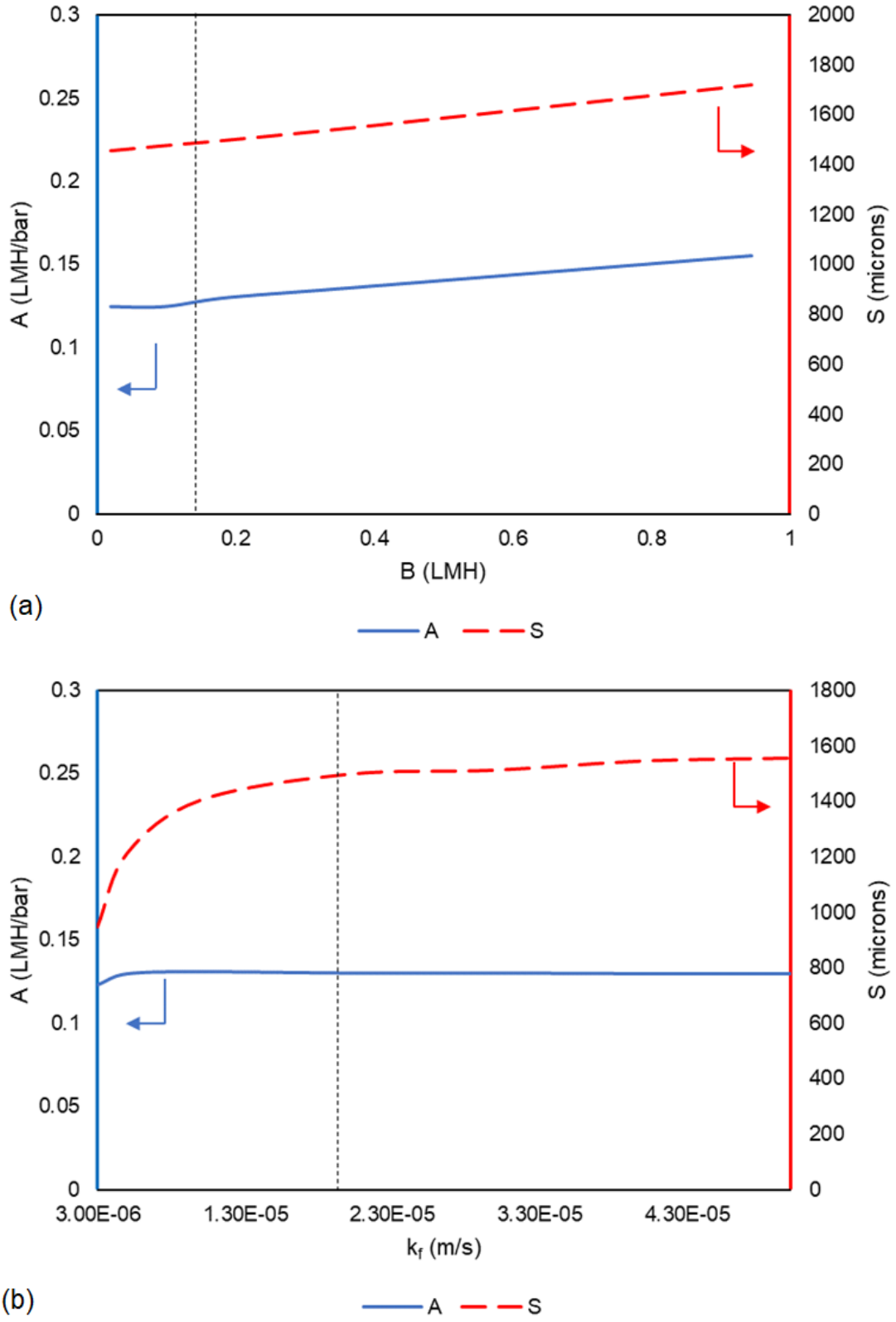

Figure 4.9: Water permeability and structural parameter as function of parameter B (a) and feed mass transfer coefficient (b). The dashed line represents the fixed value used in previous RO calculations.

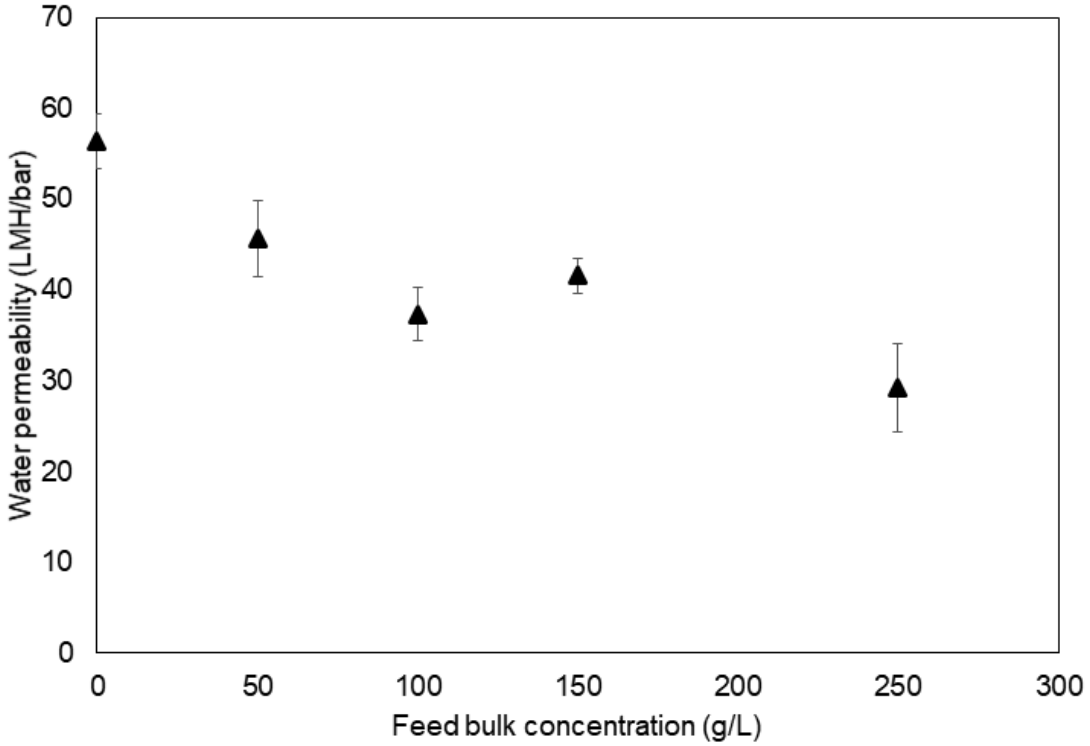

Figure 4.10: Pervaporation water permeability with feed bulk concentration. The error bars are the standard deviation for the measurements performed.

Another important point to note is that these results are also independent on salt permeation during pervaporation, since one side is corrected using water activity and the vacuum line has a measurement of the actual water vapor pressure used in Eq. 4.7.

The order of magnitude for A is not the same as the one from the previous section because the driving force, in this case, is vapor pressure, which affects differently the water chemical potential than hydraulic pressure.

It is interesting to mention temperature polarization did not play a role in this case due, mainly, to the low fluxes. The pure water and highest salinity cases were tested for temperature polarization, but the membrane temperature would be only 0.3°C below the bulk temperature at the conditions tested, which allows to assume this effect was negligible. Even if a very low heat transfer coefficient was found, as the permeate fluxes are much higher for the pure water case, the strongest effect in polarization would make the permeability calculated in this case to be more underestimated than in the brine case. In other words, the curve in Figure 4.10 would have a stronger decay with salinity if temperature polarization was considered.

When the water permeability is normalized by the pure water value (A_0) measured at similar conditions, the trend is similar to the one obtained via osmotic

processes, as shown in Figure 4.11.

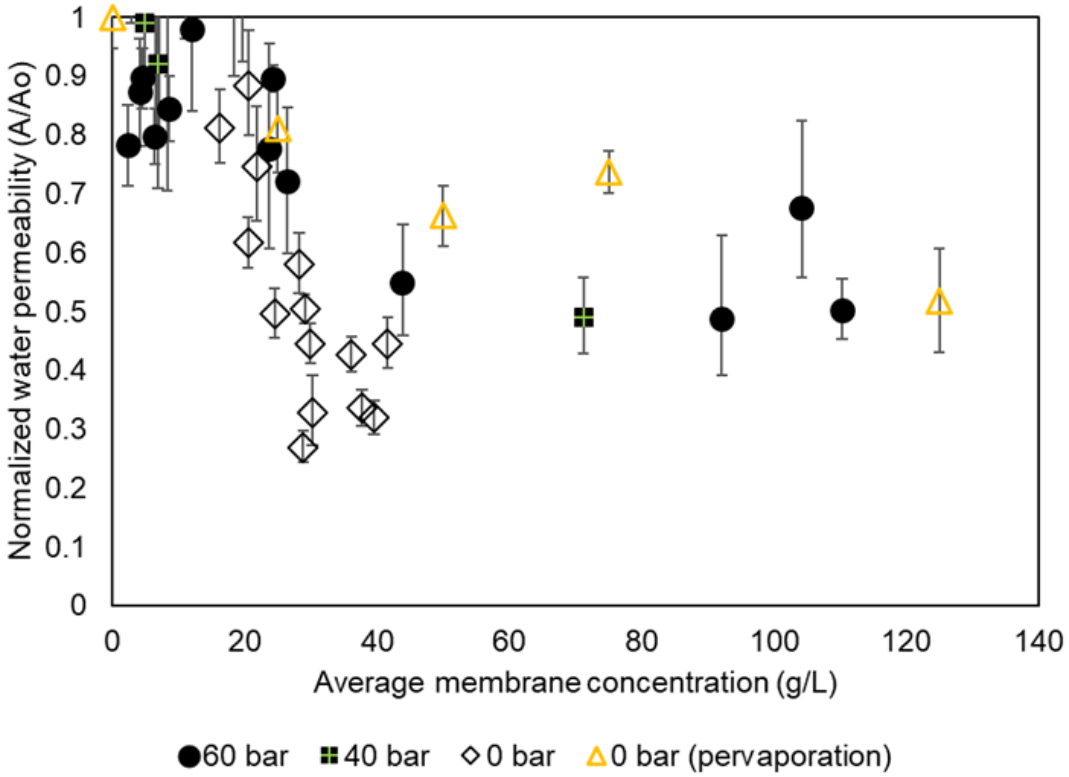

Figure 4.11: Normalized water permeability coefficient for osmotic processes and pervaporation processes.

As concentration polarization did not play an important role in the pervaporation test and the trend was very similar in both cases, it is unlikely that an underestimation in the mass transfer coefficient k_f or S had occurred. Again, the decrease in the fitted water permeability discussed in the previous section would not be sufficiently justified by uncertainties related to CP. Therefore, the data suggest the actual water permeability of the CTA membrane is changing, likely due to deswelling.

Impacts on osmotic processes

The observation that permeability changes in high salinity raises questions regarding the possible mechanisms involved. Although there are papers that reported deswelling and loss of permeabilities [12, 212], these studies were focused on nanofiltration membranes and hydrogels, respectively. While the former case involves a less rigid membrane, the latter is an extreme of high swelling. Freger [12] did not detect a significant change in high salinity for reverse osmosis polyamide membranes using AFM, which was attributed to the high rigidity of these membranes. Geise et al. [212] reported a decrease in the salt permeability coefficient for uncharged polymers, but an increase for charged hydrogels.

Conversely, there is a report of increasing permeability in high salinities for polyamide PRO membranes [156]. The authors linked the observed effects to possible charge screening effects and the decrease in the hydrated radius of ions in high salinity, which would increase the diffusivity through the polymer. However, as the reported pure water permeabilities for polyamide were increasing strongly in higher pressures, the membrane could be also susceptible to mechanical effects, as stretching/bursting, offsetting the results.

Also, it was reported that CTA membranes zeta potential in the pH range used in this work was slightly negative [147, 212, 216, 217] and similar to commercial polyamide reported values [147, 212, 216], although the permeabilities reported here did not follow the same pattern, nor the trend expected for charged polymers [212]. One possible explanation for this CTA behavior is its lack of ionizable groups [147], so it would behave more similarly to uncharged polymer. However, it should be mentioned that charged polymers with high ion capacity exchange were reported to have nearly neutral zeta potential at a wide range of pH [218]. Thus, zeta potential might not be representative of the bulk charge of the polymer, since it is an indirect measurement, nor the main reason for its permeabilities to change. A second point is that CTA membranes are substantially thicker than polyamide membranes. Therefore, while the latter may be more influenced by surface effects and charge due to ionizable groups, the former could be more prone to polymer bulk effects. Future research should focus on understanding these mechanisms and their relationship with membrane transport performance.

Another important takeaway is that the common employed assumptions on constant permeabilities could be invalid for high salinity and high pressure membrane processes. Thus, the range of testing conditions is crucial to faithfully represent real or expected operations and to allow an accurate techno-economic analysis.

4.2 Membrane physicochemical and structural properties

Face to the decrease of water and salt permeability detected in the earlier section, analytical techniques were investigated to verify the hypothesis of membrane deswelling. Due to sorption-diffusion mechanism be the most accepted for osmosis-based processes [100, 219], both bulk properties (mostly related to diffusion) and surface properties (mostly related to sorption) were investigated.

Structural investigation of RO membranes may use various techniques which may be correlated to physical entities, such as free volume for positron annihilation lifetime spectroscopy (PALS) [13, 219] or a characteristic dimension for small an-

gle neutron scattering (SANS) [220, 221]. Besides, thickness can be measured by techniques as atomic force microscopy (AFM) [12, 15, 37], in dry and liquid mode, and related to volumetric changes. AFM is also used for topographical imaging of membranes [37].

Surface affinity with water or saline solution can be investigated using contact angle [37]. Another important surface analytical method is Fourier transform infrared spectroscopy (FTIR). It can identify functional groups through specific vibrational signatures [221] and, thereby, detect relative water content in membranes [222, 223] or even thickness by membrane stacking [15].

Physicochemical properties as moisture content can also be quantified using thermogravimetric analysis (TGA) [223]. Another emerging technique for measuring moisture, swelling in liquid state, as well as fouling propensity is quartz crystal microbalance with dissipation (QCM-d) [224–227].

Due to equipment availability and suitability for liquid measurements, the techniques chosen for further studies were contact angle and QCM-d. Additionally, if there is deswelling which would cause a decrease in water permeability of roughly 50 %, it is estimated a volumetric water decrease of only 1-2 % according to Figure 4.12. Thus, techniques with high sensitivity are required.

4.2.1 Contact angle

The contact angle developed from a drop of water on a solid surface can be used as measurement of wetting or hydrophilicity [221]. For commercial polyamide membranes, it was reported the contact angle increased when the solution salinity increased from 10 mg/L to 35 g/L, suggesting the membrane wetting decreased [37].

Methodology

The captive bubble method was chosen to guarantee the commercial CTA membrane (FTS CTA, mentioned in the earlier section) would be hydrated during the whole analysis. Samples were stored overnight in ultrapure water and in a sodium chloride solution almost at saturation point (350 g/L). The solutions pH varied between 6 - 6.5. The wet membranes were quickly transferred to a custom-made cell, where they were fixed with tape in a way the selective layer would face the solution. A Rame-Hart goniometer was used.

Air was slowly released until a stable bubble was formed at the membrane surface. It is worth mentioning commercial polyamide membranes (SW30 - Dow) were also tested, but did not hold stable air bubbles, compromising their measurement. This happened probably because of the high interaction of water to this membrane [37], compatible to its extremely high water permeability [15].

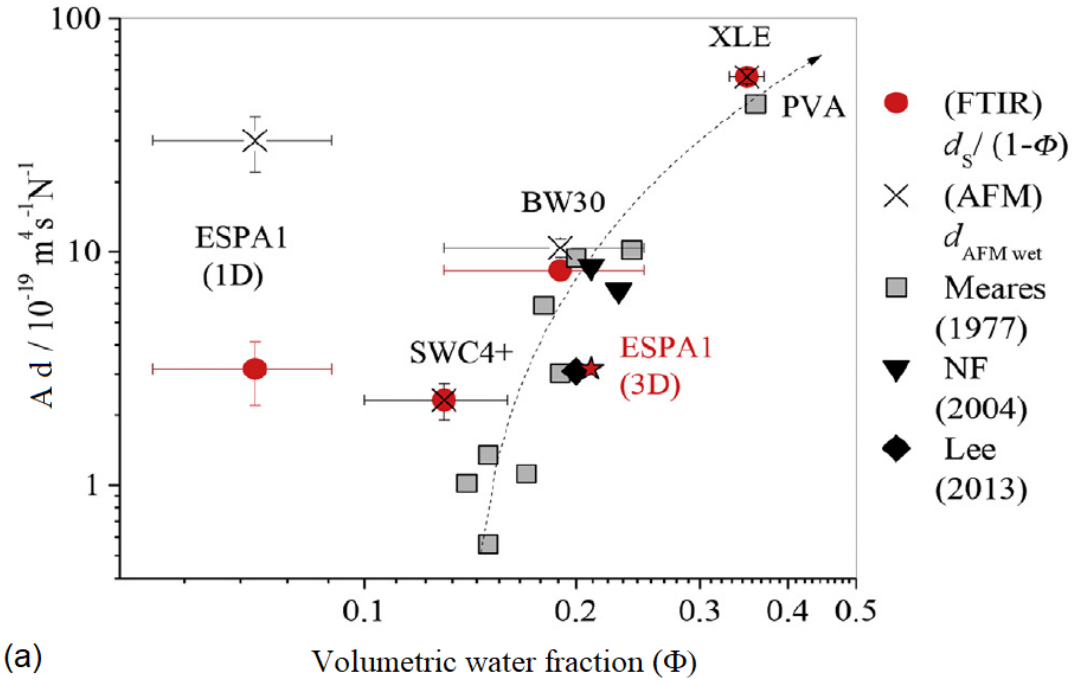

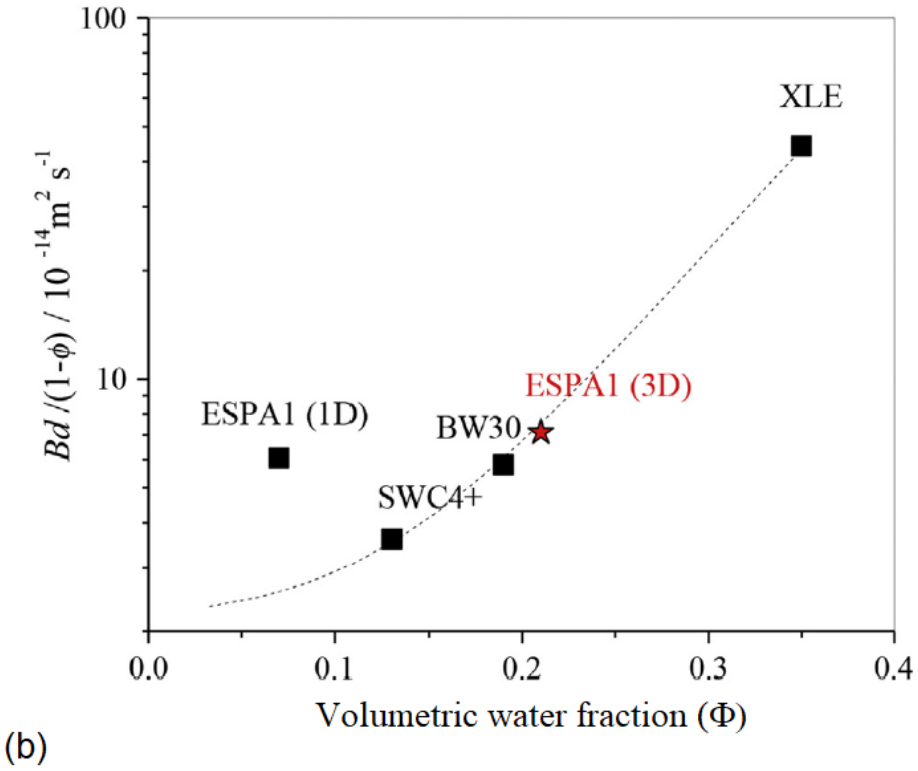

Figure 4.12: Intrinsic water (a) and salt permeabilities (b) as functions of volumetric water content [12–14]. ESPA1 and SWC4+ are commercial Hydranautics RO TFC membranes, while Dow is the manufacturer of BW30 and XLE. d corresponds to thickness. These figures were adapted from Drazevic *et al* [15], Copyright Elsevier (2013).

To ensure reprodutibility, for each of three different pieces of membrane used, three different spots were measured.

Results and discussion

The results are presented in Figures 4.13 and 4.14. There was no statistically significant increase in the contact angle for the salt solution, when compared to the DI water condition. One of the reasons for reported polyamide to increase its contact angle in saline solution is the higher influence of charge [37], which is more pronounced for polyamide than for CTA due to the presence of ionizable groups [145], although their zeta potential is similar in the studied pH range [147].

The insignificant effect of salt concentration on contact angle suggests CTA selective layer wetting is similar for low and high salinities.

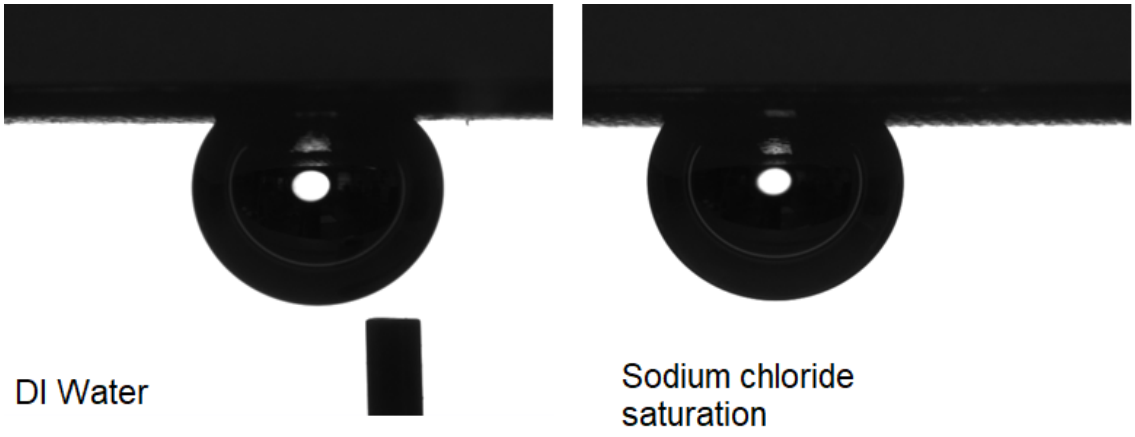

Figure 4.13: FTS CTA captive bubble contact angle in deionized water and in sodium chloride saturation point.

4.2.2 Quartz Crystal Microbalance with dissipation

The technique of QCM-d allows measurements of mass and viscoelastic/structural properties by the changes in the natural oscillating frequencies and the damping of oscillation (dissipation) of a sensor when voltage is applied [228, 229].

It can be used as a microbalance due to the relation of frequency shift with mass change in thin films [229]. In case of homogeneous, rigid films at low dissipation and no deviations in normalized frequency, a linear relation of frequency shift and mass can be applied [229, 230]. The frequency is normalized with its resonance or overtone number, which is defined as each odd harmonic resultant from the shear vibration of the crystal [229]. When the film is soft, the mass quantification follows other models [229]. Liquid solutions viscosity can also be calculated from QCM-d data [229].

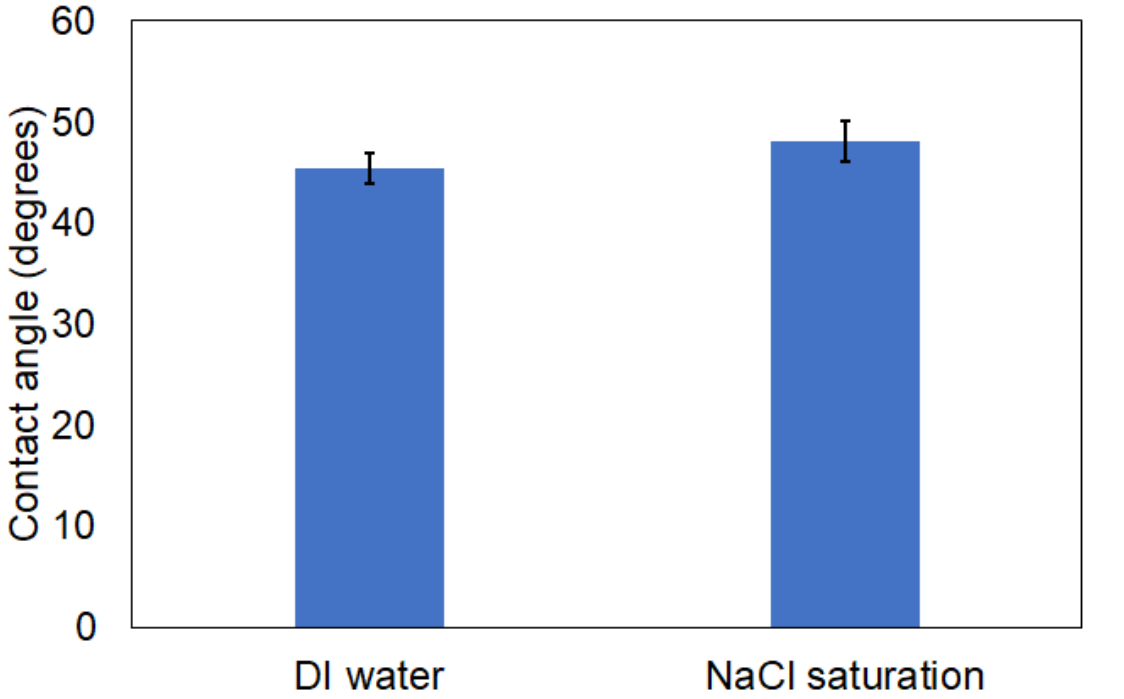

Figure 4.14: FTS CTA contact angle in deionized water and in sodium chloride saturation point.

In general, when the objective is to measure moisture content, polymer films are analyzed with air at different humidities, as sometimes with liquid water [224, 225, 227]. In case of fouling studies, a buffer with and without specific foulants is feed to the equipment, so the frequency and dissipation detected changes are associated purely to the presence of fouling agents [231, 232]. In case of saline solutions which may cause swelling/deswelling, frequency changes may be associated to mass uptake for CTA thin film.

Methodology

The preliminary experiments were performed using 5 MHz quartz sensors with gold electrodes and QSense E4 analyzer (Biolin Scientific). CTA with 43-44% acetyl content (Fisher-Scientific) was spin-coated on the sensors from 0.2-0.5%(m/v) solutions in extrapure 2,2,2-trifluorethanol (TFE; Fisher-Scientific). Before use, the crystals were cleaned three times sequentially with ultrapure water and ethanol and dried with nitrogen. After this, a spin-coater (Spin 150) program was used at 5000 rpm for 2 minutes only with solvent as an additional cleaning step. Using this same program, 3 μL of solution were dropped at once in the first 30 seconds of spinning. The films were dried overnight and tested for dissolution in water.

Before QCM-d analysis, films were spin in silica wafers and tested in AFM to check for their general aspect, homogeinety and approximate thickness made of 0.2%

CTA solution. A Nanoscope Dimension 3100 AFM in tapping mode was used for two distinct measurements: one for topology and one for thickness, in which a small scratch was made to roughly measure the depth to the silica surface. The data was interpreted using the software Gwyddion.

For QCM-d, the first QCM-d used three representative salinity concentrations: 0, 50 and 200 g/L and four crystals: two coated with the thin films and two control for bulk conditions control, fed in parallel configuration. The uncoated crystals are important to check for frequency changes caused by bulk solutions. In this firt run, a CTA solution of 0.2% was used to spin the films. The QCM-d system had its temperature controlled for 25°C.

Next, to compare frequency shift caused only by osmotic pressure difference, solutions of sodium chloride and sodium sulfate were investigated sequentially. As dissipation and frequency change may happen solely because of bulk solutions properties as density and viscosity [233], solutions of NaCl and Na_2SO_4 at equivalent $\sqrt{\rho\mu}$, but different osmotic pressures were used, according to Table 4.3. Besides, to increase the film response over the bulk response, thicker films (around 100 nm thickness, measured in AFM) were obtained using a 0.5% CTA solution. In this case, coated and non coated crystals were also applied.

In Table 4.3, each condition of fixed $\sqrt{\rho\mu}$ is reached for a calculated concentration of sodium chloride and sodium sulfate solutions, at different osmotic pressures.

Table 4.3: QCM-d experimental conditions at fixed $\sqrt{\rho\mu}$. The calculations used data from [19, 20].

Condition	1	2	3	4
$\sqrt{\rho\mu}$	0.949	0.962	0.998	1.058
NaCl (g/L)	10	20	50	100
π_{NaCl} (bar)	8.5	16.9	42.4	84.7
Na_2SO_4 (g/L)	4.7	10.7	28.9	59.2
$\pi_{Na_2SO_4}$ (bar)	2.5	5.6	15.1	31.0

Results and discussion

The AFM results, presented in Figures 4.15 and 4.16 reveal the films are thin, with approximate thickness of 25 nm and homogeneous and are suitable for QCM-d analysis. The average roughness is 189 pm, lower than reported polyamide values [37]. The low roughness of CTA supports its suitability for QCM-d analyses. It is also interesting to note there are nanopores, previously reported for CA membranes [234].

The results of the first QCM-d run are presented in Figure 4.17. The coated crystals behaved differently compared to the non-coated ones, suggesting the CTA

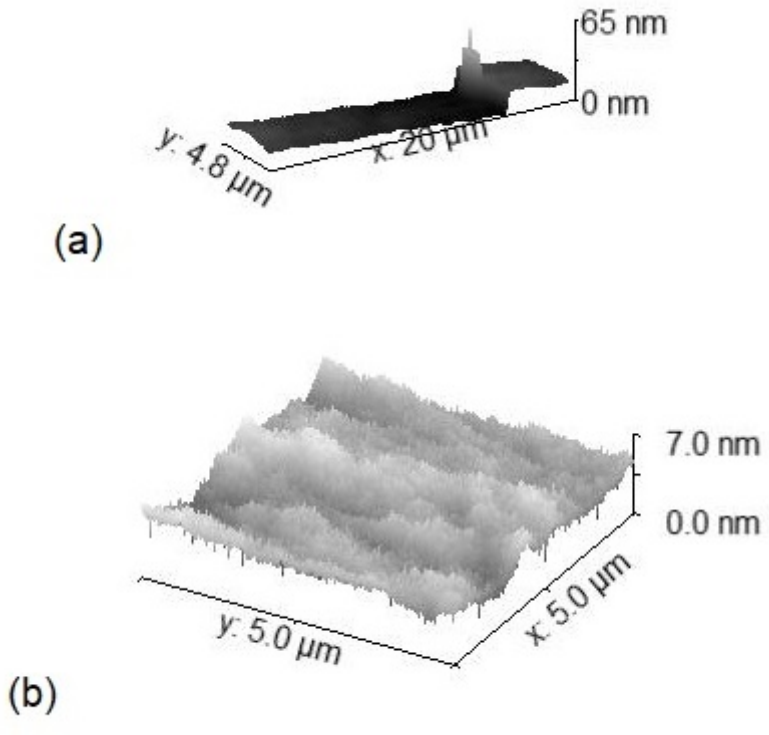

Figure 4.15: 3D view of CTA films made of 0.2% solution. (a) Thickness approximate measurement (b) General profile for the film depicted in Figure 4.16.

films changed properties when in contact with saline solutions. The frequency shift for control sensors happened due to changes in bulk solution properties (density and viscosity). If the control crystals are stablished as a baseline for solution effects, it is possible to see there is an increase of frequency shift of CTA-crystals for 50 g/L and 200 g/L conditions, when compared to their respective baseline. A decrease in frequency shift generally means film adsorption or absorption [225]. Therefore, an increase in the frequency shift could mean the film is deswelling and losing water mass.

However, as the changes caused by solution bulk properties (as density and viscosity) are high and the normalized frequency shifts for all overtones are not equivalent, it was not possible to obtain the hypothetical mass difference for each condition.

It was possible to amplify the normalized frequency shift for 50 g/L solution from the first (Figure 4.17) to the second run (condition 3 for NaCl in Figure 4.18) due to the increase of thickness. Besides, equivalent conditions of sodium chloride and sodium sulfate reached the same bulk effects, noted for the control frequency shifts. In this run, two control and one CTA-coated crystal were analyzed. The other CTA crystal presented an erratic behavior, likely related to its sensor, and

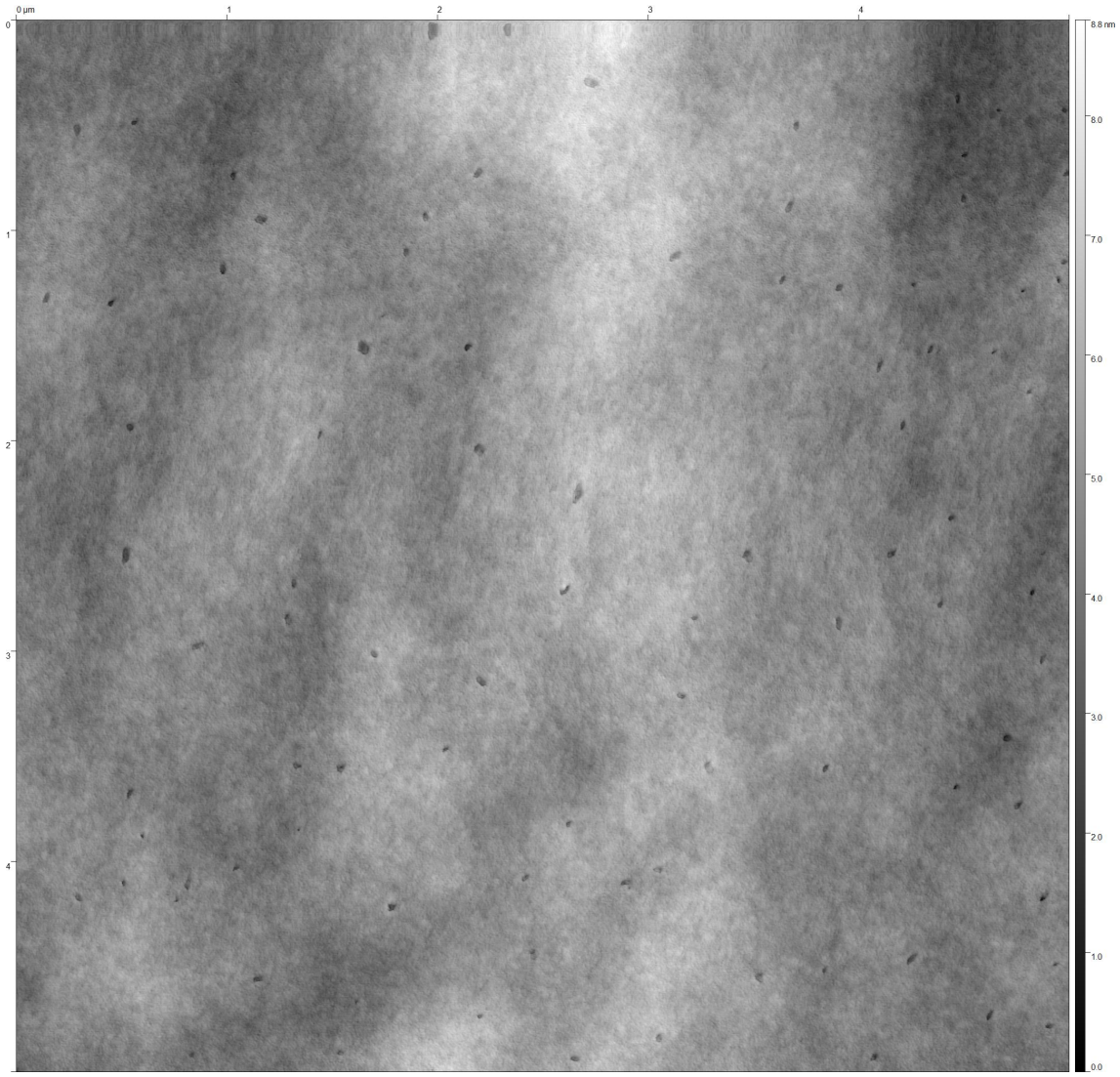

Figure 4.16: CTA film topology for a film made of 0.2% solution. The section is 5 x 5 μm^2.

was disconsidered.

At similar bulk effects, the higher the osmotic pressure, the greater the frequency shifts, supporting the hypothesis of deswelling. This behavior occurred more clearly for the highest concentration of each salt, that correspond to the highest osmotic pressure difference. However, the low salinities conditions are not replicated in sequential runs, suggesting there may be instabilities of the film (also evidenced by the final CTA shift) caused by successive changes of salinities or even for the solutions, caused by evaporation due to the long duration of experiment. It makes sense for the thicker films to detach more easily from the sensor, since they have more mass and may be more susceptible to stress caused by high ionic strength. In this run, the areal mass calculation was also not possible.

Thus, although there are signs the CTA films deswell when in contact with saline water, further studies in QCM-d and other techniques are needed to better

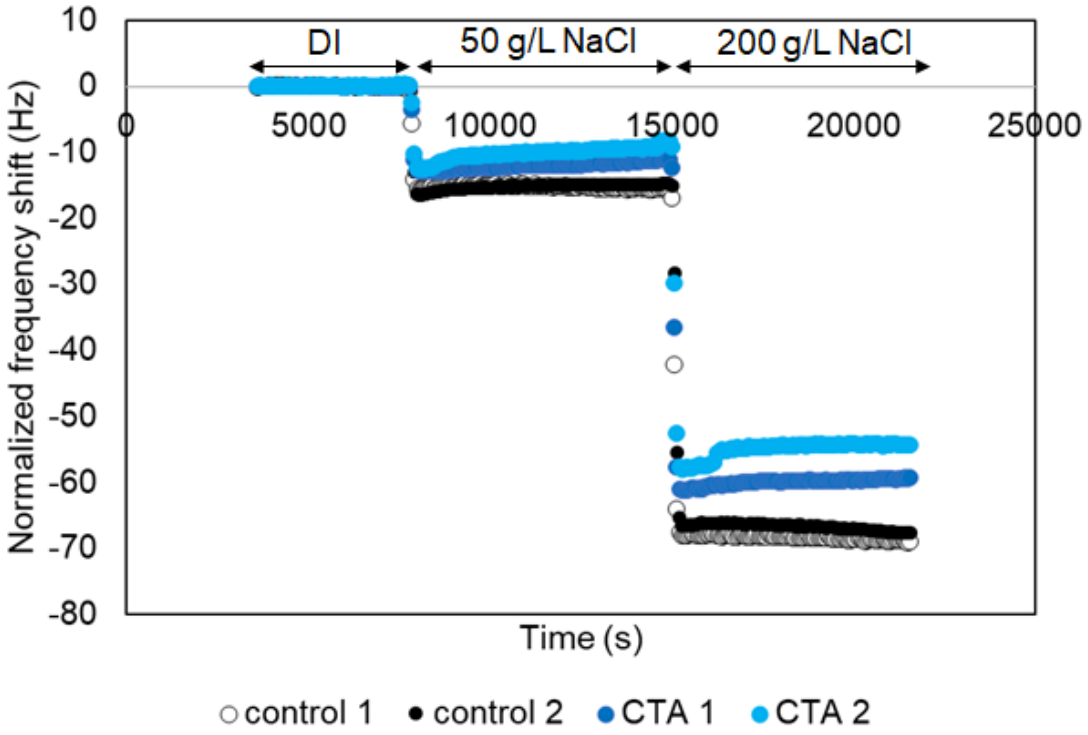

Figure 4.17: Normalized frequency shift (7th overtone) for the first run. The analysis was made with DI water, 50 g/L and 200 g/L sodium chloride solution.

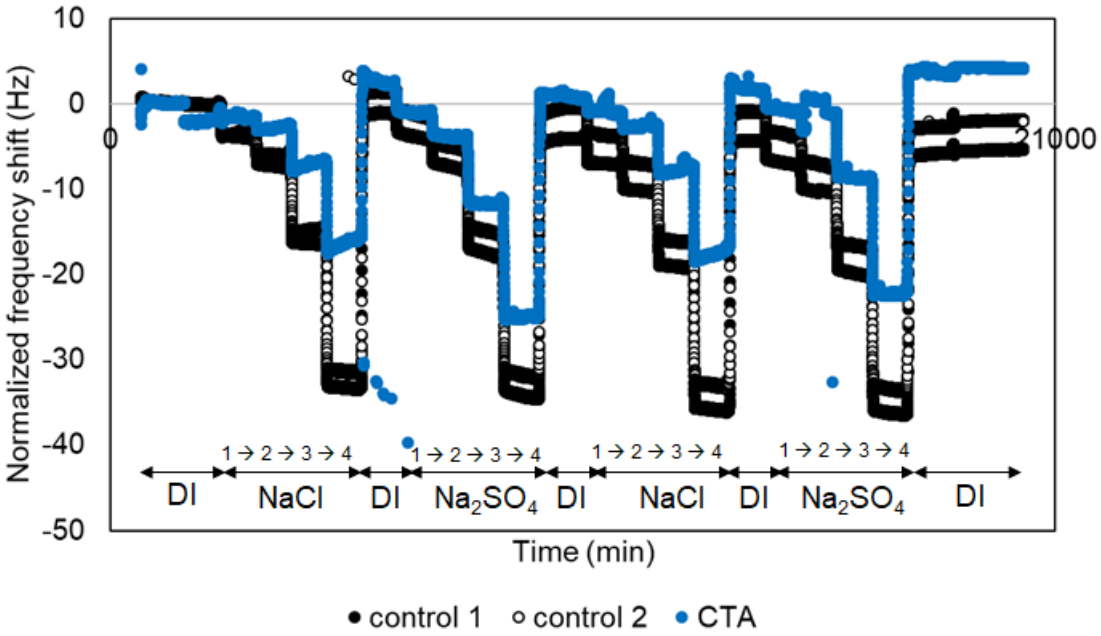

Figure 4.18: Normalized frequency shift (7th overtone) for the second run. The QCM-d analysis was performed with DI water, sodium chloride and sodium sulfate sequentially. Each number accounts for a condition, according to Table 4.3.

capture and quantify these effects. QCM-d is a very precise technique, but its application may demand intermediate investigations as delamination salinity and thickness thresholds, which may be material-dependent, and models to quantify areal mass for this case.

X-ray diffraction (XRD) was also tested aiming to associated peak angle shift to change in the polymer structure, but the results were not conclusive, even when correlating a dry and a DI-wet membrane samples, with known water content. This analysis is described in Appendix F.

4.3 Final remarks

The water permeability coefficient, as well as the salt permeability coefficient and the structural parameter were estimated for a commercial CTA membrane in variable pressure and salinity in three different labs. This work is the first to simultaneously evaluate these parameters in high salinity and pressure conditions. The results suggest CTA water permeability and salt permeability are decreasing with increasing salinity, even when concentration polarization is accounted for. Although pressure seems to have a small influence on the permeabilities, it changes significantly the structural parameter, likely due to compaction with effects on porosity decrease and tortuosity increase. Under- or overestimations of the salt permeability and mass transfer coefficient in the ranges studied cannot justify the estimated differences in water permeability.

Pervaporation tests also support the trend observed in osmotic processes under conditions in a process where concentration polarization and salt permeation have an insignificant influence. The behavior appears to be exponential, reaching a limit value after a given average salinity. The polymer is apparently behaving as an uncharged polymer which experiences an osmotic deswelling, although it possesses a small negative zeta potential. More work is necessary to completely understand and correlate the water uptake to the water permeability under variable salinity. The magnitude of the changes observed in this study highlights the importance of testing conditions on the membrane parameters estimation, as they are essential to a reliable techno-economical assessment.

QCM-d tests suggest CTA films deswell when exposed to high salinity solutions, supporting the hypothesis arised in osmotic and pervaporation experiments. However, further studies are required to properly quantify this effect over a range of concentrations and salts.

Chapter 5

Conclusions and future work

5.1 Conclusions

This work aimed to study novel RO-based technologies in cost-effective desalination of brines. It was verified through cost optimization that assisted reverse osmosis, even at high membrane cost, is cost and energy competitive, when compared to conventional processes as MVC. Besides, if the RO maximum pressure was set at lower values, the range of applicability of assisted processes would increase.

In the optimization, high structural parameters have influence on energy consumption and final cost, since the bulk driving force is used less effectively. Depeding on the S and A range and on the operating conditions, process variables as sweep concentration, flowrate and recovery may be used to damp the deleterious effect of increased support concentration polarization. Osmotically assisted reverse osmosis was found to be competitive to the conventional MVC process for wide range of membrane and economic parameters.

An experimental analysis was used to simultaneously determine the membrane parameters for different salinity and pressure conditions. Even considering parameter correlation, CP, uncertainties in mass transfer and different sorption-diffusion processes, there is a decrease of water and salt permeabilities with increasing average salinity. This decrease seems to follow a single trend regardless of the operating pressure, even considering concentration polarization, and was attributed to membrane deswelling caused by high ionic strength. Extreme pressures may turn processes as HPRO less prone to deswelling, since the membrane is more compacted.

Representative testing conditions should be seek when comparing membranes and processes in high salinity applications, since they have a strong influence on the final parameters. Moreover, simultaneous parameter estimation should be prioritized and sensitivity analysis should be applied to guarantee the parameter correlations are insignificant, specially for the pair water permeability and structural

parameter.

The RO-based process average working salinity is likely to be higher than 50 g/L, which seems to be the limiting salinity for the permeabilities decrease. Thus, for CTA membrane, the hypothesis of constant water and salt permeability in cost and energy optimization may be valid if considering the values measured at high salinity. When working in intermediate regions, the salinity effect in decreasing parameters must be considered.

Preliminary QCM-d results suggest CTA films may be facing a deswelling process, although detailed studies are needed to completely understand and correlate deswelling and permeabilities decrease. Additionally, the fact of the contact angle did not change under extreme salinity points to a predominance of diffusion effects over the sorption effects for CTA.

5.2 Suggestions for future work

With the objective of expanding the analyses discussed here, the following subjects are suggested for future studies:

- Cost comparison of desalination technologies at higher feed flowrates and more detailed salt composition.
- Expanding the transport properties analysis in high salinity for polyamide membranes and higher pressures.
- Study of the effect of different salts in the solution in the hypothetical deswelling and in scaling issues at high concentrations, as well as lab and pilot testing for the real produced or formation water.
- Investigation on a possible benefit of using higher temperatures in assisted processes, in order to increase the water permeability.
- Measurement and optimization of the head loss in the sweep side for industrial applications.
- Employment of analytical techniques as QCM-d to measure the water content and associate with transport properties under variable salinity.
- Development of membranes tailored for high salinity applications.

Bibliography

[1] BOUMA, A. T., LIENHARD, J. H. "Split-feed counterflow reverse osmosis for brine concentration", *Desalination*, v. 445, pp. 280–291, 2018.

[2] CHEN, X., YIP, N. Y. "Unlocking high-salinity desalination with cascading osmotically mediated reverse osmosis: Energy and operating pressure analysis", *Environmental science & technology*, v. 52, n. 4, pp. 2242–2250, 2018.

[3] THIEL, G. P., TOW, E. W., BANCHIK, L. D., et al. "Energy consumption in desalinating produced water from shale oil and gas extraction", *Desalination*, v. 366, pp. 94–112, 2015.

[4] BARTHOLOMEW, T. V., MEY, L., ARENA, J. T., et al. "Osmotically assisted reverse osmosis for high salinity brine treatment", *Desalination*, v. 421, pp. 3–11, 2017.

[5] MANICKAM, S. S., MCCUTCHEON, J. R. "Model thin film composite membranes for forward osmosis: Demonstrating the inaccuracy of existing structural parameter models", *Journal of membrane science*, v. 483, pp. 70–74, 2015.

[6] STRAUB, A. P., YIP, N. Y., ELIMELECH, M. "Raising the bar: Increased hydraulic pressure allows unprecedented high power densities in pressure-retarded osmosis", *Environmental Science & Technology Letters*, v. 1, n. 1, pp. 55–59, 2013.

[7] SONG, X., LIU, Z., SUN, D. D. "Energy recovery from concentrated seawater brine by thin-film nanofiber composite pressure retarded osmosis membranes with high power density", *Energy & Environmental Science*, v. 6, n. 4, pp. 1199–1210, 2013.

[8] CHOU, S., WANG, R., SHI, L., et al. "Thin-film composite hollow fiber membranes for pressure retarded osmosis (PRO) process with high power density", *Journal of membrane science*, v. 389, pp. 25–33, 2012.

[9] TIAN, M., WANG, R., GOH, K., et al. "Synthesis and characterization of high-performance novel thin film nanocomposite PRO membranes with tiered nanofiber support reinforced by functionalized carbon nanotubes", *Journal of membrane science*, v. 486, pp. 151–160, 2015.

[10] ZHANG, S., SUKITPANEENIT, P., CHUNG, T.-S. "Design of robust hollow fiber membranes with high power density for osmotic energy production", *Chemical Engineering Journal*, v. 241, pp. 457–465, 2014.

[11] BUI, N.-N., MCCUTCHEON, J. R. "Nanofiber supported thin-film composite membrane for pressure-retarded osmosis", *Environmental science & technology*, v. 48, n. 7, pp. 4129–4136, 2014.

[12] FREGER, V. "Swelling and Morphology of the Skin Layer of Polyamide Composite Membranes: An Atomic Force Microscopy Study", *Environmental Science & Technology*, v. 38, n. 11, pp. 3168–3175, 2004.

[13] LEE, J., DOHERTY, C. M., HILL, A. J., et al. "Water vapor sorption and free volume in the aromatic polyamide layer of reverse osmosis membranes", *Journal of Membrane Science*, v. 425-426, pp. 217–226, 2013.

[14] MEARES, P., STILLINGER, F., FRANKS, F., et al. "The mechanism of water transport in membranes", *Philosophical Transactions of the Royal Society of London. Series B, Biological Sciences*, v. 278, n. 959, pp. 113–150, 1977.

[15] DRAŽEVIĆ, E., KOŠUTIĆ, K., FREGER, V. "Permeability and selectivity of reverse osmosis membranes: Correlation to swelling revisited", *Water Research*, v. 49, pp. 444–452, 2014.

[16] TIBBETTS, P., BUCHANAN, I., GAWEL, L., et al. "A comprehensive determination of produced water composition". In: *Produced water*, Springer, pp. 97–112, 1992.

[17] DICKSON, A. G., GOYET, C. *Handbook of methods for the analysis of the various parameters of the carbon dioxide system in sea water. Version 2.* Relatório técnico, Oak Ridge National Lab., TN (United States), 1994.

[18] KENNISH, M. J. *Practical handbook of marine science.* Boca Raton, FL, CRC press, 2000.

[19] ABDULAGATOV, I., ZEINALOVA, A., AZIZOV, N. "Viscosity of aqueous Na2SO4 solutions at temperatures from 298 to 573 K and at pressures up to 40 MPa", *Fluid Phase Equilibria*, v. 227, n. 1, pp. 57–70, 2005.

[20] GONCALVES, F., KESTIN, J. "The viscosity of NaCl and KCl solutions in the range 25–50° C", *Berichte der Bunsengesellschaft fur physikalische Chemie*, v. 81, n. 11, pp. 1156–1161, 1977.

[21] JONES, E., QADIR, M., VAN VLIET, M. T., et al. "The state of desalination and brine production: A global outlook", *Science of the Total Environment*, v. 657, pp. 1343–1356, 2019.

[22] BUREK, P., SATOH, Y., FISCHER, G., et al. *Water futures and solution - Fast track initiative (Final report)*. Relatório técnico, International Institute for Applied Systems Analysis (IIASA), 2016.

[23] WORLD ECONOMIC FORUM. *The Global Risks Report 2019*. Relatório técnico, World Economic Forum, 2019.

[24] "Brazil may be the Owner of 20still Very Thirsty". 2016. Disponível em: <https://www.worldbank.org/en/news/feature/2016/07/27/how-brazil-managing-water-resources-new-report-scd>.

[25] "Fórum Mundial da Água: 1 em cada 6 cidades do Brasil corre risco hídrico". 2018. Disponível em: <https://g1.globo.com/df/distrito-federal/noticia/forum-mundial-da-agua-1-em-cada-6-cidades-do-brasil-corre-risco-hidrico.ghtml>.

[26] MARENGO, J. A., TORRES, R. R., ALVES, L. M. "Drought in Northeast Brazil—past, present, and future", *Theoretical and Applied Climatology*, pp. 1–12, 2016.

[27] CODAY, B. D., XU, P., BEAUDRY, E. G., et al. "The sweet spot of forward osmosis: treatment of produced water, drilling wastewater, and other complex and difficult liquid streams", *Desalination*, v. 333, n. 1, pp. 23–35, 2014.

[28] STANIC, J. "Unconventional oil and gas production drives trends in water management and treatment". In: *Water Treatment Insights-Oil and Gas Facilities*, pp. 10–15, 2014.

[29] CIHAN, A., BIRKHOLZER, J. T., BIANCHI, M. "Optimal well placement and brine extraction for pressure management during CO2 sequestration", *International Journal of Greenhouse Gas Control*, v. 42, pp. 175–187, 2015.

[30] ARENA, J. T., JAIN, J. C., LOPANO, C. L., et al. "Management and dewatering of brines extracted from geologic carbon storage sites", *International Journal of Greenhouse Gas Control*, v. 63, pp. 194–214, 2017.

[31] GREENLEE, L. F., LAWLER, D. F., FREEMAN, B. D., et al. "Reverse osmosis desalination: water sources, technology, and today's challenges", *Water research*, v. 43, n. 9, pp. 2317–2348, 2009.

[32] KHATIB, Z., VERBEEK, P. "Water to value-produced water management for sustainable field development of mature and green fields", *Journal of Petroleum Technology*, v. 55, n. 01, pp. 26–28, 2003.

[33] FIPPS, G. *Irrigation water quality standards and salinity management strategies*. Relatório técnico, Texas FARMER Collection, 2003.

[34] DAVENPORT, D. M., DESHMUKH, A., WERBER, J. R., et al. "High-Pressure Reverse Osmosis for Energy-Efficient Hypersaline Brine Desalination: Current Status, Design Considerations, and Research Needs", *Environmental Science & Technology Letters*, v. 5, n. 8, pp. 467–475, 2018.

[35] SEMIAT, R. "Energy issues in desalination processes", *Environmental science & technology*, v. 42, n. 22, pp. 8193–8201, 2008.

[36] PARK, K., KIM, D. Y., YANG, D. R. "Cost-based analysis about a newly designed two-staged reverse osmosis process with draw solute". In: *26th European Symposium on Computer Aided Process Engineering: Part A and B*, v. 38, p. 223. Elsevier, 2016.

[37] YANG, J., LEE, S., LEE, E., et al. "Effect of solution chemistry on the surface property of reverse osmosis membranes under seawater conditions", *Desalination*, v. 247, n. 1-3, pp. 148–161, 2009.

[38] BP. *BP Statistical Review of World Energy 68th edition*. Relatório técnico, British Petroleum, 2019.

[39] IGUNNU, E. T., CHEN, G. Z. "Produced water treatment technologies", *International Journal of Low-Carbon Technologies*, v. 9, n. 3, pp. 157–177, 2012.

[40] FAKHRU'L-RAZI, A., PENDASHTEH, A., ABDULLAH, L. C., et al. "Review of technologies for oil and gas produced water treatment", *Journal of hazardous materials*, v. 170, n. 2, pp. 530–551, 2009.

[41] SPE. "Challenges in reusing produced water". 2016. Disponível em: <https://www.spe.org/en/industry/challenges-in-reusing-produced-water/>.

[42] BRAZIL. "Resolution n. 393 CONAMA - Establishes provisions for the continuous release of processed water or water produced on oil and natural gas sea platforms and makes other provisions." 2007.

[43] REYNOLDS, R. R., KIKER, R. D. *Produced water and associated issues*. Relatório técnico, Oklahoma Geological Survey, 2003.

[44] BRAZIL. "Resolution n. 357 CONAMA - Establishes provisions for the classification of water bodies as well as environmental directives for their framework, establishes conditions and standards for effluent releases and makes other provisions." 2005.

[45] GOMES, A. P. P. *Gestão ambiental da água produzida na indústria de petróleo: Melhores práticas e experiências internacionais*. Tese de Mestrado, Universidade Federal do Rio de Janeiro, 2014.

[46] MINIER-MATAR, J., HUSSAIN, A., JANSON, A., et al. "Treatment of produced water from unconventional resources by membrane distillation". In: *IPTC 2014: International Petroleum Technology Conference - Doha, Qatar*, 2014.

[47] ROBINSON, D. "Oil and gas: treatment of produced waters for injection and reinjection", *Filtration+ Separation*, v. 50, n. 4, pp. 36–43, 2013.

[48] BRAZIL. "Resolution n. 396 CONAMA - Establishes provisions related to the classification and groundwater environmental directive framework and makes other provisions." 2008.

[49] BRAZIL. "Resolution n. 430 CONAMA - Provisions the conditions and standards of effluents and complements and changes Resolution 357 from March 17, 2005 issued by the National Environment Council (CONAMA)." 2011.

[50] JACOBI, P. R., CIBIM, J., LEÃO, R. D. S. "Crise hídrica na Macrometrópole Paulista e respostas da sociedade civil", *Estudos avançados*, v. 29, n. 84, pp. 27–42, 2015.

[51] ZANGAEVA, E. *Produced water challenges: influence of production chemicals on flocculation*. Tese de Mestrado, University of Stavanger, Norway, 2010.

[52] FINSTER, M., CLARK, C., SCHROEDER, J., et al. "Geothermal produced fluids: Characteristics, treatment technologies, and management options", *Renewable and Sustainable Energy Reviews*, v. 50, pp. 952–966, 2015.

[53] FIGUEREDO, K. S. L., MARTÍNEZ-HUITLE, C. A., TEIXEIRA, A. B. R., et al. "Study of produced water using hydrochemistry and multivariate statistics in different production zones of mature fields in the Potiguar Basin–Brazil", *Journal of Petroleum Science and Engineering*, v. 116, pp. 109–114, 2014.

[54] DÓREA, H. S., BISPO, J. R., ARAGÃO, K. A., et al. "Analysis of BTEX, PAHs and metals in the oilfield produced water in the State of Sergipe, Brazil", *Microchemical Journal*, v. 85, n. 2, pp. 234–238, 2007.

[55] MACKAY, D., SHIU, W.-Y. "The aqueous solubility and air-water exchange characteristics of hydrocarbons under environmental conditions", *Chemistry and physics of aqueous gas solutions. Princeton, NJ: Electrochemical Society*, pp. 93–110, 1975.

[56] BADER, M. "Seawater versus produced water in oil-fields water injection operations", *Desalination*, v. 208, n. 1-3, pp. 159–168, 2007.

[57] BEYCHOK, M. R. *Aqueous wastes from petroleum and petrochemical plants*. John Wiley & Sons, 1967.

[58] OLF. *Produced Water Chemistry and Treatment Study*. Relatório técnico, Norwegian Oil Industry Association, 1992.

[59] ANDRADE, V., ANDRADE, B., COSTA, B., et al. "Toxicity assessment of oil field produced water treated by evaporative processes to produce water to irrigation", *Water Science and Technology*, v. 62, n. 3, pp. 693–700, 2010.

[60] MUNIRASU, S., HAIJA, M. A., BANAT, F. "Use of membrane technology for oil field and refinery produced water treatment—A review", *Process safety and environmental protection*, v. 100, pp. 183–202, 2016.

[61] DORAN, G. F., CARINI, F. H., FRUTH, D. A., et al. "Evaluation of technologies to treat oil field produced water to drinking water or reuse quality". In: *SPE Annual Technical Conference and Exhibition, San Antonio, TX*. Society of Petroleum Engineers, 1997.

[62] TAO, F., CURTICE, S., HOBBS, R., et al. "Reverse osmosis process successfully converts oil field brine into freshwater", *Oil and Gas Journal;(United States)*, v. 91, n. 38, 1993.

[63] METZ, B., DAVIDSON, O., DE CONINCK, H., et al. *IPCC special report on carbon dioxide capture and storage*. Relatório técnico, Intergovernmental Panel on Climate Change, Geneva (Switzerland)., 2005.

[64] HOLLOWAY, S. "Underground sequestration of carbon dioxide—a viable greenhouse gas mitigation option", *Energy*, v. 30, n. 11-12, pp. 2318–2333, 2005.

[65] IEA. *Storing CO2 underground*. Relatório técnico, International Energy Agency, 2007.

[66] LIMA, V., EINLOFT, S., KETZER, J. M., et al. "CO2 Geological storage in saline aquifers: Paraná Basin caprock and reservoir chemical reactivity", *Energy Procedia*, v. 4, pp. 5377–5384, 2011.

[67] KETZER, J., MACHADO, C., ROCKETT, G., et al. *Brazilian Atlas of CO2 Capture and Geological Storage*. EDIPUCRS, 2015.

[68] COURT, B., CELIA, M. A., NORDBOTTEN, J. M., et al. "Active and integrated management of water resources throughout CO2 capture and sequestration operations", *Energy Procedia*, v. 4, pp. 4221–4229, 2011.

[69] DILMORE, R. M., ALLEN, D. E., JONES, J. R. M., et al. "Sequestration of dissolved CO2 in the Oriskany formation", *Environmental science & technology*, v. 42, n. 8, pp. 2760–2766, 2008.

[70] KNAUSS, K. G., JOHNSON, J. W., STEEFEL, C. I. "Evaluation of the impact of CO2, co-contaminant gas, aqueous fluid and reservoir rock interactions on the geologic sequestration of CO2", *Chemical geology*, v. 217, n. 3-4, pp. 339–350, 2005.

[71] LU, J., KHARAKA, Y. K., THORDSEN, J. J., et al. "CO2–rock–brine interactions in Lower Tuscaloosa Formation at Cranfield CO2 sequestration site, Mississippi, USA", *Chemical Geology*, v. 291, pp. 269–277, 2012.

[72] SOONG, Y., HOWARD, B. H., DILMORE, R. M., et al. "CO2/brine/rock interactions in Lower Tuscaloosa formation", *Greenhouse Gases: Science and Technology*, v. 00, pp. 1–14, 2016.

[73] RAUTENBACH, R., LINN, T. "High-pressure reverse osmosis and nanofiltration, a "zero discharge" process combination for the treatment of waste water with severe fouling/scaling potential", *Desalination*, v. 105, n. 1-2, pp. 63–70, 1996.

[74] EPA. *Effluent limitation guidelines, pretreatment standards and new source performance standards for the landfills point source category: Final Rule.* Relatório técnico, U.S. Environment Protection Agency, 2000.

[75] XIONG, R., WEI, C. "Current status and technology trends of zero liquid discharge at coal chemical industry in China", *Journal of Water Process Engineering*, v. 19, pp. 346–351, 2017.

[76] INDIA. "Environment (Protection) Fifth Amendment Rules". 2016.

[77] TONG, T., ELIMELECH, M. "The global rise of zero liquid discharge for wastewater management: drivers, technologies, and future directions", *Environmental science & technology*, v. 50, n. 13, pp. 6846–6855, 2016.

[78] ARTHUR, J. D., LANGHUS, B. G., PATEL, C. *Technical summary of oil & gas produced water treatment technologies.* Relatório técnico, All Consulting, LLC, Tulsa, OK, 2005.

[79] ÇAKMAKCE, M., KAYAALP, N., KOYUNCU, I. "Desalination of produced water from oil production fields by membrane processes", *Desalination*, v. 222, n. 1-3, pp. 176–186, 2008.

[80] CODAY, B. D., ALMARAZ, N., CATH, T. Y. "Forward osmosis desalination of oil and gas wastewater: Impacts of membrane selection and operating conditions on process performance", *Journal of Membrane Science*, v. 488, pp. 40–55, 2015.

[81] MELO, M., SCHLUTER, H., FERREIRA, J., et al. "Advanced performance evaluation of a reverse osmosis treatment for oilfield produced water aiming reuse", *Desalination*, v. 250, n. 3, pp. 1016–1018, 2010.

[82] DE ANDRADE, V. T. *Avaliação da toxicidade de água produzida tratada por processo evaporativo com a finalidade de reúso em solo.* Tese de Doutorado, Universidade Federal do Rio de Janeiro, 2009.

[83] HUTCHINGS, N. R., APPLETON, E. W., MCGINNIS, R. A., et al. "Making high quality frac water out of oilfield waste". In: *SPE Annual Technical Conference and Exhibition, Florence, Italy.* Society of Petroleum Engineers, 2010.

[84] BRAZIL. "Portaria n. º 2914, de 12 de dezembro de 2011. Estabelece os procedimentos e responsabilidades relativos ao controle e vigilância da qualidade da água para consumo humano e seu padrão de potabilidade, e dá outras providências". 2011.

[85] HAYES, T., ARTHUR, D. "Overview of emerging produced water treatment technologies". In: *11th Annual International Petroleum Environmental Conference, Albuquerque, NM*, 2004.

[86] MONDAL, S., WICKRAMASINGHE, S. R. "Produced water treatment by nanofiltration and reverse osmosis membranes", *Journal of Membrane Science*, v. 322, n. 1, pp. 162–170, 2008.

[87] ASME. "ASME Consensus Documents: Feedwater, Boiler Water, Steam, and Lay-up of Boiler Systems and Water Chemistry Monitoring". ASME, 2007.

[88] GRIMALDI, M. C., CASTRISANA, W. J., TOLFO, F. C., et al. "Produced Water Reuse for Production of Chemicals". In: *SPE International Conference on Health, Safety and Environment in Oil and Gas Exploration and Production, Rio de Janeiro, Brazil*. Society of Petroleum Engineers, 2010.

[89] NASIRI, M., JAFARI, I. "Produced water from oil-gas plants: A short review on challenges and opportunities", *Periodica Polytechnica Chemical Engineering*, v. 61, n. 2, pp. 73–81, 2017.

[90] WATSON, I. C., MORIN, O., HENTHORNE, L. *Desalting handbook for planners*. Relatório técnico, United States - Department of the Interior - Bureau of Reclamation, 2003.

[91] ETTOUNEY, H. M., EL-DESSOUKY, H. T., FAIBISH, R. S., et al. "Evaluating the economics of desalination", *Chemical Engineering Progress*, v. 98, n. 12, pp. 32–39, 2002.

[92] TZEN, E., PAPAPETROU, M. "Promotion of renewable energy sources for water production through desalination", *Desalination and Water Treatment*, v. 39, n. 1-3, pp. 302–307, 2012.

[93] DARWISH, M., AL ASFOUR, F., AL-NAJEM, N. "Energy consumption in equivalent work by different desalting methods: case study for Kuwait", *Desalination*, v. 152, n. 1-3, pp. 83–92, 2003.

[94] BLANK, J., TUSEL, G., NISANC, S. "The real cost of desalted water and how to reduce it further", *Desalination*, v. 205, n. 1-3, pp. 298–311, 2007.

[95] SHAFFER, D. L., ARIAS CHAVEZ, L. H., BEN-SASSON, M., et al. "Desalination and reuse of high-salinity shale gas produced water: drivers, technologies, and future directions", *Environmental science & technology*, v. 47, n. 17, pp. 9569–9583, 2013.

[96] VEZA, J. "Mechanical vapour compression desalination plants—A case study", *Desalination*, v. 101, n. 1, pp. 1–10, 1995.

[97] SCHUHLI, J. B. *Previsão de equilíbrio líquido vapor de misturas contendo água-hidrocarboneto-sal*. Tese de Mestrado, Dissertação de Mestrado em Engenharia Química, Rio de Janeiro-RJ, Brasil, 2007.

[98] JING-YING, M., ZENG-YI, M., JIAN-HUA, Y., et al. "Development of an evaporation crystallizer for desalination of alkaline organic wastewater before incineration", *Journal of Zhejiang University-Science A*, v. 6, n. 10, pp. 1100–1106, 2005.

[99] HEINS, W., OTHERS. "Is a paradigm shift in produced water treatment technology occurring at SAGD facilities?" *Journal of Canadian Petroleum Technology*, v. 49, n. 01, pp. 10–15, 2010.

[100] BAKER, R. W. *Membrane technology and applications*. John Wiley & Sons, 2012.

[101] AL-OBAIDANI, S., CURCIO, E., MACEDONIO, F., et al. "Potential of membrane distillation in seawater desalination: thermal efficiency, sensitivity study and cost estimation", *Journal of Membrane Science*, v. 323, n. 1, pp. 85–98, 2008.

[102] ALKHUDHIRI, A., DARWISH, N., HILAL, N. "Produced water treatment: application of air gap membrane distillation", *Desalination*, v. 309, pp. 46–51, 2013.

[103] MACEDONIO, F., ALI, A., POERIO, T., et al. "Direct contact membrane distillation for treatment of oilfield produced water", *Separation and Purification Technology*, v. 126, pp. 69–81, 2014.

[104] ZHANG, X., GUO, Z., ZHANG, C., et al. "Exploration and optimization of two-stage vacuum membrane distillation process for the treatment of saline wastewater produced by natural gas exploitation", *Desalination*, v. 385, pp. 117–125, 2016.

[105] SINGH, D., SIRKAR, K. K. "Desalination of brine and produced water by direct contact membrane distillation at high temperatures and pressures", *Journal of Membrane Science*, v. 389, pp. 380–388, 2012.

[106] KIM, J., KWON, H., LEE, S., et al. "Membrane distillation (MD) integrated with crystallization (MDC) for shale gas produced water (SGPW) treatment", *Desalination*, v. 403, pp. 172–178, 2017.

[107] LIU, Q., LIU, C., ZHAO, L., et al. "Integrated forward osmosis-membrane distillation process for human urine treatment", *Water research*, v. 91, pp. 45–54, 2016.

[108] SWAMINATHAN, J., NAYAR, K. G., LIENHARD V, J. H. "Mechanical vapor compression—Membrane distillation hybrids for reduced specific energy consumption", *Desalination and Water Treatment*, v. 57, n. 55, pp. 26507–26517, 2016.

[109] EL-SAYED, N. A., BARRUFET, M. A., EL-HALWAGI, M. M. "An integrated approach for incorporating thermal membrane distillation in treating water in heavy oil recovery using SAGD", *Journal of Unconventional Oil and Gas Resources*, v. 12, pp. 6–14, 2015.

[110] TAVAKKOLI, S., LOKARE, O. R., VIDIC, R. D., et al. "A techno-economic assessment of membrane distillation for treatment of Marcellus shale produced water", *Desalination*, v. 416, pp. 24–34, 2017.

[111] LOKARE, O. R., TAVAKKOLI, S., WADEKAR, S., et al. "Fouling in direct contact membrane distillation of produced water from unconventional gas extraction", *Journal of Membrane Science*, v. 524, pp. 493–501, 2017.

[112] ONISHI, V. C., CARRERO-PARRENO, A., REYES-LABARTA, J. A., et al. "Desalination of shale gas produced water: A rigorous design approach for zero-liquid discharge evaporation systems", *Journal of cleaner production*, v. 140, pp. 1399–1414, 2017.

[113] FRITZMANN, C., LÖWENBERG, J., WINTGENS, T., et al. "State-of-the-art of reverse osmosis desalination", *Desalination*, v. 216, n. 1-3, pp. 1–76, 2007.

[114] AL-FURAIJI, M. *Hyper-saline produced water treatment for beneficial use.* Tese de Doutorado, University of Twente, 2016.

[115] ZHANG, S., WANG, P., FU, X., et al. "Sustainable water recovery from oily wastewater via forward osmosis-membrane distillation (FO-MD)", *water research*, v. 52, pp. 112–121, 2014.

[116] MCGINNIS, R. L., HANCOCK, N. T., NOWOSIELSKI-SLEPOWRON, M. S., et al. "Pilot demonstration of the NH 3/CO 2 forward osmosis desalination process on high salinity brines", *Desalination*, v. 312, pp. 67–74, 2013.

[117] MINIER-MATAR, J., HUSSAIN, A., JANSON, A., et al. "Application of forward osmosis for reducing volume of produced/Process water from oil and gas operations", *Desalination*, v. 376, pp. 1–8, 2015.

[118] LINARES, R. V., LI, Z., YANGALI-QUINTANILLA, V., et al. "Life cycle cost of a hybrid forward osmosis–low pressure reverse osmosis system for seawater desalination and wastewater recovery", *Water research*, v. 88, pp. 225–234, 2016.

[119] DUONG, P. H., CHUNG, T.-S. "Application of thin film composite membranes with forward osmosis technology for the separation of emulsified oil–water", *Journal of Membrane Science*, v. 452, pp. 117–126, 2014.

[120] HICKENBOTTOM, K. L., HANCOCK, N. T., HUTCHINGS, N. R., et al. "Forward osmosis treatment of drilling mud and fracturing wastewater from oil and gas operations", *Desalination*, v. 312, pp. 60–66, 2013.

[121] BELL, E. A., POYNOR, T. E., NEWHART, K. B., et al. "Produced water treatment using forward osmosis membranes: Evaluation of extended-time performance and fouling", *Journal of Membrane Science*, v. 525, pp. 77–88, mar. 2017.

[122] MALTOS, R. A., REGNERY, J., ALMARAZ, N., et al. "Produced water impact on membrane integrity during extended pilot testing of forward osmosis–reverse osmosis treatment", *Desalination*, v. 440, pp. 99–110, 2018.

[123] HAN, G., DE WIT, J. S., CHUNG, T.-S. "Water reclamation from emulsified oily wastewater via effective forward osmosis hollow fiber membranes under the PRO mode", *Water research*, v. 81, pp. 54–63, 2015.

[124] BUI, N.-N., ARENA, J. T., MCCUTCHEON, J. R. "Proper accounting of mass transfer resistances in forward osmosis: Improving the accuracy of model predictions of structural parameter", *Journal of membrane science*, v. 492, pp. 289–302, 2015.

[125] ACHILLI, A., CATH, T. Y., CHILDRESS, A. E. "Selection of inorganic-based draw solutions for forward osmosis applications", *Journal of membrane science*, v. 364, n. 1-2, pp. 233–241, 2010.

[126] MCCUTCHEON, J. R., MCGINNIS, R. L., ELIMELECH, M. "Desalination by ammonia–carbon dioxide forward osmosis: influence of draw and feed solution concentrations on process performance", *Journal of membrane science*, v. 278, n. 1-2, pp. 114–123, 2006.

[127] PHUNTSHO, S., SHON, H. K., HONG, S., et al. "A novel low energy fertilizer driven forward osmosis desalination for direct fertigation: evaluating the performance of fertilizer draw solutions", *Journal of Membrane Science*, v. 375, n. 1-2, pp. 172–181, 2011.

[128] ANSARI, A. J., HAI, F. I., GUO, W., et al. "Selection of forward osmosis draw solutes for subsequent integration with anaerobic treatment to facilitate resource recovery from wastewater", *Bioresource technology*, v. 191, pp. 30–36, 2015.

[129] ZHAO, P., GAO, B., XU, S., et al. "Polyelectrolyte-promoted forward osmosis process for dye wastewater treatment–Exploring the feasibility of using polyacrylamide as draw solute", *Chemical Engineering Journal*, v. 264, pp. 32–38, 2015.

[130] AKTHER, N., SODIQ, A., GIWA, A., et al. "Recent advancements in forward osmosis desalination: a review", *Chemical Engineering Journal*, v. 281, pp. 502–522, 2015.

[131] ARENA, J. T., MCCLOSKEY, B., FREEMAN, B. D., et al. "Surface modification of thin film composite membrane support layers with polydopamine: Enabling use of reverse osmosis membranes in pressure retarded osmosis", *Journal of Membrane Science*, v. 375, n. 1-2, pp. 55–62, jun. 2011.

[132] GOH, P. S., ISMAIL, A. F., NG, B. C., et al. "Recent Progresses of Forward Osmosis Membranes Formulation and Design for Wastewater Treatment", *Water*, v. 11, n. 10, pp. 2043, 2019.

[133] QIU, M., WANG, J., HE, C. "A stable and hydrophilic substrate for thin-film composite forward osmosis membrane revealed by in-situ cross-linked polymerization", *Desalination*, v. 433, pp. 1–9, 2018.

[134] PUGUAN, J. M. C., KIM, H.-S., LEE, K.-J., et al. "Low internal concentration polarization in forward osmosis membranes with hydrophilic crosslinked PVA nanofibers as porous support layer", *Desalination*, v. 336, pp. 24–31, 2014.

[135] GMBH, O. M. S. "HIGH PRESSURE Reverse Osmosis". Disponível em: <http://www.osmo-membrane.de/en/products/chemistry/high-pressure-reverse-osmosis.html>.

[136] GUNTHER, R., PERSCHALL, B., REESE, D., et al. "Engineering for high pressure reverse osmosis", *Journal of Membrane Science*, v. 121, n. 1, pp. 95–107, 1996.

[137] DOW. "DOW Specialty Membranes". http://www.dow.com/en-us/markets-and-solutions/products/DOWSpecialtyMembranes/DOWSpecialtyMembranesXUS180808UltraHighPressureROElement, . Acessed on May 18th 2017.

[138] MCGOVERN, R. K., MCCONNON, D., LIENHARD V, J. H. "The effect of very high hydraulic pressure on the permeability and salt rejection of reverse osmosis membranes". In: *IDA World Congress on Desalination and Water Reuse, San Diego, CA*. International Desalination Association, 2015.

[139] LIN, S., ELIMELECH, M. "Staged reverse osmosis operation: Configurations, energy efficiency, and application potential", *Desalination*, v. 366, pp. 9–14, 2015.

[140] WARSINGER, D. M., TOW, E. W., NAYAR, K. G., et al. "Energy efficiency of batch and semi-batch (CCRO) reverse osmosis desalination", *Water research*, v. 106, pp. 272–282, 2016.

[141] KIM, J., KIM, J., KIM, J., et al. "Osmotically enhanced dewatering-reverse osmosis (OED-RO) hybrid system: Implications for shale gas produced water treatment", *Journal of membrane science*, v. 554, pp. 282–290, 2018.

[142] BARTHOLOMEW, T. V., SIEFERT, N. S., MAUTER, M. S. "Cost optimization of osmotically assisted reverse osmosis", *Environmental science & technology*, v. 52, n. 20, pp. 11813–11821, 2018.

[143] LI, D., YAN, Y., WANG, H. "Recent advances in polymer and polymer composite membranes for reverse and forward osmosis processes", *Progress in polymer science*, v. 61, pp. 104–155, 2016.

[144] HOMAEIGOHAR, S., ELBAHRI, M. "Graphene membranes for water desalination", *NPG Asia Materials*, v. 9, n. 8, pp. e427, 2017.

[145] CODAY, B. D., HOPPE-JONES, C., WANDERA, D., et al. "Evaluation of the transport parameters and physiochemical properties of forward osmosis membranes after treatment of produced water", *Journal of Membrane Science*, v. 499, pp. 491–502, fev. 2016.

[146] TIRAFERRI, A., ELIMELECH, M. "Direct quantification of negatively charged functional groups on membrane surfaces", *Journal of Membrane Science*, v. 389, pp. 499–508, 2012.

[147] CODAY, B. D., LUXBACHER, T., CHILDRESS, A. E., et al. "Indirect determination of zeta potential at high ionic strength: Specific application to semipermeable polymeric membranes", *Journal of membrane science*, v. 478, pp. 58–64, 2015.

[148] PARK, K., YANG, D. R., OTHERS. "Cost-based feasibility study and sensitivity analysis of a new draw solution assisted reverse osmosis (DSARO) process for seawater desalination", *Desalination*, v. 422, pp. 182–193, 2017.

[149] GEISE, G. M., PAUL, D. R., FREEMAN, B. D. "Fundamental water and salt transport properties of polymeric materials", *Progress in Polymer Science*, v. 39, n. 1, pp. 1–42, 2014.

[150] LOEB, S. "Sea water demineralization by means of an osmotic membrane", *Adv Chem Ser*, v. 38, pp. 117–132, 1962.

[151] ZHANG, H., GEISE, G. M. "Modeling the water permeability and water/salt selectivity tradeoff in polymer membranes", *Journal of Membrane Science*, v. 520, pp. 790–800, 2016.

[152] WONG, M. C., MARTINEZ, K., RAMON, G. Z., et al. "Impacts of operating conditions and solution chemistry on osmotic membrane structure and performance", *Desalination*, v. 287, pp. 340–349, 2012.

[153] MEHTA, G., LOEB, S. "Performance of permasep B-9 and B-10 membranes in various osmotic regions and at high osmotic pressures", *Journal of Membrane Science*, v. 4, pp. 335–349, 1978.

[154] KINGSBURY, R., ZHU, S., FLOTRON, S., et al. "Microstructure determines water and salt permeation in commercial ion-exchange membranes", *ACS applied materials & interfaces*, v. 10, n. 46, pp. 39745–39756, 2018.

[155] TOGO, N., NAKAGAWA, K., SHINTANI, T., et al. "Osmotically Assisted Reverse Osmosis Utilizing Hollow Fiber Membrane Module for Concentration Process", *Industrial & Engineering Chemistry Research*, v. 58, n. 16, pp. 6721–6729, abr. 2019.

[156] STRAUB, A. P., OSUJI, C. O., CATH, T. Y., et al. "Selectivity and Mass Transfer Limitations in Pressure-Retarded Osmosis at High Concentrations and Increased Operating Pressures", *Environmental Science & Technology*, v. 49, n. 20, pp. 12551–12559, 2015.

[157] CATH, T. Y., ELIMELECH, M., MCCUTCHEON, J. R., et al. "Standard methodology for evaluating membrane performance in osmotically driven membrane processes", *Desalination*, v. 312, pp. 31–38, 2013.

[158] TIRAFERRI, A., YIP, N. Y., STRAUB, A. P., et al. "A method for the simultaneous determination of transport and structural parameters of forward osmosis membranes", *Journal of Membrane Science*, v. 444, pp. 523–538, 2013.

[159] BORETTI, A., AL-ZUBAIDY, S., VACLAVIKOVA, M., et al. "Outlook for graphene-based desalination membranes", *npj Clean Water*, v. 1, n. 1, pp. 1–11, 2018.

[160] LEE, K. P., ARNOT, T. C., MATTIA, D. "A review of reverse osmosis membrane materials for desalination—development to date and future potential", *Journal of Membrane Science*, v. 370, n. 1-2, pp. 1–22, 2011.

[161] LI, L., DONG, J., NENOFF, T. M., et al. "Desalination by reverse osmosis using MFI zeolite membranes", *Journal of membrane science*, v. 243, n. 1-2, pp. 401–404, 2004.

[162] TEOW, Y. H., MOHAMMAD, A. W. "New generation nanomaterials for water desalination: A review", *Desalination*, v. 451, pp. 2–17, 2019.

[163] LERMONTOV, A., BORGES, C. P., REUTHER, P. W. T., et al. "Análise econômica da dessalinização de água do mar por osmose inversa visando abastecimento público no estado do Rio de Janeiro". In: *26º Congresso brasileiro de Engenharia Sanitária e Ambiental, Porto Alegre.*, 2011.

[164] GOMEZ, J. D., CATH, T. Y. *Assessment of Osmotic Mechanisms Pairing Desalination Concentrate and Wastewater Treatment*. Relatório técnico, 2011.

[165] FURLAN, F. F., COSTA, C. B., SECCHI, A. R., et al. "Retro-Techno-Economic Analysis: Using (Bio) Process Systems Engineering Tools To Attain Process Target Values", *Industrial & Engineering Chemistry Research*, v. 55, n. 37, pp. 9865–9872, 2016.

[166] OSIPI, S. R., SECCHI, A. R., BORGES, C. P. "Cost assessment and retro-techno-economic analysis of desalination technologies in onshore produced water treatment", *Desalination*, v. 430, pp. 107–119, 2018.

[167] SPE. "Challenges in Reusing Produced Water". http://www.spe.org/industry/challenges-in-reusing-produced-water.php. Acessed on Jan 18th 2016.

[168] ALZAHRANI, S., MOHAMMAD, A. W. "Challenges and trends in membrane technology implementation for produced water treatment: a review", *Journal of Water Process Engineering*, v. 4, pp. 107–133, 2014.

[169] WESCHENFELDER, S., FONSECA, M., BORGES, C., et al. "Application of ceramic membranes for water management in offshore oil production platforms: Process design and economics", *Separation and Purification Technology*, v. 171, pp. 214–220, 2016.

[170] BORSANI, R., REBAGLIATI, S. "Fundamentals and costing of MSF desalination plants and comparison with other technologies", *Desalination*, v. 182, n. 1-3, pp. 29–37, 2005.

[171] ROCHA, J. H. B., GOMES, M. M. S., FERNANDES, N. S., et al. "Application of electrochemical oxidation as alternative treatment of produced water generated by Brazilian petrochemical industry", *Fuel processing technology*, v. 96, pp. 80–87, 2012.

[172] WESCHENFELDER, S., BORGES, C., CAMPOS, J. "Oilfield produced water treatment by ceramic membranes: Bench and pilot scale evaluation", *Journal of Membrane Science*, v. 495, pp. 242–251, 2015.

[173] CAMPOS, J. C., BORGES, R. M. H., OLIVEIRA FILHO, A. M. D., et al. "Oilfield wastewater treatment by combined microfiltration and biological processes", *Water Research*, v. 36, n. 1, pp. 95–104, 2002.

[174] ENGINEERING, C. "CEPCI issues". http://www.chemengonline.com/issues/. Acessed on May 18th 2017.

[175] SOARES, R. D. P., SECCHI, A. "EMSO: A new environment for modelling, simulation and optimisation", *Computer Aided Chemical Engineering*, v. 14, pp. 947–952, 2003.

[176] DOW. "DOW Specialty Membranes". http://www.dow.com/en-us/markets-and-solutions/products/DOWSpecialtyMembranes/

DOWSpecialtyMembranesXUS180808UltraHighPressureROElement, . Acessed on May 18th 2017.

[177] SCHOCK, G., MIQUEL, A. "Mass transfer and pressure loss in spiral wound modules", *Desalination*, v. 64, pp. 339–352, 1987.

[178] MALEK, A., HAWLADER, M., HO, J. "Design and economics of RO seawater desalination", *Desalination*, v. 105, n. 3, pp. 245–261, 1996.

[179] DOW. "Reverse osmosis & nanofiltration – Membrane information list". http://www.dow.com/en-us/water-and-process-solutions/products/reverse-osmosis, . Accessed on April 27th 2016.

[180] CHOI, Y., CHO, H., SHIN, Y., et al. "Economic Evaluation of a Hybrid Desalination System Combining Forward and Reverse Osmosis", *Membranes*, v. 6, n. 1, pp. 3, 2015.

[181] TOW, E. W., MCGOVERN, R. K., OTHERS. "Raising forward osmosis brine concentration efficiency through flow rate optimization", *Desalination*, v. 366, pp. 71–79, 2015.

[182] EL-DESSOUKY, H. T., ETTOUNEY, H. M. *Fundamentals of salt water desalination*. Elsevier, 2002.

[183] RECOVERY, E. "PX Pressure Exchanger". http://www.energyrecovery.com/water/px-pressure-exchanger/. Acessed on May 18th 2017.

[184] VANOPPEN, M., STOFFELS, G., DEMUYTERE, C., et al. "Increasing RO efficiency by chemical-free ion-exchange and Donnan dialysis: Principles and practical implications", *Water research*, v. 80, pp. 59–70, 2015.

[185] SUMMERS, E. K., ARAFAT, H. A., LIENHARD, J. H. "Energy efficiency comparison of single-stage membrane distillation (MD) desalination cycles in different configurations", *Desalination*, v. 290, pp. 54–66, 2012.

[186] NIMDEO, Y. M., JOSHI, Y. M., MURALIDHAR, K. "Measurement of mass diffusivity using interferometry through sensitivity analysis", *Industrial & Engineering Chemistry Research*, v. 53, n. 49, pp. 19338–19350, 2014.

[187] IRENA. *Renewable Power Generation Costs in 2018*. Relatório técnico, International Renewable Energy Agency, Abu Dhabi, 2019.

[188] LARA, J. R., OSUNSAN, O., HOLTZAPPLE, M. T. "Advanced mechanical vapor-compression desalination system". In: Schorr, M. (Ed.), *Desalination, Trends and Technologies*, InTech, cap. 7, 2011.

[189] JEONG, Y. S., JUNG, J., LEE, U., et al. "Techno-economic analysis of mechanical vapor recompression for process integration of post-combustion CO 2 capture with downstream compression", *Chemical Engineering Research and Design*, v. 104, pp. 247–255, 2015.

[190] WATSON, I., MORIN, O., HENTHORNE, L. "Desalting handbook for planners". In: *Desalination research and development program report*, v. 72, United States Department of the Interior Bureau of Reclamation Technical Service Center Water Treatment Engineering and Research Group, 2003.

[191] ONGARATTO, R. S., DA CUNHA LAGE, P. L., BORGES, C. P. "Physical properties of potassium pyrophosphate and its use in osmotic evaporation", *Chemical Engineering Research and Design*, v. 104, pp. 497–502, 2015.

[192] ARNALDOS, M., TORRE, T., RODRIGUEZ, C., et al. "Feasibility evaluation of the FO-MBR process for wastewater reclamation". In: *IDA World Congress on Desalination and Water Reuse, San Diego/CA*. Society of Petroleum Engineers, 2015.

[193] HOLT, T., SIVERTSEN, E., THELIN, W., et al. "Pressure Dependency of the Membrane Structure Parameter and Implications in Pressure Retarded Osmosis (PRO)". In: Du, H., Thompson, A., Wang, X. (Eds.), *Osmotically Driven Membrane Processes. Approach, Development and Current Status*, InTech, cap. 6, 2018.

[194] ELIMELECH, M., PHILLIP, W. A. "The future of seawater desalination: energy, technology, and the environment", *science*, v. 333, n. 6043, pp. 712–717, 2011.

[195] VEIL, J. *US produced water volumes and management practices in 2012*. Relatório técnico, Veil Environmental, 2015.

[196] BOURCIER, W., WOLERY, T., WOLFE, T., et al. "A preliminary cost and engineering estimate for desalinating produced formation water associated with carbon dioxide capture and storage", *International Journal of Greenhouse Gas Control*, v. 5, n. 5, pp. 1319–1328, 2011.

[197] KAPLAN, R., MAMROSH, D., SALIH, H. H., et al. "Assessment of desalination technologies for treatment of a highly saline brine from a potential CO2 storage site", *Desalination*, v. 404, pp. 87–101, 2017.

[198] YANG, L., GROSSMANN, I. E., MAUTER, M. S., et al. "Investment optimization model for freshwater acquisition and wastewater handling in shale gas production", *AIChE Journal*, v. 61, n. 6, pp. 1770–1782, 2015.

[199] BARTHOLOMEW, T. V., MAUTER, M. S. "Multiobjective optimization model for minimizing cost and environmental impact in shale gas water and wastewater management", *ACS Sustainable Chemistry & Engineering*, v. 4, n. 7, pp. 3728–3735, 2016.

[200] BEHRER, A. P., MAUTER, M. S. "Allocating Damage Compensation in a Federalist System: Lessons from Spatially Resolved Air Emissions in the Marcellus", *Environmental science & technology*, v. 51, n. 7, pp. 3600–3608, 2017.

[201] SALIH, H. H., LI, J., KAPLAN, R., et al. "Life cycle assessment of treatment and handling options for a highly saline brine extracted from a potential CO2 storage site", *Water research*, v. 122, pp. 419–430, 2017.

[202] GAO, J., YOU, F. "Optimal design and operations of supply chain networks for water management in shale gas production: MILFP model and algorithms for the water-energy nexus", *AIChE Journal*, v. 61, n. 4, pp. 1184–1208, 2015.

[203] KARAGIANNIS, I. C., SOLDATOS, P. G. "Water desalination cost literature: review and assessment", *Desalination*, v. 223, n. 1-3, pp. 448–456, 2008.

[204] CHANG, H., LI, T., LIU, B., et al. "Potential and implemented membrane-based technologies for the treatment and reuse of flowback and produced water from shale gas and oil plays: A review", *Desalination*, v. 455, pp. 34–57, 2019.

[205] KIM, J., KIM, D. I., HONG, S. "Analysis of an osmotically-enhanced dewatering process for the treatment of highly saline (waste) waters", *Journal of Membrane Science*, v. 548, pp. 685–693, 2017.

[206] NELDER, J. A., MEAD, R. "A simplex method for function minimization", *The computer journal*, v. 7, n. 4, pp. 308–313, 1965.

[207] PITZER, K. S., PEIPER, J. C., BUSEY, R. "Thermodynamic properties of aqueous sodium chloride solutions", *Journal of Physical and Chemical Reference Data*, v. 13, n. 1, pp. 1–102, 1984.

[208] ZHANG, M., LIU, R., WANG, Z., et al. "Dehydration of forward osmosis membranes in treating high salinity wastewaters: Performance and implications", *Journal of Membrane Science*, v. 498, pp. 365–373, 2016.

[209] ALBERTON, A. L. *Estimação de parâmetros e planejamento de experimentos: estudo de incertezas e funções de informação.* Tese de Doutorado, Universidade Federal do Rio de Janeiro, 2010.

[210] PITZER, K. S. "Thermodynamics of electrolytes. I. Theoretical basis and general equations", *The Journal of Physical Chemistry*, v. 77, n. 2, pp. 268–277, 1973.

[211] RESNIK, S. L., CHIRIFE, J. "Proposed theoretical water activity values at various temperatures for selected solutions to be used as reference sources in the range of microbial growth", *Journal of Food Protection*, v. 51, n. 5, pp. 419–423, 1988.

[212] GEISE, G. M., FREEMAN, B. D., PAUL, D. R. "Sodium chloride diffusion in sulfonated polymers for membrane applications", *Journal of membrane science*, v. 427, pp. 186–196, 2013.

[213] LONSDALE, H., MERTEN, U., RILEY, R. "Transport properties of cellulose acetate osmotic membranes", *Journal of Applied Polymer Science*, v. 9, n. 4, pp. 1341–1362, 1965.

[214] SAMANTA, T., SINHA, S., MUKHERJEE, M. "Effect of added salt on swelling dynamics of ultrathin films of strong polyelectrolytes", *Polymer*, v. 97, pp. 285–294, 2016.

[215] SINGH, A., MUKHERJEE, M. "Swelling dynamics of ultrathin polymer films", *Macromolecules*, v. 36, n. 23, pp. 8728–8731, 2003.

[216] XIAO, T., NGHIEM, L. D., SONG, J., et al. "Phenol rejection by cellulose triacetate and thin film composite forward osmosis membranes", *Separation and Purification Technology*, v. 186, pp. 45–54, 2017.

[217] NGUYEN, T. P. N., YUN, E.-T., KIM, I.-C., et al. "Preparation of cellulose triacetate/cellulose acetate (CTA/CA)-based membranes for forward osmosis", *Journal of membrane science*, v. 433, pp. 49–59, 2013.

[218] GEISE, G., FREEMAN, B. D., PAUL, D. R. "Characterization of a sulfonated pentablock copolymer for desalination applications", *Polymer*, v. 51, n. 24, pp. 5815–5822, 2010.

[219] ISMAIL, A. F., MATSUURA, T. "Progress in transport theory and characterization method of Reverse Osmosis (RO) membrane in past fifty years", *Desalination*, v. 434, pp. 2–11, 2018.

[220] KULKARNI, S., KRAUSE, S., WIGNALL, G., et al. "Investigation of the pore structure and morphology of cellulose acetate membranes using small-angle neutron scattering. 1. Cellulose acetate active layer membranes", *Macromolecules*, v. 27, n. 23, pp. 6777–6784, 1994.

[221] JOHNSON, D. J., OATLEY-RADCLIFFE, D. L., HILAL, N. "State of the art review on membrane surface characterisation: Visualisation, verification and quantification of membrane properties", *Desalination*, v. 434, pp. 12–36, 2018.

[222] MURPHY, D., DE PINHO, M. N. "An ATR-FTIR study of water in cellulose acetate membranes prepared by phase inversion", *Journal of membrane science*, v. 106, n. 3, pp. 245–257, 1995.

[223] WANG, Y., KAWANO, Y., AUBUCHON, S. R., et al. "TGA and Time-Dependent FTIR Study of Dehydrating Nafion- Na Membrane", *Macromolecules*, v. 36, n. 4, pp. 1138–1146, 2003.

[224] VOGT, B. D., SOLES, C. L., LEE, H.-J., et al. "Moisture Absorption and Absorption Kinetics in Polyelectrolyte Films: Influence of Film Thickness", *Langmuir*, v. 20, n. 4, pp. 1453–1458, 2004.

[225] VOGT, B. D., SOLES, C. L., LEE, H.-J., et al. "Moisture absorption into ultrathin hydrophilic polymer films on different substrate surfaces", *Polymer*, v. 46, n. 5, pp. 1635–1642, 2005.

[226] ZAN, X., PENG, B., HOAGLAND, D. A., et al. "Polyelectrolyte uptake by PEMs: Impact of salt concentration", *Polymer Chemistry*, v. 2, n. 11, pp. 2581–2589, 2011.

[227] LIN, L., LOPEZ, R., RAMON, G. Z., et al. "Investigating the void structure of the polyamide active layers of thin-film composite membranes", *Journal of Membrane Science*, v. 497, pp. 365–376, 2016.

[228] LAATIKAINEN, M., LINDSTRÖM, M. "Measurement of sorption in polymer membranes with a quartz crystal microbalance", *Journal of membrane science*, v. 29, n. 2, pp. 127–141, 1986.

[229] REVIAKINE, I., JOHANNSMANN, D., RICHTER, R. P. "Hearing What You Cannot See and Visualizing What You Hear: Interpreting Quartz Crystal

Microbalance Data from Solvated Interfaces", *Analytical Chemistry*, v. 83, n. 23, pp. 8838–8848, 2011.

[230] VOGT, B. D., LIN, E. K., WU, W.-L., et al. "Effect of film thickness on the validity of the Sauerbrey equation for hydrated polyelectrolyte films", *The Journal of Physical Chemistry B*, v. 108, n. 34, pp. 12685–12690, 2004.

[231] WU, J., CONTRERAS, A. E., LI, Q. "Studying the impact of RO membrane surface functional groups on alginate fouling in seawater desalination", *Journal of membrane science*, v. 458, pp. 120–127, 2014.

[232] LIU, Y., MI, B. "Effects of organic macromolecular conditioning on gypsum scaling of forward osmosis membranes", *Journal of membrane science*, v. 450, pp. 153–161, 2014.

[233] TALIB, Z., BABA, Z., KUROSAWA, S., et al. "Frequency behavior of a quartz crystal microbalance (QCM) in contact with selected solutions", *American Journal of Applied Sciences*, v. 3, n. 5, pp. 1853–1858, 2006.

[234] SHIMAZU, A., IKEDA, K., MIYAZAKI, T., et al. "Application of positron annihilation technique to reverse osmosis membrane materials", *Radiation Physics and Chemistry*, v. 58, n. 5-6, pp. 555–561, 2000.

[235] WESCHENFELDER, S., BORGES, C., CAMPOS, J. "Oilfield Produced Water Treatment by Ceramic Membranes: Mass Transfer and Process Efficiency Analysis of Model Solutions", *Separation Science and Technology*, v. 50, n. 14, pp. 2190–2197, 2015.

[236] EL-SAYED, Y. "Designing desalination systems for higher productivity", *Desalination*, v. 134, n. 1, pp. 129–158, 2001.

[237] HASLEGO, C., POLLEY, G. "Designing plate-and-frame heat exchangers", *Chemical engineering progress*, v. 98, n. 9, pp. 32–37, 2002.

[238] CHIAM, C.-K., SARBATLY, R. "Study of the rectangular cross-flow flat-sheet membrane module for desalination by vacuum membrane distillation", *Chemical Engineering and Processing: Process Intensification*, v. 102, pp. 169–185, 2016.

[239] KOUTSOU, C., YIANTSIOS, S., KARABELAS, A. "A numerical and experimental study of mass transfer in spacer-filled channels: effects of spacer geometrical characteristics and Schmidt number", *Journal of Membrane Science*, v. 326, n. 1, pp. 234–251, 2009.

[240] BANAT, F. A., SIMANDL, J. "Membrane distillation for dilute ethanol: separation from aqueous streams", *Journal of Membrane Science*, v. 163, n. 2, pp. 333–348, 1999.

[241] KULIK, H. J., MARZARI, N., CORREA, A. A., et al. "Local effects in the X-ray absorption spectrum of salt water", *The Journal of Physical Chemistry B*, v. 114, n. 29, pp. 9594–9601, 2010.

Appendix A

Supplementary equations and expressions

A.1 Microfiltration (MF)

Ceramic microfiltration, which was found cheaper than conventional solutions [169], was employed as a pretreatment step in some routes. As it is not the main point of analysis, an empirical flux equation was used [235]. Besides, it was considered a complete rejection of oil and grease.

Mass balance is presented in Eq. A.1 and Eq. A.2. In this equations, $\dot{m}_{in,f}$, $\dot{m}_{out,f}$ and $\dot{m}_{out,p}$ are the the inlet feed, outlet feed and outlet permeate mass flowrates, respectively. Similarly, $c_{oil,in,f}$ and $c_{oil,out,f}$ are the inlet and outlet feed oil concentrations and $\dot{F}_{in,f}$ and $\dot{F}_{out,f}$ are the respective volumetric flowrates. This process was not discretized because of its simplicity.

$$\dot{m}_{in,f} = \dot{m}_{out,f} + \dot{m}_{out,p} \tag{A.1}$$

$$c_{oil,in,f}\dot{F}_{in,f} = c_{oil,out,f}\dot{F}_{out,f} \tag{A.2}$$

For cost estimation, membrane cost was considered as 30% of total investment cost for MF [235]. In OPEX calculations, pumping energy cost and membrane repositions (10%/year) were considered.

A.2 Forward Osmosis (FO)

FO modeling was based on Bui et al. [124] approach, which considered a more rigorous flux calculation. It is important to highlight that the modeling used in

the present study considered the PRO mode in forward osmosis, i.e., selective layer facing the draw solution, which is the higher flux mode when using only saline solutions. However, the use of FO mode, i.e., selective layer facing the feed (oil/water mixture) was recommend in a desalination study of oil solutions [123]. At this point, is not possible to conclude which of the two modes will perform better, because the oil effect was not considered.

Local water J_W and salt flux j_S are described in Eq. A.3 and Eq. A.4, respectively [124].

$$J_W = A \left\{ \frac{\pi_{ds} \exp(-\frac{J_W}{k_{ds}}) - \pi_f \exp\left[J_W(\frac{1}{k_f} + \frac{S}{D_f})\right]}{1 + \frac{B}{J_W}\left\{\exp\left[J_W(\frac{1}{k_f} + \frac{S}{D_f}) - \exp(-\frac{J_W}{k_{ds}})\right]\right\}} \right\} \tag{A.3}$$

$$j_S = BMM \left\{ \frac{c_{ds} \exp(-\frac{J_W}{k_{ds}}) - c_f \exp\left[J_W(\frac{1}{k_f} + \frac{S}{D_f})\right]}{1 + \frac{B}{J_W}\left\{\exp\left[J_W(\frac{1}{k_f} + \frac{S}{D_f}) - \exp(-\frac{J_W}{k_{ds}})\right]\right\}} \right\} \tag{A.4}$$

In these equations, A is the membrane hydraulic permeability, B is the membrane salt permeability, π_{ds} and π_f are the bulk osmotic pressures in draw solution and feed, S is membrane structural parameter, k_{ds} and k_f are the mass transfer coefficients and D_f is salt diffusivity. An important assumption for salt flux calculation is that osmotic agent is the same salt present in the feed. In this case, sodium chloride (NaCl) was chosen as a draw solution.

Admitting a countercurrent module, mass balance is described according to Eq. A.5 and Eq. A.6.

$$\Delta \dot{m}_{ds} = \Delta \dot{m}_f \tag{A.5}$$

$$\Delta \dot{m}_f = -J_W a_n \rho \tag{A.6}$$

Variables $\Delta \dot{m}_f$ and $\Delta \dot{m}_{ds}$ are feed in and draw solution massic flowrate variations in each element. Variable a_n is the n_{th} element membrane area and ρ is pure water density. Flux J_W is calculated at n_{th} element velocity and concentrations.

Volumetric ratio (VR) between draw solution and feed is calculated by Eq. A.7.

$$VR = \frac{\dot{F}_{in,ds}}{\dot{F}_{in,f}} \tag{A.7}$$

In this equation, $\dot{F}_{in,ds}$ and $\dot{F}_{in,f}$ are volumetric flowrates of draw solution and feed that get into the module, respectively.

Water recovery ratio is defined as the difference between both entrance flowrate over feed flowrate.

Salt mass balance is described according to Eq. A.8. The variables are c_{ds} and

c_f , sodium chloride molar concentrations in draw solution and feed, respectively, molar mass MM and salt flux j_S at n_{th} element membrane area.

$$MM\Delta(c_{ds}\dot{F}_{ds}) = -j_S a_n = -MM\Delta(c_f\dot{F}_f) \tag{A.8}$$

For CAPEX calculation, it was assumed that forward osmosis membrane cost is 29.4% of overall fixed cost [118], similar to MF modules. Besides that, OPEX for this system involved energy requirements for pumping and osmotic agent reposition due reverse salt flux. Additionally, FO and RO membrane cost were considered to be similar, in spite of some differences in material and fabrication could exist.

A.3 Mechanical vapor compression

MVC modeling was based on El-Dessouky and Ettouney approach [182]. This method considers an evaporator/condensator together with two exchangers for heat integration.

Total mass balance and salt balance are presented in Eq. A.9 and Eq. A.10. These equations consider densities, feed $\dot{F}_{in}$, brine $\dot{F}_{out}$ and pure water $\dot{F}_{pw}$ volumetric flowrates, as well as salt concentrations in the feed, c_{in}, and in the brine c_{out}. It was considered that no salt leaves evaporator in pure water stream. This system was not discretized because it would need a detailed sizing. Approximated estimation used here was similar to Thiel et al. [3].

$$\rho_{in}\dot{F}_{in} = \rho_{out}\dot{F}_{out} + \rho\dot{F}_{pw} \tag{A.9}$$

$$c_{in}\dot{F}_{in} = c_{out}\dot{F}_{out} \tag{A.10}$$

Energy balance in the evaporator involves conditions at entrance (h_f, T_f), brine exit (h_b,T_b), vapor that gets into the compressor (T_v, H_v) and superheated compressed vapor (T_s, H_s), as shown on Eq. A.11. Condensing temperature is T_d and the heat exchanged in evaporator is q. The vapor and liquid enthalpies are calculated from the same reference state, while $\Delta h_{vap,d}$ is the latent heat of vaporization at T_d.

$$q = \rho_{in}\dot{F}_{in}(h_b - h_f) + \rho\dot{F}_{pw}H_v = \rho\dot{F}_{pw}(H_s - H_d) + \rho\dot{F}_{pw}\Delta h_{vap,d} \tag{A.11}$$

BPE, which is detailed further, is used in T_d relation to T_b. TTD is calculated by Eq. A.12.

$$T_d = T_b - BPE_f + BPE_b + TTD \tag{A.12}$$

In an approach based on Swaminathan et al. [108], it was considered that brine and MVC pure water stream leaving preheaters at the same temperature.

In order to estimate cost, evaporator area (a_e) is calculated by a simple relation described in Eq. A.13, involving global heat transfer U and aforementioned temperatures [182].

$$a_e = \frac{q}{U(T_d - T_b)} \tag{A.13}$$

Compressor work is calculated by Eq. A.14. This expression relates heat capacity ratio for water vapor (γ), specific volume (v_v), pressures in evaporator and condenser (P_v and P_d) and isentropic efficiency η. The latter value is used for T_s calculation according to the definition of η.

$$W = \frac{\gamma}{\eta(\gamma - 1)} P_v v_v \left[\left(\frac{P_d}{P_v} \right)^{\frac{\gamma-1}{\gamma}} - 1 \right] \tag{A.14}$$

Cost calculation for MVC evaporator (C_{evap}) and compressor (C_{comp}) is based on Eq. A.15 and Eq. A.16, respectively [236].

$$C_{evap} = 430(0.582\, U\, a_e \Delta P_t^{-0.01} \Delta P_{sh}^{-0.1}) \tag{A.15}$$

$$C_{comp} = 7364 \left(\rho \dot{F}_{pw} \frac{P_d}{P_v} \right) \left(\frac{\eta}{1 - \eta} \right)^{0.7} \tag{A.16}$$

In Eq. A.15, U is in kW/m^{2}K, a_e in m^2, ΔP_t and ΔP_{sh}, which are pressure loss in tubes and shell side, are in kPa. Compressor cost A.16 needs a massic flowrate (product $\rho \dot{F}_{pw}$) in kg/s. Both costs are in US dollars.

Plate heat exchangers cost (C_{hx}) calculation considered Eq. A.17, reported by Haslego and Polley [237] for areas (A_{hx}, in ft^2) larger than 200 ft^2 and grade 1 titanium, since brines tend to be very corrosive (conservative approach). All equipment costs were multiplied by the period inflation.

$$C_{hx} = 131(A_{hx})^{0.7514} \tag{A.17}$$

A.4 Direct contact membrane distillation

MD processes use temperature difference to permeate water vapor flux. In case of direct contact membrane distillation, there is a cold permeate stream that condenses vapor. Modeling was based on Thiel et al. [3] and Summers et al. [185]. A schematic process is presented on Figure A.1.

Total mass balance, as well as salt mass balance, is described in Eq. A.18 and Eq. A.19.

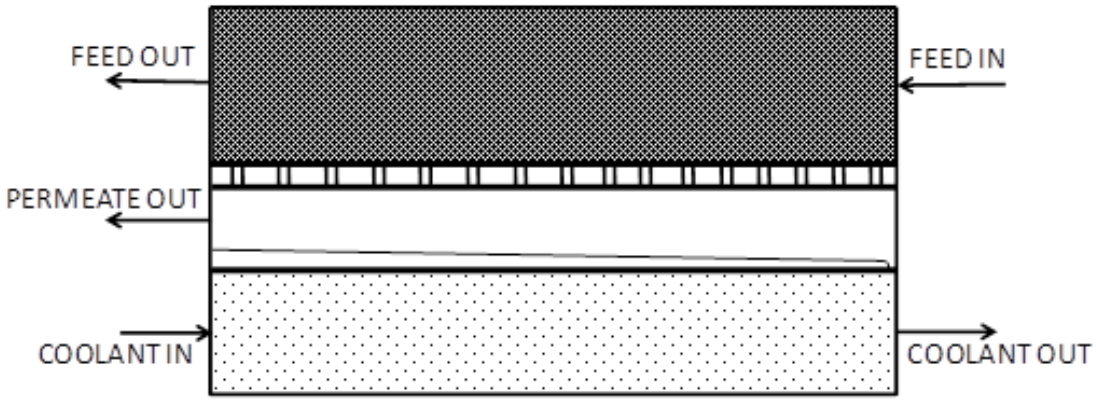

Figure A.1: DCMD simplified configuration

$$\Delta \dot{m}_f = -\Delta \dot{m}_p \tag{A.18}$$

$$\Delta(c_f \dot{F}_f) = 0 \tag{A.19}$$

Flux j_W can be calculated by vapor pressures at $T_{f,m}$ and $T_{p,m}$, which are feed and permeate temperatures on both sides of the membrane, according to Eq. A.20. Additionally, a coefficient of permeability G is used too. It is related to temperature, porosity and membrane thickness [108]. However, it was considered constant in this analysis, since the system was simulated using a specific membrane and temperatures were in a range compatible with G measurement.

$$j_W = G(P_{vap,f}(T_{f,m}) - P_{vap,p}(T_{p,m})) \tag{A.20}$$

Energy balance on feed (Eq. A.21) and permeate (Eq. A.22) sides involve heat transferred through the membrane (q_m), through the heat exchanger wall (q_c), vapor enthalpies of feed and permeate at $T_{f,m}$ and $T_{p,m}$ ($H_{v,f,m}$,$H_{v,p,m}$), volumetric flowrates of feed/concentrate ($\dot{F}_{in,f}$ and $\dot{F}_{out,f}$) and permeate ($\dot{F}_{out,p}$) and their respective massic enthalpies ($h_{in,f}$,$h_{out,f}$ and $h_{out,p}$). As in MVC calculation, the enthalpies are calculated using a single reference state. For $P_{vap,f}(T_{f,m})$ calculation, bulk colligative effects based on Raoult law were considered.

$$\rho_{in,f} \dot{F_{in,f}} h_{in,f} = \rho_{out,f} \dot{F_{out,f}} h_{out,f} + (q_m + j_W H_{v,f,m}) a_m \tag{A.21}$$

$$(q_m + j_W H_{v,p,m} - q_c) a_m = \rho \dot{F_{out,p}} h_{out,p} \tag{A.22}$$

Coolant energy balance can be described by Eq. A.23, with $\dot{F}_{in,c}$ and $\dot{F}_{out,c}$ as coolant volumetric flowrates in and out and $h_{in,c}$ and $h_{out,c}$ as their respective massic enthalpies.

$$\rho_{in,c}\dot{F_{in,c}}h_{in,c} + q_c a_m = \rho_{out,c}\dot{F_{out,c}}h_{out,c} \tag{A.23}$$

Convection in feed and permeate/coolant streams are represented in Eq. A.24 and Eq. A.25, in which $h_{f,b}$ (at $T_{f,b}$) and $h_{p,w}$ (at T_w) are feed bulk and wall massic enthalpies. It was assumed that wall temperature T_w is practically equal to permeate exit temperature $T_{out,p}$ due to low MD recovery. Convective heat transfer coefficients of feed ($h_{conv,f}$) and coolant ($h_{conv,c}$) are further detailed.

$$j_W(H_{v,f,m} - h_{f,b}) + q_m = h_{conv,f}(T_{f,b} - T_{f,m}) \tag{A.24}$$

$$j_W(H_{v,p,m} - h_{p,w}) + q_c = -h_{conv,c}(T_{c,b} - T_w) \tag{A.25}$$

Heat through membrane and heat absorbed by the coolant stream are represented according to Eq. A.26 and Eq. A.27. In these equations, K_m, K_v and K_p are membrane, water vapor and permeate thermal conductivities, ε and δ are membrane porosity and thickness, respectively.

$$q_m = \left[K_m(1-\varepsilon) + K_v\varepsilon\right]\frac{1}{\delta}\left(T_{f,m} - T_{p,m}\right) \tag{A.26}$$

$$q_c = \frac{K_p}{\delta}\left(T_{p,m} - T_w\right) \tag{A.27}$$

According to Al-Obaidani et al. [101], MD performance is more affected by temperature polarization than by CP. Therefore, in consonance to these authors and because of the low flux and recovery ratio, that drives CP, only temperature polarization was considered in this simplified modeling.

Cost modeling for MD modules considers membrane cost as 50% of total cost [101]. As proposed by El-Sayed et al. [109], modular units like membrane distillation have a capital cost almost linear with respect to capacity.

For all processes, recovery ratio is defined as volumetric flow of treated water (permeate/product) over feed volumetric flow. For each module, average values of bulk compositions were estimated based on feed and concentrate streams.

Produced water properties (mainly density and conductivity) were based in NaCl solutions parameters or extrapolated from seawater correlations [191, 238]. Enthalpy and saturation water properties were calculated by steam tables. Effect of salt concentration in water enthalpy was considered irrelevant.

A.5 Pumps

Pump power was calculated by Eq. A.28, involving pressure difference ($P_{out} - P_{in}$), massic flowrate ($\dot{m}_{in}$) and efficiency (η_p).

$$Pot = \frac{(P_{out} - P_{in})\dot{m}_{in}}{\rho\eta_p} \tag{A.28}$$

A.6 Correlations for mass transfer

FO, OARO and RO were considered in laminar flow. Mass transfer coefficient was calculated for these processes based on Reynolds number, Schmidt number, Sherwood number and d_h/L , which is the ratio between hydraulic diameter and channel length, according to Eq. A.29.

$$d_H = \frac{2(z\,W)}{(z+W)} \tag{A.29}$$

In this equation, z and W are depth and width of flow channel. Mass transfer correlation was based on Koutsou et al. [239], according to Eq. A.30.

$$Sh = 0.2Re^{0.57}Sc^{0.4} \tag{A.30}$$

Finally, mass transfer coefficient k_f is calculated using diffusivity (D_f), Sherwood number and hydraulic diameter, in consonance with Eq. A.31 for industrial spiral wound modules.

$$k_f = \frac{Sh\,D_f}{d_h} \tag{A.31}$$

A.7 Correlations for heat transfer

For MD, turbulent heat transfer correlations involving Reynolds, Nusselt (Nu) and Prandtl (Pr) numbers were based on Banat et al. [240], according to Eq. A.32. and Eq. A.33. The latter involves convection coefficient, h_{conv}, hydraulic diameter d_h and thermal conductivity K.

$$Nu = 0.023Re^{0.8}Pr^{0.3} \tag{A.32}$$

$$Nu = (d_h h_{conv})/K \tag{A.33}$$

A.8 Osmotic pressure and boiling point elevation

Osmotic pressure ϕ is calculated by Eq. A.34.

$$\pi = \frac{\phi RT\sum_i b_i}{\rho} \tag{A.34}$$

In this relation, ϕ is osmotic coefficient, $\sum_i b_i$ is the sum of species molality, R is the universal gas constant, ρ is solution density and T is operation temperature. Thermodynamic data were based on Pitzer et al. [207]. Similarly, BPE also considered a linear relation with salinity, according to Eq. A.35. Its calculation involves the same parameters of osmotic pressure relation plus density and latent heat evaluated at temperature T.

$$BPE = \frac{\phi R T^2 \sum_i b_i}{\rho h_{vap}} \tag{A.35}$$

A.9 Head loss in membrane processes

Particularly, average ΔP calculation consider the linear head loss in a membrane module (ΔP_{drop}) and feed pressure (P_{in}), as shown in Eq. A.36. Its was considered no significant pressure loss in permeate side.

$$\Delta P = P_{in} - \frac{\Delta P_{drop}}{2} \tag{A.36}$$

The head loss can be described by Eq. A.37., which considers λ as a coefficient for Reynolds between 100 and 1000, density, velocity V and other aforementioned parameters. The coefficient λ was calculated using Eq. A.38, as proposed by Schock and Miquel [177].

$$\Delta P_{drop} = \frac{\lambda \rho V^2}{2} \frac{L}{d_h} \tag{A.37}$$

$$\lambda = 6.23 Re^{-0.3} \tag{A.38}$$

A.10 Heat exchangers

Simplified model for heat exchangers were chosen for modeling. Heat exchanged is defined by Eq. A.39, involving mass flowrates ($\dot{m}_h$,$\dot{m}_c$) specific heat capacity (cp_h,cp_c) and temperature differences ($T_{out,c} - T_{in,c}$); ($T_{out,h} - T_{in,h}$) for cold and hot streams.

$$q = \dot{m}_c cp_c (T_{c,out} - T_{c,in}) = \dot{m}_h cp_h (T_{h,out} - T_{h,in}) \tag{A.39}$$

For area calculation, Eq. A.40 was used. It considers heat, global heat coefficient (U) and log mean temperature difference ($LMTD$).

$$Q = U\, A\, (LMTD) \tag{A.40}$$

Appendix B

Trust region calculation

The real trust region for the parameter estimated from the non-linear equations system was calculated using F-Fisher test at 95% confidence. Using F-Fisher test not for variances but for the least squares [209], it is possible to vary the estimated parameters around the optimal point and obtain the region, as presented in Figure B.1.

Eq. B.1 represents the least square LS method calculated for N_{exp} experiments, where y_i^{exp} are the experimental variables (water and salt flux in the present case) and y_i^1 are the calculated variables using a given model 1. In this equation, ν_y is the measurement variance.

$$LS = \frac{\Sigma_{i=1}^{n_y}(y_i^{exp} - y_i^1)^2}{N_{exp}\nu_y} \tag{B.1}$$

The suitability between different models, or with models with different parameters, could be performed using the quotient of the least squares in a F-Fisher test, as represented by Eq. B.2.

$$FF_{min} < \frac{LS_1}{LS_2} < FF_{max} \tag{B.2}$$

In Eq. B.2, FF_{min} and FF_{max} are the F-Fisher test critical values for a bicaudal test at the desired probability level and for the degrees of freedom of model 1 and 2. LS_1 and LS_2 are the least squares obtained for model 1 and 2, respectively. The degrees of freedom can be calculated using Eq. 4.6.

In Figure B.1, the points where the horizontal red line intercepts the region (at constant S) are the water permeability maximum and minimum, while the points where the vertical red line intercepts the region (at constant A) are the structural parameter maximum and minimum values for the graphs.

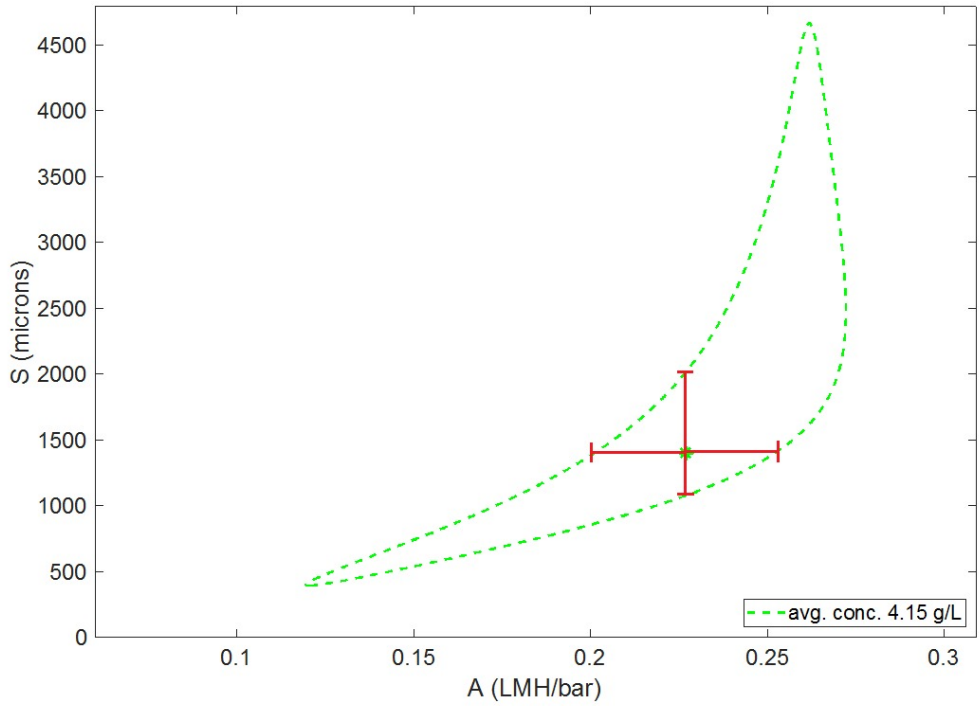

Figure B.1: Method for elaborating the error bars in a 95% trust region.

Appendix C

Osmotic experiments data

C.1 Reverse osmosis

Table C.1: RO#1 data points.

c_f (g/L)	c_p (g/L)	P (bar)	J_W (L/(h m^2))	j_S (g/(h m^2))
2.0	0.048	30	8.00	0.385
4.0	0.081	30	7.26	0.581
6.0	0.116	30	6.71	0.783
8.0	0.148	30	6.20	0.932

$A = 0.272$ LMH/bar; $B = 0.118$ LMH; $R^2(J_W) = 0.989$; $R^2(j_S) = 0.995$

Table C.2: RO#2 data points.

c_f (g/L)	c_p (g/L)	P (bar)	J_W (L/(h m^2))	j_S (g/(h m^2))
2.9	0.0170	30	6.71	0.331
7.7	0.0179	30	5.93	0.654
11.9	0.019	30	5.19	0.981
18.0	0.022	30	4.37	1.326
24.7	0.025	30	3.84	1.668

$A = 0.261$ LMH/bar; $B = 0.07$ LMH; $R^2(J_W) = 0.975$; $R^2(j_S) = 0.994$.

Table C.3: RO#3 data points.

c_f (g/L)	c_p (g/L)	P (bar)	J_W (L/(h m^2))
3.3	0.0585	60	13.78
3.4	0.0585	50	10.55
8.4	0.0585	50	9.86
8.7	0.0585	60	12.07
11.1	0.0585	60	11.54
11.2	0.0585	50	13.78

c_p assumed to be constant. $A = 0.233$ LMH/bar; $R^2(J_W) = 0.978$.

Table C.4: RO#4 data points.

c_f (g/L)	c_p (g/L)	P (bar)	J_W (L/(h m^2))
48.0	0.0585	60	4.39
48.0	0.0585	50	2.58
40.0	0.0585	50	3.56
40.0	0.0585	60	5.07

c_p assumed to be constant. $A = 0.202$ LMH/bar; $R^2(J_W) = 0.976$.

Table C.5: RO#5 data points.

c_f (g/L)	c_p (g/L)	P (bar)	J_W (L/(h m^2))
30.0	0.0585	40	4.60
30.0	0.0585	30	2.22
40.0	0.0585	40	2.87

c_p assumed to be constant. $A = 0.298$ LMH/bar; $R^2(J_W) = 0.996$.

Table C.6: RO#6 data points.

c_f (g/L)	c_p (g/L)	P (bar)	J_W (L/(h m^2))
1.3	0.0823	50	10.25
3.3	0.1136	50	9.80
4.8	0.1855	50	9.15
6.4	0.2942	50	8.66

$A = 0.204$ LMH/bar; $R^2(J_W) = 0.980$.

Table C.7: RO#7 data points.

c_f (g/L)	c_p (g/L)	P (bar)	J_W (L/(h m^2))
0.0	0.0585	60	13.29
10.0	0.0585	60	10.91
20.0	0.0585	60	9.52
30.0	0.0585	60	7.43

c_p assumed to be constant. $A = 0.219$ LMH/bar; $R^2(J_W) = 0.992$.

Table C.8: RO#8 data points.

c_f (g/L)	c_p (g/L)	P (bar)	J_W (L/(h m^2))	j_S (g/(h m^2))
11.9	0.02077	30	5.01	1.03
14.5	0.02656	30	4.32	1.58
14.5	0.03604	40	6.45	1.73

$A = 0.239$ LMH/bar; $B = 0.101$ LMH; $R^2(J_W) = 0.969$; $R^2(j_S) = 0.999$.

Table C.9: RO#9 data points.

c_f (g/L)	c_p (g/L)	P (bar)	J_W (L/(h m^2))	j_S (g/(h m^2))
5.3	0.008	30	6.85	0.52
11.2	0.010	30	5.66	0.88
19.6	0.012	30	4.48	1.29
29.8	0.016	30	3.42	1.76

$A = 0.287$ LMH/bar; $B = 0.06$ LMH; $R^2(J_W) = 0.977$; $R^2(j_S) = 0.998$.

Table C.10: RO#10 data points.

c_f (g/L)	c_p (g/L)	P (bar)	J_W (L/(h m^2))	j_S (g/(h m^2))
3.3	0.008	30	6.69	0.35
7.5	0.009	30	5.96	0.60
9.9	0.013	30	5.68	0.87
12.6	0.014	30	5.17	1.09
16.1	0.016	30	4.67	1.32

$A = 0.257$ LMH/bar; $B = 0.08$ LMH; $R^2(J_W) = 0.997$; $R^2(j_S) = 0.984$.

Table C.11: RO#11 data points.

c_f (g/L)	c_p (g/L)	P (bar)	J_W (L/(h m^2))	j_S (g/(h m^2))
2.9	0.017	30	6.71	0.33
7.8	0.018	30	5.93	0.65
11.9	0.019	30	5.19	0.98
18.0	0.022	30	4.37	1.33
23.8	0.025	30	3.84	1.67

$A = 0.261$ LMH/bar; $B = 0.07$ LMH; $R^2(J_W) = 0.984$; $R^2(j_S) = 0.997$.

Table C.12: RO#12 data points.

c_f (g/L)	c_p (g/L)	P (bar)	J_W (L/(h m^2))	j_S (g/(h m^2))
11.6	0.017	30	5.97	0.84
17.9	0.018	30	4.29	1.60
23.8	0.021	30	3.37	2.19
27.4	0.024	30	2.53	2.71
30.1	0.027	30	1.90	3.02

$A = 0.296$ LMH/bar; $B = 0.09$ LMH; $R^2(J_W) = 0.991$; $R^2(j_S) = 0.995$.

Table C.13: RO#13 data points.

c_f (g/L)	c_p (g/L)	P (bar)	J_W (L/(h m^2))
8.8	0.044	50	10.30
13.7	0.048	50	9.14
23.9	0.059	50	7.98
29.6	0.068	50	6.98
32.7	0.076	50	5.99
35.4	0.082	50	5.24

$A = 0.254$ LMH/bar; $R^2(J_W) = 0.964$.

C.2 Osmotically Assisted Reverse osmosis

Table C.14: OARO#1 data points.

c_f (g/L)	c_p (g/L)	P (bar)	J_W (L/(h m^2))
30.2	6.03	60	8.03
30.2	11.70	60	8.03
30.9	17.02	60	8.10
30.9	22.17	60	8.21
31.1	22.17	30	2.87
31.8	27.14	30	3.11

$A = 0.232$ LMH/bar; $S = 1543$ μm; $R^2(J_W) = 0.999$.

C.3 Pressure assisted osmosis

Table C.15: PAO#1 data points.

c_f (g/L)	c_{ds} (g/L)	P (bar)	J_W (L/(h m^2))
158.3	250.2	60	3.00
158.3	250.6	50	2.77
131.7	250.8	50	3.56
131.8	250.9	60	3.84
112.8	251.8	60	4.50
112.9	252.9	50	4.03
98.7	253.3	50	4.49
98.9	253.0	60	4.90

$A = 0.130$ LMH/bar; $S = 1499$ μm; $R^2(J_W) = 0.996$.

Table C.16: PAO#2 data points.

c_f (g/L)	c_{ds} (g/L)	P (bar)	J_W (L/(h m^2))
89.8	172.9	30	4.89
72.1	172.9	30	5.69
59.6	170.8	30	6.12
59.7	137.4	30	4.92
59.7	104.9	30	4.15
59.7	79.8	30	3.19
59.7	79.8	40	3.92

$A = 0.127$ LMH/bar; $S = 660$ μm; $R^2(J_W) = 0.981$.

C.4 Forward osmosis

Table C.17: PAO#3 data points.

c_f (g/L)	c_{ds} (g/L)	P (bar)	J_W (L/(h m^2))
159.0	249.6	60	2.44
159.0	249.2	50	2.27
132.0	248.2	50	2.95
132.0	247.9	60	3.32
112.9	247.3	60	3.84
112.9	246.5	50	3.52
98.5	246.3	50	3.94
98.5	245.7	60	4.22

$A = 0.175$ LMH/bar; $S = 1990$ μm; $R^2(J_W) = 0.991$.

Table C.18: PAO#4 data points.

c_f (g/L)	c_{ds} (g/L)	P (bar)	J_W (L/(h m^2))
46.1	98.6	60	6.04
46.1	99.3	50	5.07
36.9	95.4	50	5.91
36.9	98.5	60	6.44
30.7	97.7	60	7.27
26.4	97.3	60	8.37

$A = 0.187$ LMH/bar; $S = 1813$ μm; $R^2(J_W) = 0.923$.

Table C.19: PAO#5 data points.

c_f (g/L)	c_{ds} (g/L)	P (bar)	J_W (L/(h m^2))
150.0	200.0	60	2.13
119.3	199.2	60	3.31
119.3	197.7	50	2.86
99.0	195.7	50	3.40
99.0	194.2	60	3.88
84.6	192.5	60	4.27
84.6	191.0	50	3.69

$A = 0.127$ LMH/bar; $S = 1689$ μm; $R^2(J_W) = 0.967$.

Table C.20: PAO#6 data points.

c_f (g/L)	c_{ds} (g/L)	P (bar)	J_W (L/(h m^2))
50.0	98.6	50	6.12
50.0	97.2	40	4.89
40.0	95.8	40	5.86
40.0	94.5	50	6.29
40.0	93.1	60	7.37

$A = 0.142$ LMH/bar; $S = 784$ μm; $R^2(J_W) = 0.934$.

Table C.21: PAO#7 data points.

c_f (g/L)	c_{ds} (g/L)	P (bar)	J_W (L/(h m^2))
25.0	149.2	20	5.89
25.0	148.0	30	6.92
25.0	146.3	40	8.32
15.0	144.4	40	9.30
15.0	142.8	30	7.63
15.0	141.6	20	6.41

$A = 0.269$ LMH/bar; $S = 1599$ μm; $R^2(J_W) = 0.975$.

Table C.22: PAO#8 data points.

c_f (g/L)	c_{ds} (g/L)	P (bar)	J_W (L/(h m^2))
0.06	148.2	30	9.71
0.06	148.0	40	10.97
0.07	144.0	50	12.22
0.07	89.0	50	11.75
0.08	88.3	40	9.88
0.08	87.8	30	8.26

$A = 0.207$ LMH/bar; $S = 1145$ μm; $R^2(J_W) = 0.989$.

Table C.23: PAO#9 data points.

c_f (g/L)	c_{ds} (g/L)	P (bar)	J_W (L/(h m^2))
0.015	148.2	30	9.67
0.016	146.3	40	10.49
0.019	144.2	50	12.02
0.020	106.4	50	12.60
0.021	105.2	40	10.36
0.022	104.2	30	8.71

$A = 0.227$ LMH/bar; $S = 1400$ μm; $R^2(J_W) = 0.934$.

Table C.24: FO#1 data points.

c_f (g/L)	c_{ds} (g/L)	J_W (L/(h m^2))
0.49	184.4	9.93
0.49	168.6	9.05
0.49	152.2	8.56
0.49	134.2	8.15
0.49	123.2	7.09
0.49	110.3	6.70

$A = 0.116$ LMH/bar; $S = 363$ μm; $R^2(J_W) = 0.964$.

Table C.25: FO#2 data points.

c_f (g/L)	c_{ds} (g/L)	J_W (L/(h m^2))
0.5	120.6	6.92
0.5	102.2	6.06
0.5	87.7	5.39
0.5	75.8	4.42
0.5	65.67	3.83

$A = 0.083$ LMH/bar; $S = 137$ μm; $R^2(J_W) = 0.984$.

Table C.26: FO#3 data points.

c_f (g/L)	c_{ds} (g/L)	J_W (L/(h m^2))
0.1	149.2	7.33
0.1	139.8	6.90
0.1	129.3	6.71
0.1	118.0	6.23
0.1	107.0	5.81
0.1	98.0	5.61

$A = 0.131$ LMH/bar; $S = 626$ μm; $R^2(J_W) = 0.985$.

Table C.27: FO#4 data points.

c_f (g/L)	c_{ds} (g/L)	J_W (L/(h m^2))
0.1	200.0	9.28
0.1	157.6	8.11
0.1	120.9	7.34
0.1	95.8	6.18
0.1	75.1	5.29

$A = 0.194$ LMH/bar; $S = 778$ μm; $R^2(J_W) = 0.989$.

Table C.28: FO#5 data points.

c_f (g/L)	c_{ds} (g/L)	J_W (L/(h m^2))
0.1	80.3	6.48
0.1	66.3	5.87
0.1	57.4	5.28
0.1	43.6	4.37

$A = 0.211$ LMH/bar; $S = 616$ μm; $R^2(J_W) = 0.995$.

Table C.29: FO#6 data points.

c_f (g/L)	c_{ds} (g/L)	J_W (L/(h m^2))	j_S (g/(h m^2))
0.1	99.3	7.31	-1.37
0.1	89.0	6.25	-1.28
0.1	78.9	5.90	-1.16
0.1	69.6	5.29	-0.84
0.1	61.3	4.79	-0.86
0.1	52.2	4.21	-0.58

$A = 0.116$ LMH/bar; $B = 0.017$ LMH; $S = 211$ μm; $R^2(J_W) = 0.971$; $R^2(j_S) = 0.923$.

Table C.30: FO#7 data points.

c_f (g/L)	c_{ds} (g/L)	J_W (L/(h m^2))	j_S (g/(h m^2))
0.1	148.8	7.96	-1.40
0.1	138.6	7.64	-1.24
0.1	128.0	7.44	-1.24
0.1	118.3	7.18	-1.14
0.1	108.8	6.57	-0.91
0.1	99.4	6.29	-0.79

$A = 0.151$ LMH/bar; $B = 0.02$ LMH; $S = 585$ μm; $R^2(J_W) = 0.956$; $R^2(j_S) = 0.915$.

Table C.31: FO#8 data points.

c_f (g/L)	c_{ds} (g/L)	J_W (L/(h m^2))	j_S (g/(h m^2))
0.1	99.4	6.54	-1.26
0.1	90.0	5.91	-1.13
0.1	79.7	5.45	-0.97
0.1	70.2	4.95	-0.91
0.1	61.3	4.79	-0.81
0.1	52.1	4.25	-0.78

$A = 0.160$ LMH/bar; $B = 0.024$ LMH; $S = 605$ μm; $R^2(J_W) = 0.956$; $R^2(j_S) = 0.900$.

Table C.32: FO#9 data points.

c_f (g/L)	c_{ds} (g/L)	J_W (L/(h m^2))	j_S (g/(h m^2))
0.1	99.3	6.39	-1.29
0.1	89.7	5.72	-1.12
0.1	79.5	5.06	-1.01
0.1	61.4	4.49	-0.95
0.1	53.1	3.96	-0.75

$A = 0.129$ LMH/bar; $B = 0.021$ LMH; $S = 455$ μm; $R^2(J_W) = 0.959$; $R^2(j_S) = 0.84$.

Table C.33: FO#10 data points.

c_f (g/L)	c_{ds} (g/L)	J_W (L/(h m^2))	j_S (g/(h m^2))
0.1	173.7	8.00	-1.44
0.1	158.5	7.36	-1.47
0.1	143.2	6.96	-1.28
0.1	133.2	6.66	-1.19
0.1	123.2	6.22	-1.00
0.1	113.4	6.10	-0.96

$A = 0.111$ LMH/bar; $B = 0.017$ LMH; $S = 518$ μm; $R^2(J_W) = 0.974$; $R^2(j_S) = 0.89$.

Appendix D

Pervaporation experimental data

Table D.1: Pervaporation experimental data

Experiment	c_f (g/L)	J_W (L/(h m^2))	A (LMH/bar)
DI#1	0	1.138	51.12
DI#2	0	1.180	53.01
DI#3	0	1.269	57.02
DI#4	0	1.167	52.44
50#1	50	1.010	47.32
50#2	50	0.879	40.86
50#3	50	1.039	48.71
100#1	100	0.724	35.26
100#2	100	0.809	39.38
150#1	150	0.787	40.14
150#2	150	0.841	42.95
250#1	250	0.582	33.35
250#2	250	0.415	23.77
250#3	250	0.529	30.51

$P^w_{sat,v}$=2.67×10^{-3} bar T = 21°C

Appendix E

Head loss for sweep solution channels

A preliminary set of tests aimed to investigate the effect of spacers in the sweep/draw solution channel head loss under pressure. Commercial TFC membranes (SW30, Dow) and its RO feed spacers and permeate carriers were tested in the same apparatus described in Chapter 4 under variable pressure using DI water and pressures up to 50 bar. Pictures of the pristine and used membranes are depicted in Figure E.1.

The membrane deformation/imprinting was also responsible for an average increase in water permeability from 1.30 LMH/bar to 1.72 LMH/bar. In diamond spacer case, the membrane did not have a significant rejection due to extreme deformation, while for the permeate carriers support case it was measured at 97% for a solution.

These spacers were tested under variable feed pressure to check for the increase in head loss. As presented in Figure E.2, as these plastic fabrics deform, they compact and severely increase the head loss, not reaching a stable value for pressures up to 50 bar.

The MF-OARO-RO model described in Chapter 3 was used to evaluate the impact of this pressure loss in the process feasibility. The quadratic polynomial fitting presented in Figure E.2 was used and varied over 0.1 - 100% of its original value.

According to Figure E.3, the pressure drop strongly influences both flux and energy consumption. The effect of increasing mass transfer at higher flowrates is very small compared to the decrease caused by head loss. It impacts on both raising the needed feed pressure to reach the design flux and increasing the sweep solution pump size, creating a double inefficiency. In case of an industrial module, in order to make the process economically feasible, the head loss must be severely minimized. Even applying 1% of the permeate carries head loss, the energy consumption is still

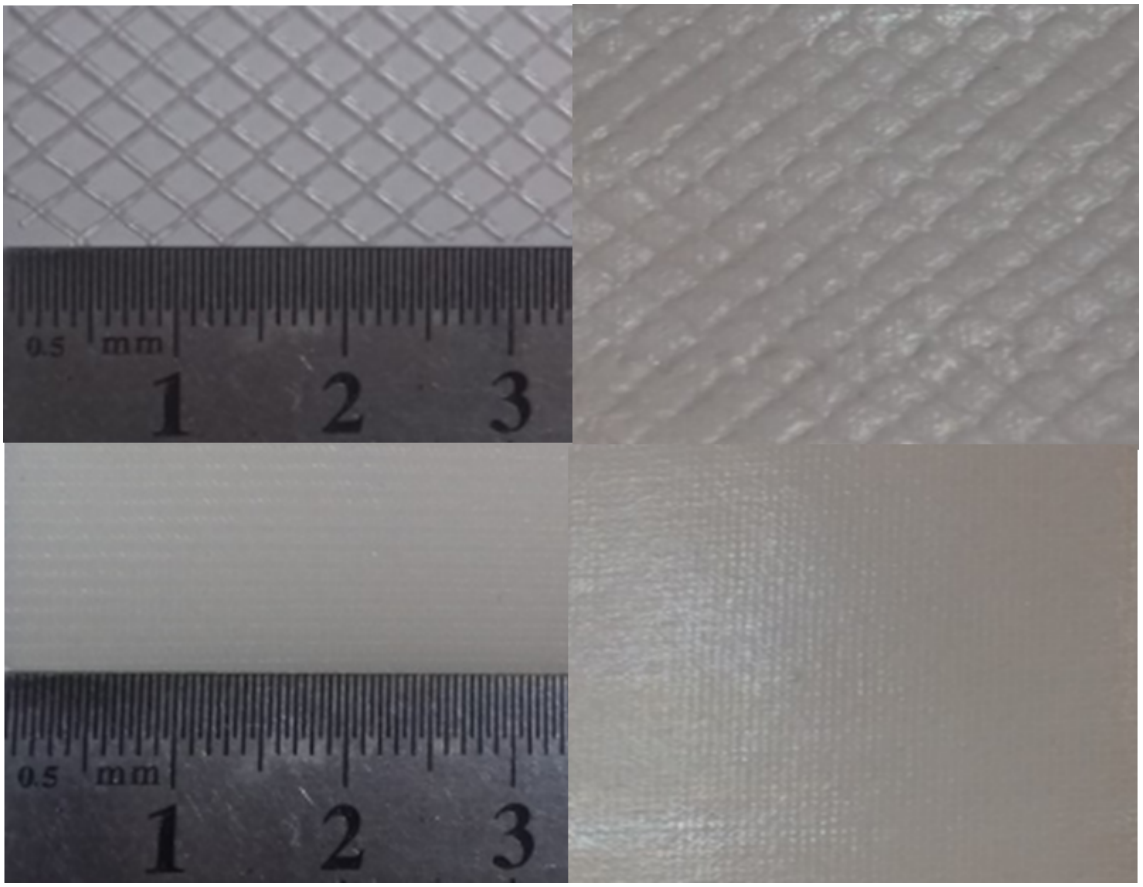

Figure E.1: Membranes before and after pressurization using (1) diamond spacers and (2) permeate carriers.

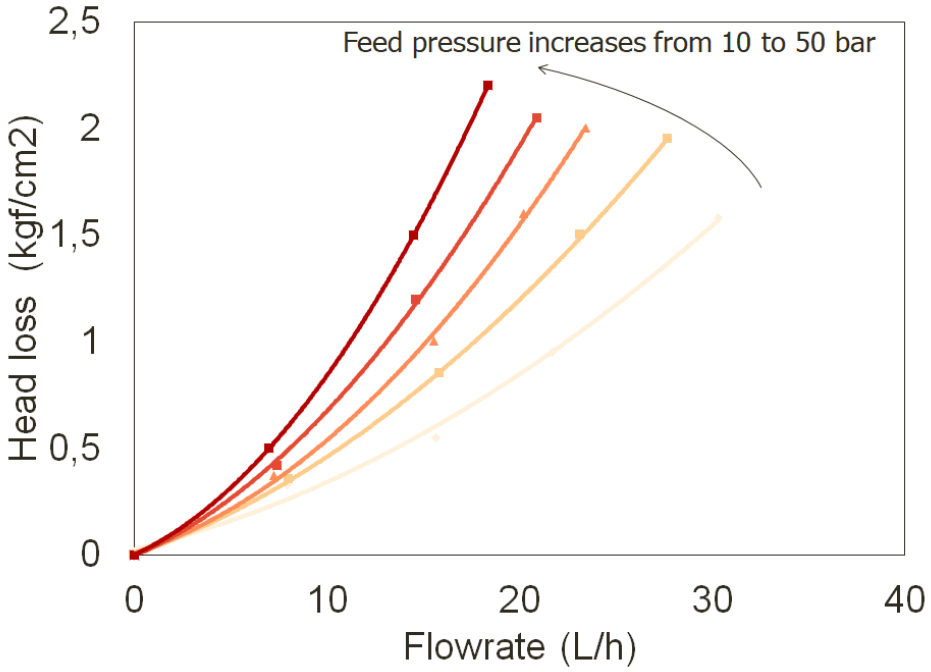

Figure E.2: Sweep channel head loss as function of flowrate and applied feed pressure for a stack of 5 permeate carriers.

strongly influenced by the draw solution velocity.

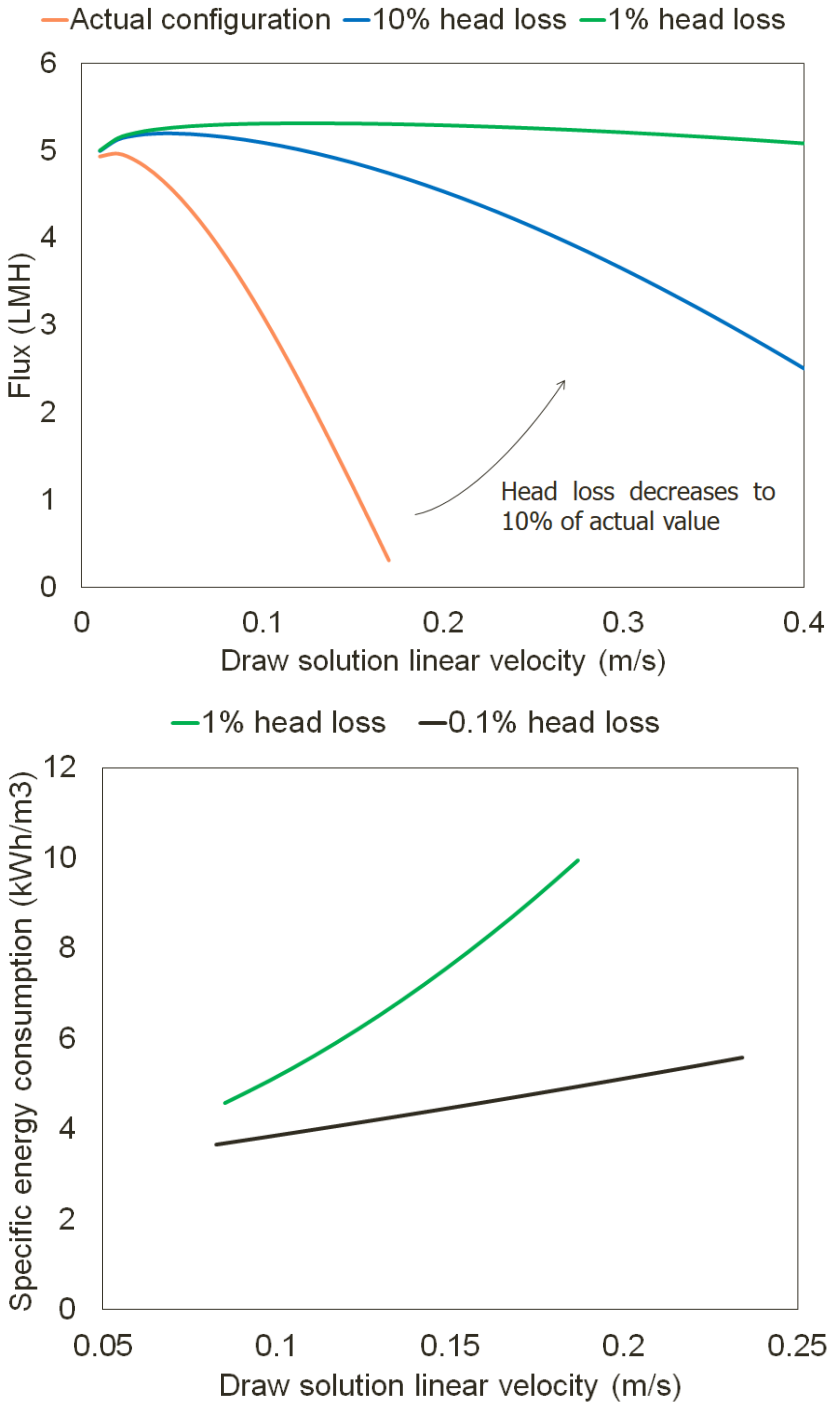

Figure E.3: Flux (a) and energy consumption (b) of OARO process with seawater feed, 20 g/L sweep solution, A = 1LMH/bar, B = 0.1 LMH and S = 1000 μm.

The metalic fabrics were investigated to minimize the effect of compaction caused by deformable spacers and proved to be suitable for high pressures, with almost absent effect of feed pressure. Although the adopted metalic fabrics were sufficient for the test purposes in Chapter 4, a head loss of 0.2 bar for each 10 cm is still high and shall be focus of further studies.

Appendix F

X-ray diffraction

Aiming to associate peak shift (and structural properties) to the hypothetical deswelling, X-ray diffraction was tested in dry, DI-wet and (150 g/L solution)NaCl-wet commercial CTA (FTS Membrane) and TFC (DOW SW30, after nonwoven cloth removal) samples. They were stored in solution or air overnight.

The analysis used a XRD Rigaku equipment (Miniflex II model). In the wet samples, the procedure was performed in phases (eg. 5 – 25, 25 – 50°), so the membrane could be wet again in the solution for a moment. The solution or DI excess was removed before the analysis using a tissue.

The higher peak at 26° for the wet CTA, when compared to the dry samples in in Figure F.1, suggests there may have been a redistribution in the lattice space between the two conditions. However, there is a decrease in the peak intensity for DI-wet and saline-wet refractograms, which was associated with absorption of X-ray by the solution [241] and apparently also happened for DI-wet and saline-wet TFC membranes in Figure F.2. As TFC is thinner, the magnitude of the change of different states was lower. Even clearer in this case, the volumetric difference between the dry and the wet TFC is not evidenced in any peak shift or intensity decrease.

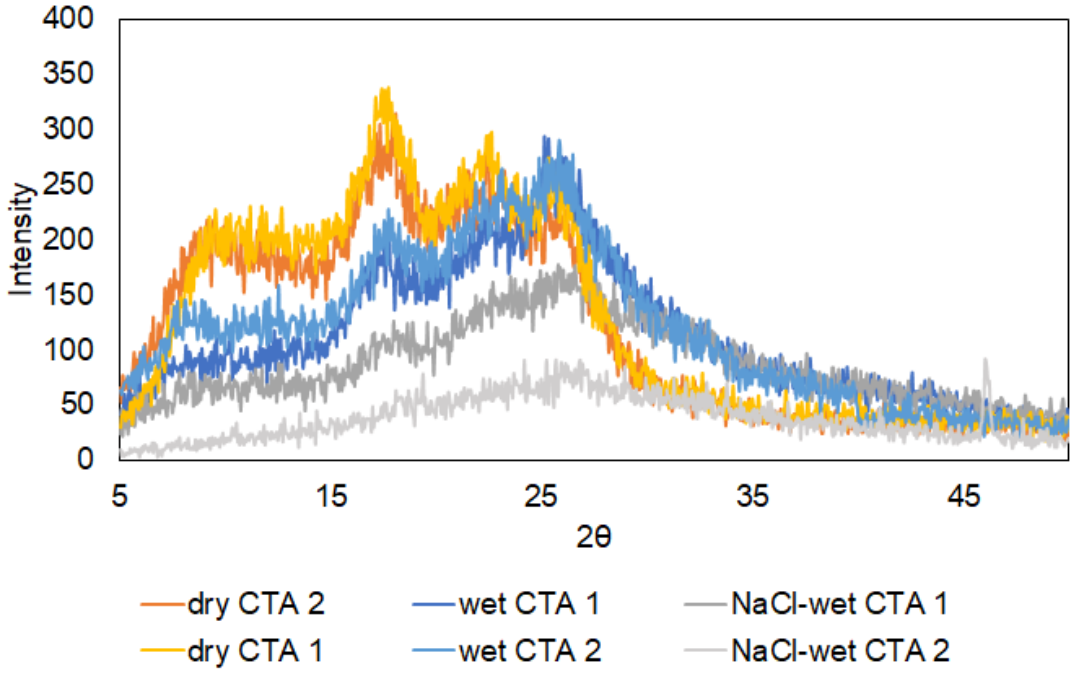

Figure F.1: Commercial dry, DI-wet and NaCl-wet CTA membrane refractograms.

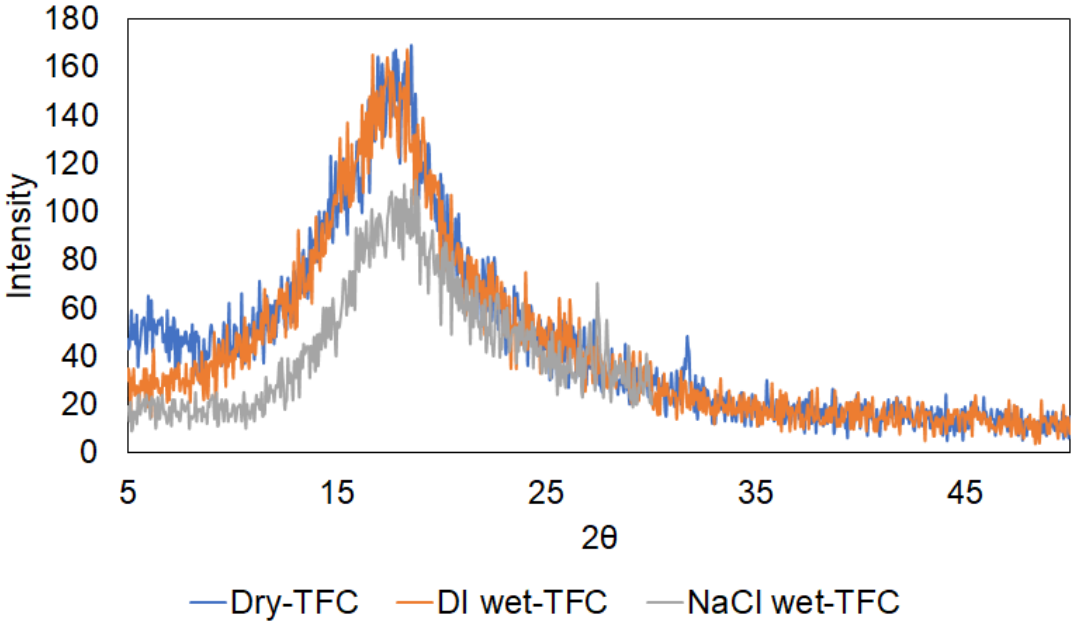

Figure F.2: Commercial dry, DI-wet and NaCl-wet TFC membrane refractograms.

Appendix G

EMSO models

G.1 MF-OARO-RO flowsheet

```
using "ROmembAssist3rig";
using "ROrigtest";
using "PXmodule";
using "auxiliary";
using "MFmemb";

    FlowSheet ROassist

    DEVICES
RO101 as ROmembAssist;
P102 as pump;
P103 as pump;
PX101 as PXmodule;
PX102 as PXmodule;
P104 as pump;
P105 as pump;
P106 as pump;
RO102 as ROmembrig;
RO103 as ROmembrig;
MF101 as MFmemb;
Fin as flow_vol(Default=2);
cons as Real(Brief="Specific energy", Lower=0, Upper=1e4, Unit='kW*h/m^3');
PXcost as currency(Brief="Capital Cost of Pressure exchangers", Default=1e3);
HPPcost as currency(Brief="Capital Cost of HP pumps", Default=1e3);
CapexRO as currency(Brief="Capital Cost of RO unit", Default=1e3); # estimated
```

```
according to SWRO
OpexT as currency(Brief="Annual Operational Cost of the unit", Default=1e4); #
estimated according to SWRO
Ecost as Real(Brief="Energy cost", Lower=1e-3, Upper=0.2, Default=0.1,
Unit='US$/(kW*h)');
CapexT as currency(Brief="Total Capital Cost", Default=1e5);
a as Real(Brief="Amortization Factor", Lower=0, Upper=1);
i as fraction(Brief="Interest Rate", Default=0.1);
spc as Real(Brief="Specific cost", Lower=0, Upper=1e4, Default=50,
Unit='US$/m^3');
Cmf as currency(Brief="Total Capital Cost", Default=1e4);
MR as Real(Brief="Ratio between draw solution and feed", Default=0.3);
NaCl as makeup(Brief="Draw solute make up");
sangria as flow_vol(Default=0.1, DisplayUnit='m^3/d');
cp as conc_mol(Default=0.05);
cpt as conc_mol(Default=0.04);
P as flow_vol(Default=2);
Ps as flow_vol(Default=0.1);

    PARAMETERS
n as Real(Brief="Plant Life", Default=20);
f as fraction(Brief="Plant Availability", Default=0.9);

    SET
f = 0.9;
n = 20;

    CONNECTIONS
Fin to MF101.Fin;

    EQUATIONS
cons = (P102.Pot+P103.Pot+P104.Pot + P105.Pot+P106.Pot)/RO102.P;
P102.F = RO101.Fin - RO101.Fout;
P102.Pout = RO101.Pin;
RO101.Pout = PX101.PinH;
P103.F = RO101.Fout;
P103.Pin = PX101.PoutL;
P103.Pout = RO101.Pin;
PX101.PinL = 0.2*'bar';
```

```
PX101.PoutH = 0.2*'bar';
MF101.RR = 0.90;
MF101.cFin = 100*'kg/m^3' ;
P104.F = RO102.Fin - RO102.Fout;
P104.Pout = RO102.Pin;
RO102.Pout = PX102.PinH;
P105.F = RO101.Fout;
P105.Pin = PX102.PoutL;
P105.Pout = RO102.Pin;
PX102.PinL = 0.2*'bar';
PX102.PoutH = 0.2*'bar';
#Cost
HPPcost = 1.419*52*'US$'*(P102.Pout*P102.F+P103.Pout*P103.F +
P104.Pout*P104.F+P105.Pout*P105.F+ P106.Pout*P106.F)/('atm*(m^3/h)');
PXcost = 1.419*52*'US$'*(PX101.PinH*RO101.Fout +
PX102.PinH*RO102.Fout)/('atm*m^3/h');
a = (i*((1+i)^n))/(((1+i)^n)-1);
CapexRO = (HPPcost + PXcost + RO101.ROMcost+RO102.ROMcost+
RO103.ROMcost)/0.45;
CapexT = a*(CapexRO + Cmf)/f;
Cmf = 720*'US$/m^2'*(MF101.Am)/0.3;
spc = (OpexT+CapexT)/((RO103.P+Ps-sangria)*360*'d');

    if RO102.Js(3)*RO102.Am > RO101.Jsa*RO101.Am then
NaCl.M = (RO102.Js(3)*RO102.Am-RO101.Jsa*RO101.Am);
OpexT = ((P102.Pot+P103.Pot + P104.Pot +
P105.Pot+P106.Pot)*Ecost*360*'d'*f + 0.333*(RO101.ROMcost +
RO102.ROMcost))/0.88 + 0.1*520*'US$/m^2'*(MF101.Am)+NaCl.M*1*'US$/kg'*360*'d';
sangria = 1e-10*'m^3/d';

    else
NaCl.M = (RO101.Jsa*RO101.Am-RO102.Js(3)*RO102.Am);
sangria*RO102.cFin = NaCl.Mol;
OpexT = ((P102.Pot+P103.Pot + P104.Pot +
P105.Pot+P106.Pot)*Ecost*360*'d'*f + 0.333*(RO101.ROMcost +
RO102.ROMcost))/0.88 + 0.1*520*'US$/m^2'*(MF101.Am);
end

    cpt*(Ps+P) = (RO102.cFin*Ps+cp*P);
```

```
P = RO103.P;
cp = RO103.cP;
P+Ps = 50*'m^3/d';

    SPECIFY
RO101.RR = 0.46;
RO101.Fin = MF101.P;
RO101.cFin = 1.85*'kmol/m^3';
MF101.cS = RO101.cFin*(58.5*'kg/kmol');
RO101.Pi = MR*RO101.Fin;
RO101.cPi =0.9*'kmol/m^3';
RO102.Fin = RO101.Po; #connection between two RO modules
RO102.cFin = RO101.cPo;
RO102.Fout = RO101.Pi;
P102.Pin = 1e-10*'atm';
P104.Pin = 0.1*'atm';
Ecost = 0.05*'US$/(kW*h)';
i = 0.10;
P102.rho = 1059.93*'kg/m^3';#RO101.rhoF(1);
P103.rho = 1059.93*'kg/m^3';#RO101.rhoF(1);
P104.rho = RO102.rhoF(1);
P105.rho = RO102.rhoF(1);
P106.rho = 1000*'kg/m^3';
MR = 0.52;
RO101.Jw(2) = 15*'l/(h*m^2)';
RO102.Jw(2) = 15*'l/(h*m^2)';
cpt = 0.0034*'kmol/m^3';
RO101.A = 2.77E-7*'m^3/(s*bar*m^2)'; #DOW SWRO30-400
RO101.B = 3E-8*'m^3/(s*m^2)';
RO101.S = 1E-4*'m';
RO101.ROcost = 80*'US$/m^2';
RO103.Fin = RO102.P;
RO103.cFin = RO102.cP;
RO103.Jw(2)=20*'l/(h*m^2)';
RO103.RR = 0.9;
P106.F = RO103.Fin;
P106.Pin = 1e-10*'atm';
P106.Pout = RO103.Pin;
```

```
    OPTIONS
GuessFile="ROassistAP";
# SecondGuessFile="TesteROpap";#"TesteROpARO";#"TesteROnm5";
Dynamic = false;

    end
```

G.1.1 MF module

```
Model MFmemb

    PARAMETERS
L as length(Brief="Length of each flow channel");
dp as length(Brief="Pore diameter");
dm as length(Brief="Diameter of each membrane channel");
A as Real(Brief="Membrane permeability", Unit = 'm^3/(s*bar*m^2)');
T as temperature;
#Oil concentration
cP as conc_mass;

    SET
cP = 0*'kg/m^3';

    VARIABLES
#Flows
in Fin as flow_vol(Brief="Inlet flowrate");
out Fout as flow_vol(Brief="Outlet flowrate");
P as flow_vol(Brief="Permeate flowrate");
#Oil concentrations
cFin as conc_mass;
cFout as conc_mass;
cS as conc_mass;
RR as fraction(Brief="Recovery");
Jw as flux_vol(Brief="Permeate flux", DisplayUnit='l/(h*m^2)');
Am as area(Brief="Total membrane area");

    EQUATIONS
"Flux calculation" # vF = 2 m/s e dP = 2 bar
Jw = ('l/(h*m^2)')*(253 - 0.0014*'m^3/(kg)'*cS - 0.30*'m^3/(kg)'*cFin +
```

```
12.7*'1/(K)'*(T-273.15*'K')-0.00187*'m^3/(K*kg)'*cFin*(T-273.15*'K')          +
0.00011*'m^6/(kg^2)'*cFin^2 - 0.066*'1/((K^2))'*(T-273.15*'K')^2);
"Mass balance"
Fin = Fout + P;
"Recovery ratio"
RR = P/Fin;
"Oil balance"
cFout*Fout = cFin*Fin;
"Area calculation"
Jw = P/Am;
```

G.1.2 OARO membrane module

```
using "types";

    Model ROmembAssist

    PARAMETERS
L as length(Brief="Length of the retangular flow channel");
W as length(Brief="Width of retangular flow channel");
R as Real(Brief="Universal gas constant", Unit = '(atm*m^3)/(K*kmol)', Default
= 0.082);
D as diffusivity;
T as temperature;
MM as molweight(Default = 58.5);
dh as length;
Lm as length(Brief="Membrane length");
Nl as Real(Brief="Number of leaves in a RO spiral wound module");
n as Real(Brief="Vant Hoff factor", Lower = 1, Upper = 5, Default = 2);
nm as Integer;

    SET
Lm = 0.0254*40*'m';
Nl = 16;
L = 0.0254*50*'m';
W = 28*0.001*0.0254*'m'; #feed spacer = 28 mil
T = 298*'K';
dh = 4*(L*W)/(2*L+2*W);
```

D = 1.33E-9*'(m^2)/s';
nm=8;

VARIABLES
A as Real(Brief="Membrane permeability", Unit = 'l/(h*bar*m^2)', DisplayUnit='l/(bar*h*m^2)');
B as Real(Brief="Salt permeability", Unit = 'm^3/(s*m^2)', DisplayUnit = 'l/(h*m^2)');
Fin as flow_vol(Brief="Feed flow");
Fout as flow_vol(Brief="Concentrate flow", Default=3.2);
Pi as flow_vol(Brief="Permeate flow", Default=2);
Po as flow_vol(Brief="Permeate out flow", Default=2);
RR as fraction(Default = 0.3, Upper = 0.9); #recovery ratio
Pin as pressure(Default = 120);
Pout as pressure(Default = 118);
lamb(nm) as Real(Default=0.47);
Fi(nm+1) as flow_vol(Brief="Feed flow");
P(nm+1) as flow_vol(Brief="Permeate+DS flow", Default=2);
# concentrations
cFin as conc_mol(Default = 1.5);
cPi as conc_mol(Default = 0.5);
cPo as conc_mol(Default=0.4);
cP(nm) as conc_mol(Default=0.45);
cPm(nm) as conc_mol(Default=0.5);
cFm(nm) as conc_mol(Default = 1.77);
cF(nm) as conc_mol(Default = 1.83);
cFout as conc_mol(Default = 4);
dCm(nm) as conc_mol(Default=1);
cFi(nm+1) as conc_mol(Default = 1.6);
cPx(nm+1) as conc_mol(Default = 0.5);
Press(nm+1) as pressure(Default=90);
# Membrane calculations
Jw(nm) as flux_vol(Default = 1e-6, DisplayUnit = 'l/(h*m^2)');
Js(nm) as flux_mass(Default=1e-7);
Jsa as flux_mass(Default=1e-7);
# Fluid properties
piFm(nm) as pressure(Default=144);
dPi(nm) as pressure(Default=50);
dP(nm) as pressure(Brief="Head loss");

```
Am as area;
Amn as area;
vF(nm) as velocity;
vP(nm) as velocity;
ReF(nm) as Real(Brief="Número de Reynolds");
ReP(nm) as Real(Brief="Número de Reynolds");
kF(nm) as Real(Brief="mass transfer coefficient", Unit = 'm/s');
ScF(nm) as Real(Brief="Schmidt number");
ShF(nm) as Real(Brief="Sherwood number");
rhoF(nm) as dens_mass;
miF(nm) as viscosity;
ROMcost as currency(Brief="Capital Cost of RO Membranes and housings",
Default=1e5);
S as length;
ROcost as Real(Brief="Polimeric RO membrane and housings cost per m^2",
Unit='US$/(m^2)');

    EQUATIONS
Pin = Press(1);
Pout = Press(nm+1);
cFi(1)=cFin;
cFi(nm+1)=cFout;
cPx(nm+1)=cPi;
cPx(1)=cPo;
Pi=P(nm+1);
Po = P(1);
Fin = Fi(1);
Fout = Fi(nm+1);
Amn = Am/nm;
RR = (Po-Pi)/Fin;

    for index in [1:nm] do
cFm(index)*Jw(index) = -B*dCm(index)+(Jw(index)*cF(index)+B*dCm(index))*
exp(Jw(index)/kF(index));
cPm(index)*Jw(index) = -B*dCm(index) +(Jw(index)*cP(index)+B*dCm(index))*exp(-
Jw(index)*S/D);
"Global Mass balance"
Fi(index) + P(index+1) = Fi(index+1) + P(index);
"Global Mass balance with flux"
```

```
Fi(index) - Fi(index+1) = Jw(index)*Amn;
"Salt mass balance"
MM*cFi(index)*Fi(index) -Js(index)*Amn = MM*cFi(index+1)*Fi(index+1);
"Salt mass balance with flux"
MM*cPx(index+1)*P(index+1) + Js(index)*Amn = MM*cPx(index)*P(index);
"Osmotic pressure - Feed average"
piFm(index) = cF(index)*R*T*n;
cP(index) = (cPx(index) + cPx(index+1))/2;
"Feed average velocity"
vF(index)*(Lm*W*Nl) = ((Fi(index)+Fi(index+1))/2);
"Permeate average velocity"
vP(index)*(Lm*W*Nl) = (P(index)+P(index+1))/2;
"Feed Reynolds"
ReF(index) = vF(index)*rhoF(index)*dh/miF(index);
"Permeate Reynolds"
ReP(index) = vP(index)*rhoF(index)*dh/miF(index);
"Feed Schmidt"
ScF(index) = miF(index)/(rhoF(index)*D);
"Feed Sherwood"
ShF(index) = 0.2*(ReF(index)^2)^(0.57/2)*(ScF(index)^2)^(0.4/2);
"Feed mass transfer coefficient"
ShF(index) = kF(index)*dh/D;
"cFm calculation"
cF(index) = (cFi(index)+ cFi(index+1))/2;
dCm(index)*(Jw(index)+B*(exp(Jw(index)/kF(index))-exp(-Jw(index)*S/D)))
=                Jw(index)*(cF(index)*exp(Jw(index)/kF(index))-cP(index)*exp(-
Jw(index)*S/D));
dPi(index) = dCm(index)*R*T*n;
"Water Flux"
Jw(index) = A*(Press(index) - dP(index)/2 - dPi(index));
"Salt flux"
Js(index) = B*MM*(dCm(index));
"Lambda calculation"
lamb(index) = 6.23*(ReF(index)^2)^(-0.3/2);
"Pressure loss"
dP(index) = (lamb(index)*rhoF(index)*Lm*vF(index)^2)/(2*dh);
"Final pressure" Press(index+1) = Press(index) - dP(index);
"DS density calculation"
rhoF(index) = (1000.8*'kg/m^3'+ 37.216*cF(index)*'g/mol');
```

```
"DS viscosity calculation"
miF(index) = (1+cF(index)*0.1173*'l/mol')*'cP';
end
ROMcost = ROcost*Am;
Jsa = sum(Js)/nm;
end
```

G.1.3 RO membrane module

```
using "types";

    Model ROmembrig

    PARAMETERS
L as length(Brief="Length of the retangular flow channel");
W as length(Brief="Width of retangular flow channel");
A as Real(Brief="Membrane permeability", Unit = 'l/(h*bar*m^2)');
B as Real(Brief="Salt permeability", Unit = 'm^3/(s*m^2)');
R as Real(Brief="Universal gas constant", Unit = '(atm*m^3)/(K*kmol)', Default
= 0.082);
D as diffusivity;
T as temperature;
MM as molweight(Default = 58.5);
Nl as Real(Brief="Number of leaves in a RO spiral wound module");
ROcost as Real(Brief="Polimeric RO membrane and housings cost per m^2",
Unit='US$/(m^2)');
n as Real(Brief="Vant Hoff factor", Lower = 1, Upper = 5, Default = 2);
nm as Integer(Brief="Number of elements");
dpt as length;

    SET
L = 0.0254*50*16*'m';
W = 28*0.001*0.0254*'m'; #feed spacer = 28 mil
A = 2.77E-7*'m^3/(s*bar*m^2)'; # DOW SWRO30-400
B = 3E-8*'m^3/(s*m^2)';
T = 298*'K';
D = 1.33E-9*'(m^2)/s';
ROcost = 40*'US$/(m^2)';
nm = 6;
```

```
dpt = 28*0.001*0.0254*'m';

    VARIABLES
Fin as flow_vol(Brief="Feed flow");
Fout as flow_vol(Brief="Concentrate flow", Default=3.2);
P as flow_vol(Brief="Permeate flow", Default=2);
Fi(nm+1) as flow_vol(Brief="Feed in flow per element", Default=1);
Pi(nm) as flow_vol(Brief="Permeate flow per element", Default=1);
RR as fraction(Default = 0.5); #recovery ratio
Pin as pressure(Default = 120);
Pout as pressure(Default = 118);
lamb(nm) as Real(Default=1);
Press(nm+1) as pressure(Default=119);
# concentrations
cFi(nm+1) as conc_mol(Default=2);
cPi(nm) as conc_mol(Default=0.008);
cFm(nm) as conc_mol(Default=1.77);
cM(nm) as conc_mol(Default=1.83);
cP as conc_mol(Default=0.008);
cFin as conc_mol(Default = 0.76);
cFout as conc_mol(Default = 4);
# Membrane calculations
Jw(nm) as flux_vol(Default = 2e-6, DisplayUnit = 'l/(h*m^2)');
Jwa as flux_vol(Default=1e-6, DisplayUnit = 'l/(h*m^2)');
Js(nm) as flux_mass(Default=1e-7);
# Fluid properties
piFm(nm) as pressure(Default=144);
piM(nm) as pressure(Default=148);
dP(nm) as pressure(Brief="Head loss");
Am as area(Default=100);
Amn as area(Default=10);
vF(nm) as velocity;
ReF(nm) as Real(Brief="Número de Reynolds");
kF(nm) as Real(Brief="mass transfer coefficient", Unit = 'm/s');
ScF(nm) as Real(Brief="Schmidt number");
ShF(nm) as Real(Brief="Sherwood number");
rhoF(nm) as dens_mass;
miF(nm) as viscosity;
ROMcost as currency(Brief="Capital Cost of RO Membranes and housings",
```

Default=1e5);
Lm as length(Brief="Membrane length");
dh as length(Brief="Hydraulic diameter");
x as length(Default=40);
mF(nm) as Real(Brief="Feed molality", Default=1, Unit='mol/kg');
phiF(nm) as Real(Brief="Osmotic coefficient", Default=0.9, Lower=0.9, Upper=1.3);

EQUATIONS
Jwa = sum(Jw)/nm;
Fin = Fi(1);
Fout = Fi(nm+1);
cFi(1)=cFin;
cFi(nm+1)=cFout;
Pin = Press(1);
Pout = Press(nm+1);
P = sum(Pi);
Am = x*L*Nl;
Amn = Am/nm;
Lm = L/nm;
"Hydraulic diameter"
dh*(2*dpt+2*x) = 4*(dpt*x);
"Recovery ratio"
RR = P/Fin;
for index in [1:nm] do
phiF(index) = 0.9144 + 0.0239*mF(index)*'kg/mol' + 0.0061*(mF(index)*'kg/mol')^2;
mF(index)*(rhoF(index)-cFm(index)*MM) = cFm(index);
"Global Mass balance"
rhoF(index)*Fi(index) = Fi(index+1)*rhoF(index) + Pi(index)*1000*'kg/m^3';
"Global Mass balance with flux"
Fi(index) - Fi(index+1) = Jw(index)*Amn;
"Salt mass balance"
MM*cFi(index)*Fi(index) -Js(index)*Amn = MM*cFi(index+1)*Fi(index+1);
"Salt mass balance with flux"
MM*cPi(index)*Pi(index) = Js(index)*Amn;
"Osmotic pressure - Feed average"
piFm(index) = phiF(index)*cFm(index)*R*T*n;
"Osmotic pressure - @Membrane"

```
piM(index) = phiF(index)*cM(index)*R*T*n;
"Feed average velocity"
vF(index)*(Nl*dpt*x) = (Fi(index)+Fi(index+1))/2;
"Feed Reynolds"
ReF(index) = vF(index)*rhoF(index)*dh/miF(index);
"Feed Schmidt"
ScF(index) = miF(index)/(rhoF(index)*D);
"Feed Sherwood"
ShF(index) = 0.2*(ReF(index)^2)^(0.57/2)*(ScF(index)^2)^(0.4/2);
"Feed mass transfer coefficient"
ShF(index) = kF(index)*dh/D;
(cM(index)-cPi(index))=(cFm(index)-cPi(index))*exp(Jw(index)/kF(index));
"cFm calculation"
cFm(index) = (cFi(index)+ cFi(index+1))/2;
"Water Flux"
Jw(index) = A*(Press(index) - dP(index)/2 - piM(index));
"Salt flux"
Js(index) = B*MM*(cM(index)-cPi(index));
"Lambda calculation"
lamb(index) = 6.23*(ReF(index)^2)^(-0.3/2);
"Pressure loss"
dP(index) = (lamb(index)*rhoF(index)*Lm*vF(index)^2)/(2*dh);
"Final pressure"
Press(index+1) = Press(index) - dP(index);
"DS density calculation"
rhoF(index) = (1000.8*'kg/m^3'+ 37.216*cFm(index)*'g/mol');
"DS viscosity calculation"
miF(index) = (1+cFm(index)*0.1173*'l/mol')*'cP';
end


    ROMcost = ROcost*Am;
cP = sum(cPi*Pi)/P;
end
```

G.1.4 MF-OARO-RO optimization routine

```
using "ROassistrigAP";
Optimization ROassistopt as ROassist
```

```
    MINIMIZE
spc;

    FREE
RO101.cPi;
RO101.RR;
MR;

    EQUATIONS
RO101.cPi <= 2.2*'kmol/m^3';
RO101.cPi >= 0.5*'kmol/m^3';
MR >= 0.3;
MR <= 1.2;
RO101.Pin <=120*'bar';

    OPTIONS
Dynamic = false;
GuessFile = "ROassistoptbga";
SecondGuessFile="ROassistbga";
NLPSolveNLA = false;
FeasiblePath = true;
NLPSolver(File = "complex",
#File = "PSO",
#File = "ipopt_emso",
MaxIterations = 5000,
RelativeAccuracy = 1e-10, AbsoluteAccuracy = 1e-10);

    GUESS
RO101.cPi = 1.9*'kmol/m^3';
end
```

G.2 MF-RO flowsheet

```
using "PXmodule";
using "auxiliary";
using "MFmemb";
using "ROrigtest3";

    FlowSheet ORSW
```

```
    DEVICES

    RO101 as ROmembrig;
P101 as pump;
P102 as pump;
P103 as pump;
PX101 as PXmodule;
MF101 as MFmemb;
Fin as flow_vol(Default=2);
cons as Real(Brief="Specific energy", Lower=0, Upper=1e4, Unit='kW*h/m^3');
PXcost as currency(Brief="Capital Cost of Pressure exchangers", Default=1e3);
HPPcost as currency(Brief="Capital Cost of HP pumps", Default=1e3);
CapexRO as currency(Brief="Capital Cost of RO unit", Default=1e3); #estimated
according to SWRO
OpexT as currency(Brief="Annual Operational Cost of the unit", Default=1e4);
#estimated according to SWRO
Ecost as Real(Brief="Energy cost", Lower=1e-3, Upper=0.2, Default=0.1,
Unit='US$/(kW*h)');
CapexT as currency(Brief="Total Capital Cost", Default=1e5);
a as Real(Brief="Amortization Factor", Lower=0, Upper=1);
i as fraction(Brief="Interest Rate", Default=0.1);
spc as Real(Brief="Specific cost", Lower=0, Upper=1e4, Default=50,
Unit='US$/m^3');
Cmf as currency(Brief="Total Capital Cost", Default=1e4);
cp as conc_mol(Default=0.05);
cpt as conc_mol(Default=0.04);
P as flow_vol(Default=2);
Ps as flow_vol(Default=0.1);

    PARAMETERS
n as Real(Brief="Plant Life", Default=20);
f as fraction(Brief="Plant Availability", Default=0.9);

    SET
f = 0.9;
n = 20;
RO101.Nl = 16;
```

```
    CONNECTIONS
Fin to MF101.Fin;

    EQUATIONS
cons = (P102.Pot+P103.Pot)/(RO101.P);
P102.F = RO101.Fin - RO101.Fout;
P102.Pout = RO101.Pin;
RO101.Pout = PX101.PinH;
P103.F = RO101.Fout;
P103.Pin = PX101.PoutL;
P103.Pout = RO101.Pin;
PX101.PinL = 0.2*'bar';
PX101.PoutH = 0.2*'bar';
MF101.RR = 0.90;
MF101.cFin = 100*'kg/m^3';
P101.F = MF101.Fin;
P101.Pin = 1e-10*'atm';
P101.Pout = 2*'bar';
#Costs HPPcost = 1.419*52*'US$'*(P101.Pout*P101.F +
P102.Pout*P102.F+P103.Pout*P103.F)/('atm*(m^3/h)');
PXcost = 1.419*52*'US$'*(PX101.PinH*RO101.Fout)/('atm*m^3/h');
a = (i*((1+i)^n))/(((1+i)^n)-1);
CapexRO = (HPPcost + PXcost + RO101.ROMcost)/0.45;
OpexT = ((P102.Pot+P103.Pot+P101.Pot)*Ecost*360*'d'*f +
0.333*(RO101.ROMcost))/0.88 + 0.1*720*'US$/m^2'*(MF101.Am);
CapexT = a*(CapexRO + Cmf)/f;
Cmf = 720*'US$/m^2'*(MF101.Am)/0.3;
spc = (OpexT+CapexT)/(RO101.P*360*'d');
cpt*(Ps+P) = (RO101.cFin*Ps+cp*P);
P = RO101.P;
cp = RO101.cP;

    SPECIFY
RO101.RR = 0.5;
RO101.Fin = MF101.P;#-Ps;
RO101.cFin = 1*'kmol/m^3';
MF101.cS = RO101.cFin*(58.5*'kg/kmol');
RO101.P = 50*'m^3/d';
P102.Pin = 1e-10*'atm';
```

```
Ecost = 0.05*'US$/(kW*h)';
i = 0.10;
P101.rho = RO101.rhoF(1);
P102.rho = RO101.rhoF(1);
P103.rho = RO101.rhoF(1);
RO101.Jw(2) = 15*'l/(h*m^2)';
cpt = 0.034*'kmol/m^3';

    OPTIONS
GuessFile="ORSW185ok";
Dynamic = false;
end
```

G.3 FO-RO flowsheet

```
using "FOrig3";
using "ROrigtest";
using "PXmodule";
using "auxiliary";

    FlowSheet Rota1

    DEVICES
FeedIn as flow_vol (Brief="Feed Stream", Default=1e-2, Lower=-1e-6, Upper=1e10,
DisplayUnit='m^3/d');
DrawSIn as flow_vol (Brief="DS Stream", Default=1e-2, Lower=-1e-6, Upper=1e10,
DisplayUnit='m^3/d');
FO101 as FOrigorous;
RO101 as ROmembrig;
P101 as pump;
P102 as pump;
P103 as pump;
PX101 as PXmodule;
sal as makeup;
cons as Real(Brief="Specific energy", Lower=0, Upper=1e4, Unit='kW*h/m^3');
PXcost as currency(Brief="Capital Cost of Pressure exchangers", Default=1e3);
HPPcost as currency(Brief="Capital Cost of HP pumps", Default=1e3);
CapexRO as currency(Brief="Capital Cost of RO unit", Default=1e3); #estimated
according to SWRO
```

```
OpexT as currency(Brief="Annual Operational Cost of the unit", Default=1e4);
#estimated according to SWRO
Ecost as Real(Brief="Energy cost", Lower=1e-3, Upper=0.2, Default=0.1,
Unit='US$/(kW*h)');
CapexFO as currency(Brief="Capital Cost of FO unit", Default=1e3);
CapexT as currency(Brief="Total Capital Cost", Default=1e4);
a as Real(Brief="Amortization Factor", Lower=0, Upper=1);
i as fraction(Brief="Interest rate", Default=0.10);
costmk as currency(Brief="Make up cost", Default=1e3);
spc as Real(Brief="Specific cost", Lower=0, Upper=1e4, Default=50,
Unit='US$/m^3');
cdsin as Real(Default=5);
cp as conc_mol(Default=0.05);
cpt as conc_mol(Default=0.04);
P as flow_vol(Default=2);
Ps as flow_vol(Default=0.1);
F as flow_vol(Default=4);

    PARAMETERS
n as Real(Brief="Plant Life", Default=20);
f as fraction(Brief="Plant Availability", Default=0.9);

    SET
f = 0.9;
n = 20;

    CONNECTIONS
FeedIn to FO101.Fin;
DrawSIn to FO101.DSin;

    EQUATIONS
FO101.DSout = RO101.Fin;
cons = (P101.Pot+P102.Pot+P103.Pot)/RO101.P;
P102.F = FO101.DSout - RO101.Fout;
FO101.cDSout = RO101.cFin;
P101.F = FO101.Fin;
P101.Pout = FO101.PinF(1);
RO101.Fout = FO101.DSin;
sal.M = (RO101.Js(3)*RO101.Am+FO101.Js(4)*FO101.Am);
```

```
P102.Pout = RO101.Pin;
RO101.Pout = PX101.PinH;
P103.F = RO101.Fout;
P103.Pin = PX101.PoutL;
P103.Pout = RO101.Pin;
PX101.PinL = FO101.PinDS(FO101.nm+1);
PX101.PoutH = FO101.PinDS(1);
cpt*(Ps+P) = (FO101.cFin*Ps+cp*P);
P = RO101.P;
cp = RO101.cP;
Ps + P = 50*'m^3/d';
#Costs
HPPcost = 1.419*52*'US$'*(P101.Pout*P101.F+P102.Pout*P102.F+P103.Pout*P103.F)/
('atm*(m^3/h)');
PXcost = 1.419*52*'US$'*(PX101.PinH*RO101.Fout)/('atm*m^3/h');
CapexRO = (HPPcost + PXcost + RO101.ROMcost)/0.45;
OpexT = (((P101.Pot+P102.Pot+P103.Pot)*Ecost*360*'d'*f +
0.33*(RO101.ROMcost+FO101.Am*RO101.ROcost)))/0.88 + costmk;
a = (i*((1+i)^n))/(((1+i)^n)-1);
CapexFO = (FO101.Am*RO101.ROcost)/0.3;
CapexT = a*(CapexFO + CapexRO)/f;
costmk = 0.3*'US$/kg'*sal.M*360*'d';
spc = (CapexT+OpexT)/(RO101.P*360*'d');
F = FeedIn + Ps;

    SPECIFY
FO101.RR = 0.10;
FO101.cFin = 1.54*'kmol/m^3';
cdsin = 2.1; #3.22
FO101.cDSin = cdsin*'mol/l';
FO101.MR = 0.48;#0.35;
FO101.A = 3.96*'l/(h*bar*m^2)';
FO101.B = 1.346*'l/(h*m^2)';
FO101.S = 1E-4*'m';
P101.Pin = 1e-10*'atm';
P102.Pin = 1e-10*'atm';
Ecost = 0.05*'US$/(kW*h)';
i = 0.10;
P102.rho = FO101.rhoDS;
```

```
P101.rho = FO101.rhoF;
P103.rho = FO101.rhoDS;
RO101.Jw(2) = 15*'l/(h*m^2)';
FO101.PinF(FO101.nm+1) = 0.2*'atm';
FO101.PinDS(1) = 0.2*'atm';
cpt = 0.085470085*'kmol/m^3';

    OPTIONS
GuessFile="Rota1xx";
Dynamic = false;
end
```

G.3.1 FO-RO optimization routine

```
using "Rota1-1-rig";

    Optimization Rota1optt as Rota1

    MINIMIZE
spc;

    FREE
FO101.MR;
cdsin;

    EQUATIONS
FO101.MR <= 0.6;
FO101.MR >= 0.30;
cdsin <= 5;
cdsin >= 1.7;
RO101.Pin <= 120*'bar';

    OPTIONS
Dynamic = false;
GuessFile = "Rota1xx";
NLPSolveNLA = false;
FeasiblePath = true;
NLPSolver(File = "complex",
#File = "PSO",
```

```
#File = "ipopt_emso",
#File = "MultiPSO",
#File = "arshj",
#File = "direct", MinimumRectangle=1e-4,MaxEvals=5000
#File = "optpp_emso",
MaxIterations = 5000,
RelativeAccuracy = 1e-10, AbsoluteAccuracy = 1e-10);

    GUESS
FO101.MR = 0.4;
cdsin = 3.5;
end
```

FO model

```
Model FOrigorous

    PARAMETERS
R as Real(Brief="Universal gas constant", Unit = '(atm*mˆ3)/(K*kmol)', Default
= 0.082);
L as length(Brief="Length of the retangular flow channel");
W as length(Brief="Width of retangular flow channel");
Nl as Integer(Brief="Number of leaves", Default = 16);
n as Integer(Brief="Vant Hoff factor", Default = 2);
T as temperature;
rhoF as dens_mass;
rhoDS as dens_mass;
miF as viscosity;
miDS as viscosity;
D as diffusivity;
MM as molweight(Default = 58.5);
dpt as length(Brief="Depth of retangular flow channel");
nm as Integer(Default=1);

    SET
T = 298*'K';
rhoF = 1050*'kg/(mˆ3)';
rhoDS = 1106*'kg/(mˆ3)';
miF = 1.14E-3*'kg/(m*s)';
```

```
miDS = 1.35E-3*'kg/(m*s)';
D = 1.33E-9*'(m^2)/s';
MM = 58.5*'kg/kmol';
#Assuming Number of leaves (similar to RO)
Nl = 8;
L = 0.0254*50*16*'m'; #1,27m
dpt = 28*0.001*0.0254*'m'; #0,0007112m
nm = 8;

    VARIABLES
A as Real(Brief="Membrane permeability", Unit = 'l/(h*bar*m^2)');
B as Real(Brief="Salt permeability", Unit = 'm^3/(s*m^2)');
S as Real(Brief="Structural parameter", Unit = 'm');
in Fin as flow_vol(Brief="Feed flow");
in DSin as flow_vol(Brief="Concentrated Draw solution flow");
out Fout as flow_vol(Brief="Concentrate feed flow", Default=2);
out DSout as flow_vol(Brief="Diluted Draw solution flow", Default=2);
MR as Real(Brief="Mass Ratio of Feed/DS", Lower = 0, Upper = 1.5, Default =
0.8);
RR as fraction(Default=0.5); #recovery ratio
Fi(nm+1) as flow_vol(Brief="Feed in flow per element", Default=1);
Di(nm+1) as flow_vol(Brief="Draw solution in flow per element", Default=1);
# concentrations
cFin as conc_mol(Default=1.5);
cFout as conc_mol(Default=3);
cDSin as conc_mol(Default=4);
cDSout as conc_mol(Default=2);
cFi(nm+1) as conc_mol(Default=2);
cDi(nm+1) as conc_mol(Default=3.5);
cFm(nm) as conc_mol(Default=2);
cDm(nm) as conc_mol(Default=3.5);
# Membrane calculations
Jw(nm) as flux_vol(Lower=1e-13, Default=1e-6, DisplayUnit='l/(h*m^2)');
Jwa as flux_vol(Lower=1e-13, Default=1e-6, DisplayUnit='l/(h*m^2)');
Js(nm) as flux_mass(Default=1e-6);
Am as area(Brief="Total membrane area", Default=50);
Amn as area(Brief="Element membrane area", Default=10);
# Fluid properties
piDSm(nm) as pressure(Default=100);
```

```
piFm(nm) as pressure(Default=100);
# Auxiliary calculation
vF(nm) as velocity(Default=0.06);
vDS(nm) as velocity(Default=0.08);
ReF(nm) as Real(Brief="Reynolds number", Default=80);
ReDS(nm) as Real(Brief="Reynolds number", Default=80);
kF(nm) as Real(Brief="mass transfer coefficient", Unit = 'm/s', Default=1e-5);
kDS(nm) as Real(Brief="mass transfer coefficient", Unit = 'm/s', Default=1e-5);
ScF as Real(Brief="Schmidt number", Default=800);
ScDS as Real(Brief="Schmidt number", Default=800);
ShF(nm) as Real(Brief="Sherwood number", Default=35);
ShDS(nm) as Real(Brief="Sherwood number", Default=35);
dpF(nm) as pressure(Brief="Feed head loss", Default=0.05);
dpDS(nm) as pressure(Brief="Draw solution head loss", Default=0.05);
PinF(nm+1) as pressure(Brief="Inlet feed pressure");
PinDS(nm+1) as pressure(Brief="Inlet DS pressure");
lambF(nm) as Real(Brief="Friction factor for Feed", Default=1.5);
lambDS(nm) as Real(Brief="Friction factor for DS", Default=1.5);
Lm as length(Brief="Membrane length");
dh as length;
x as length(Default=40);

    EQUATIONS
Fi(1)=Fin;
Fi(nm+1)=Fout;
Di(nm+1)=DSin;
Di(1)=DSout;
cFi(1)=cFin;
cFi(nm+1)=cFout;
cDi(nm+1)=cDSin;
cDi(1)=cDSout;
"Length calculation"
Am = x*L*Nl;
Amn = Am/nm;
Lm = L/nm;
"Feed Schmidt"
ScF = miF/(rhoF*D);
"Draw solution Schmidt"
ScDS = miDS/(rhoDS*D);
```

```
Jwa = sum(Jw)/nm;

    for index in [1:nm] do
"Element Mass balance"
Fi(index) + Di(index+1)=Fi(index+1)+Di(index);
"Element Mass balance with flux"
Fi(index)-Fi(index+1)=Jw(index)*Amn;
"Salt Mass balance"
MM*cFi(index)*Fi(index) +Js(index)*Amn = MM*cFi(index+1)*Fi(index+1);
"Salt Mass balance with flux"
MM*cDi(index+1)*Di(index+1) - Js(index)*Amn = MM*cDi(index)*Di(index);
"Average feed concentration"
cFm(index) = (cFi(index) + cFi(index+1))/2;
"Average draw solution concentration"
cDm(index) = (cDi(index) + cDi(index+1))/2;
"Osmotic pressure - Draw solution average"
piDSm(index) = cDm(index)*R*T*n;
"Osmotic pressure - Feed average"
piFm(index) = cFm(index)*R*T*n;
"Feed Reynolds"
ReF(index) = vF(index)*rhoF*dh/miF;
"Draw solution Reynolds"
ReDS(index) = vDS(index)*rhoDS*dh/miDS;
"Feed average velocity"
vF(index)*(Nl*dpt*x) = ((Fi(index)+Fi(index+1))/2);
"Draw solution average velocity"
vDS(index)*(Nl*dpt*x) = ((Di(index)+Di(index+1))/2);
"Feed Sherwood"
ShF(index) = 0.2*(ReF(index)^2)^(0.57/2)*(ScF^2)^(0.4/2);
"Draw solution Sherwood"
ShDS(index) = 0.2*(ReDS(index)^2)^(0.57/2)*(ScDS^2)^(0.4/2);
"Feed mass transfer coefficient"
ShF(index) = kF(index)*dh/D;
"Draw solution mass transfer coefficient" ShDS(index) = kDS(index)*dh/D;
"Water Flux"
(Jw(index)+(B)*exp(Jw(index)*(1/kF(index)+S/D)-exp(-
Jw(index)/kDS(index)))) = A*(piDSm(index)*exp(-Jw(index)/kDS(index))-
piFm(index)*exp(Jw(index)*(1/kF(index)+S/D)));
"Salt flux"
```

```
Js(index)*(Jw(index)+(B)*exp(Jw(index)*(1/kF(index)+S/D)-exp(-
Jw(index)/kDS(index)))) = B*Jw(index)*MM*(cDm(index)*exp(-
Jw(index)/kDS(index))-cFm(index)*exp(Jw(index)*(1/kF(index)+S/D)));
"Feed lambda calculation"
lambF(index) = 6.23*(ReF(index)^2)^(-0.3/2);
"DS lambda calculation"
lambDS(index) = 6.23*(ReDS(index)^2)^(-0.3/2);
"Feed head loss"
dpF(index) = (lambF(index)*rhoF*Lm*vF(index)^2)/(2*dh);
"DS head loss"
dpDS(index) = (lambDS(index)*rhoDS*Lm*vDS(index)^2)/(2*dh);
"Feed Final pressure"
PinF(index+1) = PinF(index) - dpF(index);
"DS Final pressure"
PinDS(index) = PinDS(index+1) - dpDS(index);
end
"Hydraulic diameter"
dh*(2*dpt+2*x) = 4*(dpt*x);
"Mass ratio to DS"
MR = DSin/Fin;
"Recovery ratio"
RR = (Fin - Fout)/Fin;
end
```

G.4 FO-MVC flowsheet

```
using "FOrig3";
using "auxiliary";
using "MVCcorrig";
using "HX";

    FlowSheet FOMVC

    DEVICES
FeedIn as Real (Brief="Feed Stream", Unit='m^3/h');
DrawSIn as Real (Brief="DS Stream", Unit='m^3/h');
FO101 as FOrigorous;
MVC101 as MVC;
```

```
P101 as pump;
P102 as pump;
P103 as pump;
cons as Real(Brief="Specific energy", Unit='kW*h/m^3');
HX101 as HX;
HX102 as HX;
dT as temp_delta(Default=5);
CAPEX as currency(Default=1e5);
CapexFO as currency(Default=1e5);
OPEX as currency(Default=1e5);
Membcost as Real(Brief="Membrane cost", Unit='US$/(m^2)', Default=40);
Cmvc as currency(Default=1e5);
Chx as currency(Default=1e5);
Cp as currency(Default=1e5);
a as Real(Brief="Amortization Factor", Lower=0, Upper=1);
i as fraction(Default=0.10);
Cee as Real(Brief="Electric energy cost", Default=0.05, Unit='US$/(kW*h)');
spc as Real(Brief="Specific cost", Lower=0, Upper=50, Default=2,
Unit='US$/m^3');
NaCl as makeup(Brief="Draw solute make up");
cp as conc_mol(Default=0.05);
cpt as conc_mol(Default=0.04);
P as flow_vol(Default=2);
Ps as flow_vol(Default=0.1);

    PARAMETERS
propterm as Plugin(Brief="Steam tables", Type="water", File="propterm");
n as Real(Brief="Plant Life", Default=20);
f as fraction(Brief="Plant Availability", Default=0.9);

    SET
f = 0.9;
n = 20;

    CONNECTIONS
FeedIn to FO101.Fin;
DrawSIn to FO101.DSin;

    SPECIFY
```

FO101.RR = 0.355;
FO101.cFin = 1.23*'kmol/m^3';
FO101.cDSin = 6.1*'kmol/m^3';
FO101.MR = 0.3;
FO101.PinF(FO101.nm+1) = 0.2*'bar';
FO101.PinDS(1) = 0.2*'bar';
FO101.A = 3.96*'l/(h*bar*m^2)';
FO101.B = 1.346*'l/(h*m^2)';
FO101.S = 1E-4*'m';
# MVC P101.F=FO101.Fin;
# P101.F = FO101.DSout;
P101.Pin = 1e-10*'atm';
P101.Pout = 2*'atm';
P101.rho = MVC101.rhoF;
P102.F = MVC101.Fin;
P102.Pin = 1e-10*'atm';
P102.Pout = 2*'atm';
P102.rho = MVC101.rhoF;
P103.F = FO101.DSin;
P103.Pin = 1e-10*'atm';
P103.Pout = 2*'atm';
P103.rho = FO101.rhoDS;
Membcost = 40*'US$/(m^2)';
MVC101.Fin = FO101.DSout;
MVC101.Fout = FO101.DSin;
MVC101.cFin = FO101.cDSout;
MVC101.Tfin = HX101.Tcout;
MVC101.Tb = 333*'K';
MVC101.dT = 3.64*'K';
HX101.Fh = MVC101.PWout;
HX101.Fc = MVC101.PWout;
HX101.Tcin = 298*'K';
HX101.Thin = MVC101.Td;
HX101.hhot = 3E3*'W/(K*m^2)';
HX101.hcold = 3E3*'W/(K*m^2)';
HX101.Tcout = HX102.Tcout;
HX101.Tcout = HX101.Thin - dT;
HX102.Fh = MVC101.Fout;
HX102.Fc = MVC101.Fout;

```
HX102.Tcin = 298*'K';
HX102.Thin = MVC101.Tb;
HX102.hhot = 3E3*'W/(K*m^2)';
HX102.hcold = 3E3*'W/(K*m^2)';
i = 0.10;
Cee = 0.05*'US$/(kW*h)';
dT = 6*'K'; #lower dT, higher spc
cpt = 0.034*'kmol/m^3';

    EQUATIONS
NaCl.M = FO101.Js(3)*FO101.Am;
cons = (P101.Pot+P102.Pot +P103.Pot + MVC101.Potcs)/MVC101.PWout;
Chx = 1.396*(136*('US$')*((HX101.A/('ft^2'))^2)^(0.6907/2)
+136*('US$')*((HX102.A/('ft^2'))^2)^(0.6907/2));
Cmvc = MVC101.Cmvc;
Cp = 1.419*52*'US$'*(P102.Pout*P102.F+P101.Pout*P101.F+
P103.Pout*P103.F)/('atm*(m^3/h)');
CAPEX = a*((Chx + Cmvc+Cp)/0.27 + CapexFO)/f;
CapexFO = (FO101.Am*Membcost)/0.3;
OPEX = (MVC101.Potcs+ P101.Pot)*360*'d'*Cee*f+
0.2*CapexFO+NaCl.M*360*'d'*0.3*'US$/kg';
a = (i*((1+i)^n))/(((1+i)^n)-1);
spc = (CAPEX + OPEX)/(MVC101.PWout*360*'d');
cpt*(Ps+P) = (FO101.cFin*Ps+cp*P);
P = MVC101.PWout;
cp = 1e-10*'kmol/m^3';
Ps + P = 50*'m^3/d';

    OPTIONS
GuessFile="FOMVC";#"FO101";
# SecondGuessFile="TesteFOpFOMVC";
Dynamic = false;
end
```

G.4.1 MVC model

```
using "types";

    Model MVC
```

PARAMETERS

etac as fraction(Brief="Compressor Efficiency", Default = 0.6);
R as Real(Brief="Universal gas constant", Unit = '(kJ/(K*kmol))', Default = 8.314);
MM as molweight(Default = 58.5);
Dens as dens_mass;
outer propterm as Plugin(Brief="Steam tables", Type="water", File="propterm");

VARIABLES

Fin as flow_vol(Brief="Feed flow", Default=4);
out Fout as flow_vol(Brief="Brine outlet", Default=2);
out PWout as flow_vol(Brief="Pure Water Outlet", Default=2);
RR as fraction(Default=0.5);
A as area(Default=100);
hvapb as Real(Brief="Vaporization Enthalpy at bulk", Unit = 'kJ/kg', Default = 2256);
hvapd as Real(Brief="Vaporization Enthalpy at condensator", Unit = 'kJ/kg', Default = 2256);
# concentrations
cFin as conc_mol(Default=1.5);
cFout as conc_mol(Default=3);
rhoF as dens_mass(Brief="Feed density", Default=1060);
rhoB as dens_mass(Brief="Brine density", Default=1080);
mF as Real(Brief="Feed molality", Default=1, Unit='mol/kg');
mB as Real(Brief="Brine molality", Default=3, Unit='mol/kg');
phiF as Real(Brief="Osmotic coefficient", Default=0.9, Lower=0.9, Upper=1.3);
phiB as Real(Brief="Osmotic coefficient", Default=0.9, Lower=0.9, Upper=1.5);
# Fluid properties
BPEFin as temp_delta (Brief="Boiling Point Elevation of Inlet", Default = 0.63);
BPEFout as temp_delta (Brief="Boiling Point Elevation of Brine", Default = 1);
Tv as temperature (Brief="Inlet Compressor Saturation Temperature", Default = 352);
Tfin as temperature (Brief="Feed in Temperature", Default = 352);
Ts as temperature (Brief="Compressor outlet Temperature", Default=370);
Tcin as temperature (Brief="Inlet Compressor Temperature", Default=353);
Tb as temperature (Brief="Inlet Evaporator Condensator Temperature", Default = 353);
Td as temperature (Brief="Condensator Temperature", Default = 333);

```
dT as temp_delta (Brief="aprox Td - Tb", Default = 5);
Psatd as pressure(Brief="Saturation pressure @ Td", Default=0.1);
Psatv as pressure(Brief="Saturation pressure @ Tv", Default=0.1);
Potcs as potency (Brief="Compressor Axial Potency", Default=34);
cpvapPW as Real(Brief="Molar Thermal Capacity",Unit = 'kJ/(kmol*K)', Default
= 33.9);
ghama as Real(Brief="cp/cv", Default=1.33);
q as power(Brief="Heat exchanged at evaporator", Default=150);
U as heat_trans_coeff(Default=10);
Cmvc as currency(Default=1e5);

    EQUATIONS
phiF = 0.93424+0.03957*mF*'kg/mol'+0.00289*(mF*'kg/mol')^2;
phiB = 0.93424+0.03957*mB*'kg/mol'+0.00289*(mB*'kg/mol')^2;
rhoF =(1.02297+0.03278*mF*'kg/mol'-6.0732E-4*(Tfin/'K'-
273.15))*10^3*'kg/m^3';
rhoB = (1.02297+0.03278*mB*'kg/mol'-6.0732E-4*(Tb/'K'-
273.15))*10^3*'kg/m^3';
mF*(rhoF-cFin*MM) = cFin;
mB*(rhoB-cFout*MM) = cFout;
"Global Mass balance"
rhoF*Fin = rhoB*Fout + Dens*PWout;
"Salt mass balance"
MM*cFin*Fin = MM*cFout*Fout;
"Recovery Ratio"
RR = (PWout)/Fin;
"Boiling Point Elevation - Feed"
BPEFin = 2*cFin*R*(Tfin^2)*phiF/(hvapb*Dens);
"Boiling Point Elevation - Brine"
BPEFout = 2*cFout*R*(Tb^2)*phiB/(hvapb*Dens);
"Compressor Outlet Saturation Temperature"
Td = Tb-BPEFin+BPEFout+dT;
"Compressor Inlet Saturation Temperature"
Tv = Tb-BPEFin;
"Energy Balance"
Potcs = (cpvapPW*Tcin/etac)*(((Psatd/Psatv)^((ghama-1)/(ghama)))-
1)*(PWout*Dens/(18*'g/mol'));
"Molar Thermal Capacity"
cpvapPW = 32.22*'kJ/(kmol*K)'+1.92E-3*'kJ/(kmol*K^2)'*Tcin+1.06E-
```

5*'kJ/(kmol*K^3)'*Tcin^2-3.59E-9*'kJ/(kmol*K^4)'*Tcin^3;
"ghama"
ghama = cpvapPW/(cpvapPW-R);
"Heat calculation"
q = rhoF*Fin*4.2*'kJ/(K*kg)'*(Tb - Tfin) + Dens*PWout*hvapb;
q = Dens*PWout*cpvapPW*(Ts - Td)/(18*'kg/kmol')+ Dens*PWout*hvapd;
"Vaporization heat at bulk"
hvapb = (2499.5698-2.204864*(Tb-273.15*'K')/'K'-2.304E-3*(Tb-273.15*'K')^2/'K^2')*'kJ/kg';
"Vaporization heat at condensator"
hvapd = (2499.5698-2.204864*(Td-273.15*'K')/'K'-2.304E-3*(Td-273.15*'K')
2/'K^2')*'kJ/kg';
"Sat pressure calculation"
Tv = propterm.Tsat(Psatv);
Td = propterm.Tsat(Psatd);
"Area calculation"
(U*(Td-Tb))*A = q;
"U calculation"
U = 1e-3*(1939.4+1.40562*(Tb-273.15*'K')/'K'-0.0207525*(1/'K^2')*(Tb-273.15*'K')^2+0.0023186*(1/'K^3')*(Tb-273.15*'K')^3)*'kW/(K*m^2)';
Tcin = Tb + 0.5*(BPEFin - BPEFout);
Cmvc = 1.374*(430*'US$'*(0.582*(1/('kW/(K)'))*A*U*(10^(-0.01)*10^-(0.1)))+7364*'US$'*PWout*Dens/('kg/s')*Psatd/Psatv*(etac/(1-etac))^0.7);
end

G.4.2 FO-MVC optimization

Optimization FOMVCopt as FOMVC

MINIMIZE
spc;

FREE
FO101.RR;
MVC101.dT;

EQUATIONS
MVC101.dT > 1*'K';
MVC101.dT < 4*'K';

```
OPTIONS
Dynamic = false;
GuessFile = "FOMVCteste";
NLPSolveNLA = false;
FeasiblePath = true;
NLPSolver(File = "complex",
MaxIterations = 5000,
RelativeAccuracy = 1e-10, AbsoluteAccuracy = 1e-10);

    GUESS
MVC101.dT = 2.3*'K';
MVC101.Tb = 333*'K';
end
```

G.5 MF-MVC flowsheet

```
using "MVCcorrig";
using "auxiliary";
using "HX";
using "MFmemb";

    FlowSheet TesteMVC

    PARAMETERS
propterm as Plugin(Brief="Steam tables", Type="water", File="propterm");
n as Real(Brief="Plant Life", Default=20); f as fraction(Brief="Plant Availability",
Default=0.9);
    DEVICES
MF101 as MFmemb; MVC101 as MVC;
P101 as pump;
P102 as pump;
cons as Real(Brief="Specific energy", Unit='kW*h/mˆ3');
HX101 as HX;
HX102 as HX;
dT as temp_delta(Default=5);
CAPEX as currency(Default=1e5);
OPEX as currency(Default=1e5);
Cmf as currency(Default=1e5);
Cp as currency(Default=1e5);
```

```
Cmvc as currency(Default=1e5);
Chx as currency(Default=1e5);
a as Real(Brief="Amortization Factor", Lower=0, Upper=1);
i as fraction(Default=0.10);
Cee as Real(Brief="Electric energy cost", Default=0.05, Unit='US$/(kW*h)');
spc as Real(Brief="Specific cost", Lower=0, Upper=50, Default=2,
Unit='US$/m^3');
cp as conc_mol(Default=0.05);
cpt as conc_mol(Default=0.04);
P as flow_vol(Default=2);
Ps as flow_vol(Default=0.1);

    SET
f = 0.9;
n = 20;

    CONNECTIONS
P101.F to MF101.Fin;

    SPECIFY

    P101.Pin = 1e-10*'atm';
P101.Pout = 2*'atm';
P102.F = MF101.P;
P102.Pin = 1e-10*'atm';
P102.Pout = 2*'atm';
MF101.RR = 0.90;
MF101.cFin = 100*'kg/m^3' ;
MF101.cS = 90000*'kg/m^3';
MVC101.RR = 0.5;
MVC101.cFin = 1.85*'kmol/m^3';
MVC101.Tfin = HX101.Tcout;
MVC101.Tb = 333*'K';
MVC101.dT = 2*'K';
MVC101.Fin = MF101.P-Ps;

    HX101.Fh = MVC101.PWout;
HX101.Fc = MVC101.PWout;
HX101.Tcin = 298*'K';
```

```
HX101.Thin = MVC101.Td;
HX101.hhot = 3E3*'W/(K*m^2)';
HX101.hcold = 3E3*'W/(K*m^2)';
HX101.Tcout = HX102.Tcout;
HX101.Tcout = HX101.Thin - dT;
HX102.Fh = MVC101.Fout;
HX102.Fc = MVC101.Fout;
HX102.Tcin = 298*'K';
HX102.Thin = MVC101.Tb;
HX102.hhot = 3E3*'W/(K*m^2)';
HX102.hcold = 3E3*'W/(K*m^2)';
i = 0.10;
Cee = 0.05*'US$/(kW*h)';
dT = 6*'K';
cpt = 0.034*'kmol/m^3';

    EQUATIONS
cons = (P101.Pot+MVC101.Potcs+P102.Pot)/MVC101.PWout;
Chx = 1.396*(136*('US$')*((HX101.A/('ft^2'))^2)^(0.6907/2)
+136*('US$')*((HX102.A/('ft^2'))^2)^(0.6907/2));
Cmvc = MVC101.Cmvc;
Cp = 1.419*52*'US$'*(P102.Pout*P102.F+P101.Pout*P101.F)/('atm*(m^3/h)');
Cmf = 720*'US$/m^2'*(MF101.Am)/0.3;
CAPEX = a*((Chx + Cmvc+Cp)/0.27+Cmf)/f;
OPEX = (MVC101.Potcs+ P101.Pot+P102.Pot)*360*'d'*Cee*f+
0.1*720*'US$/m^2'*(MF101.Am);
a = (i*((1+i)^n))/(((1+i)^n)-1);
spc = (CAPEX + OPEX)/(MVC101.PWout*360*'d');
cpt*(Ps+P) = (MVC101.cFin*Ps+cp*P);
P = MVC101.PWout;
cp = 1e-10*'kmol/m^3';
Ps + P = 50*'m^3/d';

    OPTIONS
GuessFile="TesteMVCup";
Dynamic = false;
end
```

G.5.1 MF-MVC optimization

```
Optimization MVCopt as TesteMVC

    MINIMIZE
spc;

    FREE
# MVC101.Tb;
# MVC101.RR;
MVC101.dT;

    EQUATIONS
# MVC101.Tb <= 353*'K';
# MVC101.Tb >= 333*'K';
# MVC101.RR <= 0.5;
# MVC101.RR >= 0.3;
MVC101.dT >= 1*'K';
MVC101.dT <= 7*'K';

    OPTIONS
Dynamic = false;
GuessFile = "MVCoptup";
SecondGuessFile = "TesteMVCup";
NLPSolveNLA = false;
FeasiblePath = true;
NLPSolver(File = "complex",
MaxIterations = 5000,
RelativeAccuracy = 1e-10, AbsoluteAccuracy = 1e-10);
end
```

G.6 MF-MVC-MD flowsheet

```
using "MVCcorrig";
using "MDIErig";
using "HX";
using "auxiliary";
using "MFmemb";
```

```
    FlowSheet MDMVC

    PARAMETERS
propterm as Plugin(Brief="Steam tables", Type="water", File="propterm");
n as Real(Brief="Plant Life", Default=20);
f as fraction(Brief="Plant Availability", Default=0.9);

    DEVICES

    MF101 as MFmemb;
MD1001 as MDsimplified1;
MVC101 as MVC;
HX101 as HX;
P101 as pump;
P102 as pump;
P103 as pump;
cons as Real(Brief="Electric energy input",Unit='kW*h/(m^3)', Default=10);
Fin as flow_vol(Default=4);
Tfin as temperature(Default=298);
cFin as conc_mol(Default=1.5);
Fout as flow_vol(Default=2);
cFout as conc_mol(Default=3);
P as flow_vol(Default=2);
dT as temp_delta(Default=5);
dTmd as temp_delta(Default=5);
r as fraction(Default=0.5);
RR as fraction(Default=0.5);
CAPEX as currency(Default=1e5);
OPEX as currency(Default=1e5);
Cmvc as currency(Default=1e5);
Cmf as currency(Default=1e5);
Cmd as currency(Default=1e5);
Chx as currency(Default=1e5);
Cp as currency(Default=1e5);
a as Real(Brief="Amortization Factor", Lower=0, Upper=1);
i as fraction(Default=0.10);
Cee as Real(Brief="Electric energy cost", Default=0.05, Unit='US$/(kW*h)');
spc as Real(Brief="Specific cost", Lower=0, Upper=50, Default=2,
Unit='US$/m^3');
```

SET
f = 0.9;
n = 20;

CONNECTIONS
Fin to MF101.Fin;

SPECIFY
P101.F = MF101.Fin;
P101.Pin = 1e-10*'atm';
P101.Pout = 2*'atm';
P102.F = MVC101.Fin;
P102.Pin = 1e-10*'atm';
P102.Pout = 2*'atm';
P103.F = MD1001.Fin;
P103.Pin = 1e-10*'atm';
P103.Pout = 2*'atm';
MD1001.Fin = MVC101.Fout;
MD1001.cFin = MVC101.cFout;
MD1001.Tfin = MVC101.Tb;
MD1001.Fout = Fout;
MD1001.cFout = cFout;
MD1001.Tcout = MVC101.Tfin;
# MD1001.Am = 30*'m^2'; #easier to vary than dTmd
MD1001.Tcin = Tfin;
MVC101.PWout = 50*'m^3/d';
r = 0.47;
dT = 3*'K';
Tfin = (25+273)*'K';
MVC101.cFin = cFin;
cFin = 1.54*'kmol/m^3';
MVC101.RR = 0.50;
MVC101.dT = 4*'K';
dTmd = 12*'K'; # does not converge under 5
MVC101.Tb = 333*'K';
MD1001.B = 22E-7*'kg/(Pa*s*m^2)';
MD1001.km = 1.2*'W/m/K';
MF101.RR = 0.90;

```
MF101.cFin = 100*'kg/m^3' ;
MF101.cS = 90000*'kg/m^3';
Cmf = 720*'US$/m^2'*(MF101.Am)/0.3;
MF101.P = MVC101.Fin;
HX101.Fh = MVC101.PWout;
HX101.Fc = (1-r)*Fin;
HX101.Tcin = Tfin;
HX101.Thin = MVC101.Td;
HX101.Tcout = MVC101.Tfin;
HX101.hhot = 3E3*'W/(K*m^2)';
HX101.hcold = 3E3*'W/(K*m^2)';
i = 0.10;
Cee = 0.05*'US$/(kW*h)';

    EQUATIONS
MD1001.Tcout = MD1001.Tfin - dTmd;
r = MD1001.C/(Fin);
RR = (P)/MVC101.Fin;
P = MD1001.P + MVC101.PWout;
cons = (MVC101.Potcs+P101.Pot)/P;
Chx = 1.369*(136*('US$')*((HX101.A/('ft^2'))^2)^(0.6907/2));
Cmd = 90*'US$/(m^2)'*MD1001.Am;
Cmvc = MVC101.Cmvc;
Cp = 1.419*52*'US$'*(P102.Pout*P102.F+P101.Pout*P101.F
+P103.Pout*P103.F)/('atm*(m^3/h)');
CAPEX = a*((Chx + Cmvc+Cp)/0.27+ Cmd/0.5 +Cmf)/f;
OPEX = (MVC101.Potcs+P101.Pot+P102.Pot+P103.Pot)*360*'d'*Cee*f +
90*'US$/(m^2)'*MD1001.Am*0.1 +0.1*720*'US$/m^2'*(MF101.Am);
a = (i*((1+i)^n))/(((1+i)^n)-1);
spc = (CAPEX + OPEX)/(P*360*'d');

    OPTIONS
GuessFile="MDMVCteste";
SecondGuessFile="TesteMVCxx";
Dynamic = false;
end
```

G.6.1 MD model

Model MDsimplified1

PARAMETERS

outer propterm as Plugin(Brief="Steam tables", Type="water");
W as length(Brief="Width of retangular flow channel");
dpt as length(Brief="Depth of retangular flow channel");
R as Real(Brief="Universal gas constant", Unit = '(atm*m^3)/(K*kmol)', Default = 0.082);
rhoF as dens_mass;
rhoP as dens_mass;
MM as molweight(Default = 58.5);
dh as length;
eps as fraction(Brief="Membrane porosity");
thk as length(Brief="Membrane thickness");
kV as conductivity(Brief="Vapor conductivity");
Press as pressure;
nm as Integer;
nl as Integer(Brief="Number of leaves in a module", Default=10);

SET

dh = 4*(dpt*W)/(2*dpt+2*W);
W = 1*'m';
dpt = 1E-3*'m';
rhoF = 1.04E3*'kg/(m^3)';
rhoP = 0.997E3*'kg/(m^3)';
Press = 1*'atm';
eps = 0.8;
thk = 200E-6*'m';
kV = 0.0188*'W/m/K';
nl = 15; # Adjustment of velocities

VARIABLES

kF as conductivity(Brief="Feed Thermal conductivity");
kP as conductivity(Brief="Permeate Thermal conductivity @ coolant");
miF as viscosity(Default=0.7);
miP as viscosity(Default=0.9);
Fin as flow_vol(Brief="Feed flow");

```
Fout as flow_vol(Brief="Concentrate feed flow");
P as flow_vol(Brief="Permeate");
C as flow_vol(Brief="Coolant flow");
RR as fraction(Brief="Recovery ratio", Default = 0.02);
B as Real(Brief="MD coefficient", Unit = 'kg/(Pa*s*m^2)');
km as conductivity(Brief="Membrane conductivity");
cFin as conc_mol;
cFout as conc_mol;
cFavg as conc_mol;
xw as fraction(Brief="Water fraction");
Jw as flux_mass(Default=1e-3, DisplayUnit='kg/(h*m^2)'); #Js assumed to be zero
Am as area(Brief="Total membrane area", Default=8);
L as length(Brief="Flat sheet lenght", Default=8);
hFin as enth_mass(Brief="Feed enthalpy");
hFout as enth_mass(Brief="Concentrate enthalpy");
hCin as enth_mass(Brief="Coolant in enthalpy");
hCout as enth_mass(Brief="Coolant out enthalpy");
hPout as enth_mass;
hPwall as enth_mass;
hPureVapF as enth_mass(Brief="Pure vapor enthalpy");
hPureVapP as enth_mass(Brief="Pure vapor enthalpy");
HtFlux as heat_flux;
qc as heat_flux;
Hvap as enth_mass;
hLsatF as enth_mass;
hLsatP as enth_mass;
hconvF as Real(Brief="Feed convective heat transfer coefficient", Unit='W/(K*m^2)');
hconvP as Real(Brief="Permeate convective heat transfer coefficient", Unit='W/(K*m^2)');
Tfin as temperature(Brief="Bulk inlet temperature", Default = 45+273.15);
Tfout as temperature(Brief="Bulk outlet temperature", Default = 43 +273.15);
Tfb as temperature(Brief="Bulk feed temperature", Default = 44+273.15);
Tcin as temperature(Brief="Bulk coolant in temperature", Default = 35+273.15);
Tcout as temperature(Brief="Bulk coolant out temperature", Default = 37+273.15);
Tc as temperature(Brief="Bulk coolant temperature", Default =36+273.15 );
Tfm as temperature(Brief="Membrane temperature @ feed side", Default = 44.5+273.15);
```

```
Tpm as temperature(Brief="Membrane temperature @ permeate side", Default = 36.5+273.15);
TsatF as temperature(Brief="Saturation temperature @ membrane", Default = 317.15);
Tpout as temperature(Brief="Permeate temperature @ exit", Default=36+273.15);
Twall as temperature(Brief="Permeate temperature @ exit", Default=35+273.15);
PvapF as pressure(Brief="vapor pressure @ TsatF @xw");
PsatF as pressure(Brief="Saturation pressure @TsatF");
PvapP as pressure(Brief="vapor pressure @ Tpm @xw=1");
vF as velocity;
ReF as Real(Brief="Feed Reynolds number");
PrF as Real(Brief="Feed Prandtl number");
NuF as Real(Brief="Feed Nusselt number");
vP as velocity;
ReP as Real(Brief="Permeate Reynolds number");
PrP as Real(Brief="Permeate Prandtl number");
NuP as Real(Brief="Feed Nusselt number");
cpF as cp_mass;
cp as cp_mass(Default=4.18);
S1 as entr_mass;
S2 as entr_mass;
S3 as entr_mass;
S4 as entr_mass;
S5 as entr_mass;
S6 as entr_mass;
S7 as entr_mass;
S8 as entr_mass;

    EQUATIONS
kF = (0.608+7.46E-4*(Tfb-273.15*'K')*(1-0.98*(1-xw))/'K')*'W/m/K';
kP =(0.608+7.46E-4*(Tc-273.15*'K')*(1-0.98*(1-xw))/'K')*'W/m/K';
cpF = 3.93*'kJ/(kg*K)';
cp = 4.2*'kJ/(kg*K)';
miF = (8.7E-1*'cP'-6.3E-3*(Tfb-273.15*'K')*'cP/K')*(1+12.9*(1-xw));
miP = (8.7E-1*'cP'-6.3E-3*(Tpout-273.15*'K')*'cP/K');
Am = L*W*nl;
"Global Mass balance"
Fin = Fout + P;
"Recovery ratio"
```

```
RR = P/Fin;
"Global Mass balance with flux"
rhoF*(Fin - Fout) = Jw*Am;
"Salt mass balance"
MM*cFin*Fin = MM*cFout*Fout;
"Feed average velocity"
vF = ((Fin+Fout)/2/nl)/(dpt*W);
"Coolant average velocity"
vP = ((P+2*C)/2/nl)/(dpt*W);
"Feed Reynolds"
ReF = vF*rhoF*dh/miF;
"Permeate Reynolds"
ReP = vP*rhoP*dh/miP;
"Water Flux"
Jw = B*(PvapF-PvapP);
"Feed Tsat calculation"
PsatF/'Pa' = exp(23.328-3841*'K'/(TsatF-45*'K'));
"Permeate Tsat calculation"
PvapP/'Pa' = exp(23.328-3841*'K'/(Tpm-45*'K'));
"Raoults law for dilute solution"
PvapF = PsatF*xw;
"Water fraction"
xw=(1/18)/(((cFin+cFout)/(2*'kmol/m^3'))/1000+(1/18));
"Average concentration on feed side"
cFavg = (cFin + cFout)/2;
"Hvap calculation"
Hvap = 2265*'kJ/kg';
Tfm = TsatF;
"Estimation for feed bulk temperature"
Tfb = (Tfin + Tfout)/2;
"Estimation for coolant bulk temperature"
Tc = (Tcin + Tcout)/2;
"Energy balance on feed side"
rhoF*Fin*hFin = rhoF*Fout*hFout + (HtFlux + hPureVapF*Jw)*Am;
"Feed in Enthalpy calculation"
[S1, hFin]= propterm.propPTl(Press, Tfin);
"Feed out Enthalpy calculation"
[S2, hFout] = propterm.propPTl(Press, Tfout);
"Energy balance on permeate side"
```

```
(HtFlux + hPureVapP*Jw)*Am = rhoP*hPout*P+qc*Am;
"Energy balance on coolant side"
rhoP*C*hCin + qc*Am = rhoP*(C)*hCout;
"Coolant in Enthalpy calculation"
[S3, hCin] = propterm.propPTl(Press, Tcin);
"Coolant out Enthalpy calculation"
[S4, hCout] = propterm.propPTl(Press, Tcout);
"Feed Prandtl number"
PrF = cpF*miF/kF;
"Coolant Prandtl number"
PrP = cp*miP/kP;
"Feed Nusselt number"
NuF = hconvF*dh/kF;
"Coolant Nusselt number"
NuP = hconvP*dh/kP;
"Nusselt correlation for feed"
# NuF = (2.76E-3)*((ReF^2)^(0.97/2))*((PrF^2)^(3.7909/2));
# NuF = 0.13*((ReF^2)^(0.64/2))*(PrF^2)^(1/6);
NuF = 0.027*((ReF^2)^.4)*((PrF^2)^0.15);
"Nusselt correlation for permeate"
# NuP = (2.76E-3)*((ReP^2)^(0.97/2))*((PrP^2)^(3.7909/2)); #Chiam (2014)
# NuP = 0.13*((ReP^2)^(0.64/2))*(PrP^2)^(1/6);
NuP = 0.027*(((ReP^2)^.4)*((PrP^2)^0.15));
"Feed convection"
Jw*(hPureVapF - (hFin+hFout)/2) + HtFlux = hconvF*(Tfb-Tfm);
"Qc flux"
qc=kP*(Tpm-Twall)/dpt;
qc + Jw*(hPureVapP - hPwall) = -hconvP*(Tc-Twall);
[S7, hPout] = propterm.propPTl(Press,Tpout);
[S8, hPwall] = propterm.propPTl(Press,Twall);
Tpout = Twall;
"Heat flux"
HtFlux = (km*(1-eps)+kV*eps)*(Tfm-Tpm)/thk;
"vapor enthalpy"
hPureVapF = Hvap + hLsatF;
[S5, hLsatF] = propterm.propPTl(Press,Tfm);
hPureVapP = Hvap+ hLsatP;
[S6, hLsatP] = propterm.propPTl(Press,Tpm);
end
```